Postępowanie wstępujące jest strategią charakterystyczną dla syntezy. Na bazie dotychczasowych informacji następuje wyprowadzenie (synteza) nowej.

2. SCHEMAT WNIOSKOWANIA WSTĘPUJĄCEGO

Mówiąc ogólnie, jeden krok wnioskowania wstępującego polega na dopasowaniu odpowiedniej liczby asercji do warunków konkluzji i wyprowadzeniu nowej asercji. Nową asercję tworzy konkluzja klauzuli ukonkretniona przez podstawienia dopasowujące. Jeżeli klauzula jest negacją (czyli nie ma konkluzji), wówczas wyprowadzona asercja jest klauzulą pustą.

Zasada postępowania została schematycznie przedstawiona na rys. 1.

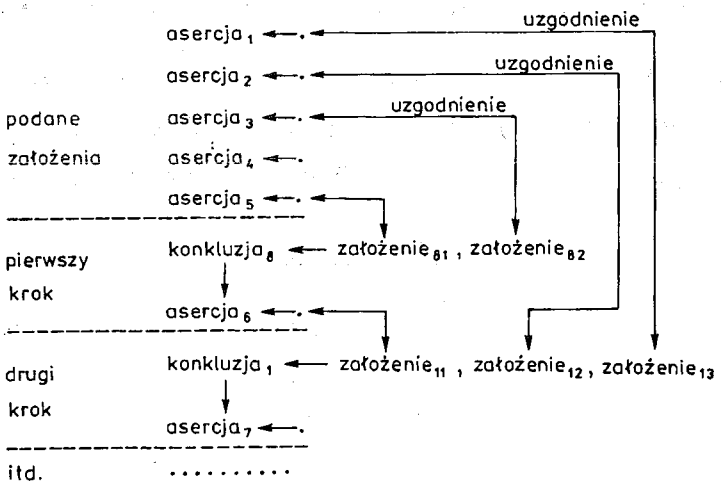

Rys. 1. Schemat wnioskowania wstępującego

Na schemacie tym, asercje oznaczone numerami 1 do 5, są podanymi założeniami. W pierwszym kroku, w wyniku uzgodnienia [2] asercji$_5$ z założeniem$_{81}$ oraz asercji$_3$ z założeniem$_{82}$, ukonkretniona została konkluzja$_8$ i przyjęta jako nowa asercja$_6$. W drugim kroku, po uzgodnieniu założeń klauzuli$_1$ i ukonkretnieniu jej konkluzji, powstaje asercja$_7$. Dalej proces powtarza się, aż do osiągnięcia klauzuli, która już nie wyprowadza nowej asercji. Konkluzją tej ostatniej klauzuli jest zwykle wyprowadzenie informacji o osiągnięciu celu.

W Prologu, ze względu na sposób zapisu asercji do bazy danych, wnioskowanie wstępujące zapisuje się zwykle w postaci reguł o następującej składni [5]:

<kontekst>: – <założenia>, assert(<konkluzje>)

gdzie *assert* jest predykatem zapisującym fakty do bazy danych. Klauzula$_1$ w przykładzie na rys. 1 może mieć w Prologu schemat następujący:

reguła$_1$: –
założenie$_{11}$, założenie$_{12}$, założenie$_{13}$,
assert(konkluzja$_1$).

3. IDENTYFIKACJA MODUŁÓW WZMACNIACZA CMOS JAKO PRZYKŁAD ZASTOSOWANIA WNIOSKOWANIA WSTĘPUJĄCEGO

Przykładem zastosowania wnioskowania wstępującego może być identyfikacja układów stosowanych w projektowaniu wzmacniaczy CMOS [8,10]. Zakłada się, że dana jest lista tranzystorów wraz z oznaczeniami węzłów, do których są podłączone. Odpowiada to danym dla programów symulacyjnych, np. SPICE [7]. Należy podać reguły, które na podstawie tej listy pozwolą na identyfikację układów elementarnych, jak zwierciadło prądowe, inwerter przeciwsobny itp. Rozpoznane układy elementarne będą z kolei służyć do identyfikacji większych bloków konstrukcyjnych (stopień różnicowy, stopień końcowy itp.), w końcu całego wzmacniacza. Identyfikacja układów jest ważnym elementem procesu automatycznej interpretacji wyników symulacji [4].

Dla elementów i układów przyjęto reprezentację o strukturze ramowej [3], np.:

układ ([rodzaj (...), typ (...), we (...), wy (...), zasilanie (...)])

Rozważmy jako pierwszą regułę identyfikującą zwierciadło prądowe (rys. 2).

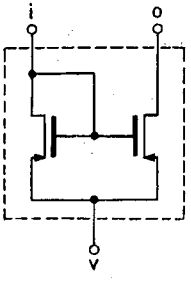

Rys. 2. Schemat zwierciadła prądowego

```
(R1)
   układ ([rodzaj (zwierciadło_prądowe),
           typ (t),
           we (i),
           wy (o),
           zasilanie (v)]) ←
       układ ([rodzaj (tranzystor),
               typ (vt),
               źródło (v),
               bramka (i),
               dren (o)]),
       różne ([v, i, o]),
       układ ([rodzaj (tranzystor),
               typ (t),
               źródło (v),
```

bramka(*i*),
dren(*i*)]).

Funktory o nazwach *we, wy, bramka* itp. służą do zapisu połączeń między układami. Zapis ten jest realizowany przez podanie wspólnej zmiennej dla zacisków połączonych ze sobą w jeden węzeł. Zmiennymi są tu *i, o, v* (oznaczenia węzłów) oraz *t* (typ tranzystora).

Należy ponadto podać, które zaciski nie mogą być ze sobą połączone. Takie niezamierzone połączenie, może wyniknąć z uzgodnienia różnych zmiennych z tą samą stałą [2]. Jako przykład rozważmy następującą sytuację: pierwsze założenie klauzuli R8 zostało uzgodnione z asercją:

układ([rodzaj(tranzystor),
typ(PMOS),
źródło(3),
bramka(1),
dren(1)]) ←.

Wynikiem unifikacji będą przypisania:

$$\{\ t=\text{PMOS},\ v=3,\ i=1,\ o=1\ \}.$$

Zakładając, że predykat różne(...) nie został użyty, zauważmy że drugie założenie klauzuli R1 po ukonkretnieniu ma postać identyczną jak zapisana wyżej asercja – daje się więc z nią uzgodnić. Wynikiem tych uzgodnień i ukonkretnienia konkluzji będzie więc asercja

układ([rodzaj(zwierciadło_prądowe),
typ(PMOS),
we(1),
wy(1),
zasilanie(3)]) ←.

Reprezentuje ona zwierciadło prądowe o zwartym wejściu i wyjściu. Predykat różne([...]) zapobiega powtarzaniu się symboli na liście [3], która jest jego argumentem.
W podobny sposób można zapisać regułę identyfikującą parę różnicową (rys. 3).

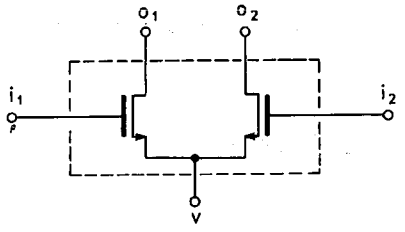

Rys. 3. Schemat pary różnicowej

(R2)
układ ([rodzaj (para_różnicowa),
typ (t),
we (i_1),
we (i_2),
wy (o_1),
wy (o_2),
zacisk (w)]) ←
układ ([rodzaj (tranzystor),
typ (t),
źródło (w),
bramka (i_1),
dren (o_1)]),
układ ([rodzaj (tranzystor),
typ (t),
źródło (w),
bramka (i_2),
dren (o_2)]),
różne ([i_i, i_2, o_1, o_2, w]).

Trzecia reguła określa sposób identyfikacji stopnia różnicowego (rys. 4).

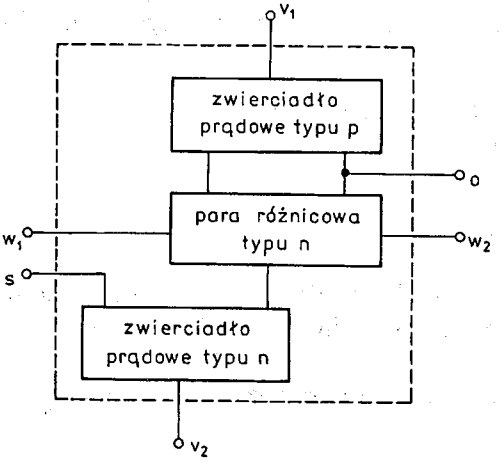

Rys. 4. Schemat blokowy stopnia różnicowego

(R3)
układ ([rodzaj (stopień_różnicowy),
typ (t_1),
we (w_1),
we (w_2),
wy (o),

zasilanie (v_1),
zasilanie (v_2),
zacisk (s)]) ←
układ ([rodzaj (para_różnicowa),
typ (t_1),
we (i_1),
we (i_2),
wy (o_1),
wy (o_2),
zasick (w)]),
układ ([rodzaj (zwierciadło_prądowe),
typ (t_1),
we (s),
wy (w),
zasilanie (v_2)]),
zmień_typ (t_1, t_2),
układ ([rodzaj (zwierciadło_prądowe),
typ (t_2),
we (i),
wy (o),
zasilanie (v_1)]),
dopasuj ([i_1, i_2, o_1, o_2, w_1, w_2, i, o]).

Na uwagę zasługują tu dwa predykaty pomocnicze *zmień_typ* i *dopasuj*. Zadaniem pierwszego jest zapewnienie różnych typów pary różnicowej i obciążenia. Operację tą można zrealizować przy pomocy dwóch asercji

zmień_typ (PMOS, NMOS) ←.
zmień_typ (NMOS, PMOS) ←.

Zadaniem drugiego predykatu jest „dopasowanie" oznaczeń zacisków pary różnicowej do obciążenia. Operację tą można zrealizować przy pomocy dwóch asercji:

dopasuj ([i_1, i_2, o_1, o_2, i_1, i_2, o_1, o_2]) ←.
dopasuj ([i_1, i_2, o_1, o_2, i_2, i_1, o_2, o_1]) ←.

Druga asercja odpowiada „obrotowi" pary różnicowej wokół osi symetrii.

Należy też zwrócić uwagę na brak w założeniach klauzuli R3 predykatu różne (...). Indywidualne nazwy zacisków zostały bowiem zapewnione na etapie identyfikacji układów elementarnych.

W oparciu o te trzy reguły, spróbujmy prześledzić sposób wnioskowania wstępującego, na przykładzie identyfikacji układu przedstawionego na rys 5.

Struktura topologiczna tego układu będzie reprezentowana przez asercje:

(A1) układ ([rodzaj (tranzystor),
typ (NMOS),
źródło (Vss),

bramka (1),
dren (1)]) ←.

(A2) układ ([rodzaj (tranzystor),
typ (NMOS),
źródło (Vss),
bramka (1),
dren (*wy*)]) ←.

(A3) układ ([rodzaj (tranzystor),
typ (PMOS),
źródło (2),
bramka (−),
dren (1)]) ←.

(A4) układ ([rodzaj (tranzystor),
typ (PMOS),
źródło (2),
bramka (+),
dren (wy)]) ←.

(A5) układ ([rodzaj (tranzystor),
typ (PMOS),
źródło (Vdd),
bramka (3),
dren (3)]) ←.

(A6) układ ([rodzaj (tranzystor),
typ (PMOS),
źródło (Vdd),
bramka (3),
dren (2)]) ←.

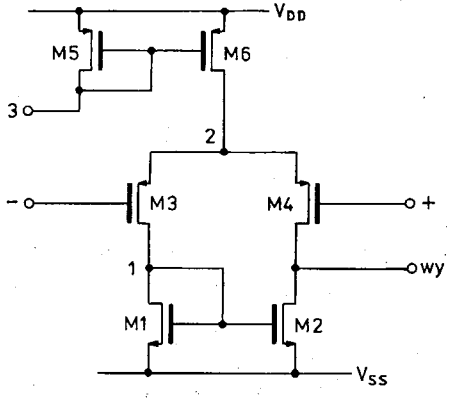

Rys. 5. Schemat stopnia różnicowego

Przebieg wnioskowania można przedstawić w postaci drzewa dwudzielnego (rys. 6). W każdej ścieżce występują na przemian węzły asercji i klauzule. W procesie budowania drzewa stosuje się strategię poszukiwania „wszerz" [2].

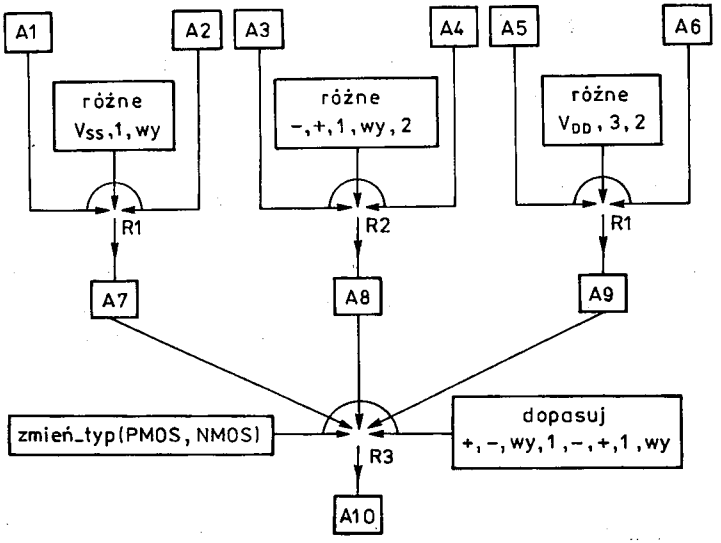

Rys. 6. Drzewo wnioskowania – połączenie gałęzi łukiem oznacza koniunkcję

Wyprowadzone w trakcie wnioskowania asercje mają postać:

(A7) układ ([rodzaj (zwierciadło_prądowe),
typ (NMOS),
we (1),
wy (wy),
zasilanie (Vss)]) ← .

(A8) układ ([rodzaj (para_różnicowa),
typ (PMOS),
we (+),
we (−),
wy (*wy*),
wy (1),
zacisk (2)]) ← .

(A9) układ ([rodzaj (zwierciadło_prądowe),
typ (PMOS),
we (3),
wy (2),
zasilanie (Vdd)]) ← .

(A10) układ ([rodzaj (stopień_różnicowy),
typ (PMOS),
we (−),
we (+),
wy (wy),
zasilanie (Vss),
zasilanie (Vdd),
zacisk (3)]) ← .

Przedstawiony przykład został zaimplementowany z niewielkimi zmianami w Prologu. Program może być łatwo rozszerzony o nowe reguły, identyfikujące pozostałe bloki konstrukcyjne wzmacniacza.

4. IMPLEMENTACJA REGUŁ IDENTYFIKACJI W PROLOGU

Przedstawiony niżej program, napisany w Turbo Prologu, jest przykładem implementacji reguł R1, R2 i R3 identyfikujących moduły wzmacniaczy CMOS. Dla poprawienia czytelności program i wydruki zostały uzupełnione polskimi literami.

```
domains
    file          = lista_tranzystorów
    specyfikacje  = specyfikacja*
    specyfikacja  = nazwa(string); rodzaj(symbol); typ(symbol);
                    we(symbol); wy(symbol),
                    źródło(symbol); bramka(symbol); dren(symbol);
                    zacisk(symbol) i zasilanie(symbol)
    lista  = symbol*
    nazwy  = string*

database
    układ(specyfikacje)
    nr_układ(integer)
    rozpoznane(nazwy)

predicates
    reguła(integer)                 różne(lista)
    zapisz_rozpoznane(nazwy)        zapisz(specyfikacje)
    należy_do(symbol, lista)        nazwa_układu(string)
    zmień_typ(symbol, symbol)       dopasuj(lista)
    czytaj_dane   czytaj            rozpoznaj(integer)

clauses
    reguła(1): -
        układ([ nazwa(T1),   rodzaj(tranzystor), Typ,
                źródło(V),   bramka(We), dren(Wy) ]),
        różne([ V, We, Wy ]),
        układ([ nazwa(T2),   rodzaj(tranzystor), Typ,
        źródło(v), bramka(We), dren(We)]).
        zapisz_rozpoznane([ T1, T2]),
        zapisz([ rodzaj(zwierciadło_prądowe),   Typ,
                we(We), wy(Wy), zasilanie(V) ]).
    reguła(2): -
        układ([ nazwa(T1),   rodzaj(tranzystor), Typ,
                źródło(W),   bramka(We1), dren(Wy1) ]),
```

```
    układ ([ nazwa T2),     rodzaj (tranzystor), Typ,
            źródło(W),      bramka (We2), dren (Wy2) ]),
    różne (W, We1, We2, Wy1, Wy2 ]),
    zapisz_rozpoznane ([T1, T2 ]),
    zapisz_rozpoznane ([T2, T1]),
    zapisz ([ rodzaj (para_różnicowa), Typ,
            we (We1), we (We2), wy (Wy1), wy (Wy2), zacisk (W) ]).

reguła (3): –
    układ ([ nazwa (U1),    rodzaj (para_różnicowa), typ (T1),
            we (I1), we (I2), wy (Wy1), wy (Wy2), zacisk (W) ]),
    układ ([ nazwa (U2), rodzaj (zwierciadło_prądowe), typ (T1),
            we (S), wy (W), zasilanie (V2) ]),
    zmień_typ ( T1, T2),
    układ ([ nazwa (U3), rodzaj (zwierciadło_prądowe),    typ (T2),
            we (We), wy (Wy), zasilanie (V1) ]).
    dopasuj ([ I1, I2, Wy1, Wy2, We1, We2, We, Wy ]),
    zapisz_rozpoznane ([U1, U2, U3]),
    zapisz ([rodzaj (stopień_różnicowy),    typ (T1),
            we (We1), we (We2), wy (Wy),
            zasilanie (V1), zasilanie (V2), zacisk (S) ]),
zapisz_rozpoznane (Układy): –rozpoznane (Układy), !, fail.
zapisz_rozpoznane (Układy): –
    write ("Układy: ", Układy), nl,
    asserta (rozpoznane (Układy)).
zapisz (Układ): –
    nazwa_układu (Nazwa),
    nl, write ("tworzą układ: ", Nazwa), nl, write (Układ), nl,
    assertz (układ ([nazwa (Nazwa) : Układ])).
różne ([ ]): –!.
różne ([W:Reszta]): –należy_do (W, Reszta), !, fail.
różne ([ _:Reszta]): –różne (Reszta).

należy_do (G:_]): –!.
należy_do (G, [_:Reszta]): –należy_do (G, Reszta).

nazwa_układu (Nazwa): –
    nr_układu (Nr),!, retract (nr_układu (_)), Nr1 = Nr+1,
    str_int (Str, Nr1), concat ("Ukł", Str, Nazwa),
    assertz (nr_układu (Nr1))
    nazwa_układu ("Ukł1"): –assertz (nr_układu (1)).

zmień_typ ("PMOS", "NMOS"): –!.
zmień_typ ("NMOS", "PMOS").
dopasuj ([I1, I2, Wy1, Wy2, I1, I2, Wy1, Wy2]): –!.
dopasuj ([I1, I2, Wy1, Wy2, I2, I1, Wy2, Wy1]).
```

```
czytaj_dane: –
    writec ("Podaj nazwę pliku z listą tranzystorów: "),
    readln (NazwaPliku),
    opeenread (lista_tranzystorów, NazwaPliku),
    readdevice (lista_tranzystorów),
    czytaj,
    closefile (lista_tranzystorów).
czytaj: –
    not (eof (lista_tranzystorów)),!,
    readln (Opis1),
    front token (Opis1, Nazwa, Opis2),
    front token (Opis2, Dren, Opis3),
    front token (Opis3, Bramka, Opis4),
    front token (Opis4, Źródło, Opis5),
    front token (Opis5, Typ, _),
    asserta (układ ([nazwa (Nazwa), rodzaj (tranzystor), typ (Typ),
                źródło (Źródło), bramka (Bramka), dren (Dren) ])),
    czytaj.
czytaj: –readdevice (keyboard).

rozpoznaj (4): –!.
rozpoznaj (Nr): –reguła (Nr),
                write ("zgodnie z reguła nr ", Nr), nl, nl, !,
                rozpoznaj (Nr).
rozpoznaj: –Nr1 = Nr + 1, rozpoznaj (Nr1).
goal  czytaj_dane, rozpoznaj (1).
```

Dane dla programu podawane są w postaci zbliżonej do formatu przyjętego w programie SPICE [7], tj. <nazwa> <dren> <bramka> <źródło> <typ>. Układ z rys. 5 będzie opisany następująco:

```
M1   1   1   Vss   NMOS
M2   wy  1   Vss   NMOS
M3   1   –   2     PMOS
M4   wy  +   2     PMOS
M5   3   3   Vdd   PMOS
M6   2   3   Vdd   PMOS
```

Wynikiem działania programu jest wydruk, który pokazuje rozpoznane moduły wzmacniacza.

```
Układy: ["M6", "M5"]
tworzą układ: Ukł1
[rodzaj ("zwierciadło_prądowe"), typ ("PMOS"),
 we ("3"), wy ("2"), zasilanie ("Vdd")]
zgodnie z regułą nr 1
```

```
Układy: ["M2", "M1"]
tworzą układ: Ukł2
[rodzaj ("zwierciadło_prądowe"), typ ("NMOS"),
 we ("1"), wy ("wy"), zasilanie ("Vss")]
zgodnie z regułą nr1

Układy: ["M4", "M3"]
Układy: ["M3", "M4"]
tworzą układ: Ukł3
[rodzaj ("para_różnicowa"), typ ("PMOS"), we ("+"), we ("–"),
 wy ("wy"), wy ("1"), zacisk ("2")]
zgodnie z regułą nr 2

Układy: ["Ukt3", "Ukł1", "Ukł2"]
tworzą układ: Ukł4
[rodzaj ("stopień_różnicowy"), typ ("PMOS"), we ("–"), we ("+"),
 wy ("wy"), zasilanie ("Vss"), zasilanie ("Vdd"), zacisk ("3")]
zgodnie z regułą nr3
```

W pełnej wersji, program zawiera 16 reguł i jest w stanie rozpoznać 72 różne wersje wzmacniacza.

PODSUMOWANIE

W drugiej części pracy przedstawiono zasadę wnioskowania wstępującego. Struktura przestrzeni poszukiwań wstępujących jest bardziej skomplikowana niż w przypadku przestrzeni poszukiwań zstępujących [9]. Co za tym idzie, przeszukiwanie tych przestrzeni jest trudniejsze.

W praktyce rzadko stosuje się do przestrzeni poszukiwań wstępujących strategie inne niż poszukiwanie wszerz [9]. Poszukiwanie wszerz polega na rozważeniu wszystkich asercji o głębokości n, zanim będzie wygenerowana jakakolwiek asercja o głębokości n+1. Głębokość asercji jest o jeden większa niż największa spośród głębokości asercji, z których ją wyprowadzono. W przedstawionym przykładzie asercje A1 – A6 mają głębokość zero (zostały podane), asercje A7 – A9 mają głębokość 1 (zostały wyprowadzone z asercji o głębokości zero). Natomiast asercja A10 ma głębokość 2. W przytoczonym programie przykładowym i w pełnej wersji programu, poszukiwanie wszerz zrealizowano przez odpowiednie ponumerowanie reguł.

Identyfikacja układów jest ważnym etapem automatycznej interpretacji wyników analizy układów [4]. Interpretacja taka nie jest praktycznie możliwa, jeżeli nie zostaną określone funkcje układu oraz modułów z których jest zbudowany.

Zainteresowanym Czytelnikom autor udostępni pełny tekst prototypowego systemu identyfikacji układów.

BIBLIOGRAFIA

1. J. L. Alty, M. J. Coombs: *Expert Systems. Concepts and Examples.* NCC Publ. 1984
2. H. Budzisz: *Przetwarzanie wiedzy o układach elektronicznych, cz. 1.* Unifikacje i reguły przetwarzania, Kwart. Elektr. i Telekom. 1991, 37, zesz. 3–4
3. H. Budzisz: Reprezentacja wiedzy o układach elektrotechnicznych, cz.1 i cz. 2, Kwart. Elektr. i Telekom. 1991, 37, zesz. 1–2, ss. 23–33
4. H. Budzisz: *Interpretacja wyników symulacji programem* SPICE *przy użyciu systemu reguł,* XII KK TOiUE, Rzeszów 1989, ss. 403–408
5. W. F. Clocksin, C. S. Mellish: *Programming in Prolog.* Springer Verlag, Berlin, Heidelberg 1984, 2–nd ed.
6. B. R. Gaines: *Induction of inference rules for expert systems.* Fuzzy Sets and Systems, 1986, vol. 18, pp. 315–328
7. PSPICE *User's Manual.* MicroSim Corp., 1986
8. D. C. Stone, J. E. Schroeder, R. H. Kaplan, A. R. Smith: *Analog* CMOS *Building Blocks for Custom and Semicustom Applications.* IEEE j.of Solid – State Circuits, vol. SC–19, No 1, Feb. 1984, pp. 55–61
9. R. Kowalski: *Logika w rozwiązywaniu zadań,* Warszawa: WNT, 1989
10. Y. P. Tsividis, P. Antognetii, eds.: *Design of* MOS VLSI *Circuits for Telecommunications.* Prentice–Hall Inc., 1985

H. BUDZISZ

KNOWLEDGE PROCESSING IN THE DOMAIN OF ELECTRONIC CIRCUITS

Part 2: Forward reasoning

Summary

Rules of inference are very general statements of the relationshipe between assumptions and conclusions forming clauses. In forward reasoning technique, discussed in this part of the paper, the complete computation cycle of inference engine corresponds to the repeated applications of the modus ponendo ponens rule. In each step of the process, conclusions are generated which in turn become new assertions within the knowledgebase. As an example illustrating the way of reasoning a problem of CMOS amplifier modules identyfication has been shown. A Prolog implementation of the inference has also been presented.

Część 3: Wnioskowanie zstępujące

W interpretacji proceduralnej klauzul hornowskich, reguła wnioskowania modus tollendo tollens jest rozumiana jako uaktywnienie procedury. Przy tej interpretacji, wnioskowanie zstępujące jest ciągiem wywołań procedur, z których każda wywołuje następne procedury. Proces jest uruchamiany przez cel początkowy, a kończy się po osiągnięciu asercji. Asercje interpretuje się jako procedury rozwiązujące cel bezpośrednio, bez redukowania go do podcelów. Jako przykład ilustrujący technikę wnioskowania zstępującego, przedstawiono problem weryfikacji projektu układu cyfrowego CMOS. Pokazano też sposób implementacji metody w Prologu.

1. WPROWADZENIE

Aby wykazać w języku klauzul, że zbiór założeń implikuje pewną konkluzję, przy zastosowaniu strategii zstępującej [2] zakładamy, że konkluzja nie jest prawdziwa i pokazujemy, że negacja konkluzji jest sprzeczna z założeniami (*reductio ad absurdum*).

Na przykład z $\neg$*stabilny(x)* oraz *stabilny(x)*←*pasywny(x)* wynika $\neg$*pasywny(x)*, czyli „jeżeli układ nie jest stabilny to znaczy, że nie jest pasywny". Klasycznym błędem logicznym jest natomiast wyciągnięcie na podstawie prawdziwości *stabilny(x)* oraz *stabilny(x)*←*pasywny(x)*, wniosku *pasywny(x)*, czyli „jeżeli układ jest stabilny to jest pasywny".

Sprowadzenie wywodu do wykazania sprzeczności jest nieco nienaturalne i dlatego wygodniej jest zastosować proceduralną interpretację wnioskowania zstępującego [8,9]

W interpretacji proceduralnej, klauzulę hornowską [2], postaci:

$$B \leftarrow A_1, \ldots, A_n, n \geqslant 0$$

utożsamia się z procedurą

$$<\text{nagłówek}> \leftarrow <\text{treść}>.$$

Nagłówkiem jest konkluzja B (cel, jaki należy osiągnąć), a treścią ciąg wywołań procedur $A_1, \ldots, A_n$ (ciąg celów pomocniczych).

Przy tej interpretacji, w rozumowaniu zstępującym, wychodzi się od celu (końcowej konluzji), sprowadza się go do celów pomocniczych itd. do chwili, gdy wszystkie cele pomocnicze zostaną osiągnięte, tj. uzgodnione z asercjami. Asercję interpretuje się jako procedurę, która rozwiązuje cel bezpośrednio, bez redukowania go do podcelów. O postępowaniu zstępującym mówi się też że jest sterowane celem (ang. goal – directed).

2. SCHEMAT WNIOSKOWANIA ZSTĘPUJĄCEGO

W każdym kroku wnioskowania zstępującego, aby osiągnąć aktualny w tym kroku cel, należy najpierw osiągnąć cele pomocnicze. W kolejnych krokach następuje więc „rozbicie" celu głównego na coraz prostsze cele pomocnicze. W wyniku takiego postępowania, tworzy się drzewo, którego przykład pokazany został na rys. 1.

Ze schematu tego wynika, że cel jaki należy osiągnąć, reprezentuje konkluzja klauzuli$_7$. W pierwszym kroku należy osiągnąć dwa cele pomocnicze wyrażone w założeniu$_{71}$ i założeniu$_{72}$. W wyniku uzgodnień z konkluzją$_2$ i konkluzją$_5$ okazuje się, że należy osiągnąć następne cele pomocnicze. Dalej proces powtarza się, aż wszystkie liście tego drzewa będą asercjami.

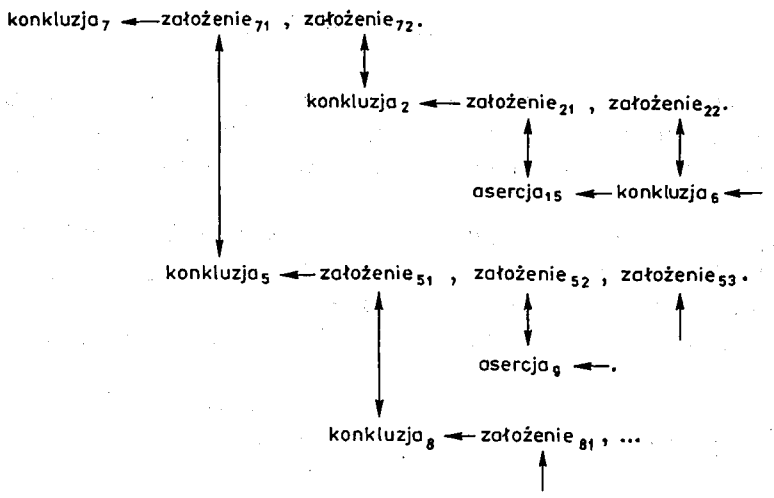

Rys. 1. Schemat wnioskowania zstępującego

3. PRZYKŁAD ZASTOSOWANIA POSTĘPOWANIA ZSTĘPUJĄCEGO DO WERYFIKACJI PROJEKTU UKŁADU CYFROWEGO

Podstawowymi elementami, które służą do realizacji układów cyfrowych w technologii CMOS, są tranzystory PMOS i CMOS (rys. 2a i 2b), które w układach cyfrowych są często w uproszczeniu traktowane jako przełączniki dwustanowe (zwarte i rozwarte).

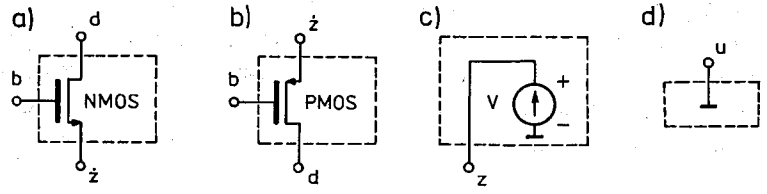

Rys. 2. Podstawowe elementy składowe do budowy układów cyfrowych w technologii CMOS: a) klucz na tranzystorze NMOS, b) klucz na tranzystorze PMOS, c) zasilanie, d) uziemienie

Przy takim modelu, właściwości tranzystorów można opisać następująco:

$$\forall b, \acute{z}, d \in \{0,1\}\ [(b=1 \rightarrow \acute{z}=d) \rightarrow \mathrm{NMOS}(b, \acute{z}, d)]$$
$$\forall b, \acute{z}, d \in \{0,1\}\ [(b=0 \rightarrow \acute{z}=d) \rightarrow \mathrm{PMOS}(b, \acute{z}, d)]$$

gdzie: stałe 0 i 1 oznaczają stany logiczne.

Pierwsze sformułowanie można odczytać następująco: jeżeli stan logiczny 1 na bramce spowoduje zwarcie źródła z drenem, to mamy do czynienia z tranzystorem NMOS. W drugim zapisie na bramce występuje stan logiczny 0. Po odpowiednich przekształceniach [3], otrzymuje się następujący zapis w języku klauzul:

(R1) NMOS $(b, \acute{z}, d) \leftarrow$ równe $(b,0)$
(R2) NMOS $(b, \acute{z}, d) \leftarrow$ równe $(\acute{z},d)$

(R3) PMOS(b, $\acute{z}$, d)←równe(b,1)
(R4) PMOS(b, $\acute{z}$, d)←równe($\acute{z}$,d)

Istotnie, tranzystor NMOS nie może być traktowany jako przełącznik tylko wtedy, gdy $b=1$, i $\acute{z} \neq d$, czyli

$$(b = 1) \wedge \neg \text{równe}(\acute{z}, d)$$

Wszystkie inne kombinacje wartości b, $\acute{z}$ i d są dopuszczalne.
Negując więc powyższe wyrażenie, otrzymuje się:

$$(b = 0) \vee \text{równe}(\acute{z}, d)$$

co odpowiada warunkom klauzul R1 i R2. Podobne rozumowanie można przeprowadzić dla tranzystora PMOS.

Dwa pozostałe elementy służące do budowy układu: zasilanie i uziemienie (rys. 2c i 2d), można opisać następująco:

(R5) zasilanie(z) ← równe(z,1)
(R6) uziemienie(u) ← równe(u,0)

Predykat równe(...) zdefiniowany jest przy pomocy asercji:

(A1) równe(0,0)←
(A2) równe(1,1)←

Stałe 0 i 1 oznaczają stany logiczne.

Rozważmy dalej jako przykład dwa proste układy cyfrowe: inwerter i bramkę NAND. Opis funkcjonalny inwertera sprowadza się do zapisu:

$$\forall\, we,wy \in \{0,1\}\ [\text{inwerter}(we,wy) \rightarrow (we \neq wy)]$$

Po odpowiednich przekształceniach zapis ten można przedstawić w postaci klauzulowej:

(R7) ← inweter(we,wy), równe(we,wy).

czyli „nieprawda, że układ jest inwerterem i stan na wejściu jest równy stanowi na wyjściu układu". Z drugiej stony topologię inwertera (rys. 3b) można opisać klauzulą

(R8) inwerter(we,wy)←zasilanie(v),
uziemienie(u),
PMOS(we,v,wy),
NMOS(we,u,wy).

Należy wykazać, że układ z rys. 3b, opisany klauzulą R8 rzeczywiście realizuje funkcję inwertera opisaną klauzulą R7. Drzewo dowodu z zastosowaniem mechanizmu wnioskowania zstępującego i strategii poszukiwania „w głąb" [2], przedstawione zostało na rys. 4.

Wychodząc z klauzuli R7 należy wykazać, że przynajmniej jedno z założeń nie jest prawdziwe. Pierwsze założenie *inwerter (we,wy)* daje się uzgodnić z konkluzją klauzuli

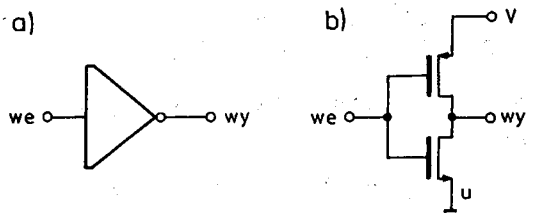

Rys. 3. Inwerter: a) symbol, b) typowa implementacja w technologii CMOS

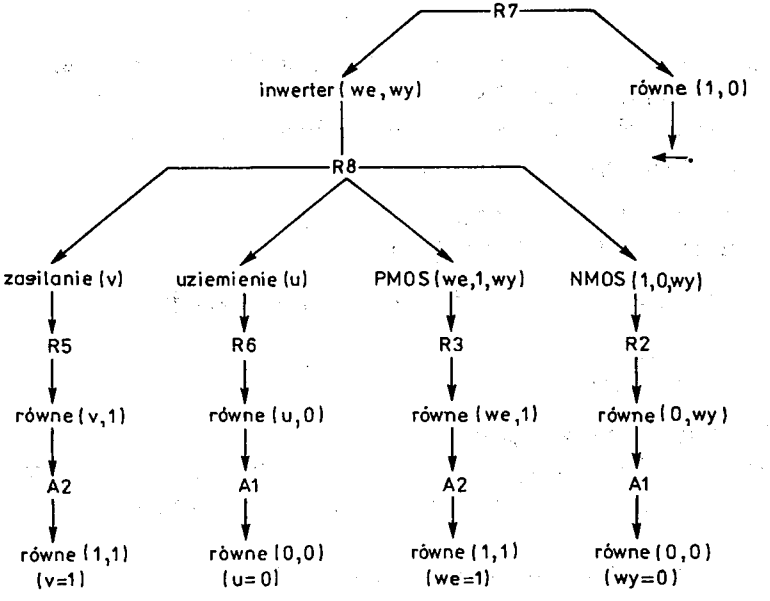

Rys. 4. Drzewo wnioskowania dowodu poprawności implementacji inwertera

R8 i zostaje rozbite na cztery podcele. W wyniku uzgodnienia predykatu *zasilanie (v)* za pośrednictwem klauzuli R5 z asercją A2, pod zmienną v podstawiona zostaje wartość logiczna 1. Z kolei uzgodnienie predykatu *uziemienie (u)* poprzez R6 z asercją A1, prowadzi do podstawienia $\{u=0\}$. Ukonkretniony predykat PMOS(*we*,1,*wy*), poprzez R3 daje się uzgodnić z A2, w wyniku czego otrzymuje się podstawienie $\{we=1\}$. W końcu uzgodnienie predykatu NMOS(1,0,*wy*) prowadzi do podstawienia $\{wy=0\}$. Ponieważ wszystkie założenia klauzuli R8 udało się uzgodnić, musimy przyjąć, że ukonkretniony predykat *inwerter*(1,0) jest prawdziwy. Jednak drugie założenie R8, które w wyniku ukonkretnienia przyjmuje postać *równe* (1,0), nie daje się uzgodnić z żadną asercją, a więc ma wartość *fałsz*. Ostatecznie prawdziwe okazuje się zaprzeczenie wyrażone przez klauzulę R7.

Dla kompletności dowodu należałoby zbudować drugą wersję drzewa dowodowego, w którym predykat PMOS(*we*,1,*wy*) zostaje uzgodniony z konkluzją klauzuli R4.

Przechodząc do drugiego przykładu, opis funkcjonalny bramki NAND można przedstawić następująco:

$$\forall\, we_1, we_2, wy \in \{0,1\}$$
$$\text{NAND}(we_1, we_2, wy) \rightarrow [(we=1) \wedge (we_2=1)] \rightarrow (wy=0)] \wedge$$
$$[(we_1=0) \vee (we_2=0)] \rightarrow (wy=1)]$$

co daje się przekształcić do postaci klauzulowej:

(R9a) ← NAND(we_1, we_2, wy),
równe(we_1, 0),
równe(wy, 0).

(R9b) ← NAND(we_1, we_2, wy),
równe(we_2, 0),
równe(wy, 0).

(R9c) ← NAND(we_1, we_2, wy),
równe(we_1, 1),
równe(we_2, 1),
równe(wy, 1).

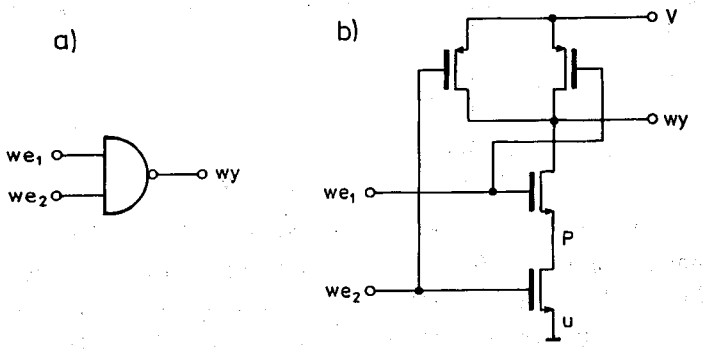

Rys. 5. Bramka NAND: a) symbol, b) typowa implementacja w technologii CMOS

Z kolei opis topologiczny (rys. 5) prowadzi do klauzuli:

(R10) NAND(we_1, we_2, wy)← zasilanie(v),
uziemienie(u),
PMOS(we_1, v, wy),
PMOS(we_2, v, wy),
NMOS(we_1, p, wy),
NMOS(we_2, u, p).

Weryfikacja takiego układu jest już bardziej złożona. Jak łatwo zauważyć predykaty *zasilanie (u)* i *uziemienie (u)* zawsze prowadzą do podstawień $\{v=1, u=0\}$. Regułę (R10) można więc uprościć do postaci:

(R10') NAND(we_1, we_2, wy)←PMOS(we_1, 1, wy),
PMOS(we_2, 1, wy),
NMOS(we_1, p, wy),
NMOS(we_2, 0, p).

Proces uzgadniania założeń reguły (R10') z regułami (R1)–(R6) oraz asercjami (A1) i (A2) prowadzi do podstawień:

(P1) $\{ we_1 = 0, we_2 = 0, wy = 1 \}$
(P2) $\{ we_1 = 0, we_2 = 1, wy = 1 \}$
(P3) $\{ we_1 = 1, we_2 = 0, wy = 1 \}$
(P4) $\{ we_1 = 1, we_2 = 1, wy = 0 \}$

Rys. 6 przedstawia szczegółowo proces uzgadniania prowadzący do podstawień (P4).

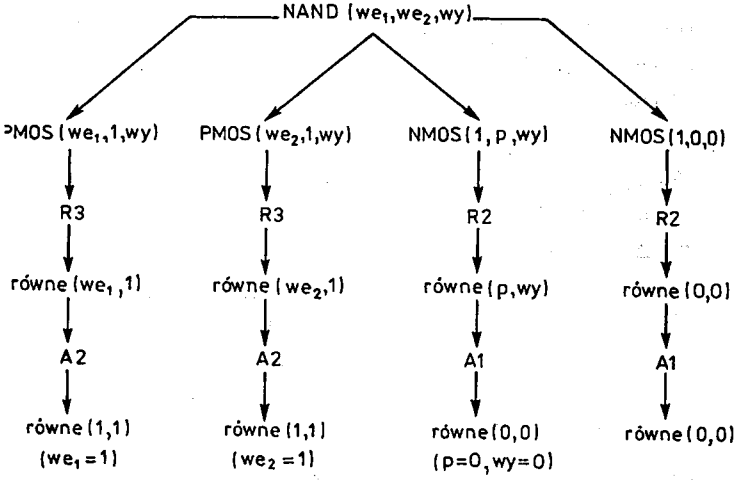

Rys. 6. Przykład uzgadniania zmiennych predykatu NAND

Podstawiając kolejno wartości zmiennych wygenerowane przez predykat NAND do reguł (R9a), (R9b) i (R9c) można stwierdzić, że wszystkie zaprzeczenia są prawdziwe (tzn. przynajmniej jedno założenie w każdej klauzuli nie jest prawdziwe). Warto zauważyć, że podstawiena (P1)–(P4) przedstawiają definicję bramki NAND, a sekwencje predykatów równe(...) w regułach (R9a)–(R9c) określają stany zabronione. Jeżeli stany dopuszczalne i zabronione są sprzeczne, to projekt jest poprawny.

4. IMPLEMENTACJA REGUŁ WERYFIKACJI W PROLOGU

Przedstawiony niżej program napisany w Turbo Prologu jest przykładem implementacji reguł weryfikacji omówionych przykładów. Dla poprawienia czytelności, tekst programu uzupełniono polskimi literami.

```
predicates
  _PMOS (symbol, symbol, symbol)
  _NMOS (symbol, symbol, symbol)
  zasilanie (symbol)
  uziemienie (symbol)
  inwerter (symbol, symbol)
```

```
    _NAND (symbol, symbol, symbol)
    równe (symbol, symbol)
clauses
    równe (X, X).
    _NMOS (B, _, _): – równe (B, "0").
    _NMOS (_, Z, D): – równe (Z, D).
    _PMOS (B, _, _): – równe (B, "1").
    _PMOS (_, Z, D): – równe (Z, D).
    zasilanie (Z): – równe (Z, "1").
    uziemienie (U): – równe (U, "0").
    inwerter (We, Wy): – zasilanie (V), uziemienie (U),
                         _PMOS (We, V, Wy), _NMOS (We, U, Wy).
_NAND (We1, We2, Wy): – zasilanie (V), uziemienie (U),
                        _PMOS (We2, V, Wy), _PMOS (We1, V, Wy),
                        _NMOS (We1, P, Wy), _NMOS (We2, U, P).
```

Odpowiedzią ne cel sformułowany w klauzuli (R7) jest *fałsz*, zgodnie z przedstawionym poprzednio wywodem (teksty przedstawione dalej w ramkach, zostały skopiowane z ekranu).

```
Goal: inwerter (We, Wy), równe (We, Wy)
False
```

Predykat *inwerter* można też wykorzystać w inny sposób. Na pytanie: "jakie są dopuszczalne stany na wejściu i wyjściu inwertera?", odpowiedź jest następująca:

```
Goal: inwerter (We, Wy)
We=1, Wy=0
We=0, Wy=1
2 Solutions
```

Odpowiedzią na pytanie: "czy prawdą jest, że inwerter ma stan na wejściu 1 i stan 0 na wyjściu?", jest stwierdzenie: *prawda*.

```
Goal: inwerter ("1", "0")
True
```

Podobnie dla bramki NAND. Na pytanie: "jakie są dopuszczalne stany na obu wejściach i wyjściu bramki NAND?", odpowiedzią jest wykaz czterech rozwiązań.

```
Goal: _NAND (We1, We2, Wy)
We1,=1,   We2=1,   Wy=0
We1=0,    We2=1,   Wy=1
We1=1,    We2=0,   Wy=1
We1=0,    We2=0,   Wy=1
4 Solutions
```

Program może być łatwo rozszerzony na układy bardziej złożone. Rozszerzoną wersję programu zawierają m.in. opis bramki NOR i pełnego sumatora jednobitowego, autor udostępni zainteresowanym Czytelnikom.

PODSUMOWANIE

We wnioskowaniu zstępującym, przestrzeń poszukiwań przybiera postać drzewa koniunkcyjno-alternatywnego (ang. and-or tree) [8]. Do przeszukiwania takiego drzewa stosuje się zwykle technikę poszukiwania "w głąb". Jeżeli poszukiwanie zakończy się niepowodzeniem, następuje nawrót w kierunku korzenia do najbliższego węzła alternatywnego, w celu zbadania dalszych możliwości osiągnięcia postawionych lub wyprowadzonych celów.

Przy rozwiązywaniu niektórych problemów korzystne jest stosowanie obu sposobów wnioskowania — zstępującego i wstępującego [9]. Jest to możliwe wówczas, gdy dane są zarówno założenia początkowe jak i końcowy cel, a poszukuje się drogi jaką należy dojść do celu. Taka dwukierunkowa strategia poszukiwania daje w efekcie zmniejszenie przestrzeni poszukiwań.

BIBLIOGRAFIA

1. J. L. A l t y, M. J. C o o m b s: *Expert Systems.* Concepts and Examples, NCC Publ. 1984
2. H. B u d z i s z: *Przetwarzanie wiedzy o układach elektronicznych, cz. 1. Unifikacje i reguły przetwarzania.* Kwart. Elektr. i Telekom. 1991, 37, z. 3–4
3. H. B u d z i s z: *Reprezentacja wiedzy o układach elektronicznych,* cz. 1 i cz. 2, Kwart. Elektr. i Telekom. 1991, 37, z. 3–4
4. H. B u d z i s z: *Weryfikacja projektu układu cyfrowego oparta na systemie reguł* (XIII KK TOiUE, Bielsko-Biała 1990, ss.193–198)
5. W. F. C l o c k s i n, C. S. M e l l i s h: *Programming in Prolog.* Springer Verlag, Berlin, Heidelberg, 1984, 2-nd ed.
6. M. G o r d o n: *Why higher–order logic is a good formalism for specifying and verifying hardware,* Proc. of 1985 Edinburgh Workshop on VLSI, pp. 153–177
7. C. L o b, R. S p i c k e l m i e r, A. R. N e w t o n: *Circuit Verification Using Rule-Based Expert Systems.* Proc. IS CAS'85, pp. 881–884
8. R. K o w a l s k i: *Logika w rozwiązywaniu zadań.* Warszawa: WNT, 1989
9. R. K o w a l s k i: *Algorithm = Logic + Control.* Communication of the ACM, July 1979, vol. 22, No 1, pp. 424–436

H. BUDZISZ

KNOWLEDGE PROCESSING IN THE DOMAIN OF ELECTRONIC CIRCUITS
Part 3: Backward reasoning

Summary

In the procedural interpretation of Horn caluses, modus tollendo tollens rule of reasoning is interpreted as procedure invocation. In top-down problem-solving, we reason backwards from the conclusions, repeatedly reducing goals to subgoals until eventually all subgoals are solved directly by the original assertions. The process of reasoning is activated by the initial goal statement. A rule-based verification of digital CMOS circuits design has been chosen to exemplify backward reasoning. Prolog implementation has also been shown.

KWARTALNIK ELEKTRONIKI I TELEKOMUNIKACJI, 1991, 37, Z. 3—4, ss. 423—434

621.3.069:681.31

Reprezentacja wiedzy o układach elektronicznych Część II. Sieci semantyczne i reprezentacja ramowa

HENRYK BUDZISZ

Instytut Elektroniki, Wyższa Szkoła Inżynierska w Koszalinie

Otrzymano 1990.07.05

Autoryzowano do druku 1991.01.15

W pierwszej części pracy przedstawiono zastosowanie języka klauzul do reprezentacji wiedzy o układach elektronicznych [1]. Jest to reprezentacja podstawowa na której oparte są struktury tworzące sieci powiązań między obiektami. Sieć semantyczna jest grafem reprezentującym związki między obiektami. Związki te tworzą często struktury hierarchiczne, dla których projektuje się mechanizmy dziedziczenia właściwości, dostępu do wartości domyślnych i do procedur obliczeniowych. Obiekty stereotypowe, łączące elementy lub układy z ich właściwościami, tworzą struktury ramowe. Struktury te są również organizowane w sieci semantyczne.

1. SIECI SEMANTYCZNE

Zależności (asercje) dwuargumentowe [1] przedstawia się często jako graf skierowany, nazywany siecią semantyczną [2,3,7,8]. Węzły grafu reprezentują obiekty, a krawędzie związki między nimi. Rys. 1 przedstawia sieć semantyczną dla przykładu opisu inwertera [1].

Taka graficzna reprezentacja jest dużym ułatwieniem w projektowaniu i przy modyfikacjach opisu, gdyż uwidacznia strukturę powiązań pomiędzy obiektami. Sieć semantyczna służy często do zapisu hierarchicznych powiązań między obiektami. Powiązania te zapisuje się zwykle przy pomocy predykatów *klasa* lub *jest_to*. Tworzy się w ten sposób strukturę drzewiastą (rys. 2).

Przez analogię do drzewa genealogicznego, używa się tu określeń „ojciec" i „dziecko" („przodek" i „potomek"). Tak więc na rys. 2, obiekt *układ_nieliniowy* jest „ojcem" obiektów *modulator* i *detektor* oraz „dziadkiem" modulatorów *FM* i *AM*. Każdy obiekt lub klasa obiektów mają zwykle pewne określone cechy. Powiązania między obiektami i ich własnościami tworzą złożoną sieć semantyczną. Przykład takiej sieci przedstawiony jest na rys. 3. Zawiera ona dwa drzewa hierarchiczne (układów i sygnałów) oraz powiązania między nimi, a także opis niektórych właściwości obiektów.

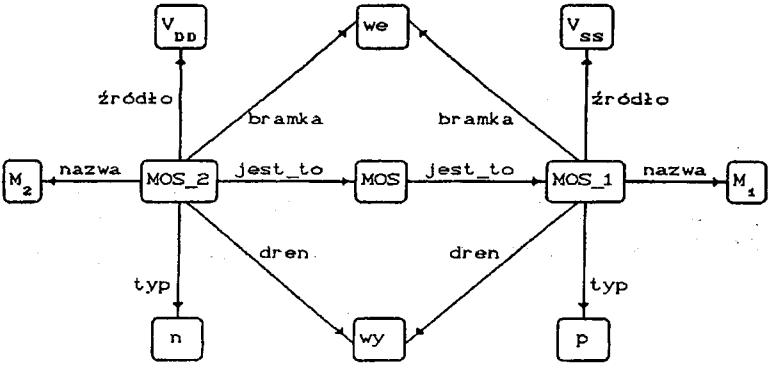

Rys. 1. Sieć semantyczna opisu inwertera

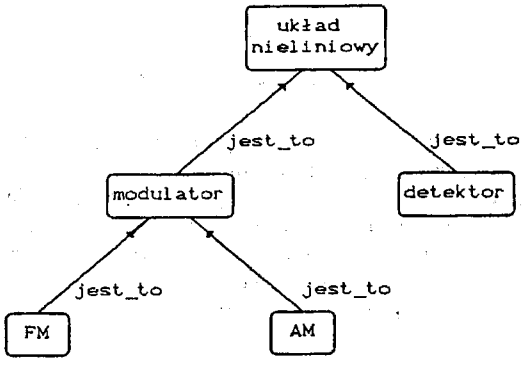

Rys. 2. Przykład drzewa hierarchicznego

Jest to już więc gotowa struktura, dla której łatwo sporządzić bazę wiedzy. Poniżej przedstawiono jako przykład fragment takiej bazy.

właściwość (układ_elektroniczny, we, sygnał_elektryczny) ←.
właściwość (układ_elektroniczny, wy, sygnał_elektryczny) ←.
jest_to (układ_analogowy, układ_elektroniczny) ←.
właściwość (układ_analogowy, we, sygnał_ciągły) ←.
właściwość (układ_analogowy, wy, sygnał_ciągły) ←.
jest_to (układ_liniowy, układ_analogowy) ←.
jest_to (układ_nieliniowy, układ_analogowy) ←.
właściwość (układ_liniowy, spełnia, zasada_superpozycji) ←.
← właściwość (układ_nieliniowy, spełnia, zasada_superpozycji).
jest_to (filtr, układ_liniowy) ←.
właściwość (filtr, we, sygnał_sinusoidalny) ←.
właściwość (filtr, wy, sygnał_sinusoidalny) ←.
jest_to (wzmacniacz, układ_liniowy) ←.
jest_to (detektor, układ_nieliniowy) ←.
. . . . . .

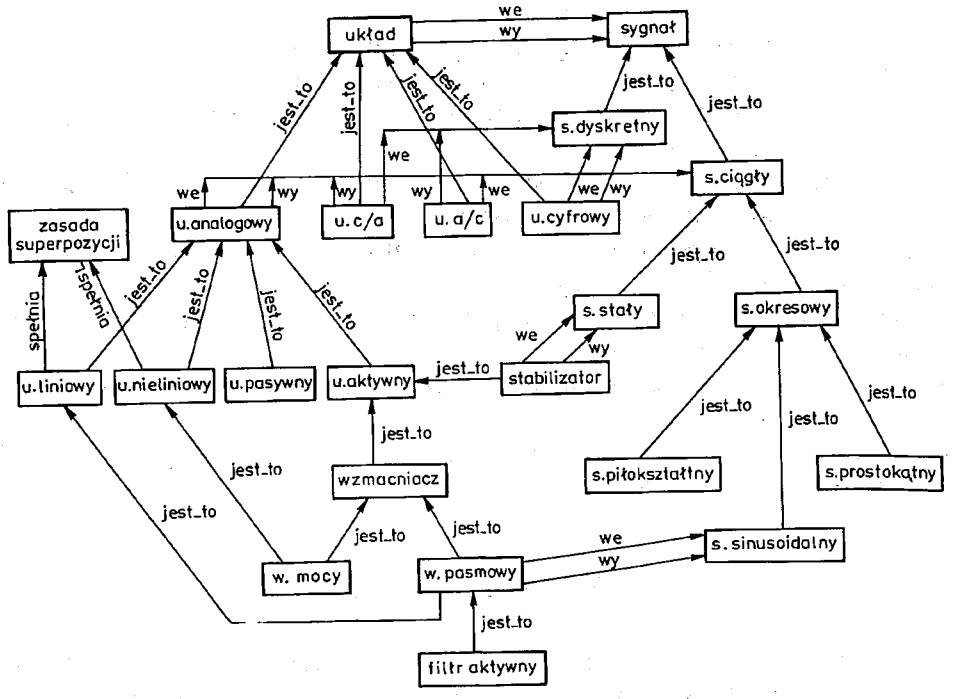

Rys. 3. Przykład hierarchicznej sieci semantycznej

Do opisu właściwości użyto predykatu trójargumentowego, który łączy różne właściwości. Umożliwia to tworzenie opisu wielu różnych cech bez potrzeby powiększania liczby predykatów. Duża liczba predykatów o różnych nazwach, utrudnia budowę mechanizmów obsługi sieci. Takie scalające predykaty można oznaczyć na rysunku specjalnym symbolem (rys. 4).

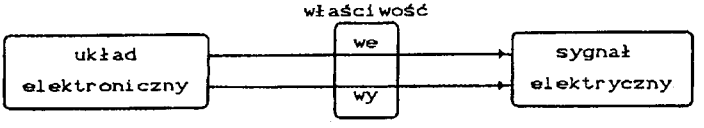

Rys. 4. Oznaczenie graficzne predykatu scalającego

Przedstawiony przykład uwypukla wspomniane już dwie ważne w praktyce cechy – dużą elastyczność przy modyfikacjach bazy oraz rozwlekłość opisu. Przedstawiony sposób zapisu sieci semantycznej jest tylko jednym z kilku możliwych [6]. Do obsługi sieci hierarchicznej stosuje się zwykle mechanizmy [7,8], które umożliwiają między innymi:

- dziedziczenie właściwości po przodkach i przekazywanie ich potomstwu,
- korzystanie z właściwości domyślnych,
- korzystanie z procedur obliczeniowych,

– określenie właściwości uzależnione od kontekstu.

Mechanizmy te korespondują ze sposobem rozumowania człowieka. Na przykład określenie *„sumator szeregowy"* kojarzy się z właściwościami:

– przetwarza sygnały cyfrowe, bo wszystkie układy cyfrowe mają takie właściwości (własność odziedziczona),

– realizuje przeniesienie, bo wszystkie sumatory tak robią (własność odziedziczona, ale z innej klasy układów niż poprzednia).

– jest taktowany zegarem, bo większość sumatorów jest realizowana jako układy synchroniczne (własność domyślna),

– jest 8-bitowy, bo sumatory szeregowe 16 i 32-bitowe są rzadko stosowane w praktyce (własność domyślna),

– działanie jest oparte na algorytmie dodawania binarnego (procedura obliczeniowa).

Inne też będzie rozumienie określenia „sumator", jeśli zostanie użyte w kontekście wiążącym go z układami analogowymi.

2. STRUKTURY RAMOWE

Obiekt prosty, wraz z właściwościami, które uznaje się za jego nieodłączne atrybuty, tworzy obiekt złożony, często nazywany obiektem stereotypowym [7,8]. Do reprezentacji obiektu stereotypowego stosuje się strukturę składającą się z węzła reprezentującego obiekt prosty oraz pewnej liczby nazwanych pól* [4,7,8]. Struktura taka, schematycznie przedstawiona na rys. 5, nazywana jest ramą (ang. frame).

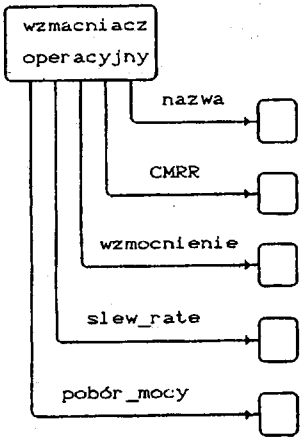

Rys. 5. Przykład reprezentacji ramowej

* określenie pole (termin ang. slot), przyjęto ze względu na duże podobieństwo struktury ramowej do rekordu.

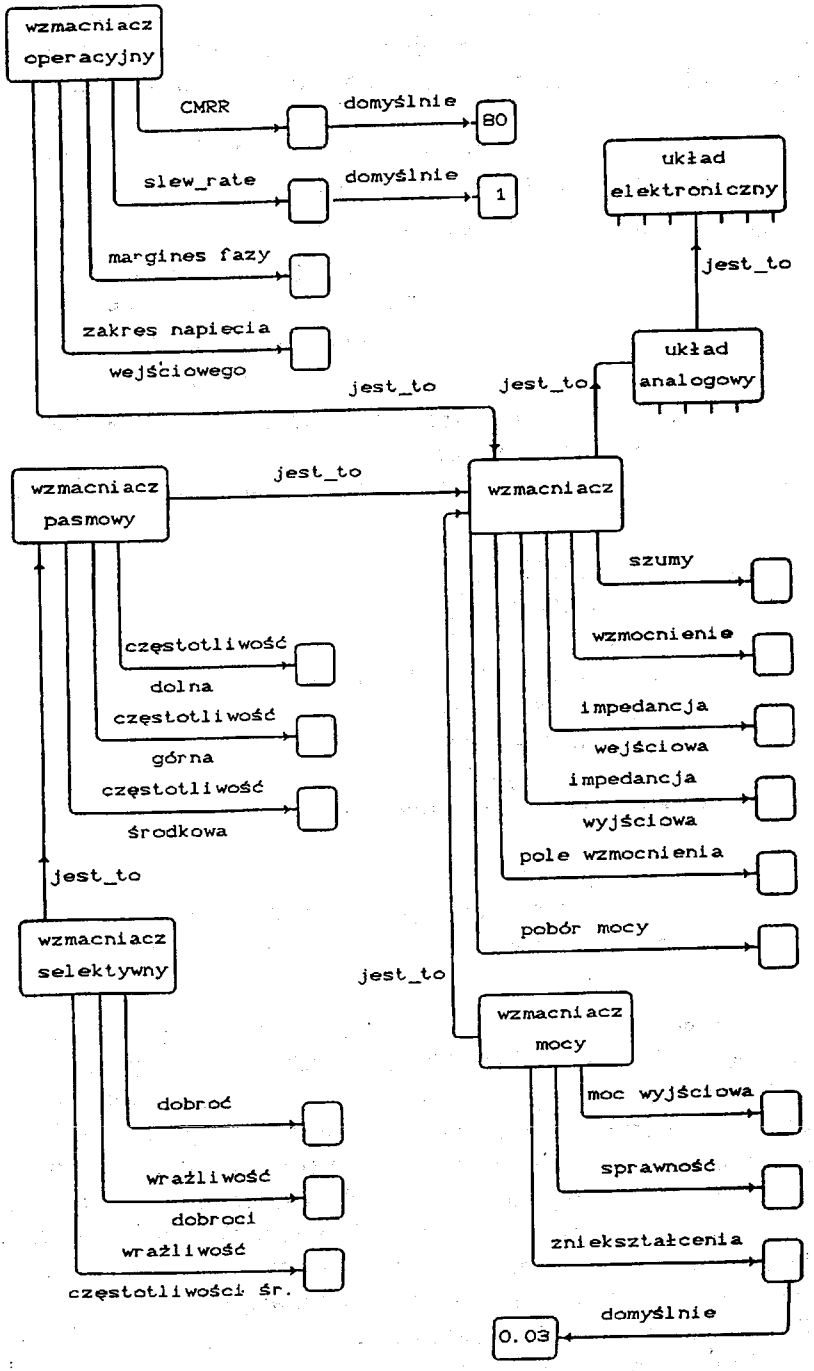

Rys. 6. Przykład sieci łączącej ramy

Podczas definiowania struktury ramowej, część pól jest zwykle obiektami pustymi. Wypełnianie tych pól następuje w trakcie przetwarzania wiedzy. Operacja ta nazywana jest konkretyzacją ramy, a wielkość wypełniająca – wypełniaczem (ang. filler). Stąd w literaturze angielskojęzycznej można też spotkać się z określeniem *slot-and-filler representation.*

Wygodnym sposobem zapisu struktury ramowej w języku klauzul (również w Prologu) jest predykat z termami w postaci list [6], np:

```
układ(wzmacniacz_operacyjny, [wzmocnienie([?]),
                              CMRR([?, domyślnie, 80]),
                              slew_rate([?, domyślnie, 10]),
                              pobór_mocy([?]) ←.
```

Symbol „?" przyjęto jako oznaczenie wartości nieokreślonej.

Ramy nie występują zwykle jako struktury samodzielne, lecz tworzą sieć semantyczną (najczęściej drzewo hierarchiczne – rys. 6).

Zapis sieci ram w języku klauzul, jest podobny do zapisu zwykłej sieci semantycznej, np.:

```
układ(wzmacniacz, [jest_to(układ_analogowy),
                   wzmocnienie([?]),
                   szumy([?]),
                   impedancja_wejściowa([?]),
                   impedancja_wyjściowa([?]),
                   pole_wzmocnienia([?]),
                   pobór_mocy([?])]) ←.
układ(wzmacniacz_mocy, [jest_to(wzmacniacz),
                        moc_wyjściowa([?]),
                        sprawność([?]),
                        zniekształcenia([?, domyślnie, 0.03])]) ←.
układ(wzmacniacz_pasmowy, [jest_to(wzmacniacz), ...]) ←.
    . . . . . .
```

Podobnie jak w zwykłej sieci semantycznej, ramy mogą zawierać wartości domyślne i wskaźniki do procedur obliczeniowych. Konstruuje się też dla nich mechanizm dziedziczenia. Jako przykład niech posłuży poszukiwanie w sieci hierarchicznej podobnej do przedstawionej na rys. 6, wartości parametru *p* dla układu *u*. Przeszukiwanie struktur drzewiastych najwygodniej przeprowadza się przy zastosowaniu rekursji. Warunkiem ograniczającym głębokość rekursji będzie założenie, że rama o nazwie *układ_elektroniczny* jest przodkiem wszystkich pozostałych obiektów w sieci. Algorytm poszukiwania może być następujący:

1. Aktualnie rozpatrywaną ramą jest rama o nazwie *u*.
2. Jeżeli aktualną ramą jest *układ_elektroniczny*, to parametr *p* nie jest stosowany do opisu układu *u* – koniec poszukiwań.
3. Jeżeli parametr *p* znajduje się na liście parametrów aktualnej ramy, to poszukiwana wartość została odnaleziona – koniec poszukiwań.

4. Znajdź przodka aktualnej ramy na podstawie właściwości *jest_to* i uczyń go nową aktualną ramą – wróć do kroku 2.

W dodatku zamieszczono przykład implementacji w Prologu sieci ram oraz mechanizm dostępu do wartości parametrów, a także przykłady testujące.

Ramy stanowią pewien szkielet, według którego można rozpoznawać lub wybierać obiekty. Ramy ukonkretnione stoją najniżej w hierarchii – są liśćmi drzewa hierarchicznego. Ukonkretnienie ramy można interpretować jako przejście od obiektu stereotypowego do obiektu rzeczywistego. Przykładem konkretyzacji ramy *wzmacniacz_operacyjny* może być zapis:

```
układ (μA709A, [jest_to (wzmacniacz_operacyjny),
                wzmocnienie ([25000]),
                pole_wzmocnienia ([5E6]),
                pobór_mocy ([0.075]),
                impedancja_wejściowa ([7E5]),
                CMRR ([80]),
                slew_rate ([0.3]) ]) ←.
```

Wypełnione pola „przesłaniają" (patrz: dodatek) te same pola występujące u przodków. Pozostałe pola, odziedziczone po przodkach nadal obowiązują dla ramy μA709A, mimo że są puste. Mogą zostać wypełnione w trakcie dalszej konkretyzacji.

PODSUMOWANIE

W wielu opracowaniach m.in. [3,7,8,9], opis metod reprezentacji wiedzy ogranicza się do schematów graficznych. Na łamach artykułów prowadzone są dyskusje na temat deklaratywnej lub proceduralnej postaci reprezentacji. Dodatkowe zamieszanie wprowadza mnogość terminów używanych do określenia tych samych pojęć. Prof. R. Kowalski skomentował tę sytuację lapidarnym stwierdzeniem [9]:

„There is only one language suitable for representing information – whether declarative or procedural – and that is first-order logic"

Kierując się tą myślą, w pracy przedstawiono kilka powszechnie stosowanych metod reprezentacji wiedzy, sprowadzając ich opis do zapisu w języku klauzul [5]. Umożliwia to ich późniejszą łatwą implementację w Prologu lub innym języku programowania logicznego. Prezentacja oparta została na przykładach zastosowań do opisu układów elektronicznych.

Czynione są próby opracowania uniwersalnych systemów reprezentacji i przetwarzania wiedzy. Nie znalazły one jednak szerszego zastosowania w praktyce, ponieważ każda dziedzina zastosowań ma swoją własną specyfikę w tym zakresie.

DODATEK

Przedstawiony niżej program jest przykładem implementacji w Prologu (Turbo Prolog wer. 1.1) hierarchicznej sieci ram podobnej do przedstawionej na rys. 6 oraz

mechanizmu dostępu do wartości parametrów z zastosowaniem dziedziczenia. Dla poprawy czytelności, tekst programu został przedstawiony z użyciem polskich liter, które w oryginale oczywiście nie występują.

Sekcja *predicates* zawiera deklaracje predykatów, a sekcja *domains* deklaracje dziedzin ich argumentów. Podstawową częścią programu jest sekcja *clauses* zawierająca definicje klauzul.

Asercje *układ* służą do opisu hierarchicznej sieci ram. Zapis jest podobny do reprezentacji ram w języku klauzul (pkt. 2). Funktor *ma* służy do zapisu właściwości układu i został wprowadzony w celu ominięcia ograniczeń występujących w Turbo Prologu.

Algorytm poszukiwania wartości parametrów zapisany został przy pomocy predykatu *znajdź_wartość*, zawierającego wywołanie rekursywne. Do jego definicji użyto predykatów pomocniczych *należy_do* i *drukuj*.

```
domains
    parametry = parametr*
    parametr  = jest_to(symbol); ma(lista)
    lista     = symbol*

predicates
    układ(symbol, parametry)
    znajdź_wartość(symbol, symbol);
    należy_do(parametr, parametry)
    drukuj(symbol, lista)

clauses
/*** definicja sieci ram opisujących układy elektroniczne ***/
    układ(układ_elektroniczny, []).
    układ(układ_analogowy,
          [jest_to(układ_elektroniczny),
          ma([wejście, sygnał_ciągły]),
          ma([wyjście, sygnał_ciągły])]).
    układ(wzmacniacz,
          [jest_to(układ_analogowy),
          ma([szumy, "?"]),
          ma([wzmocnienie, ">1"]),
          ma([impedancja_wejściowa, "?", domyślnie, duża]),
          ma([impedancja_wyjściowa, "?", domyślnie, mała]),
          ma([pole_wzmocnienia, "?"]),
          ma([pobór_mocy, "?"])]).
    układ(wzmacniacz_operacyjny,
          [jest_to wzmacniacz),
          ma(["CMRR", "?", domyślnie, "80"]),
          ma([slew_rate, "?", domyślnie, "1"]),
          ma([margines_fazy, "?"]),
```

```
                    ma([zakres_napięcia_wejściowego, "?"])]).
            układ(miA709A,
                    [jest_to(wzmacniacz_operacyjny),
                    ma([wzmocnienie, "25000"]),
                    ma([pole_wzmocnienia, "5E6"]),
                    ma([slew_rate, "0.3"])]).
/*** mechanizm odszukiwania wartości parametrów ***/
znajdź_wartość(układ_elektroniczny, Parametr): -
    write("Parametr: ", Parametr),
    write(", nie jest stosowany do opisu tego układu"), nl, !.
znajdź_wartość(Nazwa_układu, Parametr): -
    układ(Nazwa_układu, Parametry),
    należy_do(ma([Parametr : Wartość]), Parametry), !,
    drukuj(Parametr, Wartość).
znajdź_wartość(Nazwa_układu, Parametr): -
    układ(Nazwa_układu, Parametry),
    należy_do(jest_to(Przodek), Parametry),
    znajdź_wartość(Przodek, Parametr).
należy_do(Parametr, [Parametr _]): -!.
należy_do(Parametr, [_: Parametry]): -
    należy_do(Parametr, Parametry).
drukuj(Parametr, [„?", domyślnie, Wartość]): -
    write(„Wartość parametru: ", Parametr),
    write(", nie została określona"), nl,
    write(      Wartość domyślna: ", Wartość), nl, !.
drukuj(Parametr, [„?" _]): -
    write(„Wartość parametru: ", Parametr),
    write(", nie została określona"), nl, !.
drukuj(Parametr, [Wartość _]): -
    write(„Parametr: ", Parametr, ", ma wartość: ", Wartość),
    nl.
```

Program został przetestowany na kilku przykładach. Tekst ujęty w ramki został skopiowany z ekranu.

Test 1:

```
Goal: znajdź_wartość(miA709A, wzmocnienie)
Parametr: wzmocnienie, ma wartość: 25000
```

W tym przykładzie wartość parametru *wzmocnienie*, została znaleziona bezpośrednio na liście parametrów ramy *miA709A*. Pole *wzmocnienie* przesłoniło takie samo pole w ramie *wzmacniacz*.

Test 2:

```
Goal: znajdź_wartość(miA709A, „CMRR")
Wartość parametru: CMRR, nie została określona
      Wartość domyślna: 80
```

Test 3:

```
Goal: znajdź_wartość(miA709A, impedancja_wejściowa)
Wartość parametru: impedancja_wejściowa, nie została
określona
      Wartość domyślna: duża
```

W tych dwóch przykładach znalezione zostały wartości domyślne odziedziczone po przodkach. W następnym przykładzie, odziedziczona zostanie wartość pola *wzmocnienie,* która o ile nie zostanie przesłonięta, obowiązuje dla wszystkich wzmacniaczy.

Test 4:

```
Goal: znajdź_wartość(wzmacniacz_operacyjny, wzmocnienie)
Parametr: wzmocnienie, ma wartość: >1
```

Ostatni przykład dotyczy parametru *dobroć,* który nie jest stosowany do opisu wzmacniacza operacyjnego, ani jego przodków.

Test 5:

```
Goal: znajdź_wartość(wzmacniacz_operacyjny, dobroć)
Parametr: dobroć, nie jest stosowany do opisu tego układu
```

PODZIĘKOWANIE

Autor dziękuje prof. M. Białko i prof. A. Guzińskiemu z Wydziału Elektroniki Politechniki Gdańskiej za uważne przeczytanie całości i uwagi, które pozwoliły na wprowadzenie istotnych ulepszeń w tekście.

BIBLIOGRAFIA

1. H. Budzisz: *Reprezentacja wiedzy o układach elektronicznych,* Cz. I, Kwart. El. i Tel. 1990, 36, z. 1–2, ss 23–33
2. H. Budzisz, K. Wawryn, A. Guziński: *Systemy ekspertowe — nowe podejście do automatyzacji projektowania,* IX KK TOiUE, Wrocław 1986, ss. 17–28
3. N. Finder (ed): *Associative networks — the representation and use of knowledge in computers.* Academic Press, New York, 1979

4. P. G a ł k a, M. B i a ł k o: *Przetwarzanie wiedzy o układach elektronicznych reprezentowanej w postaci ram w języku Turbo Prolog.* XI KK TOiUE, Łódź 1988, ss. 298 – 303
5. R. K o w a l s k i: *Logika w rozwiązywaniu zadań.* WNT 1989
6. N. S. L e e: *Programming with P-Shell.* IEEE Expert, Summer 1986, pp. 50 – 63
7. N. J. N i l s s o n: *Principles of Artificial Intelligence.* Tioga Publishing Co., 1980
8. P. H. W i n s t o n: *Artificial Intelligence.* Addison-Wesley Publ. Co., 1984
9. R. J. B r a c h m a n, B. C. S m i r h: Eds., SIGART Newsletter: *Special Issue on Knowledge Representation,* vol. 70, Feb. 1980

H. BUDZISZ

KNOWLEDGE REPRESENTATION IN THE DOMAIN OF ELECTRONIC CIRCUITS

Part II: Semantic networks and frame representation

S u m m a r y

In the first part of the paper [1] there were discussed methods of knowledge representation in the clause language. This is the basic representation concept which enables development of associative network structures. Semantic net is a directed graph which identifies objects with nodes and relations between them with arcs. These relations are often used to build hierarchical structures provided with some specific mechanisms like inheritance of properties, acces to default values and object-oriented computational procedures. A collection of semantic net nodes and slots that together describe a stereotyped object, named a frame, have been used to determine relations between circuits and their properties.

KWARTALNIK ELEKTRONIKI I TELEKOMUNIKACJI, 1991, 37, Z. 3–4, ss. 435–447

621.315.592:546.3/.9

Numerical analysis of influence of external cooling conditions and assembling gaps on thermal behaviour of integrated circuits

STANISŁAW KUCYPERA, JANUSZ SKOREK

Instytut Techniki Cieplnej, Politechnika Śląska, Gliwice

Received 1990.06.22

Authorized 1991.03.14

A mathematical model of temperature distribution within integrated circuits has been worked out on the base of discrete control volume method. Control volume approach to the problem of heat transfer allows to consider geometry of semiconductor device, multilayer structure, nonlinear properties of materials, time dependent heat generation and other factors which can have a significant influence on thermal behaviour of working device. Experimental and numerical results have been compared to verify the accuracy of the mathematical model. The analysis of influence of fitting defects and external cooling conditions on the temperature of active zone of integrated circuit has been carrying out. Some numerical examples are presented.

1. INTRODUCTION

Temperature of active zone of working semiconductor devices, including integrated circuits, is one of the most important factor determining reliability of electronic devices due to the fact that reliability of complex electronic device is determined by the reliability of unique semiconductor element.

Thermal analysis of semiconductor devices is difficult because of complex external and internal geometry, conditions of heat transfer and nonlinear properties of materials. To determine temperature distribution and heat flow within semiconductor device both experimental and theoretical methods are developed. The cost of experiment is rather high and due to that the mathematical modeling of thermal processes occurring in semiconductor devices become the most popular.

In addition, theoretical approach to the thermal analysis allows to consider the problem of influence of wide range of factors on thermal behaviour of device what is not always possible by experiments. To determine temperature distribution the

boundary problem of heat transfer has to be solved. Two essential approaches to deal with that problem are used: analytical and numerical [1], [2].

Analytical approach provides obvious advantages as accuracy and general form of obtained solution. On the other hand these methods can be used only for solving simple boundary problems. To solve complex problems of heat transfer (e.g. odd geometry of the body, nonlinear properties of materials, radiation) wide range of numerical methods is successfully used. Additionaly in thermal analysis of semiconductor devices the following problems has be taken into account: multi layer and complicated internal structure of device, heat generation, convective and radiative heat transfer on the outer surface of device.

Among the numerical methods which are used to deal with boundary problems of heat transfer the following are considered to be the most effective [2]:

- finite difference method (FDM),
- finite element method (FEM),
- control volume method (CVM),
- boundary element method (BEM).

Presented mathematical model of the temperature distribution within integrated circuits has been evaluated on the base of control volume method [2], [3]. In contrary to FEM or BEM control volume method has very clear and simple physical interpretation and can be is especially effective for solving complex problems of heat transfer.

2. MATHEMATICAL MODEL OF TEMPERATURE DISTRIBUTION WITHIN INTEGRATED CIRCUIT

Mathematical model of temperature distribution has been worked out taking into account the following general assumptions [4]:

a) Three-dimensional temperature field in cartesian or cylindrical geometry is considered.

b) Steady-state or transient temperature field is taken into account.

c) Multi layer structure of the semiconductor device is considered.

d) Heat generation in the layer of semiconductor is taken into account.

e) Influence of gaseous gapes in the structure of integrated circuit on its thermal state may be considered,

f) Convective and radiative heat transfer on the external surfaces is taken into account.

g) Non-linear thermal properties of materials and temperature depedence of heat transfer coefficients are considered.

In the control volume formulation of heat transfer problems analyzed body has to be divided into arbitrary chosen number of elements (control volumes) with centrally situated node. Temperature of node represents the temperature of control volume. For each element of analyzed domain the energy balance is evaluated in order to obtain set of equatios in the nodes temperature distribution. The energy balance equations represents the first law of thermodynamics written for each element.

Basic equation of energy balance for the element i can be written in the following form [3]:

$$\sum_j \dot{Q}_{ji} + \sum_i \dot{Q}_{fi} + V_i \dot{q}_{vi} = V_i \rho_i c_{pi} \frac{T_i^{k+1} - T_i^k}{\Delta\tau}, \tag{1}$$

where:

$\dot{Q}_{ji}$ – heat flux rate from adjacent element j to element i,
$\dot{Q}_{fi}$ – heat flux on the external surface of element i,
$\dot{q}_{vi}$ – density of internal heat sources in the element i,
ρ_i – density of material,
V_i – volume of the element,
c_{pi} – specific heat of material,
k – index of time step,
$\Delta\tau$ – time step rate,
T_i^{k+1}, T_i – temperature of the node i at $k+1$ and k step of time.

Assuming one – dimensional and adiabatic heat conduction between adjacent elements volumes the heat flux rate $\dot{Q}_{ji}$ can be written as

$$\dot{Q}_{ji} = \frac{1}{R_{ij}} - \left(T_j^{k+1} - T_i^{k+1}\right), \tag{2}$$

where:

R_{ij} – thermal resistance between elements i and j.

Thermal resistance R_{ij} can be calculated from the following general formula [3] (see figure 1):

$$R_{ij} = \int_{l_{ij}} \frac{\mathrm{d}l}{\lambda(l)\,\mathrm{F}(l)}, \tag{3}$$

where:

λ – thermal conductivity,
$F(l)$ – area of the surface perpendicular to the line l.

Integration in (3) is performed along the line l_{ij} which joins nodes i and j.

For the elements of regular geometry e.g. rectangle or cubicoid thermal resistance can be expressed in very simple form:

$$R_{ij} = \frac{\Delta l}{\lambda F_{ij}} \tag{4}$$

where:

Δl – distance between nodes i and j.

When thermophysical properties are different in adjacent elements thermal resistance R_{ij} can be calculated as a sum:

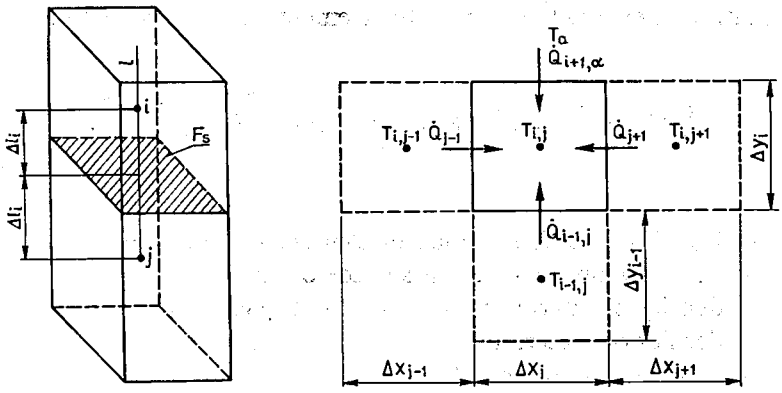

Fig. 1. Difference elements (control volumes)

$$R_{ij} = R_i + R_j = \frac{\Delta l_i}{\lambda_i F_{ij}} + \frac{\Delta l_j}{\lambda_j F_{ij}}, \tag{5}$$

where:

$\Delta l_i, \Delta l_j$ – distance between node i or j to the surface between elements.

When very thin layer of any material or gaseous gap is situated between two elements, this additional resistance can be added to R_{ij}:

$$R_{ij} = R_i + R_j + \frac{\delta}{\lambda_g F_{ij}} \tag{6}$$

where:

δ – gap thickness,

λ_g – thermal conductivity of gas.

Heat power within device is generated in the junction of semiconductor. At the presented model one assumes that heat power is generated on the surface of semiconductor and can be treated as a flat (surfacial) heat source. When heat source is located between two adjacent elements (see figure 1) heat flux $\dot{Q}_{ji}$ from element j to element i is calculated from relationship

$$\dot{Q}_{ji}^{k+1} = \frac{1}{R_i + R_j}\left(T_j^{k+1} - T_i^{k+1}\right) + F_s \frac{R_j}{R_i + R_j}\dot{q}_s, \tag{7}$$

where:

$\dot{q}_s$ – density of surfacial heat source (W/m^2),

F_s – area of heat source.

Temperature of semiconductor junction is assumed to be equal to the temperature T_s on the surface of heat source and can be calculated from formula:

$$T_s = \frac{R_j}{R_i+R_j}T_i + \frac{R_i}{R_i+R_j}T_j + F_s\frac{R_j R_i}{R_i+R_j}\dot{q}_s \tag{8}$$

On the external surfaces of the device the boundary condition of third kind has been involved. Both, free convection and radiation is taken into consideration.

Overall heat transfer coefficient α is a sum of convective α_c and radiative α_r heat transfer coefficients:

$$\alpha = \alpha_c + \alpha_r \tag{9}$$

Convective heat transfer coefficient is calculated from following relationship [5]:

$$\alpha_k = \mathrm{H}(\mathrm{T}_{fi} - \mathrm{T}_a)^n \tag{10}$$

where:

T_{fi} – temperature on the external surface of the element,

T_a – temperature of the fluid.

Radiative heat transfer coefficient α_r is calculated from relationship:

$$\alpha_r = \varepsilon_f \mathrm{C}_c 10^{-8}(\mathrm{T}_{fi}^2 + \mathrm{T}_a^2)(\mathrm{T}_{fi} + \mathrm{T}_a) \tag{11}$$

where:

ε – emissivity of the surface,

$\mathrm{C}_c = 5.67\ \mathrm{W/m^2K^4}$.

Unknown boundary temperature T_{fi} is evalued from equation of energy balance on the external surface of element i:

$$S_{fi}(\alpha_c + \alpha_r)(T_a^{k+1} - T_{fi}^{k+1}) = \frac{1}{R_{fi}}\left(T_{fi}^{k+1} - T_i^{k+1}\right), \tag{12}$$

where:

R_{fi} – thermal resistance between external surface and node i.

Either α_c or α_r depends on temperature T_{fi} hence to evaluate T_{fi} iterative procedure has to be applied.

Heat transfer through the gaseous assembling gaps is considered to be forced only by conduction. Because of very small thickness of the gap heat transfer by convection does not occur (what results from Rayleigh criteria [5]). Due to the relatively low temperature within device heat radiation in the gap has a small contribution comparing to the conduction what justify above assumption.

Energy balance equations elaborated for each element of analyzed domain leads to the set of N algebraic equations with respect to the N unknown nodal temperatures T_i^{k+1}, $i=1,2,\ldots N$:

$$\mathbf{A}\,\mathbf{T}^{k+1} = \mathbf{T}^k + \mathbf{B} \tag{13}$$

where:

$\mathbf{A}$ – square matrix of dimensions $N*N$,

$\mathbf{T}^{k+1}, \mathbf{T}^k$ – vectors of nodal temperature at $k+1$ and k step of time.

Calculations one begins at time $\tau=0$ ($k=0$) where initial temperature distribution $\mathbf{T}(0)$ is known.

To solve set of equations the (13) standard Gauss method has been used. Due to the nonlinearity of problem (nonlinear thermophysical properties of materials, nonlinearity of radiative and convective heat transfer coefficient) additional iterative procedure of solution has to be applied.

3. COMPARISON OF EXPERIMENTAL AND NUMERICAL RESULTS

Experimental and numerical results for the silicon integrated circuit in Flat Pack (FP) potting (figure 2) has been compared to verify the accuracy of worked out mathematical model.

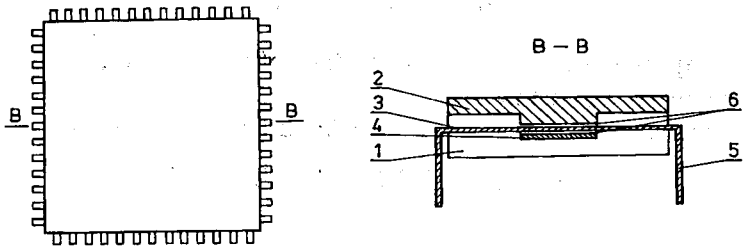

Fig. 2. Shape and cross-section of silicon Flat Pack integrated circuit

1 – silicon resin
2 – radiator
3 – scrap
4 – semiconductor (e. g. silicon)
5 – current leads
6 – air gaps

The silicon region of measured FP integrated circuit has dimensions 4.5*4.5*0.2 mm. On the upper surface of silicon 4 transistors BD – 127 type are symmetrically situated. The layer of semiconductor is mounted within potting with copper or aluminium radiator. To provide equalization of temperature distribution within layer of semiconductor during the measurements the thermal power was generated in all 4 transistors.

To improve accuracy of calculations each transistor has been represented by separated control volume. The control volume mesh of analyzed integrated circuit is shown in the figure 3.

In experiment the junction temperature of integrated circuit has been pointed out indirectly by measurements of forward voltage in semiconductor. The impulse method of measurements has been applied.

To come to the point graphs of the following relationship

$$U_f = f(T_j), \tag{14}$$

where:

U_f – forward voltage,

T_j – temperature of the junction

have been worked out for a fixed value of current intensity I_m.

Temperature T_j of the device was kept constant during each measurement. The range $T_j \in [20^0\text{C}, 130^0\text{C}]$ was considered. It has been estimated [6] that average relative error of evaluating of temperature T_j is not greater than 1%.

Scheme of used measurement network is shown in the figure 4.

Measurement and calculations of steady-state temperature distribution (including junction temeperature) were carried on for various rate of thermal power (figure 5).

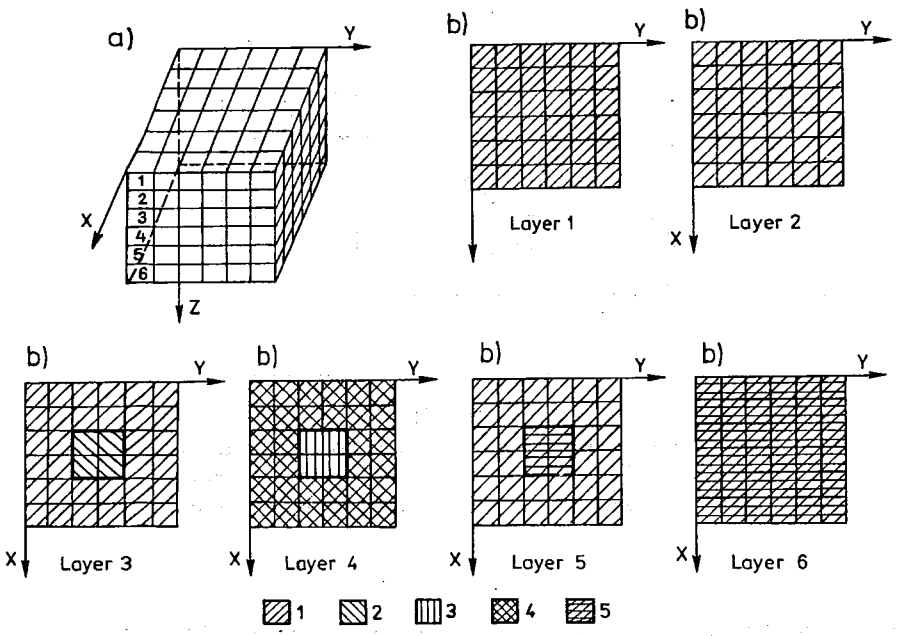

Fig. 3. Control volume mesh of FLATPACK integrated circuit a) 3-D grid b) 2-D grid within x, y layer
1 – resin (MG – 15)
2 – semiconductor (silicon)
3 – scrap (kovar)
4 – resin and currend leads
5 – radiator (aluminium or copper)
Dimension of control volume elements:
$\Delta x_i = \Delta y_i = 3{,}375$ mm (i = 1, 2, 5, 6)
$\Delta x_i = \Delta y_i = 2{,}25$ mm (i = 3, 4)
$\Delta z_1 = \Delta z_2 = 0{,}5$ mm; $\Delta z_3 = \Delta z_4 = 0{,}2$ mm; $\Delta z_5 = 0{,}4$ mm; $\Delta z_6 = 0{,}6$ mm

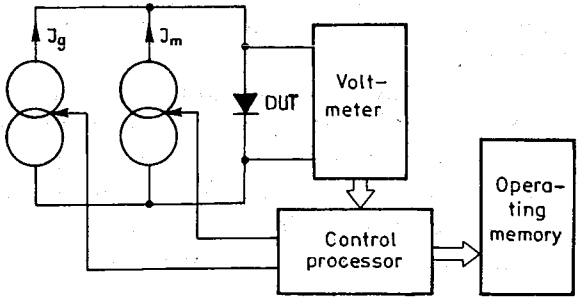

Fig. 4. Scheme of measurement network

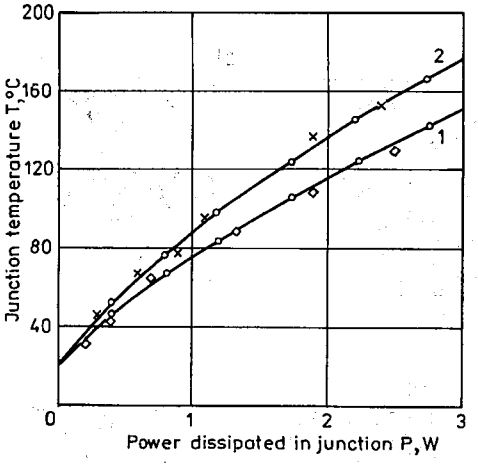

Fig. 5. Steady-state junction temperature of integrated circuit
o — calculations 1 — vertical position of device
x, ◇ — measurements 2 — horizontal position of device

Agreement between of experimental and numerical results is quite sufficient. Calculated values of junction temperature vary from experimental results less than 8 percent. The same level of accuracy has been obtained in the cases of investigations of different types of integrated circuits.

4. THERMAL ANALYSIS OF INFLUENCE OF ASSEMBLING GAPS AND EXTERNAL COOLING CONDITIONS ON THE TEMPERATURE OF ACTIVE ZONE OF INTEGRATED CIRCUIT

The integrated circuits as well as other semiconductor devices have non-homogeneous internal structure. These non-homogeneities have different influence on temperature distribution within semiconductor device. For example calculations pointed out that assumptions of homogeneous structure of open work instead of real structure leads to the variation of temperature of the active zone integrated circuit not more than 1 K.

The most significant influence on temperature distribution have asembling gaps occuring between layers of potting of integrated circuits as a result of non-ideal technological process. Thermal conductivity of gas mixture within gaps is much more less than conductivity of silicon or other materials of which consists the integrated circuit. This even very thin layers of gas causes the significant increasing of total thermal resistance between active zone and outer surface of device.

External condition of heat transfer (cooling conditions) have also significant influence on the temperature distribution within integrated circuit.

Using evaluated mathematical model and computer code the influence of the following factors on the temperature of active zone integrated circuit has been analyzed:

1). Thickness and location of assembling gaps.
2) Insulation of the one of frontal faces.
3) Position of the device on the mouting plate (horizontal or vertical).
4) Ambient temperature.
5) Emissivity of external surface of device.
6) Velocity of coolant and position of the device in relation to the direction of the coolant flow in the case of forced convection.

One assumes also that density of generated thermal power is calculated from the relationship:

$$q_s = \frac{P}{F_s} \tag{15}$$

where:

P – global electric power,

F_s – area of all working transistors.

Thermophysical properties of materials (used for calculations) are shown in table 1 [7], [8].

Properties of materials Table 1

Material	Density ρ kg/m³	Specific heat c_p J/kg K	Conductivity λ W/m K
Aluminium	2700.0	896.0	229.0
Kovar*	2981.0	1374.0	18.0
Silicon	2330.0	710.0	128.0
Copper	8930.0	381.0	393.0
Plastic* M15	1923.0	715.0	1.257

* – producer information

In all analyzed cases (except no. 2) one assumes that frontal surfaces on the bottom side of integrated circuit is insulated (what simulates the fitting on the mounting plate). On the other surfaces heat transfer to the environment by convection and radiation is taking into consideration and the boundary conditions of third kind are involved.

Results of calculations of steady-state temperature distribution within integrated circuit in FP potting are shown in figures 6 – 11. The influence of air assembling gap of thickness 10 μm located between radiator and open-work on the temperature of silicon is shown in the figure 6. Analyzed integrated circuit is supplied with radiator.

The influence of insulation of the one of frontal surfaces on the temperature of silicon is shown in the figure 7. Insulation causes that conditions of heat transfer into surrounding become worse and as a result temperature of active zone increases.

The influence of position of integrated circuit (horizontal or vertical) on the silicon temeprature is shown in the figure 8. In the case of horizontal position the heat transfer coefficient on the frontal surface is about 30% higher than in vertical position, but it causes rather inconsiderable variation of temperature distribution within integrated circuit.

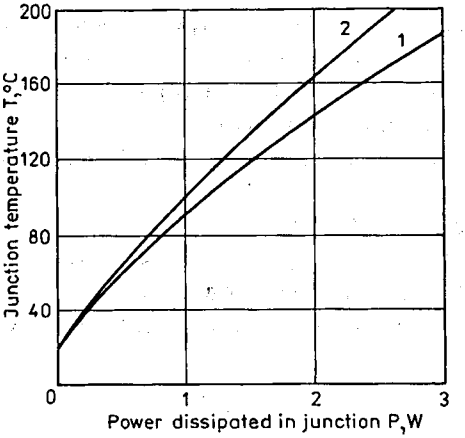

Fig. 6. Steady-state junction temperature of integrated circuit
1 — without any assembling gaps
2 — a gap between radiator and open-work

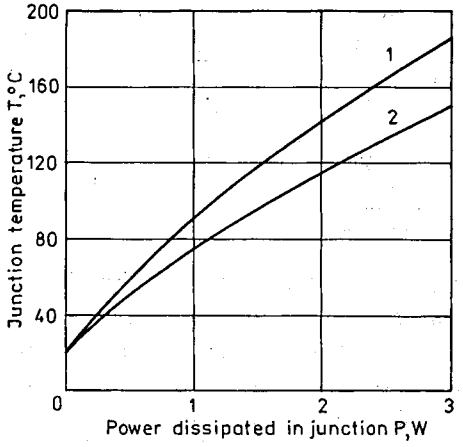

Fig. 7. Steady-state junction temeperature of integrated circuit mounted in vertical position
1 — one frontal surface insulated
2 — all surfaces are not insulated

The influence of ambient temeprature on the silicon temperature is shown in the figure 9. The integrated circuits with cooper and aluminium radiator are considered. The influence of ambient temperature is greater in the case of device with aluminium radiator, due to the lower value of emissivity of aluminium.

The influence of emissivity of external surfaces what determines density of radiative heat flux on the temperature distribution is shown in the figure 10. From the figure

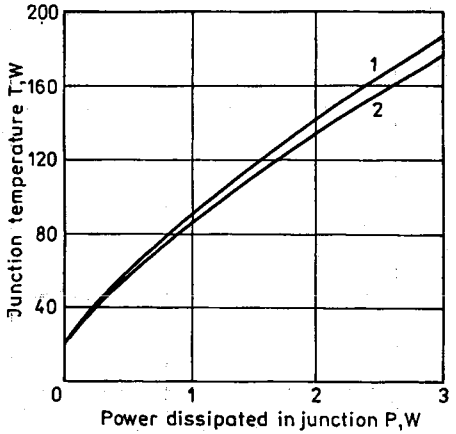

Fig. 8. Steady-state junction temperature of integrated circuit when one frontal surface in insulated
1 – vertical position of device
2 – horizontal position of device

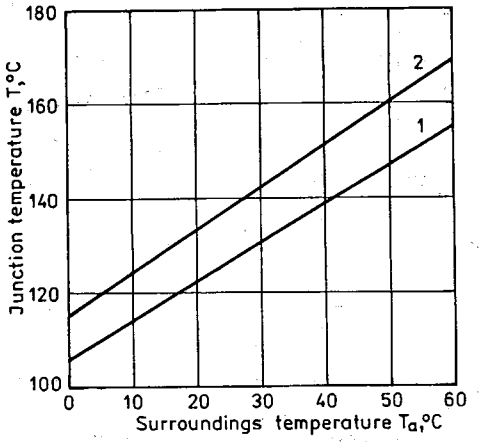

Fig. 9. Steady-state junction temeprature as a function of ambient temeprature
1 – device with cooper radiator
2 – device with aluminium radiator

results that convection has greater influence on the heat transfer intensity than radiation. It results from the fact of relatively low temperature of the surfaces. Taking into consideration two extreme values of the emissivity i. e. $\varepsilon = 0$ anf $\varepsilon = 1$ one obtains difference of silicon temperature less than 17°C.

Different cases of natural and forced convection on the surfaces of integrated circuit are shown in the figure 11. The influence of velocity of cooling air on the temperature of silicon is considered.

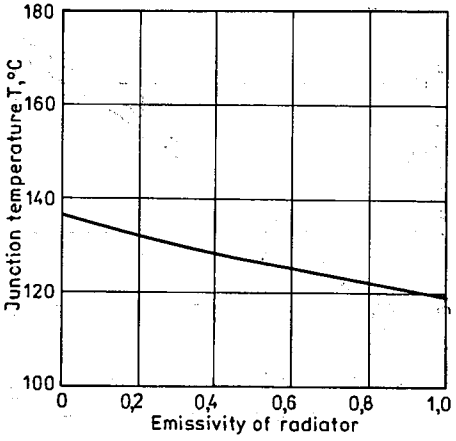

Fig. 10. The influence of emissivity of external surfaces on the temperature distribution

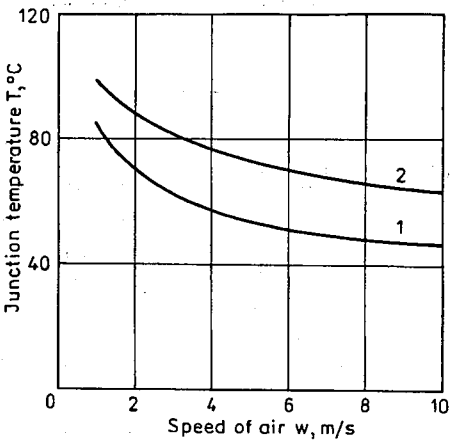

Fig. 11. Steady-state junction temperature in different cooling conditions
1 — forced convection on frontal and lateral surfaces
2 — forced convection on frontal surfaces and free convection on lateral surfaces

CONCLUSIONS

The experimental verification has confirmed sufficient agreement between measurements and numerical results obtained using described mathematical model.

Worked out model can be used in practice for designing and improving of construction of semiconductor devices as well as for investigation of optimal conditions of exploitation (for example cooling condition).

The control volume method on the base of which is evaluated mathematical model allows to consider in simple way the influence of great number of factors on the thermal behaviour of integrated circuit.

REFERENCES

1. H. S. Carslaw, J. C. Jaeger: *Conduction of heat in solids*. Clarendon, Oxford, 1959
2. Y. Jaluria, K. E. Torrance: *Computational heat transfer*. Hemisphere Publishing Corporation 1986
3. J. Szargut: *Metody numeryczne w obliczeniach cieplnych pieców przemysłowych*. Wyd. Śląsk, Katowice 1977
4. E. Kostowski, S. Kucypera, J. Skorek: *Analiza parametrów termodynamicznych przyrządów półprzewodnikowych przy użyciu metod numerycznych*. Unpublished report. Insitute of Thermal Technology Gliwice, 1987, 1988
5. S. Wiśniewski: *Wymiana ciepła*. Warszawa: PWN, Warszawa, 1979
6. S. Kucypera: *Analiza procesów wymiany ciepła w przyrządach półprzewodnikowych*. D. Sc. thesis. Inst. of Thermal Technology, Gliwice, 1988
7. S. Stępień: *Poradnik konstruktora sprzętu elektronicznego*. Warszawa: WNT, 1976
8. A. L. Zacharov, E. J. Asvadurova: *Rascet teplowych parametrov poluprovodnikovych priborov*. Radio i sviaz. Moskva, 1983

S. KUCYPERA, J. SKOREK

MODELOWE BADANIE WPŁYWU ZEWNĘTRZNYCH PARAMETRÓW EKSPLOATACYJNYCH I SZCZELIN MONTAŻOWYCH NA ROZKŁAD TEMPERATURY W OBSZARZE CZYNNYM UKŁADÓW SCALONYCH

Streszczenie

W oparciu o dyskretną metodę bilansów elementarnych opracowano model matematyczny pola temperatury w przyrządach półprzewodnikowych. Zastosowanie metody bilansów elementarnych umożliwia w stosunkowo prosty sposób rozwiązywać złożone problemy wymiany ciepła z uwzględnieniem np. złożonej geometrii obszaru, wielowarstwowej struktury, nieliniowych właściwości materiałów i innych czynników mających znaczący wpływ na stan cieplny przyrządu półprzewodnikowego.

W celu weryfikacji dokładności modelu matematycznego zostały przeprowadzone również pomiary temperatury z zastosowaniem metody impulsowej. W oparciu o opracowany model dokonano analizy wpływu zewnętrznych warunków chłodzenia oraz defektów montażowych na rozkład temperatury w strefie czynnej układów scalonych. Wyniki obliczeń zilustrowano na wykresach.

KWARTALNIK ELEKTRONIKI I TELEKOMUNIKACJI, 1991, 37, Z. 3–4, ss. 449–470

621.397.331.53

Detekcja cech obrazów w środowisku Systemu Przetwarzania Informacji Wizyjnej VIPS

TOMASZ OSTROWSKI, PIOTR BAJKOWSKI
KONRAD WICYŃSKI, RYSZARD MUSIAŁ

Instytut Automatyki Przemysłowej, Politechnika Szczecińska

Otrzymano 1990.10.24

Autoryzowano do druku 1991.02.01

W dziedzinie cyfrowego przetwarzania obrazów zagadnieniem o istotnym znaczeniu staje się redukcja informacji 2D sygnału, w celu ekstrakcji cech obrazu istotnych dla danego obszaru zastosowań. Praca dotyczy implementacji, pod Systemem Przetwarzania Informacji Wizyjnej VIPS, trzech metod detekcji cech, opartych na gaussowskiej i morfologicznej filtracji oraz przestrzenno-częstotliwościowej dekompozycji 2D sygnału. Przedstawione są rezultaty działania algorytmów na obrazach rzeczywistych i testowych.

1. WSTĘP

W dziedzinie cyfrowego przetwarzania obrazów pojawia się problem działania na cechach obiektów, które są reprezentowane w szerokim zakresie skali z uwzględnieniem wzajemnego oddziaływania cech reprezentowanych na różnych skalach organizacji obrazu (np. zmienność poziomu szarości obrazu może przybierać określoną postać w zależności od wybranej skali reprezentacji). Wynika stąd potrzeba przetwarzania obrazów na różnych poziomach skali. Posiadanie narzędzi, umożliwiających otrzymanie hierarchicznej reprezentacji obrazu w funkcji parametru skali, może umożliwić właściwą selekcję informacji, niezbędnej dla opisu i interpretacji obiektów [4].

Celem naszej pracy była implementacja możliwie bogatego i uniwersalnego zbioru operatorów dla uzyskania hierarchicznej struktury reprezentacji obrazu, z możliwością elastycznego kształtowania w zależności od konkretnego problemu przetwarzania obrazów.

Przy doborze operatorów oparto się na następujących metodach detekcji cech obiektów:

– operator zawężający pasmo częstotliwości, działający na zasadzie wykrywania przejść przez zero rezultatu splotu obrazu z filtrem uzyskan przez działanie

laplasjanem na funkcję o kształcie gaussowskiego rozkładu normalnego (Marr-Hildreth, Laplacian of Gaussian, LoG, lub $\nabla^2 G$ operator).

– operator realizujący morfologiczny filtr otwierający przez złożenie operacji obliczania lokalnego minimum i maksimum sygnału w obszarze elementu strukturalizującego,

– operator dokonujący rozkładu sygnału obrazu na zbiór przestrzennie zorientowanych pasm częstotliwości.

Układ pracy odpowiada kolejności wynienionych wyżej metod detekcji cech obiektów. Implementacji algorytmów dokonano w języku C, w formie operacji dołączonych do środowiska Systemu Przetwarzania Informacji Wizyjnej VIPS, wykonanego w Instytucie Automatyki Przemysłowej Politechniki Szczecińskiej [15].

2. DETEKCJA CECH OBIEKTÓW PRZEZ LoG FILTRACJĘ O ZMIENNEJ SKALI

Literatura w dziedzinie cyfrowego przetwarzania obrazów podaje kilka równoważnych postaci analitycznych operatora $\nabla^2 G$, różniących się jedynie stałą multiplikatywną nie zmieniającą kształtu operatora [3], [5], np.:

$$\nabla^2 = (\partial^2/\partial^2 x + \partial^2/\partial^2 y); \tag{1}$$

$$g(x, y) = \exp[-(x^2 + y^2)/2\sigma^2]; \tag{2}$$

$$\nabla^2 G = \nabla^2 g(x, y) = -1/\sigma^2 [2 - (x^2 + y^2)/\sigma^2] \exp[-(x^2 + y^2)/2\sigma^2]; \tag{3}$$

gdzie σ jest odchyleniem standardowym krzywej Gaussa.

Przez skalę operatora rozumiemy wymiar okna operatora, które jest dobierane tak, aby wynosiło w przybliżeniu 4σ. Taki wymiar okna zapewnia uwzględnienie istotnych wartości współczynników dyskretnej postaci operatora.

Ze względu na bezpośredni związek z wymiarem okna σ nazywane jest parametrem skali operatora.

Detekcja cech operatorem $\nabla^2 G$ polega na obliczaniu splotu $f(x,y) * \nabla^2 G$, gdzie $f(x,y)$ jest funkcją reprezentującą sygnał obrazu (poziom szarości) dla pixela o współrzędnych (x,y), a następnie znalezieniu miejsc przejść przez zero wyników obliczeń [5].

Przejścia przez zero występują w pobliżu tych pixeli obrazu, gdzie zachodzą zmiany poziomu sygnału, to znaczy w okolicach krawędzi. W celu wyeliminowania przejść przez zero, które nie odpowiadają zmianom sygnału o odpowiednio dużej intensywności, lub powstają z powodu obecności szumu w obrazie, wybieramy tylko przejścia o odpowiednio dużym nachyleniu, większym od zadanego progu th.

Przez zastosowanie operatora ∇^2G o różnych wartościach parametru skali otrzymujemy różniące się opisy sygnału obrazu. W ogólności, dla małej skali operatora otrzymujemy drobniejsze (bardziej subtelne) detale obrazu, lecz operator jest mniej odporny na zakłócenia, natomiast dla dużej skali otrzymujemy mniej

subtelne cechy obrazu, a operator wykazuje lepsze możliwości redukcji zakłóceń [1]. Jednakże zasadniczym elementem leżącym u podstaw tej koncepcji jest nie problem redukcji szumów, lecz zdolności do śledzenia zachowań tych samych cech w zależności od skali, na której są analizowane [2].

W celu zmniejszenia ilości obliczeń zrealizowaliśmy nasz $\nabla^2 G$ operator przez złożenie dwóch jednowymiarowych operatorów o postaci analitycznej:

$$\nabla^2 G' = (1 - x^2/\sigma^2)\exp[-x^2/2\sigma^2]; \tag{4}$$

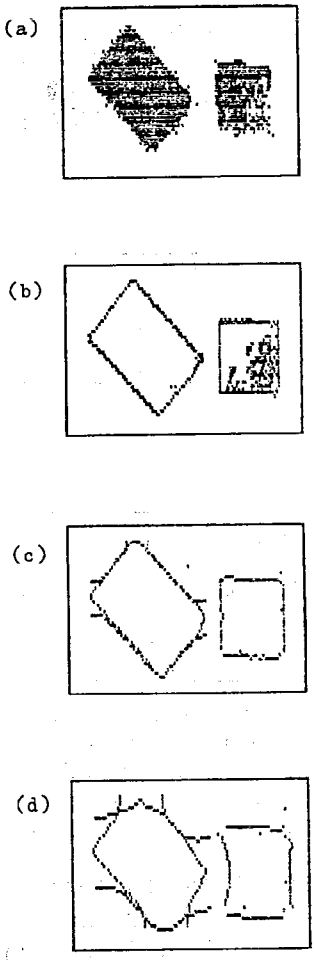

Rys. 1. Detekcja cech operatorem $\nabla^2 G$ (a) Obraz szary 50×113, 16 poziomów, zbinaryzowany przy wydruku. (b) Przejścia przez zero otrzymane dla $\sigma=2$, th=0, czas wykonywania operacji, t=4 min. 15 s. (c) Przejścia przez zero, $\sigma=5$, th=0, t=8 min. 10 s. (d) Przejścia przez zero, $\sigma=10$, th=0, t=14 min. 45 s. (e) Odpowiedź operatora $\nabla^2 G'$ na krawędź

Czasy realizacji wszystkich operacji (rys. 1 – 12) zmierzone zostały dla IBM PC 8 MHz bez koprocesora

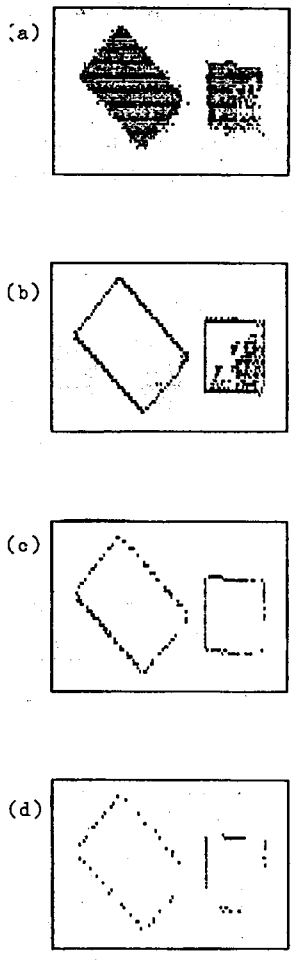

Rys. 2. Detekcja cech operatorem $\nabla^2 G$. (a) Obraz szary 50×113, 16 poziomów, zbinaryzowany przy wydruku. (b) Przejścia przez zero otrzymane dla $\sigma = 2$, th $= 0$, czas wykonywania operacji, t $= 4$ min. 15 s. (c) Przejścia przez zero, $\sigma = 2$, th $= 1$, t $= 4$ min. 15 s. (d) Przejścia przez zero, $\sigma = 2$, th $= 2$, t $= 4$ min. 15 s.

działających odpowiednio w kierunkach poziomym i pionowym. Przejście przez zero jest lokalizowane dla pixela o współrzędnych (x,y), jeżeli zostało stwierdzone w tym punkcie przy działaniu operatora w kierunku poziomym lub pionowym (logicznie OR). Odpowiedź operatora na lokalną zmianę poziomu szarości (krawędź) przedstawiona jest poglądowo na rysunku 1e.

W celu zapewnienia maksymalnej elastyczności doboru skali reprezentacji obrazu zdecydowano się na implementację $\nabla^2 G$ operatora w postaci zmiennoprzecinkowej. W przypadku wyboru konkretnych wartości parametrów skali dla danego obszaru zastosowań, można dokonać przekształcenia operatorów na postać o współczynnikach całkowitych metodą podaną w [3].

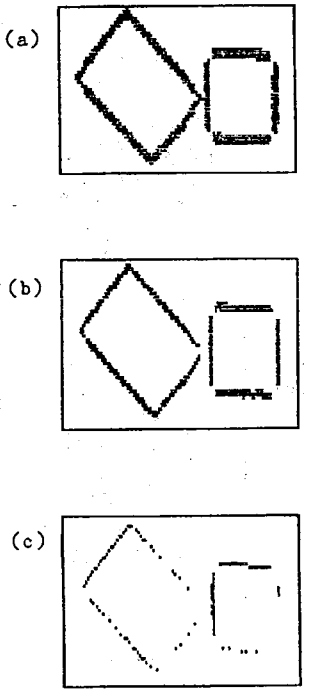

Rys. 3. Detekcja cech operatorem $\nabla^2 G$, w którym wykrywanie przejść przez zero zastapione zostało progowaniem sygnału splotu (wartość progu określa parametr th_p). Obraz wejściowy identyczny jak na rysunkach 1 i 2. (a) Krawędzie wykryte dla $\sigma=2$, $th_p=1$, czas wykonywania operacji, t = 3 min. 25 s. (b) Krawędzie, $\sigma=2$, $th_p=2$, t = 3 min. 25 s. (c) Krawędzie, $\sigma=2$, $th_p=3$, t = 3 min. 25 s.

Rysunki 1 – 5 przedstawiają wyniki działania operatora $\nabla^2 G$ na obrazie rzeczywistym dla różnych wartości parametru skali σ i różnych rozdzielczości obrazu.

Można zaobserwować, że wraz ze zwiększeniem parametru skali poprawia się zdolność redukcji szumów operatora, natomiast kontury obiektów ulegają zniekształceniu. Zastąpienie wykrywania przejść przez zero progowaniem sygnału splotu powoduje pogrubienie krawędzi i utrudnia lokalizację wykrytych cech.

3. MORFOLOGICZNA FILTRACJA OTWIERAJĄCA O ZMIENNEJ SKALI

Filtracja morfologiczna dokonuje ekstrakcji cech przez wybór odpowiedniego kształtu elementu strukturalizującego. Metodą tą można dokonać ekstrakcji interesujących cech obiektu takich jak: krawędzie, zaokrąglenia, dziury, rogi, kliny i szczeliny, działając elementem strukturalizującym o odpowiednio dobranym kształcie. Szczegółowy opis podstaw teoretycznych morfologii matematycznej i jej za-

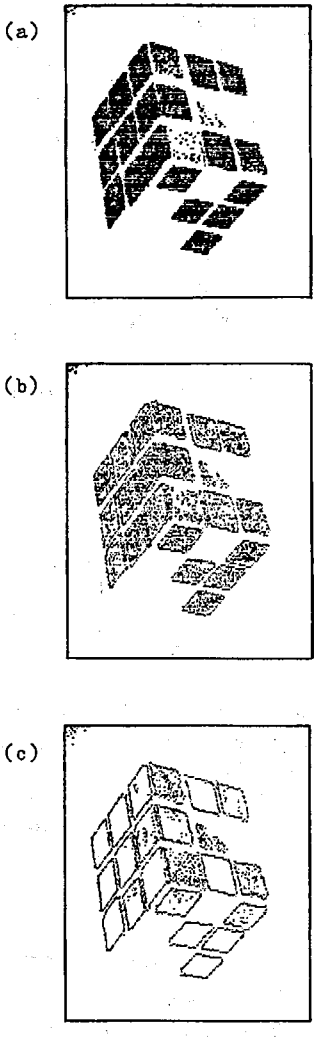

Rys. 4. Detekcja cech operatorem $\nabla^2 G$. (a) Obraz szary 233×175, 16 poziomów, zbinaryzowany przy wydruku, „kostka Rubika". (b) Przejścia przez zero otrzymane dla $\sigma = 1$, th $= 0$, czas wykonywania operacji, t = 21 min. 25 s. (c) Przejścia przez zero, $\sigma = 2$, th $= 0$, t = 31 min. 20 s.

stosowań w dziedzinie przetwarzania obrazów można znaleźć w opracowaniach Serry [7] i Haralicka [6].

Podstawowe operacje morfologiczne można zdefiniować następująco [9].

D e f i n i c j a (dylacja).

Niech F i B będą podzbiorami dyskretnej przestrzeni Z^2. Dylację zbioru F zbiorem B oznaczamy przez $F \oplus B$ i definiujemy jako:

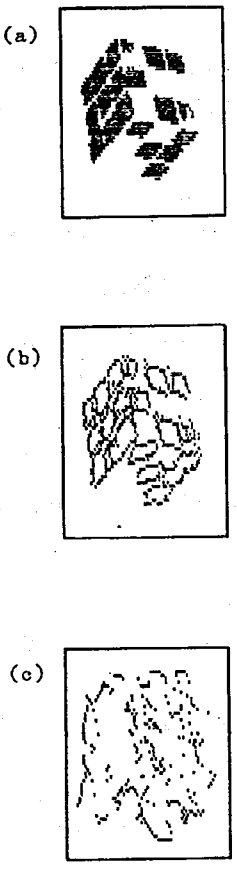

Rys. 5. Detekcja cech operatorem $\nabla^2 G$. (a) Obraz szary 61×78, 16 poziomów, zbinaryzowany przy wydruku, „kostka Rubika". (b) Przejścia przez zero otrzymane dla $\sigma = 2$, th = 0, czas wykonywania operacji, t = 3 min. 35 s. (c) Przejścia przez zero, $\sigma = 10$, th = 0, t = 12 min. 10 s.

$$F \oplus B = \{ z \in Z^2 \mid z = a + b, \text{ dla pewnych } a \in F \text{ i } b \in B \}. \tag{5}$$

Załóżmy, że $\Lambda \subset Z^2$ jest podprzestrzenią dyskretną, na której określono funkcję binarną (obraz) $f(x,y)_{(x,y)\in\Lambda}$, a $B \subset \Lambda$ jest elementem strukturalizującym. Dylację funkcji (obrazu) $f(x,y)$ elementem B można zdefiniować przy użyciu podstawowych operacji logicznych następująco [8]:

$$\{f \oplus B\}(x, y) = \mathrm{OR}_{(i,j)\in B}\{f(x-i, y-j)\}. \tag{6}$$

W przypadku wykonywania operacji dylacji na obrazie szarym, logiczne działanie OR należy zastąpić operacją obliczania lokalnego maksimum, z wartości poziomów szarości pixeli obrazu w obszarze elementu strukturalizującego [14]:

$$\{f \oplus B\}(x, y) = \max_{(i,j)\in B}\{f(x-i, y-j)\}. \tag{7}$$

D e f i n i c j a (erozja)

Jeżeli F i B są podzbiorami dyskretnej przestrzeni Z^2, to erozję zbioru F zbiorem B oznaczamy przez $F \ominus B$ i definiujemu jako:

$$F \ominus B = \{z \in Z^2 \mid z + b \in F, \text{ dla każdego } b \in B\}. \tag{8}$$

Podobnie jak w przypadku dylacji, erozję obrazu $f(x,y)_{x,y)\in\Lambda}$ elementem strukturalizującym $B \subset \Lambda$ realizujemy przez podstawowe operacje logiczne:

$$\{f \ominus B\}(x, y) = \text{AND}_{(i,j)\in B}\{f(x+i, y+j)\}. \tag{9}$$

Jeżeli wykonujemy erozję na obrazie szarym, logiczne AND należy zastąpić obliczeniem lokalnego minimum, z wartości poziomów szarości pixeli obrazu w obszarze elementu strukturalizującego:

$$\{f \ominus B\}(x, y) = \min_{(i,j)\in B}\{f(x+i, y+j)\}. \tag{10}$$

Przy wykorzystaniu pojęć dylacji i erozji można zdefiniować następujące dwie złożone operacje:

D e f i n i c j a (otwarcie)

Otwarcie zbioru F zbiorem B oznaczamy $F \bullet B$ i definiujemy jako złożenie erozji z dylacją:

$$F \bullet B = \{F \ominus B\} \oplus B. \tag{11}$$

D e f i n i c j a (domknięcie)

Domknięcie zbioru F zbiorem B oznaczamy $F \bullet B$ i definiujemy jako złożenie dylacji z erozją:

$$F \bullet B = [F \oplus B] \ominus B. \tag{12}$$

Podobnie jak w omawianej poprzednio $\nabla^2 G$ filtracji również dla filtracji morfologicznej można zdefiniować pojęcia skali i jej parametru. Przez skalę filtracji filtra morfologicznego rozumiemy wielkość użytego elementu strukturalizującego, a przez parametr skali konkretny wymiar geometryczny tego elementu, na przykład długość boku kwadratu, lub średnicę koła, jeżeli takie zostały użyte elementy strukturalizujące.

Szczególnie interesującą operacją morfologiczną jest otwarcie kołem (dyskiem) średnicy D, ze względu na niewprowadzanie dodatkowych przejść przez zero funkcji krzywizny konturu obiektu, przy zwiększeniu skali filtracji [9]. Algorytm filtracji został tak zaprojektowany, że umożliwia interakcyjne, graficzne zdefiniowanie elementu strukturalizującego o dowolnym kształcie i wymiarach, a więc możliwe jest wykonanie filtracji morfologicznej o dowolnej skali. Rysunki 6–10 przedstawiają wyniki takich filtracji wraz z użytymi elementami strukturalizującymi (kształt elementu strukturalizującego określa cechę podlegającą detekcji).

Zrealizowana w ten sposób morfologiczna filtracja otwierająca, stwarza możliwość reprezentacji obrazów w abstrakcyjnej przestrzeni skali filtracji, pod kątem doboru żądanych cech.

(a)

Rys. 6. Morfologiczna filtracja otwierająca o zmiennej skali
(a) Obraz wejściowy binarny 135×278 „rycina"

(b)

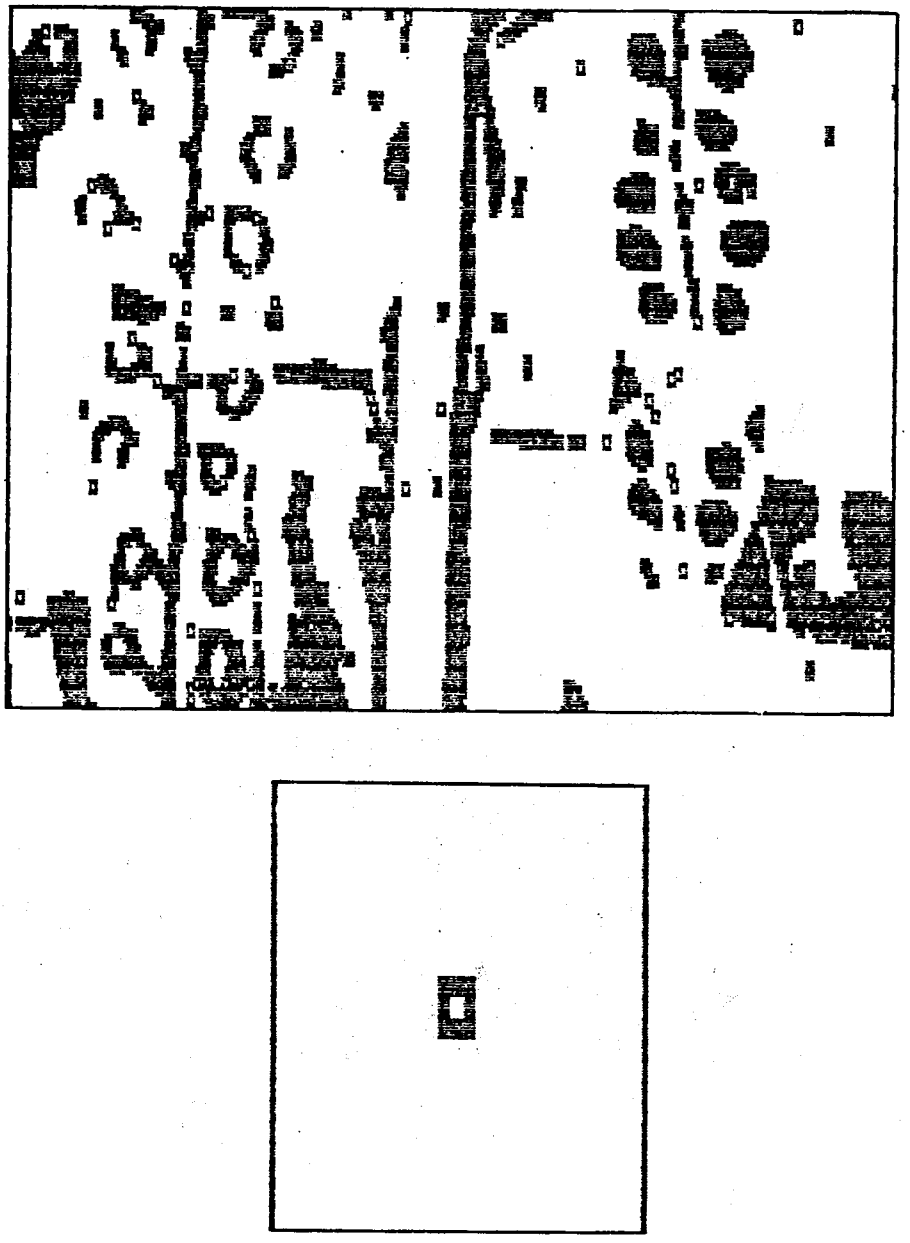

Rys. 6. Morfologiczna filtracja otwierająca o zmiennej skali
(b) Otwarcie obrazu (a) „pierścieniem" średnicy D=3. Czas wykonywania operacji, t=1 min 10 s

(c)

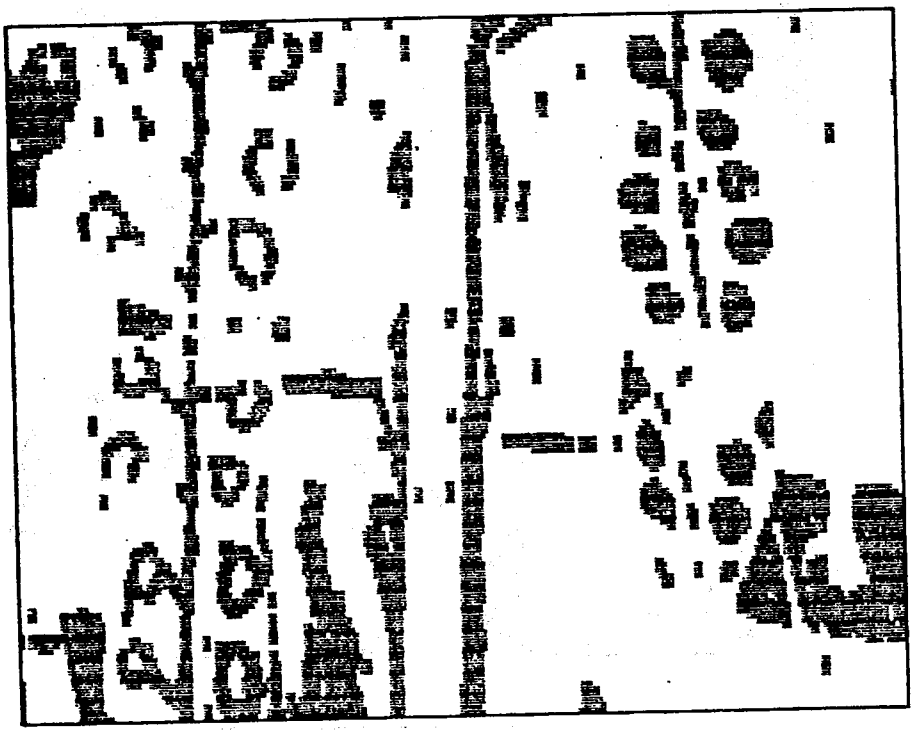

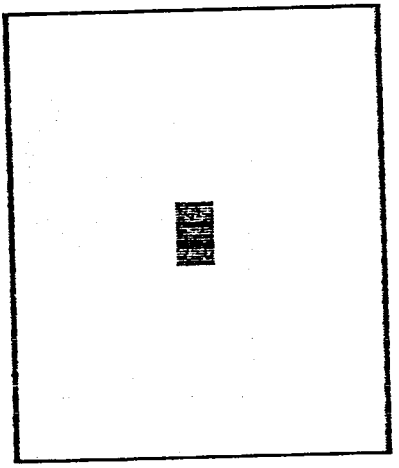

Rys. 6. Morfologiczna filtracja otwierająca o zmiennej skali
(c) Otwarcie obrazu (a) „dyskiem" średnicy D=3. Czas wykonywania operacji, t=1 min 10 s

(d)

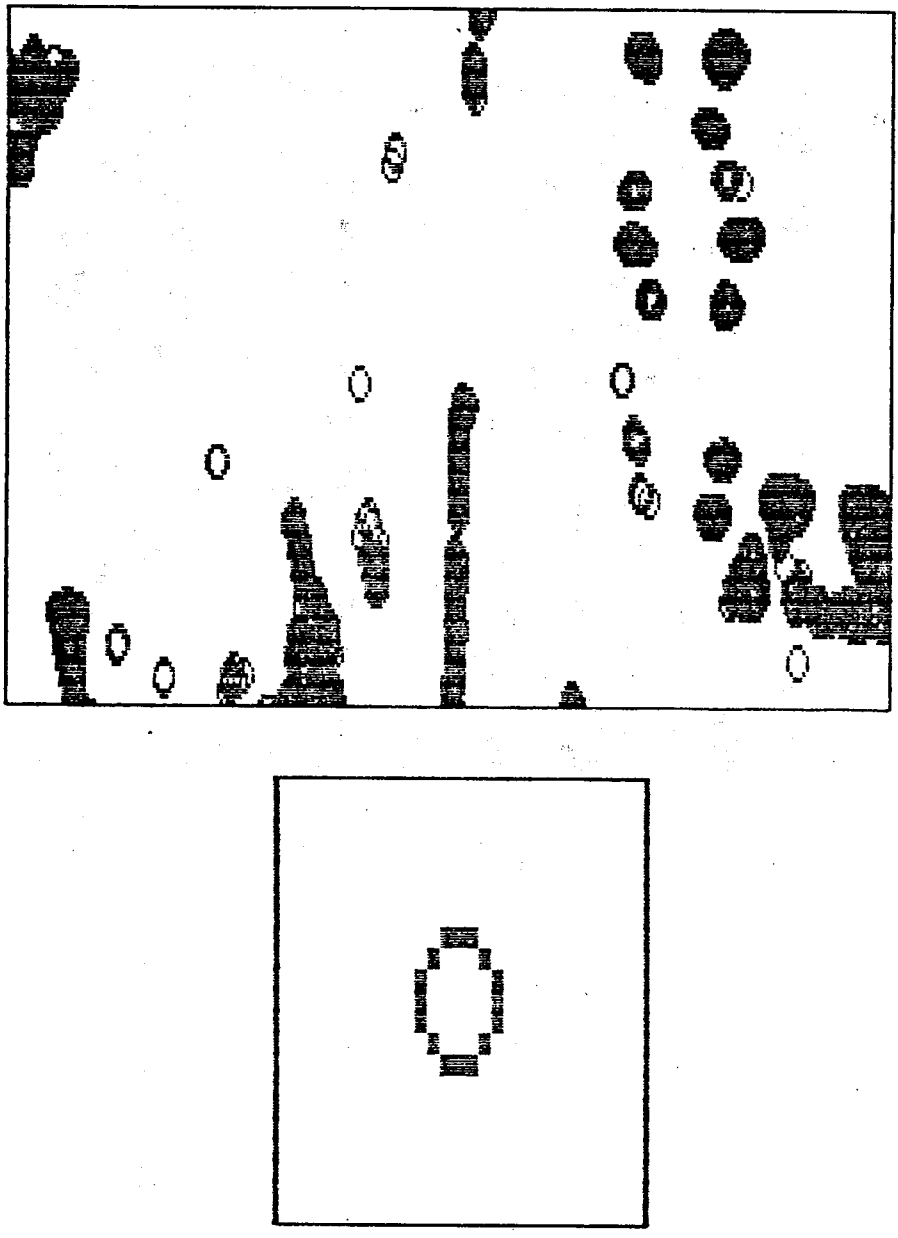

Rys. 6. Morfologiczna filtracja otwierająca o zmiennej skali
(d) Otwarcie obrazu (a) „pierścieniem" średnicy D=7. Czas wykonywania operacji, t=4 min 10 s

(e)

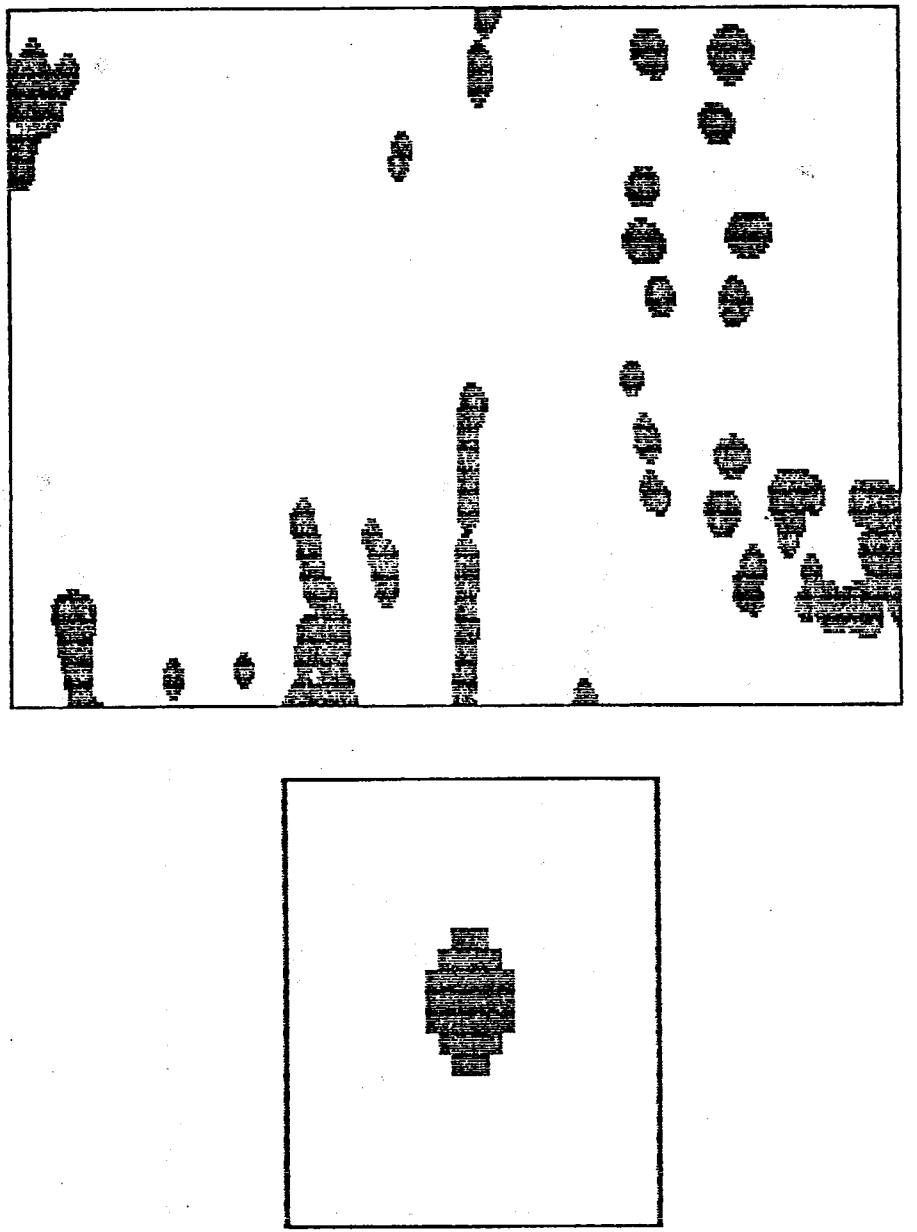

Rys. 6. Morfologiczna filtracja otwierająca o zmiennej skali
(e) Otwarcie obrazu (a) „dyskiem" średnicy D=7. Czas wykonywania operacji, t=4 min 40 s

(f)

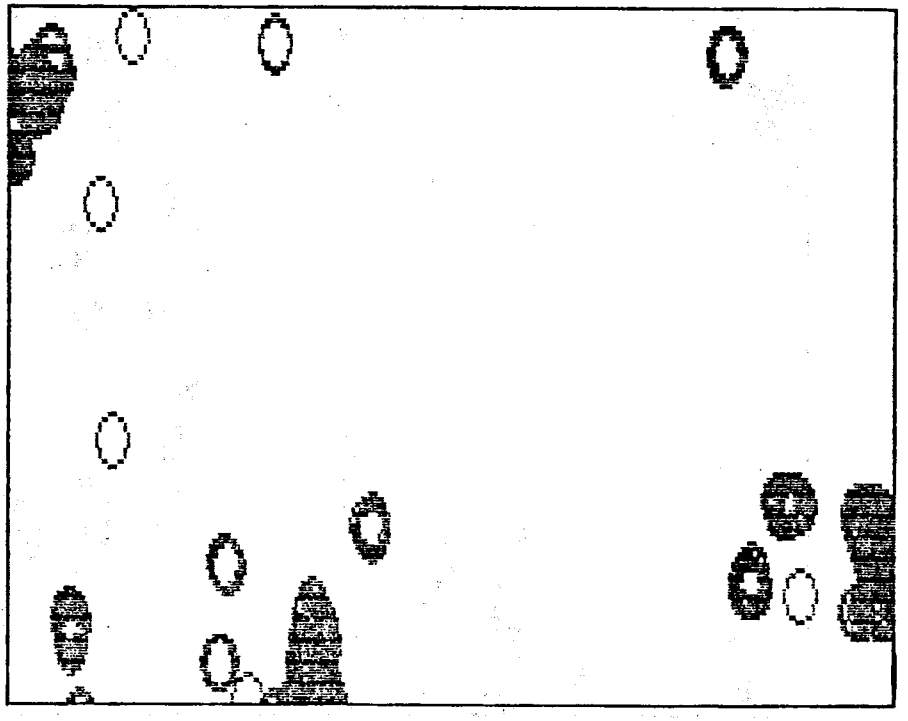

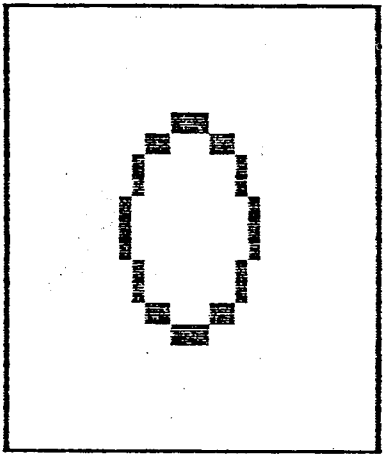

Rys. 6. Morfologiczna filtracja otwierająca o zmiennej skali
(f) Otwarcie obrazu (a) „pierścieniem" średnicy D=11. Czas wykonywania operacji, t=9 min 10 s

(g)

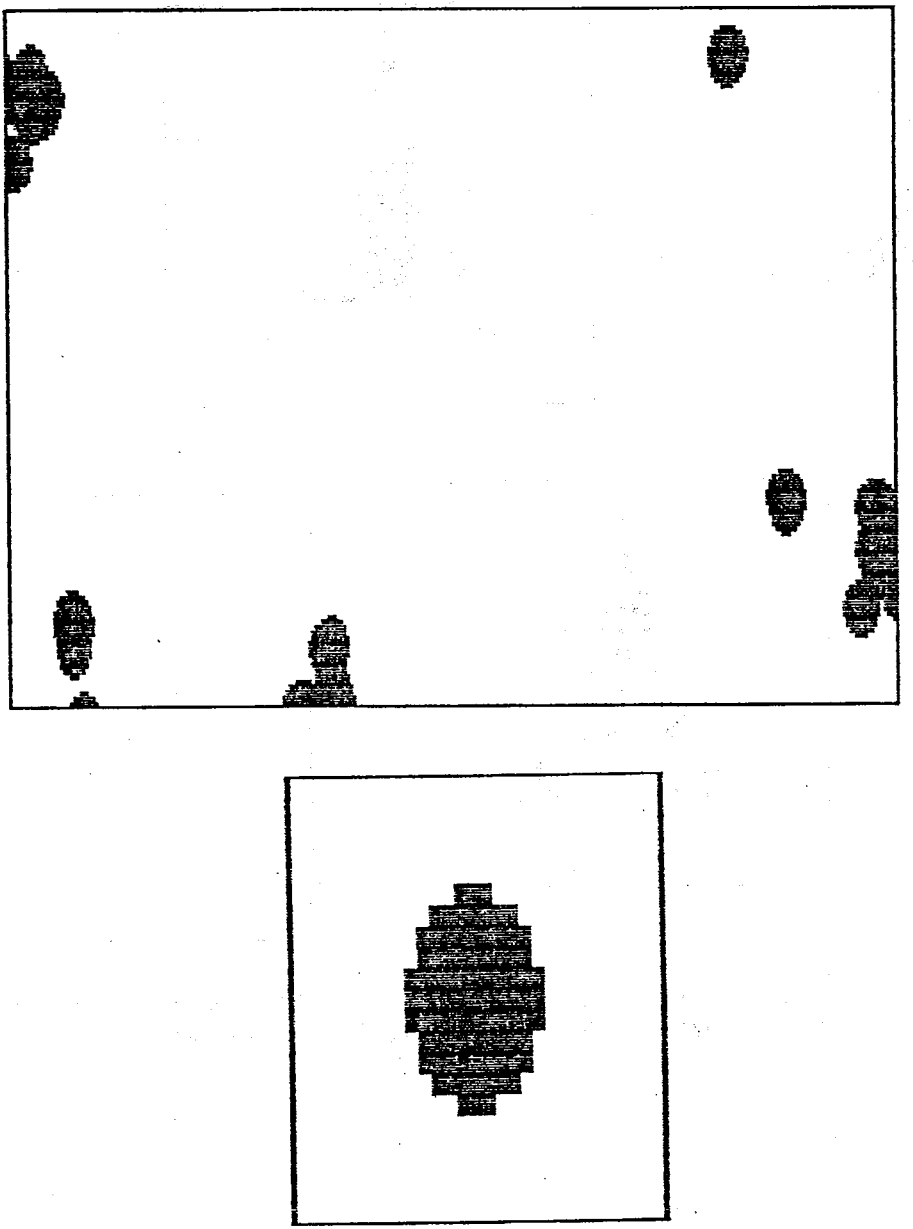

Rys. 6. Morfologiczna filtracja otwierająca o zmiennej skali
(g) Otwarcie obrazu (a) „dyskiem" średnicy D = 11. Czas wykonywania operacji, t = 10 min 40 s

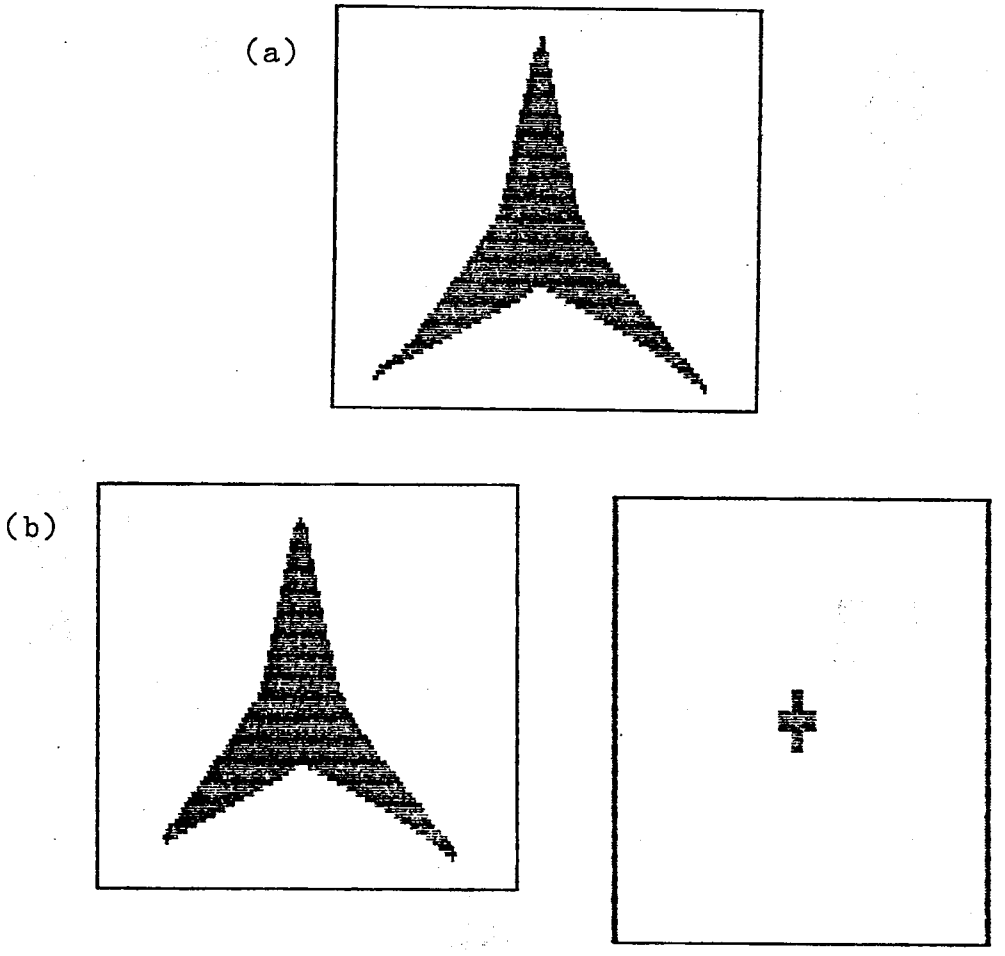

Rys. 7. Ewolucja konturu obiektu, poddanego morfologicznej filtracji otwierającej o zmiennej skali (a) Obraz testowy binarny 80 × 133. (b) Otwarcie obrazu (a) „dyskiem" średnicy D = 3, czas wykonywania operacji, t = 30 s

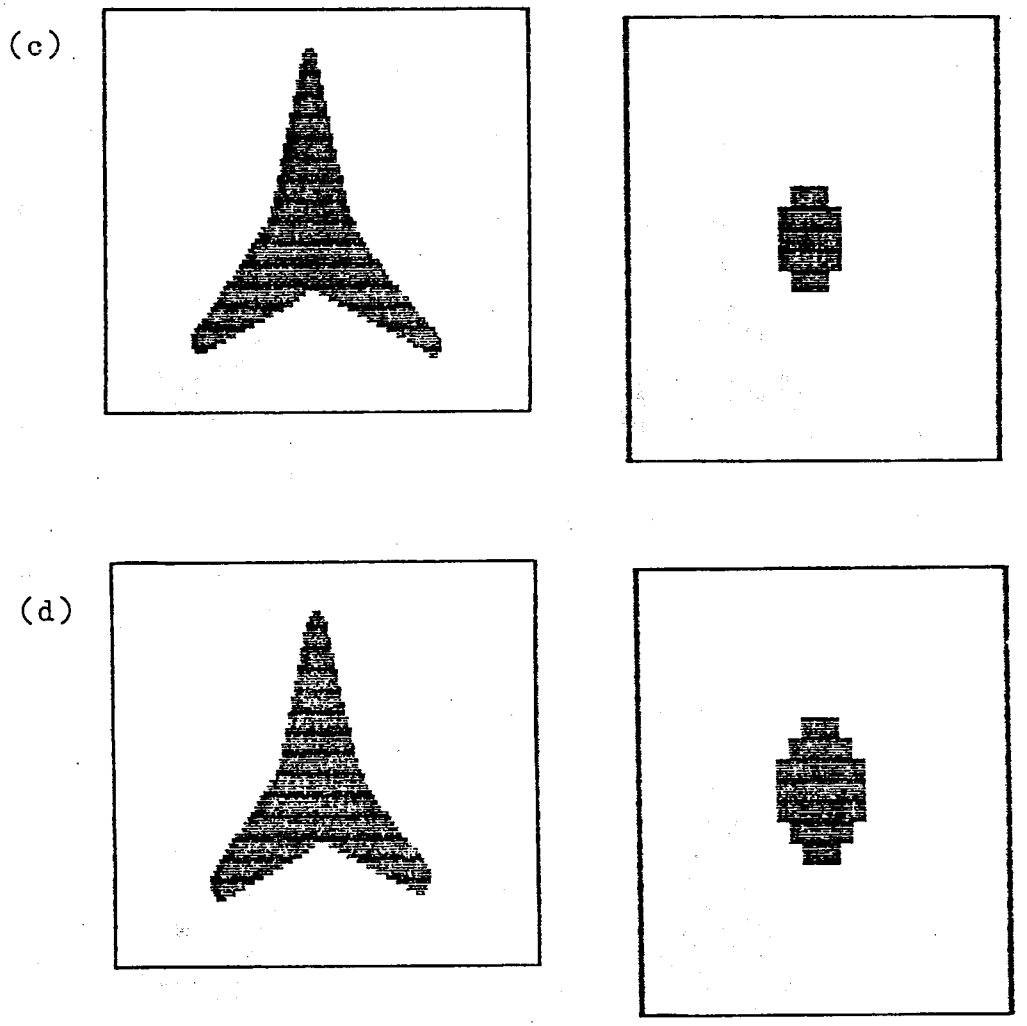

Rys. 7. Ewolucja konturu obiektu, poddanego morfologicznej filtracji otwierającej o zmiennej skali (c) Otwarcie obrazu (a) „dyskiem", D = 5, t = 45 s. (d) Otwarcie obrazu (a) „dyskiem", D = 7, t = 1 min 15 s

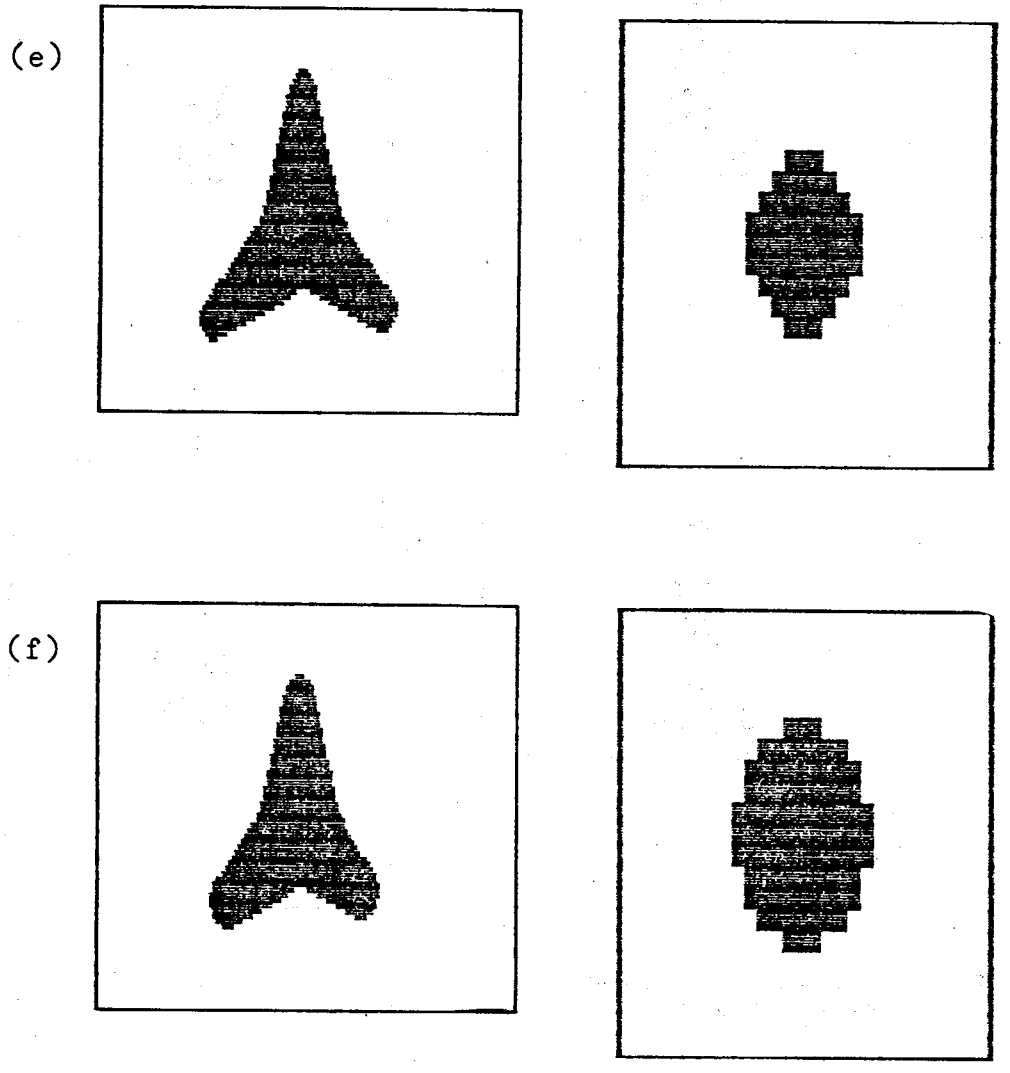

Rys. 7. Ewolucja konturu obiektu, poddanego morfologicznej filtracji otwierającej o zmiennej skali. (e) Otwarcie obrazu (a) „dyskiem", D=9, t=2 min. (f) Otwarcie obrazu (a) „dyskiem", D=11, t=3 min

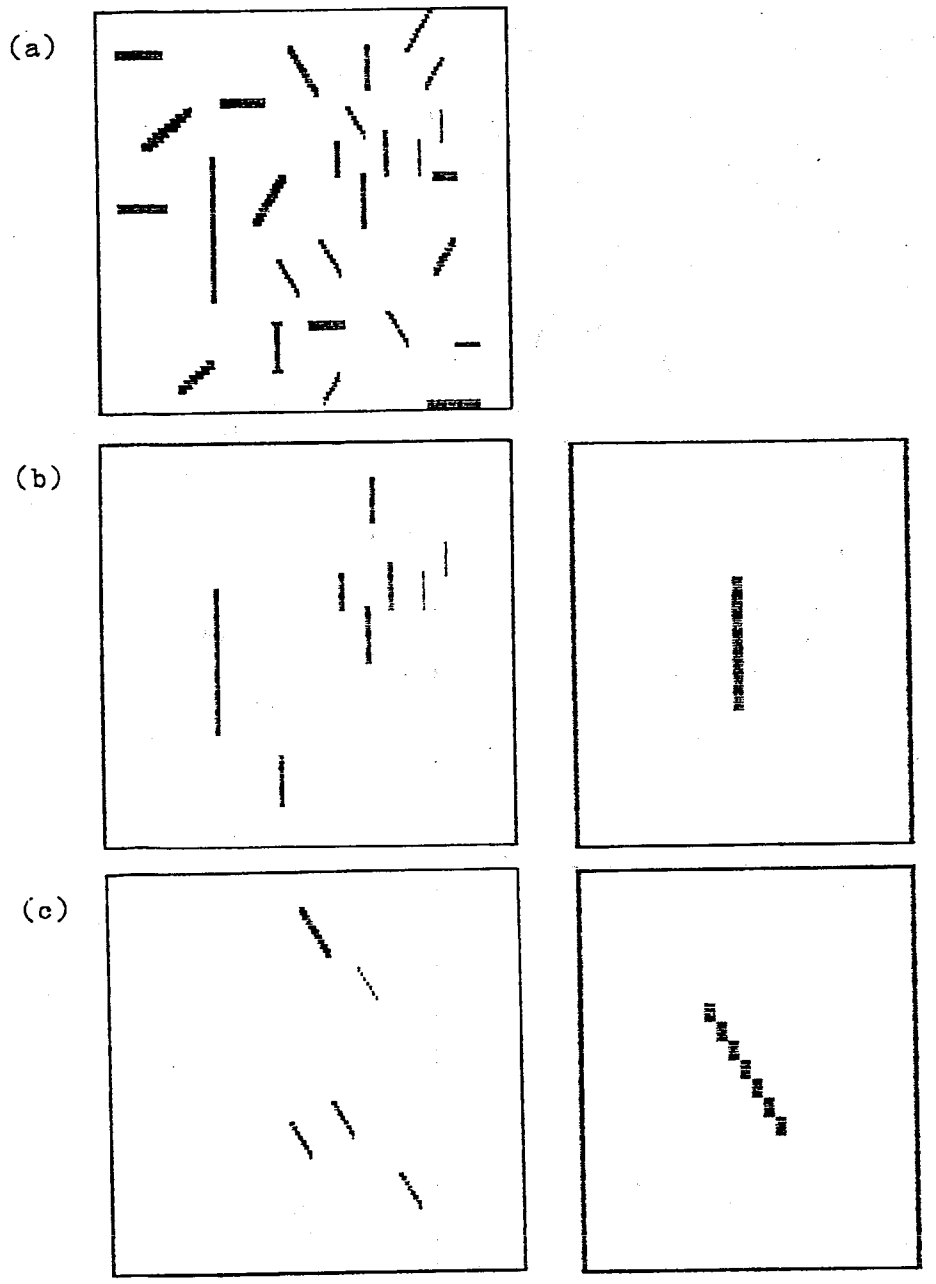

Rys. 8. Redukcja obiektów filtrem otwierającym
(a) Obraz testowy 85×143. (b) Otwarcie obrazu (a) „odcinkiem pionowym" o długości l=7, czas wykonywania t=35 s. (c) Otwarcie obrazu (a) „odciniem skośnym", l=7, t=1 min 25 s

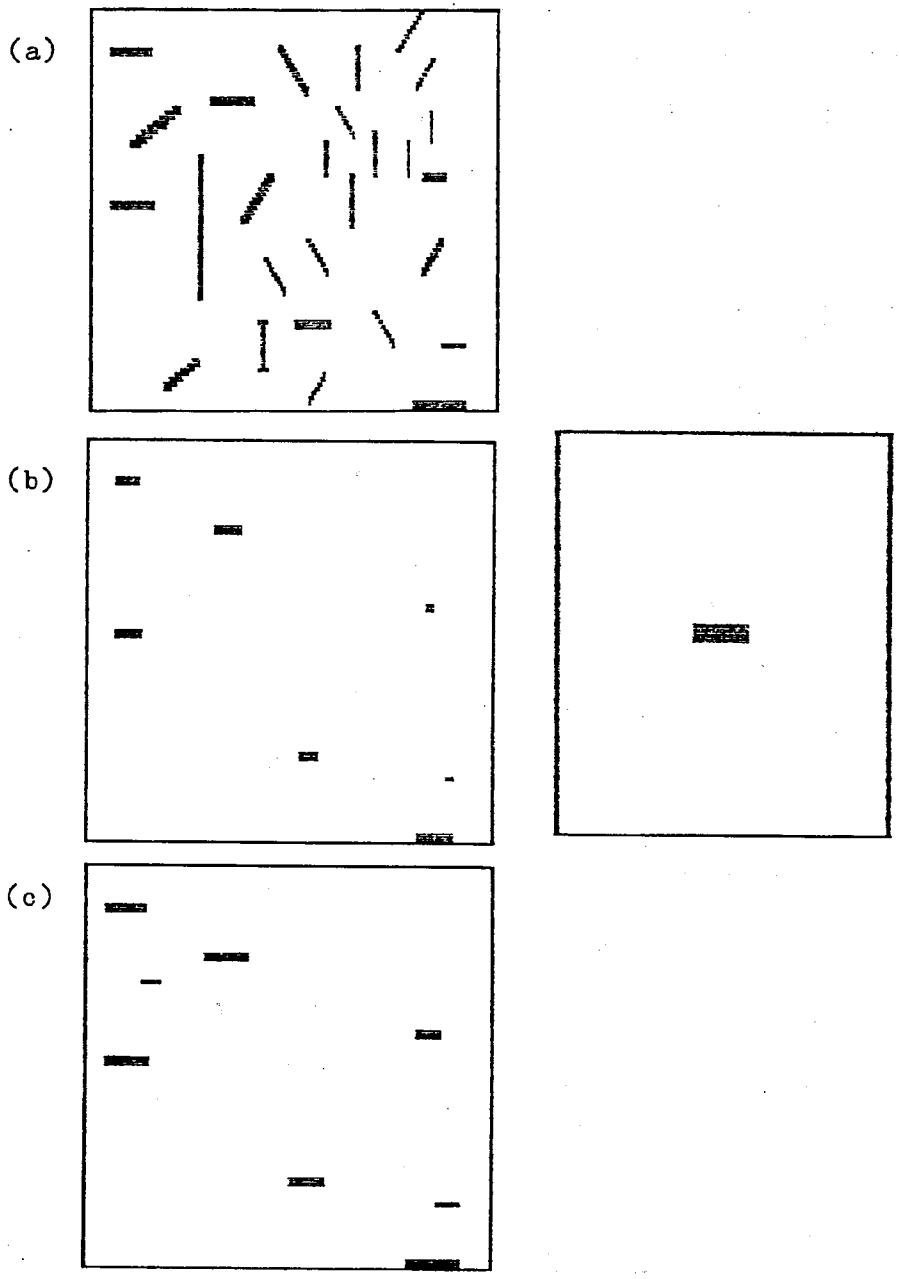

Rys. 9. Redukcja obiektów w obrazie filtrem otwierającym
(a) Obraz testowy binarny 85 × 143. (b) Erozja obrazu (a) „odcinkiem poziomym", l=7, t=5 s. (c) Dylecja obrazu (b) takim samym elementem strukturalizującym, t=15 s

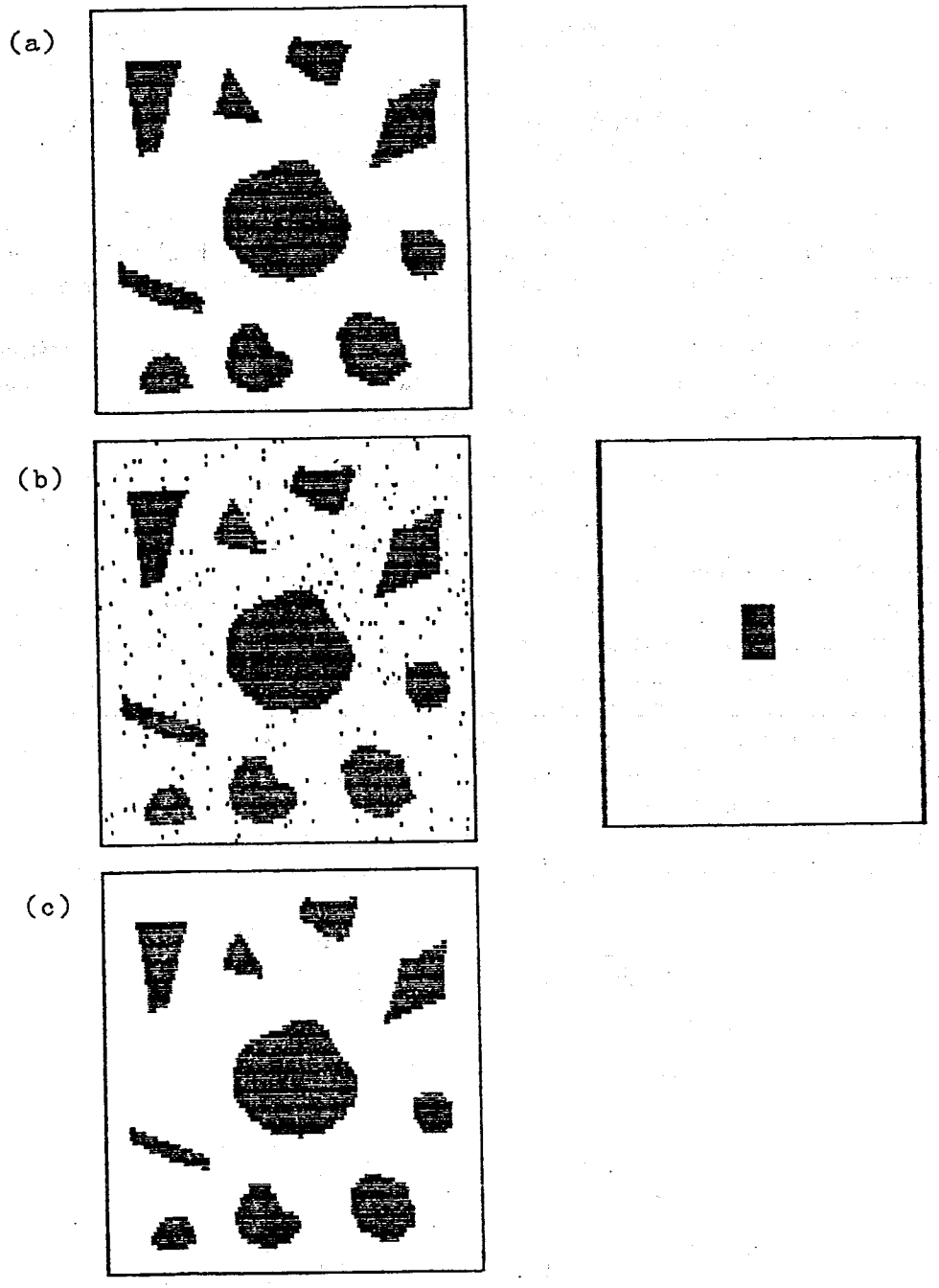

Rys. 10. Redukcja szumu impulsowego przy pomocy filtra otwierającego
(a) Obraz testowy binarny 136 × 90. (b) Obraz (a) zaszumiony – 5% szum impulsowy. (c) Otwarcie obrazu (b) „dyskiem", D = 3, t = 25 s

4. REPREZENTACJA OBRAZU OPARTA NA KONCEPCJI ORTONORMALNEJ PRZESTRZENNO-CZĘSTOTLIWOŚCIOWEJ DEKOMPOZYCJI 2D SYGNAŁU

Ta część pracy zawiera opis operatora, dokonującego transformacji 2D sygnału obrazu na zbiór czterech obrazów o czterokrotnie mniejszej rozdzielczości, których poziomy szarości posiadają dobre właściwości lokalizacyjne w dziedzinach przestrzennej i częstotliwościowej.

Działanie operatora polega na wykrywaniu zmian poziomu sygnału o określonej orientacji przestrzennej, poprzez rozwinięcie funkcji reprezentującej wartości sygnału obrazu względem bazy ortonormalnej i reprezentację obrazu współczynnikami rozwinięcia, z czterokrotnie zmniejszoną rozdzielczością.

Do niedawna panowało przekonanie, że nie istnieje prosta ortonormalna baza rozwinięcia w przestrzeni $L^2(R)$ fukcji całkowalnych z kwadratem o dobrych własnościach lokalizacyjnych jednocześnie w dziedzinach przestrzennej i częstotliwościowej. Dopiero stosunkowo niedawno Grossmann i Morlet [10] wprowadzili klasę funkcji zwanych w oryginalnej terminologii „wavelets" (fale pierwotne), jako funkcje $\psi(x)$, których translacje i dylacje $\sqrt{s}\psi(sx-t)_{(s,t)\in R^2 \times R}$ mogą być użyte do rozwinięcia w przestrzeni funkcji całkowalnych z kwadratem $L^2(R)$. Funkcje te są nowym narzędziem analizy funkcjonalnej, będącym uogólnieniem bazy Haara. Posługiwanie się nimi wykazuje silną koncepcyjną analogię z analizą fourierowską, z tą różnicą, że rozwinięcie na *„wavelety"* umożliwia dyskryminację określonej orientacji przestrzennej kanałów częstotliwościowych.

Praktyczna realizacja dekompozycji sygnału polega na przemiennym użyciu dwóch jednowymiarowych filtrów H i Q, nazywanych filtrami zwierciadlanymi, we

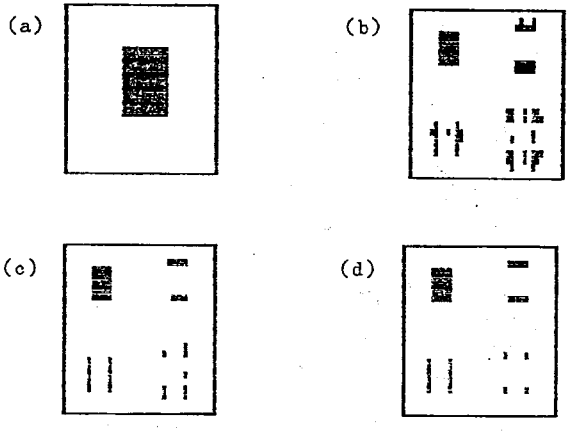

Rys. 11. Działanie algorytmu przestrzenno-częstotliwościowej dekompozycji sygnału „wavelet" Parametry: th_1, th_2, th_3, th_4, określają poziom progowania w obszarach A. D1, D2, D3, parametr η określa wielkość okna filtracji $(2\eta+1)$. (a) Obraz testowy binarny 26×37. (b) Wynik działania algorytmu na obrazie (a), $th_1=0{,}2$, $th_2=0.1$, $th_3=0.1$, $th_4=0.01$, $\eta=5$, t=28 s. (c) Wynik działania algorytmu, $th_1=0.3$, $th_2=0.17$, $th_3=0.17$, $th_4=0.03$, $\eta=5$, t=28 s. (d) Wynik działania algorytmu, $th_1=0.3$, $th_2=0.17$, $th_3=0.017$, $th_4=0.05$, $\eta=3$, t=28 s

wzajemnie prostopadłych kierunkach i dwukrotnym zmniejszeniu rozdzielczości na każdym etapie rozwinięcia.

Rysunki 11 – 12 przedstawiają wynik działania algorytmu na obrazach testowych. Może być on interpretowany jako dekompozycja sygnału na zbiór niezależnych, przestrzennie zorientowanych pasm częstotliwości.

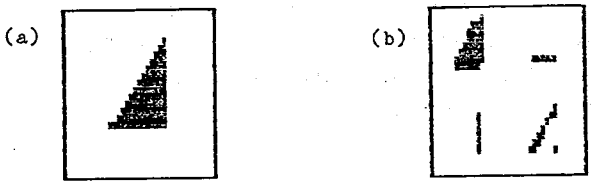

Rys. 12. Działanie algorytmu przestrzenno-częstotliwościowej dekompozycji sygnału „wavelet" Parametry: th_1, th_2, th_3, th_4, określają poziom progowania w obszarach A. D1, D2, D3, parametr η określa wielkość okna filtracji $(2\eta+1)$. (a) Obraz testowy binarny 26×37. (b) Wynik działania algorytmu na obrazie (a), $th_1=0{,}2$, $th_2=0.05$, $th_3=0.05$, $th_4=0.05$, $\eta=3$, t=28 s

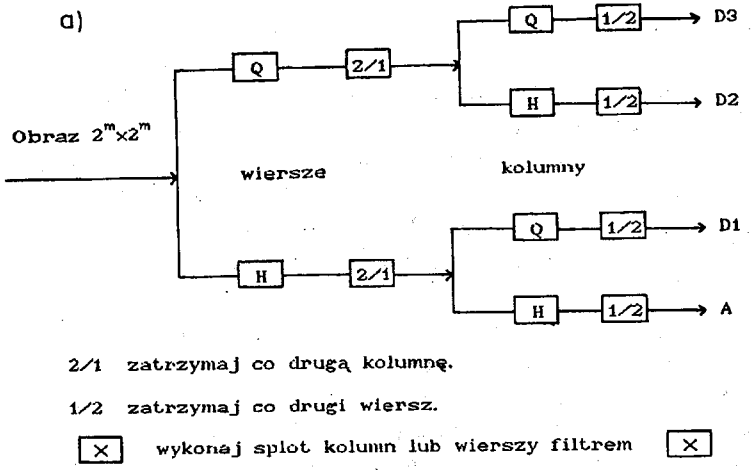

b)

A	D1
D2	D3

c)

n	H(n)
0	0.542
1	0.307
2	-0.035
3	-0.078
4	0.023
5	-0.030
6	0.012
7	-0.013
8	0.006
9	0.006
10	-0.003
11	-0.002

H(-n) = H(n);

Rys. 13. (a) Struktura algorytmu „wavelet". (b) Rozmieszczenie obrazów wyjściowych. (c) Współczynniki filtrów

Struktura algorytmu oraz parametry filtrów [10] przedstawiono na rysunku 13. Interpretacja obrazów jest następująca:
A odpowiada niskim częstotliwościom,
D1 podaje wysokie częstotliwości (krawędzie) w kierunku pionowym,
D2 wysokie częstotliwości w kierunku poziomym,
D3 wysokie częstotliwości w pionie i poziomie (rogi).

Algorytm może być realizowany kaskadowo, przy czym sygnałem wejściowym stopnia n kaskady jest obraz A na wyjściu stopnia $n-1$. Ilość stopni w kaskadzie można interpretować jako parametr skali.

5. PODSUMOWANIE I KIERUNEK DALSZYCH PRAC

W pracy przedstawiono rezultaty implementacji pod systemem VIPS trzech algorytmów detekcji cech lokalnych w obrazie. Ze względu na oparcie systemu VIPS o klasyczną architekturę von Neumanna (IBM PC) czasy realizacji algorytmów są znaczne (duża ilość działań zmniennoprzecinkowych dla obliczenia splotów i operacji logicznych w przypadku filtrów morfologicznych). Pewną kompensatą tej niedogodności może być dołączona do systemu operacja zmniejszania obrazu do dowolnych wymiarów, pozwalająca dobrać minimalną rozdzielczość dla danego obszaru zastosowań. Również reprezentacja pod systemem VIPS sygnału obrazu na szesnastu poziomach szarości (oraz quasi binarny) nie pozwala na efektywną pracę z *„waveletami"*, wymagającymi reprezentacji obrazu o dużej precyzji i znacznej pamięci operacyjnej systemu.

Zaprezentowane rezultaty należy traktować jako bazę do dalszych badań. Zamiarem autorów nie była optymalizacja parametrów stosowanych algorytmów, lecz stworzenie, w ramach posiadanych możliwości sprzętowych, maksymalnie uniwersalnego narzędzia, umożliwiającego *„strojenie"* algorytmów w zależności od postawionego celu. Cel ten będzie inaczej zdefiniowany np. w metalografii a inaczej w robotyce. W pierwszym przypadku można osiągnąć ciekawe rezultaty stosując operacje morfologiczne, w drugim preferowane będą detektory działające na zasadzie wykrywania przejść przez zero.

Na uwagę zasługuje spójne podejście do problemu detekcji cech, oparte na pojęciu skali filtracji i jej parametru.

Dokonana dla wybranego zbioru parametrów skali ekstrakcja cech umożliwia, po wyposażeniu operatorów w zdolność rejestracji atrybutów cech, takich jak: orientacja, kontrast itp., wykonanie grupowania lokalnego cech na każdym poziomie skali według metodyki podanej niżej, a następnie przejście do wyższych poziomów przetwarzania opartych na wiedzy, zgodnie z powszechnie akceptowaną koncepcją „stożka przetwarzania" (processing cone) [5].

Realizacja tych celów wymaga jednak zastosowania systemu przetwarzania obrazów o znacznie zwiększonej, przez zastosowanie architektury równoległej mocy, obliczeniowej.

Metodyka konstrukcji symbolicznego opisu sceny przez grupowanie wykrytych cech lokalnych [11], [12], [13].

6. DODATEK

1. Łączenie wykrytych krawędzi.
2. Aproksymacja połączonych krawędzi odcinkami linii prostych.
3. Detekcja dla każdej linii wszystkich linii z nią sąsiadujących, wykonana przez skanowanie dla każdego pixela linii, obrazu w kierunku do niej prostopadłym, do momentu napotkania linii sąsiadującej odpowiednio z lewej i z prawej strony.
4. Obliczenie dla każdej linii średniego poziomu szarości pixeli w obszarze między tą linią i wszystkimi liniami sąsiadującymi odpowiednio z lewej i prawej strony.
5. Umowna orientacja linii tak, aby obszar o niższym średnim poziomie szarości znajdował się z prawej strony, a obszar o wyższym średnim poziomie szarości z lewej strony linii.
6. Utworzenie struktury danych, realizującej symboliczny opis sceny w formie atrybutowego grafu relacyjnego z wierzchołkami reprezentującymi linię i jej atrybuty takie jak: położenie, orientacja, średni poziom sygnału sąsiadujących obszarów oraz z gałęziami (wskaźnikami), odpowiadającymi relacjom, np. lewego i prawego sąsiedztwa (rysunek 14).

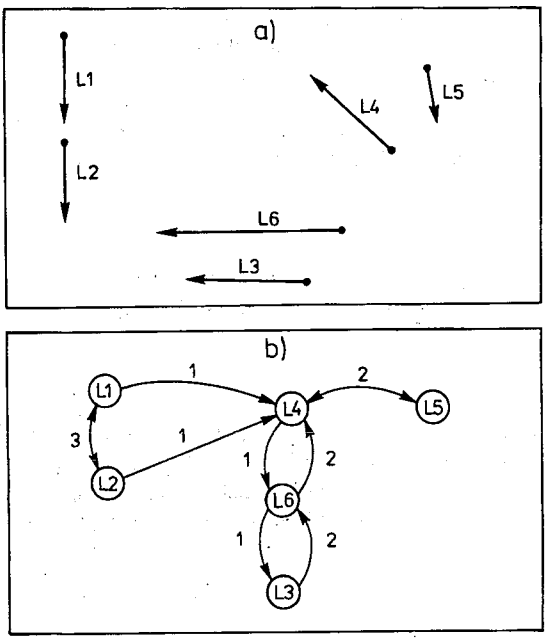

Rys. 14. (a) Rysunek liniowy. (b) Opis strukturalny rys. (a).
Relacje są oznaczone następująco: 1-lewy, 2-prawy, 3-współliniowy. Utworzony w ten sposób opis obrazu może być wejściem do zadań wyższego poziomu

BIBLIOGRAFIA

1. A. L. Yuille and T. A. Poggio: *Scaling theorems for zero crossings.* IEEE Trans. Pattern Anal. Machine Intell., vol. PAMI–8, no 1, pp. 15–25, Jan. 1986
2. Y. Lu and R. C. Jain: *Behavior of edges in scale space.* IEEE Trans. Pattern Anal. Machine Intell., vol. PAMI–11, no 4, pp. 337–356, April 1989
3. W. E. L. Grimson and E. C. Hildreth: *Comments on „Digital step edges from zero crossings of second directional derivatives".* IEEE Trans. Pattern Anal. Machine Intell., vol PAMI–7, no 1, pp. 121–127, Jan. 1985
4. *Multiresolution Image Processing and Analysis.* A Rosenfeld, ed., New York, Springer Verlag, 1984
5. *VLSI Image Processing.* R. J. Offen, ed., London, Collins Professional and Technical Books, 1985
6. R. M. Haralick, S. R. Sternberg and X. Zhuang: *Image analysis using mathematical morphology.* IEEE Trans. Pattern Anal. Machine Intell., vol PAMI–9, no 7, pp. 532–550, July 1987
7. J. Serra: *Introduction to mathematical morphology.* Comput. Vision, Graphics, Image Processing, vol. 35, pp. 283–305, Sept. 1986
8. F. Y. Shih and R. Mitchell: *Threshold decomposition of gray scale morphology into binary morphology.* IEEE Trans. Pattern Anal. Machine Intell., vol. PAMI–11, no 1, pp. 31–42, Jan. 1989
9. M. Chen and P. Yan: *A multiscaling approach based on morphological filtering.* IEEE Trans. Pattern Anal. Machine Intell., vol. PAMI–11, no 7, pp. 694–700, July 1989
10. S. G. Mallat: *A theory for multiresolution signal decomposition: the wavelet representation.* IEEE Trans. Pattern Anal. Machine Intell., vol. PAMI–11, no 7, pp. 674–693, July 1989
11. R. Nevatia and K. R. Babu: *Linear feature extraction and description.* Comput. Vision. Graphics, Image Processing, vol. 13, pp. 257–269, 1980
12. T. Pavlidis, S. L. Horowitz: *Segmentation of plane curves.* IEEE Trans. Comput., vol. C–23, no. 8, pp. 860–870, Aug. 1974
13. R. Horaud, T. Skordas: *Stereo correspondence through feature grouping and maximal cliques.* IEEE Trans. Pattern Anal. Machine Intell., vol. 11, no. 11, pp. 1168–1180, Nov. 1989
14. P. Maragos: *Pattern spectrum and multiscale shape representation.* IEEE Trans. Pattern Anal. Machine Intell., vol. 11, no. 7, pp. 701–716, July 1989
15. J. Biardzki, R. Musiał, T. Ostrowski, K. Wicyński: *System Przetwarzania Informacji Wizyjnej dla komputera klasy IMB PC–VIPS.* Komunikaty III Sympozjum Techniki Laserowej, str. 308–309, Szczecin, Zakład Poligraficzny Politechniki Szczecińskiej, 1990

T. OSTROWSKI, P. BAJKOWSKI, K. WICYŃSKI, R. MUSIAŁ

FEATURE DETECTION IN DIGITAL PICTURES USING IMAGE PROCESSING SYSTEM VIPS

Summary

In the domain of digital image processing, the crucial problem is the reduction of the informational content of the images for the purpose of application oriented feature detection. This paper concerns three methods of feature detection based on the Gaussian and morphological filtration, and space-frequency decomposition of 2D signal. The experiments with real and test images performed under Image Processing System VIPS are presented.

KWARTALNIK ELEKTRONIKI I TELEKOMUNIKACJI, 1991, 37, Z. 3–4, ss. 475–531

621.317.08

On the digital nonuniform sampling phase-locked loops in the presence of noise

MARIUSZ ŻÓŁTOWSKI

Instytut Telekomunikacji, Politechnika Gdańska

Recived 1990.10.12

Authorized 1991.01.18

Part I

The dynamics of the discrete-time phase-locked loop is considered in systematic way. The general expressions from which the basic parameters of the discrete-time phase-locked loops in the presence of noise are obtained have been derived. The Markov theory based approach is used together with ergodic theory. The different aspects of loop's dynamics are shown. The theoretical insight of this paper seems to be more complete as before. For example, the problem of evolution of the invariant measure under the increasing impact of noise while the chaotic phenomenon occurs in the deterministic case may interest the reader. The paper consists of two parts. Part I is devoted to the theory while Part II provides ilustrating examples.

1. INTRODUCTION

The dynamics of nonuniform sampling digital phase-locked loops in the presence of noise has been mainly considered in the papers of Weinberg and Liu [2], Lindsey and Chie [1,3]. Bitjucki and Serdiakov [7] Varanasi and Gupta [13] more recently. The continous state space of dynamics is of concern in the mentioned papers. The case of discrete state space while the effects of quantizations are taken into account has been considered by Holmes [5] Cessna and Levy [6], D'Andrea and Russo [4] first of all. It has been considered in [9] also. In this paper the expressions for the basic parameters of the discrete time phase-locked loops including the mean squared value of the steady state phase error process, the mean time to acquire, the mean time to skip the cycle and their variances are given. The problem is concerned within Markov approach together with ergodic one. The paper consists of two parts. Part I is devoted to the theory mainly while Part II provides numerical and computer modelling based results.

2. THE BASIC DEFINITIONS AND RELATIONS

Let X be the space equivalent to the space of states of the dynamical system and $\mathscr{B}_x$ the family of Borel subsets of X. Then the stochastic operator $P(x,A)$ acting upon $(X,\mathscr{B}_x)$; $x \in X$, $A \in \mathscr{B}_x$, is defined as follows:

1) $P(x, A)$ is a probabilistic measure of any $A \in \mathscr{B}_x$ for every $x \in X$

2) $P(x, A)$ is a measurable function of x in respect to $\mathscr{B}_x$ field for every fixed $A \in \mathscr{B}$. (1)

Normalized measure σ on $(X, \mathscr{B}_x)$ is called an invariant measure of stochastic operator P if

$$\sigma(A) = \int_X P(x, A)\, d\sigma(x) \quad \text{for any } A \in \mathscr{B}_x. \tag{2}$$

Now, let M stands for the set of sequences

$$M = \{ x = (\ldots, x_{-1}, x_0, x_1, \ldots,) : x_{i_1} \in C_1, \ldots, x_{i_r} \in C_r\} \tag{3}$$
$$1 \leqslant r < \infty,\ i_1, \ldots, i_r \text{ are integers and } C_1, \ldots, C_r \in \mathscr{B}_x.$$

The set

$$A = \{ x : x_i \in C_0, x_{i+1} \in C_1, \ldots, x_{i+r} \in C_r\} \tag{4}$$

is called a cylinder, $-\infty < i < \infty$, $r \geqslant 0$, $C_0, \ldots, C_r \in \mathscr{B}_x$.
Then the measure of any A is

$$\mu(A) = \int_{C_0} d\sigma(x_i) \int_{C_1} P(x_i, dx_{i+1}) \ldots \int_{C_r} P(x_{i+r-1}, dx_{i+r}). \tag{5}$$

This measure can be extended to M according to Kolmogorov theorem:
The measurable space $(M, \mathscr{B}_M, \mu)$ is obtained

$$(M, \mathscr{B}_M, \mu) = \bigtimes_{i=-\infty} (X, \mathscr{B}_x, \sigma)_i, \tag{6}$$

while product measure μ is generated by

$$\mu = \bigtimes_{n=-\infty}^{\infty} \sigma. \tag{7}$$

The measure μ is invariant while concerning any C because σ is invariant. Its extension is also invariant. The second meaning of invariant measure is the stationary one.

The dynamical system modelled as shift on $(M, \mathscr{B}_M, \mu)$ according to

$$\varphi(x_i) = x_{i+1},\ i = \ldots, -1, 0, 1, \ldots \tag{8}$$

is called the automorphism of Markov. The natural interpretation of $P(x,A)$ is as transition function in view of (1) to (8).
The transition function can be given in terms of its density;

$$P(x, A) = \int_A q(x, y)\,\mathrm{d}y. \tag{9}$$

The $\mathscr{B}_x$ measurable function satisfies

$$q(x, y) \geqslant 0, \qquad \int_X q(x, y)\,\mathrm{d}x = 1 \tag{10}$$

$x,y \in X$ and the integration is performed in respect to Lebesgue measure of space X, $\dim X=m$, $x=x^1,\ldots,x^m$.
The density of transition function in n steps can be given in reccurent form as

$$q^{(n)}(x, y) = \begin{cases} q(x, y) & n = 1 \\ \int_X q^{(n-1)}(z, y)\, q(x, z)\,\mathrm{d}z & n > 1. \end{cases} \tag{11}$$

Whereas the transition function in n steps or n-th iteration of stochastic operator P is

$$P^{(n)}(x, A) = \int_A q^{(n)}(x, y)\,\mathrm{d}y. \tag{12}$$

Generally the transition function in n steps satisfies the equation of Smoluchowski

$$P^{(k+m)}(x, A) = \int_A P^{(k)}(y, A)\, P^{(m)}(x, \mathrm{d}y) \tag{13}$$

$$k + m > 1,\ k \geqslant 1.$$

Suppose the initial density p of the point x_0 is given. Then the transition function in n steps is modified according to

$$P^{(n)}(x_0, A) \stackrel{df}{=} \int_X p(x)\, P^{(n)}(\mathrm{d}x, A), \quad n = 1,\ldots. \tag{14}$$

Moreover the density of the transition function in n steps is

$$q^{(n)}(x_0, y) \stackrel{df}{=} q^{(n)}(x, y)p(x), \quad \mathrm{n} = 1,\ldots \tag{15}$$

The expressions (14) and (15) define new function in terms of the previous ones. Also

$$\int_X p(x)\,\mathrm{d}x = 1\,. \tag{16}$$

Moreover the measure of any cylinder is not invariant in this case;

$$\sigma_0(x) = p(x)$$

and

$$\sigma_n(A) = \int_X P(x, A)\,\mathrm{d}\sigma_{n-1}(x) \tag{17}$$

according to the equation of Smoluchowski. Now the resulting cartesian measurable space is

$$(M, \mathscr{B}_M, \mu) = \overset{\infty}{\underset{n=0}{\mathrm{X}}} (X, \mathscr{B}_X, \sigma_n)_n \tag{18}$$

and the product measure μ is

$$\mu = \overset{\infty}{\underset{n=-\infty}{\mathrm{X}}} \sigma_n\,. \tag{19}$$

The shift on this space is known as Markov shift or discrete time stochastic Markov process, nonstationary generally.
If the state space X consists of N elements then A is an subset of the set of N elements. Suppose the probabilities $P_{x,y}$ are given

$$P_{x,y} \geqslant 0\,; \quad \sum_{y \in X} P_{x,y} = 1\,, \quad x \in X. \tag{20}$$

Then the transition function in one step is

$$P_{x,A} = \sum_{y \in A} P_{x,y}\,. \tag{21}$$

The discrete time counterpart of Smoluchowski equation is

$$P_{x,A}^{(k+m)} = \sum_{y \in A} P_{y,A}^{(k)}\, P_{x,y}^{(m)} \tag{22}$$
$$k + m > 1, \quad k \geqslant 1\,.$$

It gives the transition probability in $k+m$ steps in terms of the transition probabilities in k and m steps.
If $k+m=n$, $k=1$, $A=y$ then the resulting equation

$$P_{x,y}^{(n)} = \sum_{z \in X} P_{z,y} P_{x,z}^{(n-1)} \tag{23a}$$

$$P_{x,y}^{(1)} = P_{x,y}$$

is the discrete time counterpart of (11). Suppose the initial distribution of probability is given

$$P_{x_0} \geqslant 0, \qquad \sum_{x_0 \in X} P_{x_0} = 1. \tag{23b}$$

Then the new probability of transition in n steps is

$$P_{x_0,A}^{(n)} = \sum_{z_0 \in X} P_{z_0,A}^{(n)} P_{z_0} \tag{23c}$$

given in terms of previous one and the initial distribution of probability P_{x_0}. Markov process with the stete space X discrete is called a Markov chain. The invariant stationary probability P_x satisfies

$$P_x = \sum_{z \in X} P_{z,x} P_z, \qquad x \in X \tag{23d}$$

3. ON THE EXISTENCE OF INVARIANT MEASURES

The anticipation of the bahaviour of dynamical systems include the knoledge about their states while the discrete time n tends to infinity. This is called a steady state behaviour and its properties are usually specified in details. The steady state in Markov process case is considered in terms of the invariant, stationary distribution of probability. The conditions under which it is well established are of interest.

Theorem 1. Continous state space [10]

Given the family $\mathscr{B}_X \subset X$ of Borel sets. Suppose there exist
1) measure m: $0 < m(x) < \infty$
2) set $C \subset X$: $m(C) > 0$
3) constants; integer $m \geqslant 1$, $\delta > 0$ such that

$$q^m(x, y) \geqslant \delta \quad \text{if} \quad x \in X, \quad y \in C \subset X$$

$q^m(x,)$ stands for the density of probabilistic measure $P^{(m)}(x,)$ absolutely continous in measure m;

$$P^{(m)}(x, A) = \int_A q^{(m)}(x, y)\, \mathrm{d}m(y).$$

Then there exists stationary invariant distribution P of probability satisfying

$$P(A) \geqslant \delta m(A) \text{ for } A \subset C$$

and

$$|P^{(n)}(x, A) - P(A)| \leqslant (1 - \sigma m(C))^{\left(\frac{n}{m}\right)-1}, \quad n = 1,...$$

The set C of theorem 1 has the physical meaning of the set which is reachable within the finite number of steps. The proof of the theorem 1 is given in appendix 1.
The discrete state space counterpart of theoterm 1 is;

Theorem 2.

Suppose there is Markov chain of N states and the probabilities $P_{x,v}^{(m)}$ of transition in m steps are given. If there exist; integer $m \geqslant 1$ and set C of $M_c \geqslant 1$ elements y and

$$\min_{\substack{x \in X \\ y \in C}} P_{x,y}^{(m)} = \delta > 0$$

Then the stationary, invariant probability distribution P_x, $x \in X$ exists Moreover

$$\forall_{x} \in C,\ P_x \geqslant \delta$$

and

$$|P_{x,y}^{(n)} - P_x| \leqslant (1 - M\delta)^{\left(\frac{n}{m}\right)-1}, \quad n = 1,...$$
$$x \in X, \quad y \in C.$$

The meaning of set C is similar to that of theorem 1. It is the set of reachable states within the finite number of steps. The proof of theorem 2 is given in appendix 2.

4. SOME CONSEQUENCES OF THE EXISTANCE OF INVARIANT MEASURE

It is possible to consider the dynamical system from the ergodic point of view while the invariant measure exists.

Definition of the metrical system

Let $\varphi^{\alpha}: X \to X, \alpha \in \mathfrak{A}$ stands for the continous semigroup of measure preserving mappings [8,11]; ($\mathfrak{A}$ metrical semigroup with zero)

$$\forall_{\alpha \in \mathfrak{A}} \forall_{A \in \mathscr{B}_X} \mu(\varphi^{-\alpha}(A)) = \mu(A)$$

System $(X, \mathscr{B}_X, \mu, \varphi^{\alpha})$, X — space, $\mathscr{B}_X$ — family of Borel sets, μ — measure, φ^{α} — continous group of measure preserving mappings [8,11] is a metrical model of dynamical system.
One sets $\mathfrak{A} = Z^{+}$ (the set of nonnegative integers) and φ as a shift in the stochastic discrete time Markov process case.

The properties of the metrical systems are well characterized [8,11]

Theorem of Poincaré

Let $(X,\mathscr{B}_X,\mu,\varphi)$ is the metrical model of dynamical system and $A\subset\mathscr{B}_X,\mu(A)>0$. Then the set

$$B = \{x \in A: \varphi^n(x) \notin A,\ n = 1,2,\ldots\} \quad \text{is of zero measure.}$$

It means that the probability of not returning to any set A of positive measure is equal zero.

Theorem of Birkhoff [8]

Let $(X,\mathscr{B}_X,\mu,\varphi)$ be the metrical model of dynamical system. Then the series

$$\frac{1}{n}\sum_{k=o}^{n-1} f\circ\varphi^k(x) \text{ converges to } f^*(x) \text{ in } L^p(X,\mathscr{B}_X,\mu),$$

$p \geqslant 1$ for every $f \in L^p(X,\mathscr{B}_X,\mu)$.
The case while $p=1$ is called the individual one;

$$\int f^*\,d\mu = \int f\,d\mu \qquad \text{and} \qquad f^*\circ\varphi(x) = f^*(x).$$

Theorem of Bogolubov and Krylov [8,11]

Suppose X is a compact metric space and $\varphi: X \to X$ is a continous mapping. Then there exists φ — invariant probabilistic measure on X. The measure of the theorem of Bogolubov and Krylov concentrates on the set of nonwandering points only [8].

DEFINITION

The point $x \in X$ is a wandering point of diffeomorphism φ if it belongs to neighbourhood U and

$$\bigcup_{|n|>0} \varphi^n(U) \cap U = \Phi$$

A nonwandering point is this point which is not wandering. The set of nonwandering points is denoted as $\Omega(\varphi)$.

System for which the unique probabilistic measure exists is called unioqely ergodic. The next theorem characterizes this case.

Theorem [8,11]

Suppose μ is normalized, φ invariant measure of compact space X while φ is homeomorphism. Then the following statements are equivalent;

1) system (X, φ) is uniquely ergodic

2) If function f is continous on $X; f \in C(X)$ then

$$\lim_{n\to\infty}\frac{1}{n}\sum_{k=o}^{n-1} f(\varphi^k(x)) = \int_X f(x)\,d\mu \overset{df}{=} \mu(f)$$

for every $x \in X$.

3) If $f \in C(X)$ then

$$\frac{1}{n} \sum_{k=o}^{n-1} f(\varphi^k(x))$$

converge uniformly to $\mu(f)$.
Let us construct a measure of Bogolubov and Krylov theorem.
Suppose $\Omega(\varphi)$ consists of disjoint sets while X compact;

$$\Omega(\varphi) = \bigcup_k \Omega_k(\varphi) \tag{24}$$

while each of it is invariant under φ.
One can choose first

$$\operatorname{mes}(\Omega_k(\varphi)) = \operatorname{mes}(\mathscr{A}_k(\varphi))/\operatorname{mes}(X)$$

$$\mathscr{A}_k(\varphi) \stackrel{df}{=} \{x \in X: \operatorname{dist}(\varphi^n(x), \Omega_k(\varphi)) \underset{n\to\infty}{\to} 0\}$$

dist means the distance in the sense of Hausdorff.
Secondly, the measure $\operatorname{mes}(\Omega_k(\varphi))$ can be distributed uniformly on $\Omega_k(\varphi)$ if it consists of periodic orbit for example.
Thus the measure of $X \backslash \Omega(\varphi)$ is equal zero.
If $k > 1$ then the unique ergodicity does not occur obviously, for even the system is not ergodic at all in this case;

DEFINITION

System $(X, \mathscr{B}_X, \mu, \varphi)$ is the metrical model of ergodic dynamical system if

$$\varphi^{-\alpha}(A) \underset{\alpha \in \mathfrak{A}}{=} A \Rightarrow \mu(A) = 0 \quad \text{or } \mu(A) = 1$$

i.e the measure of any invariant sets under φ^α is either 1 or 0. Thus there is not trivial subsystem in this case.
The following theorem holds true in the ergodic case:

Theorem of Kac

Given ergodic system $(X, \mathscr{B}_X, \mu, \varphi)$. Let $A \in \mathscr{B}_X$, $\mu(A) > 0$ and B is the set of theorem of Poincaré.
Then

$$\underset{x \in A-B}{\forall} \int_A n(x)\,d\mu = 1$$

and $n(x)$ is the first time instant to return to A;

$$n(x) = \min\{n \geqslant 1: \varphi^n(x) \in A\}.$$

The proof this theorem is given in appendix 2.
It turns out that space X is compact while the synchronization system is considered. However the notion of covering space should be introduced. The result of covering represents itself a compact space.

DEFINITION

Suppose X and Y are topological spaces and Π: $Y \to X$ is a continous mapping. We call the mapping Π a covering if every $x_0 \in X$ belongs to neighbourhood U and $\Pi^{-1}(U)$ is a disjoint union of open subsets of Y. Moreover every subset of this union is mapped onto U by Π in homeomorphic way locally. Y is the covering space and X is the base one. Usually R^m is a covering space and torus $T^m = X_m S^1$ a base one in the case of discrete time phase-locked loop of m^{th} order. S^1 is a circule.

5. MEAN AND MEAN SQUARED VALUE IN STATIONARY STATE

Suppose the stationary distribution of probability is given. Then the mean value $m(x)$ and the variance $v(x)$ of the stationary state can be determined according to (dim $X=m$)

$$m(x) = \int_X x\, q(x)\, \mathrm{d}x, \tag{25}$$

$$v(x) = \int_X (x - m(x))^2\, q(x)\, \mathrm{d}x = \int_X x^2\, q(x)\, \mathrm{d}x - m^2(x). \tag{26}$$

This is the case of continous space while the stationary probability is given in terms of its density. Moreover

$$m_x = \sum_X x\, P_x \tag{27}$$

and

$$v_x = \sum_X (x - m_x)^2\, P_x = \sum_X x^2\, P_x - m_x^2 \tag{28}$$

in the discrete case of state space X. The stationary distribution is given in terms of probabilities P_x. The time instants of reaching any set will be considered further in the uniquely ergodic case.

6. MEAN NUMBER AND VARIANCE OF MEAN NUMBER OF STEPS TO REACH THE ABSORBING SET

Suppose $x_0 \in X$ ($\dim X = m$) is an initial state. Let $A_s \subset (X)$ stands for the absorbing set and $q(x_0, z)$ for the density of transition from x_0 to z in one step. On the other hand let $Q_k(x_0)$ stands for the probability of abosorbtion in step k from the initial state x_0. Then

$$Q_0(x_0) = 0 \qquad \left(x_0 \in X \backslash A_s\right) \tag{29}$$

$$Q_1(x_0) = 1 - \int_{X \backslash A_s} q(x_0, z)\,\mathrm{d}z \tag{30}$$

and

$$Q_{k+1}(x_0) = \int_{X \backslash A_s} q(x_0, z)\, Q_k(z)\,\mathrm{d}z, \quad k = 1, 2, 3, \ldots \tag{31}$$

This is for continous space X. Whereas for the discrete counterpart;

$$Q^0_{x_0} = 0, \qquad x \in X \backslash A_s \tag{32}$$

$$Q^1_{x_0} = 1 - \sum_{z \in X \backslash A_s} P_{x_0, z} \tag{33}$$

and

$$Q^{k+1}_{x_0} = \sum_{z \in X \backslash A_s} P_{x_0, z}\, Q^k_z \tag{34}$$

Q_z^k of (32–34) $k=0,1,\ldots$ stands for the probability of absorbing in step k while the z state initial, wheras $P_{x_0,z}$ for the transition probability in one step from x_0 to z.

The relations (29)–(31) and (32)–(34) make the calculations of the probability of absorbtion in subsequent doiscrete time steps possible. Let us find the mean number of steps and its variance to reach the absorbing set.

Let

$$Q(\mathscr{x}, x_0) \overset{\mathrm{df}}{=} \sum_{n=o}^{\infty} Q_n(x_o)\, \mathscr{x}^{-n} = \mathscr{Z}\{Q_n(x_o)\} \tag{35a}$$

and

$$Q_{x_0,}(\mathscr{x}) \overset{\mathrm{df}}{=} \sum_{n=0}^{\infty} Q_{x_0}{}^n\, \mathscr{x}^{-n} = \mathscr{Z}\{Q^n_{x_0}\} \tag{35b}$$

$\mathscr{Z}$ – stands for $\mathscr{Z}$– Laurent transformation.

If

$$0 < \epsilon_1 \leqslant \int_{X \setminus A_s} q(x_0, z)\,dz \leqslant 1 - \epsilon_2 < 1 \tag{36a}$$

and

$$0 < \epsilon_1 \leqslant \sum_{z \in X \setminus A_s} P_{x_0,z} \leqslant 1 - \epsilon_2 < 1 \tag{36b}$$

then the series of (35) and (36) are uniformly bounded by the power series including $|z|=1$.

It may be proved (see appendix 3) that the mean number of steps to absorbtion $m_1(x_0)$ (m_{1x_0}) satisfy the equations ;

$$m_1(x_0) - \int_{X \setminus A_s} q(x_0, z)\, m_1(z)\,dz = 1 \tag{37a}$$

$$m_1(x_0) \stackrel{\text{df}}{=} \sum_{k=0}^{\infty} k\, Q_k(x_0)$$

$$m_{1,x_0} - \sum_{z \in X \setminus A_s} P_{x_0,z}\, m_{1,z} = 1 \tag{37b}$$

$$m_{1,x_0} \stackrel{\text{df}}{=} \sum_{k=0}^{\infty} k\, Q^k(x_0),$$

while x_0 is the initial state ($x_0 \in X \setminus A_s$).

The first equation refers to the continous space while the discrete space is of concern in the second one.

On the other hand the mean square numbers of steps to absorbtion

$$m_2(x_0) \stackrel{\text{df}}{=} \sum_{k=0}^{\infty} k^2\, Q_k(x_0) \tag{38a}$$

$$m_{2,x_0} \stackrel{\text{df}}{=} \sum_{k=0}^{\infty} k^2\, Q^k_{x_0} \tag{38b}$$

satisfy the following equations respectively (see appendix 3);

$$m_2(x_0) - \int_{X \setminus A_s} q(x_0, z)\, m_2(z)\,dz = 2m_1(x_0) - 1 \tag{39a}$$

$$m_{2,x_0} - \sum_{z \in X \setminus A_s} P_{x_0,z}\, m_{2,z} = 2m_{1,x_0} - 1. \tag{39b}$$

The variances of the number of steps to absorbtion are given by

$$v(x_0) \stackrel{\text{df}}{=} m_2(x_0) - m_1(x_0)^2 \tag{40a}$$

$$v_{x_0} \stackrel{\text{df}}{=} m_{2,x_0} - m_{1,x_0}^2 \tag{40b}$$

The expressions given in this chapter are valid for the state space X of any dimension.

7. MEAN AND MEAN SQUARE NUMBER OF STEPS TO REACH A SUBSET OF ABSORBING SET

Mean and mean square number of steps to reach a subset of absorbing set may be of interest in some applications. Suppose $x_0 \in X$ is an initial state and the absorbing set A_s is a disjoint union of sets A_s^i, $i=1.....P$;

$$A_s = \bigcup_{i=1}^{P} A_s^i \quad \text{and} \quad A_s^i \bigcap_{i \neq j} A_s^i = \Phi. \tag{41}$$

Let $q(x_0, z)$ stand still for the density of transition from x_0 to z in one step. On the other hand $Q_k^i(x_0)$ stands for the probability of absorbtion in k step by the set A_s^i from the initial state x_0.
Then

$$Q_0^i(x_0) = 0, \qquad x_0 \in X \backslash A_s \tag{42a}$$

$$Q_1^i(x_0) = 1 - \int_{X \backslash A_s^i} q(x_0, z)\,\mathrm{d}z \tag{42b}$$

and

$$Q_{k+1}^i(x_0) = \int_{X \backslash A_s} q(x_0, z)\, Q_k^i(z)\,\mathrm{d}z \tag{42c}$$

$$k = 1, 2, 3, \ldots, \qquad i = 1, 2, 3, \ldots, P.$$

The discrete counterparts of (42) are;

$$Q_{x_0}^{i,o} = 0, \qquad x_0 \in X \backslash A_s \tag{43a}$$

$$Q_{x_0}^{i,1} = 1 - \sum_{z \in X \backslash A_s^i} P_{x_0,z} \tag{43b}$$

$$Q_{x_0}^{i,k+1} = \sum_{z \in X \backslash A_s} P_{x_0,z}\, Q_z^{i,k} \tag{43c}$$

$$i = 1, \ldots, P, \qquad k = 1, 2, 3, \ldots$$

$Q_{x_0}^{i,k}$ of (43) stands for the probability of absorbtion in step k from the initial step x_0. The following equations have been obtained from (42) and (43) to characterize this case in terms of the notions of the previous chapter (see appendix 4). For the probabilities
$P_a^i(x_0)$ (P_{a,x_0}^i) of absorbtion by set A_s^i from x_0;

$$P_a^i(x_0) - \int_{X\setminus A_s} q(x_0, z) P_{a,i}(z)\,dz = 1 - \int_{X\setminus A_s^i} q(x_0, z)\,dz \tag{44a}$$

and

$$P_{a,x_0}^i - \sum_{z\in X\setminus A_s} P_{x_0,z} P_{a,z}^i = 1 - \sum_{z\in X\setminus A_s^i} P_{x_0,z} \qquad i = 1, \ldots, P \tag{44b}$$

For the mean number of steps $m_1^i(x_0)$ (m_{1,x_0}^i) to absorbtion by set A_s^i from the initial state x_0;

$$m_1^i(x_0) - \int_{X\setminus A_s} q(x_0, z) m_1^i(z)\,dz = 1 - \int_{X\setminus A_s^i} q(x_0, z)\,dz + \int_{X\setminus A_s} q(x_0, z) P_a^i(z)\,dz \tag{45a}$$

and

$$m_{1,x_0}^i - \sum_{z\in X\setminus A_s} m_{1,z}^i P_{x_0,z} = 1 - \sum_{z\in X\setminus A_s^i} P_{x_0,z} + \sum_{z\in X\setminus A_s} P_{x_0,z} P_{a,z}^i \tag{45b}$$

$$i = 1, \ldots, P.$$

Finally the mean square numbers of steps $m_2^i(x_0)$, m_{2,x_0}^i to absorbtion by set A_s^i satisfy

$$m_2^i(x_0) - \int_{X\setminus A_s} q(x_0, z) m_2^i(z)\,dz = m_1^i(x_0) + \int_{X\setminus A_s^i} q(x_0, z) m_1^i(z)\,dz \tag{46a}$$

and

$$m_{2,x_0}^i - \sum_{z\in X\setminus A_s} P_{x_0,z} m_{2,z}^i = m_{1,x_0}^i + \sum_{z\in X\setminus A_s^i} P_{x_0,z} m_{1,z}^i . \tag{46b}$$

Suppose the density p of the initial x_0 is given. Then the all parameters depedent on x_0 can be weighted by this density and the mean parameters not depedent on x_0 are immediatly obtained in Markov case this way. Before the concrete examples of practical interest are presented in part II of this paper some general considerations will be given in next chapter.

8. DYNAMICS OF THE SYNCHRONIZATION SYSTEM IN THE PRESENCE OF NOISE

Let us try to consider the dynamics without and with noise with the attention focussed on the distribution of invariant measure. A measure of Krylov and Bogolubov theorem is given in previous chapter. Before starting with the problem what happens to that measure under the impact of noise let us proceed with some

additional notions. The problem just adressed can be considered in parallel with the discussion on the concept of attractor [12]. Not giving own definition one can postulate that some kind of invariance under the impact of noise should be taken into good account perhaps while the attractor is to be revelated from the set of nonwandering points.

Definition of orbital stability or Lapunov stability [12]

Suppose the mapping $\varphi: X \to X$ is continous and $\Omega_K(\varphi)$ is a disjoint subset of the set $\Omega(\varphi)$ of nonwandering points of φ,

$$\varphi(\Omega_k(\varphi)) = \Omega_k(\varphi)$$

1) Then $\Omega_k(\varphi)$ is Lapunov stable if it has arbitrary small neighbourhoods U: $\varphi(U) \subset U(\Omega_k(\varphi) \subset U)$
2) It is asymptotically stable if it is Lapunov stable and also satisfies the Auslander – Bhatia – Seibert condition [12];

The set $\{x \in X: \varphi^{k_n}(x) \subset \Omega_k(\varphi)\}$ is an open set.

In other words

$$\Omega_k(\varphi) = \bigcap_{n=0} \varphi^n(U); \quad \varphi^0(U) \stackrel{\text{df}}{=} U$$

Moreover the dynamics of any system under the model of Markov is given in terms of the semigroup of stochastic Markov operators;

$$P_{n+m} = P_m \circ P_n, \quad n \geqslant 1, m \geqslant 1 \tag{47}$$

according to the equation of Smoluchovski.
Now if the semigroup φ^α of continous mappings forms a topological model of dynamical system without disturbing noise then it is the limiting case while the impact of noise tends to zero.

DEFINITION 8

A couple (φ, M), M manifold and $\varphi: M \to M$ diffeomorphism is the topological model of axiom A system if
1) $\Omega(\varphi)$ is a hiperbolic set i.e tangent bundle $T(M)|_{\Omega(\varphi)}$ follows the partition

$$T(M)|_{\Omega(\varphi)} = E^+ \oplus E^-$$

$d\varphi: E^+ \to E^-$ is contracting whereas $d\varphi: E^- \to E^-$ is expanding
2) periodic points are dense in $\Omega(\varphi)$.
Thus every $\Omega_k(\varphi)$ of partition (24) Lapunov stable is asymptotically stable in the axiom A case.

Common observation is that the measure of Krylov, Bogolubov theorem constructed in previous chapter is affected under the model of Markov in the following way:

1) Invariant, stationary measure of stochastic operator P of system under the presence of noise concentrates around $\Omega_k(\varphi)$ Lapunov stable in noiseless case (Axiom A system with the state space X compact).

2) The effect of noise can make the system uniquelly ergodic if its impact is strong enough. Truncated distributions assumed due to the finite peak value property to get consistency in this case.

3) The rate of convergence to stationary case uniquely ergodic one depends on parameter δ of theorem 1 and 2 and is greater while the impact of noise is greater.

However, smooth model is valid in the case of synchronization system while the quantization effect are either negligible or are accounted for in terms of additional noise, called the quantization one. Secondly the model in terms of Markov chain (the state space discrete in quantized case) is ill conditioned from the computational point of view while the impact of noise tends to zero. The noiseless model is suitable in this case. Suppose the stationary distribution of probability is given in the uniquely ergodic case. Then the absorbtion by any set A_s^i can be considered qualitively according to the theorem of Poincaré. The absorbing set A_s^i is used to model the cycle slipping or acquistion phenomena in the presence of noise [1,2,3,4,5,6,7,9]. The compact state space X of the synchronization system is the base space of the operation of covering [8]. This formal operation follows the physical meaning of the state of synchronization system given in terms of instantenous phase error or phase error shortly in view of its cyclic nature. The mean time to return to set A is

$$\bar{n} = \int_A \frac{n(x)\,\mathrm{d}P}{\int_A \mathrm{d}P}, \quad \bar{n} = \frac{\sum_{x\in A} n(x)\,P_x}{\sum_{x\in A} P_x} \tag{48a}$$

while P of (48a) stands for stationary measure.
In view of Kac theorem

$$\bar{n} = \frac{1}{\int_A \mathrm{d}P} \quad \text{or} \quad \bar{n} = \frac{1}{\sum_{x\in A} P_x} \tag{48b}$$

Thus the distribution of stationary, invariant measure can provide information about qualitative behaviour of synchronization system.
Obviously the high concentration of probabilistic around the state of phase entrainment means the very short time to return from the state of cycle slipping and vice versa. The expressions (48) can be useful for estimations. The detailed analysis however should follow the results of chapter VI. Finally due to one input one output property of the digital phase locked loop the distribution of probability on the base space $X = T^n$ can be reduced to marginal one on the S^1 – circle space in the case of loop of any order. See for example the paper of Weinberg and Liu [2] for the second order case.

CONCLUSIONS

The dynamics of discrete-time phase – locked loop can be well characterized within the notions of the general theory of dynamical systems including ergodic approach.

The Markov model is useful to derive the expressions for basic parameters of the phase-locked loop under the impact of noise. However it is feasible for simpler nevertheless important cases only [1,2,3] just like ones to be considered in Part II.

The computer based modelling is advantageous for every detailed cases and is well established while the ergodic properties occur. Some expressions being derived while concerning the parameters in Markov case have not been found by the author elsewhere and seems to be new. The transition from probabilistic measure in noiseless case to the one of disturbed by noise can be complicated. It may conserve the most of properties of the noiseless case on first stage and leads tosthe uniquely ergodic case while the impact of noise is strong. This latter limit case occurs near treshold in synchronization systems.

The existence of chaotic transient hang up phenomenon in the loop of second order may be of interest. It is considered in Part II. Just the transition from noiseless case to disturbed by noise one is characterized.

The convergence to steady state distribution depends on the mixing properties of system under consideration [11].

REFERENCES

1. W. C. Lindsey, C. M. Chie: *A survey of digital phase-locked loops.* Proc. IEEE, vol. 69, no 4, April, pp. 410–431, 1981
2. A. Weinberg, B. Liu: *Discrete time analysis of nonuniform sampling first and second-order digital phase locked loops.* IEEE Trans. Commun., vol. COM–22, no 2, pp. 123–137, February, 1974
3. W. C. Lindsey, C. M. Chie: *Acquisition behaviour of a first-order digital phase-locked loop.* IEEE Transactions on Communications, vol. COM–26, no 9, pp. 1364–1367, Sept., 1978
4. N. A. D' Andrea, F. Russo: *Multilevel quantized DPLL behaviour with phase and frequency step plus noise input.* IEEE Transactions on Communications, vol. COM–28, no 3, pp. 1373–1381, August, 1980
5. J. K. Holmes: *Performance of a first-order transition sampling digital phase-locked loop using random – walk models.* IEEE Transactions on communications, vol. COM–20, no 2, pp. 94–104, April, 1972
6. J. K. Cessna, D. M. Levy: *Phase and transient times for a binary quantized digital phase – locked loop in white gaussian noise.* IEEE Transactions on Communications, vol. COM–20, no 2, pp. 94–104, April, 1972
7. W. I. Bitjucij, P. N. Sierdiukóv: *Ocenka vriemieni do zryva sinchronizma v impulsnoj sistemie FAPCZ.* Radiotechnika, pp. 95–97, 1973
8. W. Szlenk: *Wstęp do teorii gładkich układów dynamicznych.* Warszawa: PWN, 1982
9. M. Żółtowski: *O śledzeniu zakłóconego przebiegu sinusoidalnego przy pomocy cyfrowej pętli fazowej I – rzędu z dwuwartościową korekcją fazy.* Rozprawy Eletrotechniczne, 1983, 29, zesz 1, ss. 201–216
10. J. L. Doob: *Stochastic Processes,* New York, 1953
11. S. W. Fomin, I. P. Kornfeld, J. G. Sinaj: *Teoria ergodynamiczna.* Warszawa: PWN, 1987
12. J. Milnor: *On the concept of Attractor.* Commun. Math. Phys., pp. 177–195, 99, 1985
13. S. V. Varanasi, S. C. Gupta: *Random phase tracking of nonuniformly sampled signals.* ICASSP 83, Boston, pp. 699–702

APPENDIX 1

THE PROFF OF THEOREM 1 [10]

Let $E \subset C \subset X$ and

$$m_E^{(m)} = \inf_X P^{(m)}(x, E) \tag{A1-1}$$

$$M_E^{(m)} = \sup_X P^{(m)}(x, E). \tag{A1-2}$$

Then

$$P^{(m+1)}(x, E) = \int_X P^{(m)}(y, E) P(x, \mathrm{d}y)$$

$$\leqslant \sup_y P^{(m)}(y, E) \int_X P(x, \mathrm{d}y) = M_E^m. \tag{A1-3}$$

Also

$$P^{(m+1)}(x, E) \geqslant \inf_y P^{(m)}(y, A) \int_X P(x, \mathrm{d}y) = m_E^{(m)}. \tag{A1-4}$$

From (A1-3) and (A1-4)

$$M_E^{(m+1)} \leqslant M_E^{(m)} \quad \text{and} \tag{A1-5}$$

$$m_E^{(m+1)} \geqslant m_E^{(m)}. \tag{A1-6}$$

Thus

$$m_E^{(1)} \leqslant m_E^{(2)} \leqslant \ldots \leqslant \ldots \leqslant M_E^{(2)} \leqslant M_E^{(1)}. \tag{A1-7}$$

Moreover

$$\psi(E) = \sup_{x \in X} P^{(m)}(x, E) - \sup_{y \in X} P^{(m)}(y, E) \tag{A1-8}$$

is an additive function of set E.
Then there exists Hahn partition $S^+ \cup S^-$ of the space X;

$$S^+ \cup S^- = X; \quad S^- = CS^+ \tag{A1-9}$$

C stands for complement.

$$\psi(E) \geqslant 0 \quad \text{for any} \quad E \subset S^+ \subset \mathscr{B}_X$$

$$\psi(E) \leqslant 0 \quad \text{for any} \quad E \subset S^- \subset \mathscr{B}_X$$

Also

$$\psi(S^+) + \psi(S^-) = \psi(S^+) + \psi(X \setminus S^+) = 0 \tag{A1-10}$$

Next

$$\psi(S^+) = P^{(m)}(x, S^+) - P^{(m)}(y, S^+) = 1 - P^{(m)}(x, S^-) - P^{(m)}(y, S^+) =$$

$$= 1 - \int_{S-} q^{(m)}(x, z)\, m(\mathrm{dz}) - \int_{S+} q^{(m)}(y, z)\, m(\mathrm{dz})$$

$$\leqslant 1 - \delta m(C). \qquad \text{(A1-11)}$$

Moreover

$$M_E^{(m+n)} - m_E^{(m+n)} = \sup_x \int_X P^{(n)}(z, E)\, P^{(m)}(x, \mathrm{dz}) - \inf_y \int_X P^{(n)}(z, E)\, P^{(m)}(y, \mathrm{dz}) =$$

$$= \sup_{x,\, y} \int_X P^{(n)}(z, E)\, \psi(\mathrm{dz}) = \sup_{x,\, y} \left(\int_{S+} P^{(n)}(z, E)\, \psi(\mathrm{dz}) + \int_{S-} P^{(n)}(z, E)\, \psi(\mathrm{dz}) \right) \leqslant$$

$$\leqslant \sup_{x,\, y} \left(\int_{S+} M_E^{(n)}\, \psi(\mathrm{dz}) + \int_{S-} m_E^{(n)}\, \psi(\mathrm{dz}) \right) = \sup_{x,\, y} \psi(S^+)\,(M_E^{(n)} - m_E^{(n)}) \leqslant$$

$$\leqslant (1 - \delta m(C))\,(M_E^{(n)} - m_E^{(n)}), \qquad \text{(A1-12)}$$

$$M_E^{(m)} - m_E^{(m)} = \sup_{x,\, y} \{P^{(m)}(x, E) - P^{(m)}(y, E)\} = \sup_{x,\, y} \psi(E) \leqslant \sup_{x,\, y} \psi(S^+) \leqslant$$

$$\leqslant 1 - \delta \mathrm{m}(C). \qquad \text{(A1-13)}$$

From (A1-13) and (A1-12):

$$M_E^{(km)} - m_E^{(km)} \leqslant M_E^{(m+(k-1)m)} - m_E^{(m+(k-1)m)} \leqslant (1 - \delta m(\mathrm{C}))(M_E^{(k-1)m} - m_E^{(k-1)m}) \leqslant$$

$$\leqslant (1 - \delta m(C))^2\,(M_E^{(k-2)m} - m_E^{(k-2)m}) \leqslant (1 - \delta m(C))^{k-1}\,(M_E^{(m)} - m_E^{(m)})$$

$$\leqslant (1 - \delta m(C))^k. \qquad \text{(A1-14)}$$

Now it follows that $M_E^{(n)}$ and $m_E^{(n)}$ tend to the limit $P(E)$ while $n \to \infty$ because

$$|P^{(n)}(x, E) - P(E)| \leqslant M_E^{(n)} - m_E^{(n)} \leqslant (1 - \delta m(C))^{\left(\frac{n}{m}\right)^{-1}} \underset{n \to \infty}{\to} 0. \qquad \text{(A1-15)}$$

If $B \subset C$ then

$$P(B) \geqslant m_B^{(m)} \geqslant \delta m(B), \qquad \text{(A1-16)}$$

because

$$m_B^{(m)} = \inf_{x \in X} P^{(m)}(x, B) = \inf_{x \in B} \int_B q^{(m)}(x, y)\, \mathrm{dm}(y) \geqslant \delta m(B) \qquad \text{(A1-17)}$$

Thus function P takes nonnegative values and $P(x)=1$. It is also additive whilebeing the limit of iniformly convergent series of additive function Eventually it is a probabilistic measure. Taking the limit in

$$P^{(m+n)}(x, E) = \int_X P^{(m)}(y^E) P^{(n)}(x, \mathrm{d}y), \tag{A1-18}$$

while $n \to \infty$ one gets

$$P(E) = \int_X P^{(m)}(y, E) P(\mathrm{d}y) = \int_X P^{(m)}(y, E) p(y) \mathrm{d}y. \tag{A1-19}$$

This last equation shows that P is invariant, stationary distribution of probability. Its density satisfies

$$p(x) = \int_X q^{(m)}(y, x) p(y) \mathrm{d}y. \tag{A1-20}$$

APPENDIX 2

THE PROOF OF THEOREM 2 [10]

Let

$$m_y^{(m)} = \min_x P_{x,y}^{(m)} \quad \text{and} \quad M_y^{(m)} = \max_x P_{x,y}^{(m)}. \tag{A2-1}$$

Then

$$m_y^{(m+1)} = \min_x \sum_z P_{z,y}^{(m)} P_{x,z} \geqslant \min_x \sum_z m_y^{(m)} P_{x,z} = m_y^{(m)} \tag{A2-2}$$

$$M_y^{(m+1)} = \max_x \sum_z P_{z,y}^{(m)} P_{x,z} \leqslant \max_x \sum_z M_y^{(m)} P_{x,z} = M_y^{(m)}. \tag{A2-3}$$

Thus

$$m_y^{(1)} \leqslant m_y \leqslant \ldots \leqslant M_y^{(2)} \leqslant M_y^{(1)}. \tag{A2-4}$$

Next the sets S^+ and S^- can be defined for any x, x' from X.

$$S^+ = \{ z \in X: P_{x,z}^{(m)} \geqslant P_{x',z}^{(m)} \} \tag{A2-5}$$

$$S^- = \{ z \in X: P_{x,z}^{(m)} < P_{x',z}^{(m)} \}. \tag{A2-6}$$

Of course

$$\sum_{z\in S^+}(P^{(m)}_{x,z} - P^{(m)}_{x',z}) + \sum_{z\in S^-}(P^{(m)}_{x,z} - P^{(m)}_{x',z}) = 0. \tag{A2-7}$$

If M_+ elements of set C belong to set S^+ then

$$\sum_{z\in S^+}(P^{(m)}_{x,z} - P^{(m)}_{x',z}) \leqslant \sum_{z\in S^+} P^{(m)}_{x,z} - M_+\delta =$$

$$= 1 - \sum_{z\in S^-} P^{(m)}_{x,z} - M_+\delta \leqslant 1 - (M - M_+)\delta - M_+\delta = 1 - M\delta. \tag{A2-8}$$

The last relations are useful in further estimations:

$$M^{(n+m)}_y - m^{(n+m)}_y = \max_x \sum_z P^{(n)}_{z,y} P^{(m)}_{x,z} - \min_{x'} \sum_z P^{(n)}_{z,y} P^{(m)}_{x',z} =$$

$$= \max_{x,\ x'} \sum_z P^{(n)}_{z,y}(P^{(m)}_{x,z} - P^{(m)}_{x',z}) \leqslant$$

$$\leqslant \max_{x,\ x'} \left\{ \sum_{z\in S^+} M^{(n)}_y (P^{(m)}_{x,z} - P^{(m)}_{x',z}) + \sum_{z\in S^-} m^{(n)}_y (P^{(m)}_{x,z} - P^{(m)}_{x',z}) \right\} \leqslant$$

$$\leqslant (1 - M\delta)(M^{(n)}_y - m^{(n)}_y). \tag{A2-9}$$

(A2-7)
(A2-8)

Also

$$M^{(m)}_y - m^{(m)}_y = \max_{x,\ x'} (P^{(m)}_{x,y} - P^{(m)}_{x',y}) \leqslant$$

$$\leqslant \sum_{z\in S^+} (P^{(m)}_{x,y} - P^{(m)}_{x',y}) \underset{(A2-9)}{\leqslant} 1 - M\delta. \tag{A2-10}$$

Thus

$$M^{(km)}_y - m^{(km)}_y \leqslant (1 - M\delta)^k. \tag{A2-11}$$

Eventually $M^{(n)}_y$ and $m^{(n)}_y$ tend while $n \nearrow \infty$ to the common limit P_y which is invariant, and stationary distribution of probability; (n>m)

$$|P^{(n)}_{x,y} - P_y| \leqslant M^{(n)}_y - m^{(n)}_y \leqslant (1 - M\delta)^{\left(\frac{n}{m}\right)^{-1}} \tag{A2-12}$$

and

$$\underset{y\in C}{\forall} P_y \geqslant m^{(m)}_j = \min_x P^{(m)}_{x,y} = \delta > 0.$$

APPENDIX 3

THE PROOF OF THE THEOREM OF KAC

Let

$$A_n = \{ x \in A \setminus B : n(x) = n \} . \tag{A3-1}$$

Then the sets
$\varphi^k(A_n)$, $n = 1,\ldots\ 0 \leqslant k < n$ are disjoint and

$$\bigcup_{n \geqslant 0} \varphi^n(A) = \bigcup_{n \geqslant 1} \bigcup_{k=0}^{n-1} \varphi^k(A_n) . \tag{A3-2}$$

Thus

$$\mu\left(\bigcup_{n \geqslant 0} \varphi^n(A) \right) = \sum_{n=1}^{\infty} \sum_{k=0}^{n-1} \mu(\varphi^k(A_n)) = \sum_{n=1}^{\infty} n\mu(A_n) = 1 \tag{A3-3}$$

at view of ergodicity.

APPENDIX 4

MEAN AND MEAN SQUARE NUMBER OF STEPS TO ABSORBTION

While calculating the derivatives of the series of (35) one obtains

$$\frac{\partial Q(z,\ x_0)}{\partial z} = -\sum_{n=0}^{\infty} n Q_n(x_0)\ z^{-n-1} \tag{A4-1a}$$

$$\frac{\partial^2 Q(z,\ x_0)}{\partial z^2} = \sum_{n=0}^{\infty} (n+1) n Q_n(x_0)\ z^{-(n+2)} \tag{A4-2a}$$

and

$$\frac{\partial Q_{x_0}(z)}{\partial z} = -\sum_{n=0}^{\infty} n Q_{x_0}^n\ z^{-n-1} \tag{A4-1b}$$

$$\frac{\partial^2 Q(z,\ x_0)}{\partial z^2} = \sum_{n=0}^{\infty} (n+1) n Q_{x_0}^n\ z^{-n-1} . \tag{A4-2b}$$

In view of (A3-1)

$$m_1(x_0) = -\left. \frac{\partial Q(z,\ x_0)}{\partial z} \right|_{z=1} \tag{A4-3a}$$

$$m_{1,x_0} = -\left. \frac{\partial Q_{x_0}(z)}{\partial z} \right|_{z=1} \tag{A4-3b}$$

and

$$m_2(x_0) = \left.\frac{\partial^2 Q(\mathrm{z}, x_0)}{\partial \mathrm{z}^2}\right|_{\mathrm{z}=1} - m_1(x_0) \tag{A4-4a}$$

$$m_{2,x_0} = \left.\frac{\partial^2 Q(z, x_0)}{\partial \mathrm{z}^2}\right|_{z=1} - m_{1,x_0}. \tag{A4-4b}$$

Moreover according to (29)–(31)

$$Q(\mathrm{z}, x_0) = \sum_{k=0}^{\infty} Q_k(x_0)\,\mathrm{z}^{-k} =$$

$$= \left(1 - \int_{X\setminus A_z} q(x_0, z)\,\mathrm{d}z\right)\mathrm{z}^{-1} + \sum_{k=2}^{\infty} \int_{X\setminus A_z} q(x_0, z)\,Q_{k-1}(z)\,\mathrm{z}^{-k}\,\mathrm{d}z =$$

$$= \left(1 - \int_{X\setminus A_z} q(x_0, z)\,\mathrm{d}z\right)\mathrm{z}^{-1} + \mathrm{z}^{-1} \int_{X\setminus A_z} q(x_0, z) \sum_{k=1}^{\infty} Q_k(z)\,\mathrm{z}^{-k}\,\mathrm{d}z =$$

$$= \left(1 - \int_{X\setminus A_z} q(x_0, z)\,\mathrm{d}z\right)\mathrm{z}^{-1} + \mathrm{z}^{-1} \int_{X\setminus A_z} q(x_0, z)\,Q(\mathrm{z}, z)\,\mathrm{d}z \tag{A4-5a}$$

Whereas for the discrete state space

$$Q_{x_0}(\mathrm{z}) = \left(1 - \sum_{z\in X\setminus A_z} P_{x_0,z}\right)\mathrm{z}^{-1} + \mathrm{z}^{-1} \sum_{z\in X\setminus A_z} P_{x_0,z}\,Q_z(\mathrm{z}). \tag{A4-5b}$$

Next

$$\frac{\partial Q(\mathrm{z}, x_0)}{\partial \mathrm{z}} = -\left(1 - \int_{X\setminus A_z} q(x_0, z)\,\mathrm{d}z\right)\mathrm{z}^{-2} +$$

$$- \mathrm{z}^{-2} \int_{X\setminus A_z} q(x_0, z)\,Q(\mathrm{z}, z)\,\mathrm{d}z + \mathrm{z}^{-1} \int_{X\setminus A_z} q(x_0, z)\,\frac{\partial Q(\mathrm{z}, z)}{\partial \mathrm{z}}\,\mathrm{d}z \tag{A4-6a}$$

and

$$\frac{\partial Q_{x_0}(\mathrm{z})}{\partial \mathrm{z}} = -\left(1 - \sum_{z\in X\setminus A_z} P_{x_0,z}\right)\mathrm{z}^{-2} - \mathrm{z}^{-2} \sum_{z\in X\setminus A_z} P_{x_0,z}\,Q_z(\mathrm{z}) +$$

$$+ \mathrm{z}^{-1} \sum_{z\in X\setminus A_z} P_{x_0,z}\,\frac{\partial Q_z(\mathrm{z})}{\partial \mathrm{z}}. \tag{A4-6b}$$

In view of (A4–3) and (A4–6):

$$m_1(x_0) - \int_{X\setminus A_s} q(x_0, z)\, m_1(z)\, dz = 1 \tag{A4-7a}$$

$$m_{1,x_0} - \sum_{z\in X\setminus A_s} P_{x_0,z}\, m_{1,z} = 1. \tag{A4-7b}$$

Now calculating the second derivatives of (A4-6) in respect to $\mathscr{x}$ variable one gets

$$\frac{\partial^2 Q(\mathscr{x}, x_0)}{\partial \mathscr{x}^2} = 2\left(1 - \int_{X\setminus A_s} q(x_0, z)\, dz\right)\mathscr{x}^{-3} +$$

$$+ 2\mathscr{x}^{-3} \int_{X\setminus A_s} q(x_0, z)\, Q(z, \mathscr{x})\, dz - \mathscr{x}^{-2} \int_{X\setminus A_s} q(x_0, z) \frac{\partial}{\partial \mathscr{x}} Q(\mathscr{x}, z)\, dz +$$

$$- \mathscr{x}^{-2} \int_{X\setminus A_s} q(x_0, z) \frac{\partial Q(\mathscr{x}, z)}{\partial \mathscr{x}} dz + \mathscr{x}^{-1} \int_{X\setminus A_s} q(x_0, z) \frac{\partial^2 Q(\mathscr{x}, z)}{\partial \mathscr{x}^2} dz \tag{A4-8a}$$

and

$$\frac{\partial^2 Q_{x_0}(\mathscr{x})}{\partial \mathscr{x}^2} = 2\left(1 - \sum_{z\in X\setminus A_s} P_{x_0,z}\right)\mathscr{x}^{-3} + 2\mathscr{x}^{-3} \sum_{z\in X\setminus A_s} P_{x_0,z}\, Q_z(\mathscr{x}) +$$

$$- \mathscr{x}^{-2} \sum_{z\in X\setminus A_s} P_{x_0,z} \frac{\partial Q_z(\mathscr{x})}{\partial \mathscr{x}} - \mathscr{x}^{-2} \sum_{z\in X\setminus A_s} P_{x_0,z} \frac{\partial Q_z(\mathscr{x})}{\partial \mathscr{x}} +$$

$$+ \mathscr{x}^{-1} \sum_{z\in X\setminus A_s} P_{x_0,z} \frac{\partial^2 Q_z(z)}{\partial \mathscr{x}^2}. \tag{A4-8b}$$

At view of (A4-8), (A4-4) and (A4-7)

$$m_2(x_0) + m_1(x_0) = 2 + 2 \int_{X\setminus A_s} q(x_0, z)\, m_1(z)\, dz +$$

$$+ \int_{X\setminus A_s} q(x_0, z)(m_2(z) + m_1(z))\, dz =$$

$$= 2 + 3(m_1(x_0) - 1) + \int_{X\setminus A_s} q(x_0, z)\, m_2(z)\, dz. \tag{A4-9}$$

The following equations are obtained eventually

$$m_2(x_0) - \int_{X\setminus A_s} q(x_0, z)\, m_2(z)\, \mathrm{d}z = 2m_1(x_0) - 1 \qquad \text{(A4-10a)}$$

for X continous and

$$m_{2,x_0} - \sum_{z \in X\setminus A_s} P_{x_0,z}\, m_{2,z} = 2m_{1,x_0} - 1 \qquad \text{(A4-10b)}$$

for X discrete.

APPENDIX 5

THE MEAN AND THE MEAN SQUARE NUMBER OF STEPS TO ABSORBTION BY THE SUBSET OF ABSORBING SET

Let $Q^i(\mathscr{z}, x_0)$ stand for $\mathscr{z}$ transform of the sequence of probabilities of absorbtion by set A_s^i in subsequent steps. Then according to (42) and (43) respectively

$$Q^i(\mathscr{z}, x_0) = \left(1 - \int_{X\setminus A_s} q(x_0, z)\,\mathrm{d}z\right)\mathscr{z}^{-1} + \mathscr{z}^{-1}\int_{X\setminus A_s} q(x_0, z)\, Q^i(\mathscr{z}, z)\,\mathrm{d}z \qquad \text{(A5-1a)}$$

for the continous case and

$$Q^i_{x_0}(\mathscr{z}) = \left(1 - \int_{z\in X\setminus A_s^i} P_{x_0,z}\right)\mathscr{z}^{-1} + \mathscr{z}^{-1}\sum_{z\in X\setminus A_s} P_{x_0,z}\, Q^i_z(\mathscr{z}) \qquad \text{(A5-1b)}$$

for the discrete one.

Let $P^i_a(x)$ $(P^i_{a,x})$ stand for the probability of absorbtion by the set A^i_s if the initial state x is given. Then from (A5-1)

$$P^i_a(x_0) = Q^i(\mathscr{z}, x_0)\Big|_{\mathscr{z}=1} = 1 - \int_{X\setminus A_s^i} q(x_0, z)\,\mathrm{d}z + \int_{X\setminus A_s} q(x_0, z)\, P_{a,i}(z)\,\mathrm{d}z \qquad \text{(A5-2a)}$$

and

$$P^{\ i}_{a,x_0} = Q^i_{x_0}(\mathscr{z})\Big|_{\mathscr{z}=1} = 1 - \sum_{z\in X\setminus A_s^i} P_{x_0,z} + \sum_{z\in X\setminus A_s} P_{x_0,z}\, P^i_{a,z}. \qquad \text{(A5-2b)}$$

Let us consider the derivatives of $Q^i(\mathscr{z}, x_0)$ $(Q^i_{x_0}(\mathscr{z}))$ now;

$$\frac{\partial Q^i(\varkappa, x_0)}{\partial \varkappa} = -\left(1 - \int_{X\setminus A_s^i} q(x_0, z)\,dz\right)\varkappa^{-2} - \varkappa^{-2} \int_{X\setminus A_s} q(x_0, z)\, Q^i(\varkappa, z)\,dz + \\ + \varkappa^{-1} \int_{X\setminus A_s} q(x_0, z) \frac{\partial Q^i(\varkappa, z)}{\partial \varkappa}\,dz \qquad \text{(A5–3a)}$$

and

$$\frac{\partial Q^i_{x_0}(\varkappa)}{\partial \varkappa} = -\left(1 - \sum_{z\in X\setminus A_s^i} P_{x_0,z}\right)\varkappa^{-2} - \varkappa^{-2} \sum_{z\in X\setminus A_s} P_{x_0,z}\, Q^i_z(\varkappa) + \\ + \varkappa^{-1} \sum_{z\in X\setminus A_s} P_{x_0,z} \frac{\partial Q^i_z(\varkappa)}{\partial \varkappa}. \qquad \text{(A5–3b)}$$

Also, let $m_1^i(x_0)$ (m_{1,x_0}^i) stands for the mean number of steps to absorbtion by set A_s^i from x_0. Then (see A5–3)

$$m_1^i(x_0) = 1 - \int_{X\setminus A_s^i} q(x_0, z)\,dz + \int_{X\setminus A_s} q(x_0, z)\, P_a^i(z)\,dz + \\ + \int_{X\setminus A_s} q(x_0, z)\, m_1^i(z)\,dz \qquad \text{(A5–4a)}$$

and

$$m_{1,x_0}^i = 1 - \sum_{z\in X\setminus A_s^i} P_{x_0,z} + \sum_{z\in X\setminus A_s} P_{x_0,z} P_{a,z}^i + \\ + \sum_{z\in X\setminus A_s} P_{x_0,z} m_{1,z}^i. \qquad \text{(A5–4b)}$$

Now consider the second derivative of $Q^i(\varkappa, x_0)$ ($Q^i_{x_0}(\varkappa)$). One gets

$$\frac{\partial^2 Q^i(\varkappa, x_0)}{\partial \varkappa^2} = 2\left(1 - \int_{X\setminus A_s^i} q(x_0, z)\,dz\right)\varkappa^{-3} + \\ + 2\varkappa^{-3} \int_{X\setminus A_s} q(x_0,z)\, Q^i(\varkappa, z)\,dz - \varkappa^{-2} \int_{X\setminus A_s} q(x_0, z) \frac{\partial}{\partial \varkappa} Q^i(\varkappa, z)\,dz + \\ - \varkappa^{-2} \int_{X\setminus A_s} q(x_0, z) \frac{\partial Q^i(\varkappa, z)}{\partial \varkappa}\,dz + \varkappa^{-1} \int_{X\setminus A_s} q(x_0,z) \frac{\partial^2 Q^i(\varkappa, z)}{\partial \varkappa^2}\,dz \qquad \text{(A5–5a)}$$

for the continous case and

$$\frac{\partial^2 Q^i_{x_0}(\mathscr{x})}{\partial \mathscr{x}^2} = 2\left(1 - \sum_{z\in X\setminus A_s^i} P_{x_0,z}\right)\mathscr{x}^{-3} + 2\mathscr{x}^{-3}\sum_{z\in X\setminus A_s} P_{x_0,z}\, Q^i_z(\mathscr{x}) +$$

$$- \mathscr{x}^2 \sum_{z\in X\setminus A_s} P_{x_0,z}\frac{\partial Q^i_z(\mathscr{x})}{\partial \mathscr{x}} - \mathscr{x}^{-2}\sum_{z\in X\setminus A_s} P_{x_0,z}\frac{\partial Q^i_z(\mathscr{x})}{\partial \mathscr{x}} +$$

$$+ \mathscr{x}^{-1}\sum_{z\in X\setminus A_s} P_{x_0,z}\frac{\partial^2 Q^i_z(\mathscr{x})}{\partial \mathscr{x}^2} \qquad \text{(A5–5b)}$$

for the discrete one.
Now, the mean square number of steps to absorbtion by A^i_s is from (A5–5)

$$m^i_2(x_0) + m^i_1(x_0) = 2\left(1 - \int_{X\setminus A_s^i} q(x_0, z)\,\mathrm{d}z\right) + 2\int_{X\setminus A_s} q(x_0, z)\,P^i_a(z)\,\mathrm{d}z +$$

$$+ 2\int_{X\setminus A_s} q(x_0, z)\,m^i_1(z)\,\mathrm{d}z + \int_{X\setminus A_s} q(x_0, z)\,(m^i_2(z) + m^i_1(z))\,\mathrm{d}z.$$

Next from (A5–4)

$$m^i_2(x_0) = -1 + \int_{X\setminus A_s^i} q(x_0, z)\,\mathrm{d}z - \int_{X\setminus A_s} q(x_0, z)\,P^i_a(z)\,\mathrm{d}z +$$

$$- \int_{X\setminus A_s} q(x_0, z)\,m^i_1(z)\,\mathrm{d}z + 2\left(1 - \int_{X\setminus A_s^i} q(x_0, z)\,\mathrm{d}z\right) +$$

$$+ 2\int_{X\setminus A_s} q(x_0, z)\,P^i_a(z)\,\mathrm{d}z + 3\int_{X\setminus A_s} q(x_0, z)\,m^i_1(z)\,\mathrm{d}z +$$

$$+ \int_{X\setminus A_s} q(x_0, z)\,m^i_2(z)\,\mathrm{d}z =$$

$$= 1 - \int_{X\setminus A_s^i} q(x_0, z)\,\mathrm{d}z + \int_{X\setminus A_s} q(x_0, z)\,m^i_2(z)\,\mathrm{d}z +$$

$$+ \int_{X\setminus A_s} q(x_0, z)\,P^i_a(z)\,\mathrm{d}z + 2\int_{X\setminus A_s} q(x_0, z)\,m^i_1(z)\,\mathrm{d}z =$$

$$= m_1^i(x_0) + \int_{X\setminus A_\varepsilon} q(x_0, z) m_1^i(z)\,dz + \int_{X\setminus A_\varepsilon} q(x_0, z) m_2^i(z)\,dz.$$

Finally

$$m_2^i(x_0) - \int_{X\setminus A_\varepsilon} q(x_0, z) m_2^i(z)\,dz = m_1^i(x_0) + \int_{X\setminus A_\varepsilon} q(x_0, z) m_1^i(z)\,dz \qquad \text{(A5–6a)}$$

for the continous case, and

$$m_{2,x_0}^i - \sum_{z\in X\setminus A_\varepsilon} P_{x_0,z} m_{2,z}^i = m_{1,x_0}^i + \sum_{z\in X\setminus A_\varepsilon} P_{x_0,z} m_{1,z}^i \qquad \text{(A5–6b)}$$

for the discrete one.

M. ŻÓŁTOWSKI

O CYFROWYCH PĘTLACH FAZOWYCH Z NIEJEDNOSTAJNYM PRÓBKOWANIEM W OBECNOŚCI ZAKŁÓCEŃ LOSOWYCH

Część I

Streszczenie

W pracy rozważono w sposób systematyczny dynamikę pętli z czasem dyskretnym. Podano wyprowadzenia ogólnych wyrażeń, z których można otrzymać podstawowe parametry pętli z czasem dyskretnym w obecności zakłócającego szumu. Zastosowano wyniki teorii Markowa i teorii ergodycznej. Pokazano różne aspekty dynamiki pętli. Uzyskany wgląd w zagadnienie wydaje się być bardziej wnikliwy niż to było dotychczas. Na przykład problem ewolucji inwariantnej miary, gdy rośnie wpływ szumu i gdy w przypadku deterministycznym ma miejsce zjawisko chaosu przejściowego może zainteresować czytelnika. Praca składa się w dwóch części. Część pierwsza jest poświęcona teorii, podczas gdy w drugiej czytelnik znajdzie ilustrujące przykłady.

On the digital nonuniform sampling phase-locked loops in the presence of noise

Part II

The nonuniform sampling phase-locked loop (DPLL) was modified in aim to get improved acquisition [2,3]. Its performance in the presence of noise was verified within the approach of part I. Especially the influence of modification on the cycle slipping phenomenon

was of interest. The carried out calculations have not shown the degradation of significant value. Unmodified DPLL of second order exhibits chaotic transient hang up phenomenon [2,3]. This phenomenon while affected has been studied in the presence of noise. The hang up phenomenon in modyfied loop does not occur.

1. INTRODUCTION

The sinusoid zero – crossing nonuniform sampling phase-locked loop of second order showed the existence of chaotic transient hang up phenomenon and phase entrainment which is different from required N:1 one [2,3]. The hang up phenomenon of acquisition process was observed also in the loop of first-order due to quantization around the any unstable state of equilibrium [5]. Though the unique ergodicity occurs under the great impact of noise the modification was made in order to change the set of

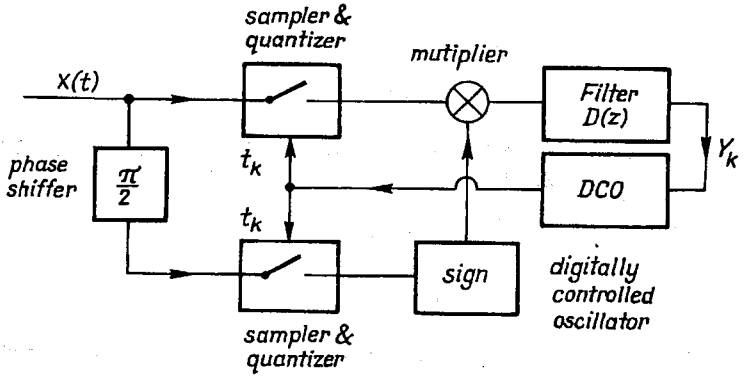

Fig. 1. Modified nonuniform sampling digital phase-locked loop

nonwandering points in aim to get convergence exactly to the only point of N:1 phase entrainment of base space in the case of loop of any order. The model of the modified loop is shown in fig. 1.

The influence of noise on the cycle slipping phenomenon is of interest after the modyfication. The hang up phenomenon in the modyfied loop case is not to occur [2].

2. MODIFIED NONUNIFORM SAMPLING DIGITAL PHASE-LOCKED LOOP OF FIRST ORDER IN THE PRESENCE OF GAUSSIAN ADDITIVE NOISE

The model of the modified loop of first-order in the negligible quantization effects case is derived in appendix I. While the input waveform is detuned in phase and frequency from the local reference the equation of the loop in the presence of noise is (see appendix I);

$$\varphi_{k+1} = \varphi_k - K_1 \operatorname{sign}(A\cos\varphi_k + N_k^c)\sin\varphi_k + \Lambda +$$

$$-\frac{K_1}{A}\operatorname{sign}(A\cos\varphi_k + N_k^c)\,N_k \tag{1}$$
$$k = 0, 1, \ldots$$

$\varphi_k(k=0,1,\ldots)$ is the phase error process which describes the deviation from the N:1 phase entrainment (zerocrossings of input waveform). A is amplitude of not disturbed input waveform, Λ stands for detunation, K_1 for the gain of the loop dependent on the loop's filter and of input phase.
Moreover

$$E\{N_k N_m\} = 0 \qquad \text{for } k \neq m \tag{2a}$$
$$E\{N_k^c N_m^c\} = 0 \qquad \text{for } k \neq m \tag{2b}$$
$$E\{N_k\} = E\{N_k^c\} = 0 \tag{2c}$$
$$E\{N_k N_k^c\} = 0 \tag{2d}$$
$$E\{N_k^2\} = E\{N_k^{c2}\} = \sigma_N^2 \tag{2e}$$

and samples N_k, N_k^c are gaussian, $k=0,1,\ldots$[1] .
Now the density of transition from state x to state z in one step can be obtained (see part I for necessary details)
The coordinates of points y and y' of fig. 2 follow the equations obtained from (1)

$$y = x - K_1 \sin x + \Lambda \tag{3a}$$
$$y' = x + K_1 \sin x + \Lambda. \tag{3b}$$

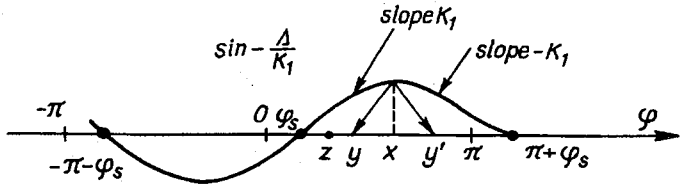

Fig. 2. The ilustration of acquisition in the modified loop of first order [2, 3]

The y of (3a) is the new coordinate of phase error while $N_k=0$ and $A\cos x+N_k^c>0$. Whereas y' of (3b) is the new coordinate of phase error while $N_k=0$ and $A\cos x+N_k^c\leqslant 0$. For the operation of multiplication by signum does not change the distribution of $N_k(k=0,1,\ldots)$ the density of transition in one step is

$$q(x,z) = p\left(\frac{z - x + K_1\sin x - \Lambda}{K_1/A}\right)\int_{-A\cos x}^{\infty} p(z)\,dz + p\left(\frac{z - x - K_1\sin x - \Lambda}{K_1/A}\right)\int_{-\infty}^{-A\cos x} p(z)\,dz \tag{4a}$$

[1] Truncated gaussian distribution can be considered, while the probabilities of events out of the interval of interest are extremely small.

and $p(z)$ is the density of $N(0,\sigma_N^2)$ gaussian noise of 0 mean value and $\delta_N{}^2$ variance. The density of (4a) can be given an equivalent form

$$q(x, z) = q\left(\frac{z - x + K_1 \sin x - \Lambda}{K_1/\sqrt{2S_0}}\right)\left(\frac{1}{2} + \operatorname{erf}\left(\sqrt{2S_0}\cos x\right)\right) + \\ + q\left(\frac{z - x - K_1 \sin x - \Lambda}{K_1/\sqrt{2S_0}}\right)\left(\frac{1}{2} - \operatorname{erf}\left(\sqrt{2S_0}\cos x\right)\right) \tag{4b}$$

and

$$q(u/c) \stackrel{\text{df}}{=} \frac{1}{\sqrt{2\pi}\,C} e^{-\frac{u^2}{2C^2}} \tag{4c}$$

$$\operatorname{erf}(u) \stackrel{\text{df}}{=} \frac{1}{\sqrt{2\pi}} \int_0^u e^{-\frac{x^2}{2}}\,dx \tag{4d}$$

$$S_0 \stackrel{\text{df}}{=} \frac{A^2}{2\delta_N{}^2}. \tag{4e}$$

The parameter S_0 of (4e) is the signal to noise power ratio.
In view of cyclic nature of phase error the dynamics of the loop should be considered on S^1 — circle base space instead of covering R while the steady state distribution is looked for. The recuired equations are derived in appendix 2.
The density on S^1 — circle manifold evolves according to

$$\tilde{q}^{(k+1)}(\tilde{x}_0, \tilde{y}) = \int_{-\pi}^{\pi} \tilde{q}^{(k)}(\tilde{x}_0, \tilde{z})\,\tilde{q}(\tilde{z}, \tilde{y})\,d\tilde{z} \tag{5a}$$

while

$$\tilde{q}^{(k)}(\tilde{x}_0, \tilde{y}) \stackrel{\text{df}}{=} \sum_{n=-\infty}^{\infty} q^{(k)}(\tilde{x}_0, \tilde{y} + 2\pi)\,dz \tag{5b}$$

and

$$\tilde{q}(\tilde{z}, \tilde{y}) = \sum_{l=-\infty}^{\infty} q(\tilde{z}, \tilde{y} + 2\pi l), \qquad k = 0, 1, \ldots \tag{5c}$$

However due to additional symetry which results from the modification (see fig. 3) the density of probability of modified loop evolves according to

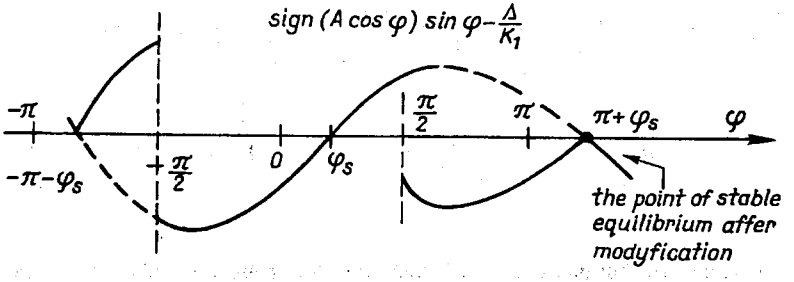

Fig. 3. The effective nonlinearity of the modified loop

$$\tilde{q}^{(k+1)}(\tilde{x}_0, \tilde{y}) = \int_{\pi/2}^{\pi/2} \tilde{q}^{(k)}(\tilde{x}_0, \tilde{z})\,\tilde{q}(\tilde{z}, \tilde{y})\,d\tilde{z} \qquad k = 0, 1, \ldots \tag{6a}$$

with

$$\tilde{q}^{(k)}(\tilde{x}_0, \tilde{y}) = \sum_{n=-\infty}^{\infty} q^{(k)}(\tilde{x}_0, \tilde{y} + \pi n) \tag{6b}$$

and

$$\tilde{q}(z, y) = \sum_{l=-\infty}^{\infty} q(\tilde{z}, \tilde{y} + \pi l) \tag{6c}$$

Now $\tilde{x}_0, \tilde{y}, \tilde{z}$ are from $S^1 = <-\pi/2, \pi/2>$. In view of part I the steady state invariant density q exists and satisfies

$$\tilde{q}(\tilde{y}) = \int_{-\pi/2}^{\pi/2} \tilde{q}(z)\,\tilde{q}(\tilde{z}, \tilde{y})\,d\tilde{z}. \tag{7}$$

Now, the cycle slipping can be characterized in terms of the results of part I. The cycle slipping phenomenon occurs while the trajectory of the phase error leaves the defined set around the state of phase entrainment. This set is $E_s \stackrel{df}{=} <-\pi + \varphi_s, \pi + \varphi_s>$ closed interval in this case, while φ_s is the point of phase entrainment in the absence of noise.

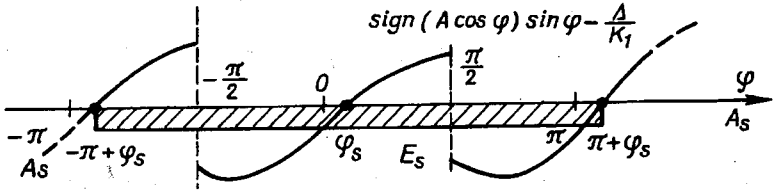

Fig. 4. The ilustration of absorbing set $A_s = R \setminus E_s$ in the cycle slipping phenomenon case. Modified digital phase-locked loop of first-order

The mean m_1^{sc} and mean square m_2^{sc} number of steps to slip the cycle satisfy (see Part I) the following equations, while x_0 is the initial state;

$$m_1^{sc}(x_0) - \int_{-\pi+\varphi_s}^{\pi+\varphi_s} q(x_0, z)\,m_1^{sc}(z)\,dz = 1 \tag{8a}$$

$$m_2^{sc}(x_0) - \int_{-\pi+\varphi_s}^{\pi+\varphi_s} q(x_0, z)\,m_2^{sc}(z)\,dz = 2m_1^{sc}(x_0) - 1 \tag{8b}$$

The variance of the number of steps v^{sc} to slip the cycle is

$$v^{sc}(x_0) = m_2^{sc}(x_0) - m_1^{sc}(x_0)^2. \tag{8c}$$

Additionaly the results of part I allow one to study the cycle slipping phenomenon to the right and to the left.

Let

$$A_{R,s} \stackrel{\text{df}}{=} \{x : x \geqslant \pi + \varphi_s\} \tag{9a}$$

be the „Right" absorbing set and

$$A_{L,s} \stackrel{\text{df}}{=} \{x : x \leqslant -\pi + \varphi_s\} \tag{9b}$$

be the „Left" absorbing set.

Thus

$$A_s = A_{L,s} \cup A_{R,s} \tag{9c}$$

The absorbtion by $A_{R,s}$ means the cycle slipping to the right while the absorbtion by $A_{L,s}$ means the cycle slipping to the left.

The probabilities of absorbtion to the right and to the left satisfy the equations; x_0 is the initial state

$$P_a^R(x_0) - \int_{X \setminus A_s} q(x_0, z) P_a^R(z)\,dz = 1 - \int_{X \setminus A_{R,s}} q(x_0, z)\,dz \tag{10a}$$

$$P_a^L(x_0) - \int_{X \setminus A_s} q(x_0, z) P_a^L(z)\,dz = 1 - \int_{X \setminus A_{L,s}} q(x_0, z)\,dz. \tag{10b}$$

Whereas mean numbers of steps to cycle slipping to the right and to the left from the initial state x_0 satisfy

$$m_1^R(x_0) - \int_{X \setminus A_s} q(x_0, z) m_1^R(z)\,dz = 1 - \int_{X \setminus A_{R,s}} q(x_0, z) P_a^R(z)\,dz \tag{11a}$$

$$m_1^L(x_0) - \int_{X \setminus A_s} q(x_0, z) m_1^L(z)\,dz = 1 - \int_{X \setminus A_{L,s}} q(x_0, z) P_a^L(z)\,dz. \tag{11b}$$

On the other hand the mean square numbers of steps to slip the cycle to the right and to the left from the initial state x_0 satisfy

$$m_2^R(x_0) - \int_{X \setminus A_s} q(x_0, z) m_2^R(z)\,dz = m_1^R(x_0) + \int_{X \setminus A_{R,s}} q(x_0, z) m_1^R(z)\,dz \tag{12a}$$

$$m_2^L(x_0) - \int_{X \setminus A_s} q(x_0, z) m_2^L(z)\,dz = m_1^R(x_0) + \int_{X \setminus A_{L,s}} q(x_0, z) m_1^L(z)\,dz \tag{12b}$$

Whereas the variances v^R and v^L are

$$v^R(x_0) = m_2^R(x_0) - m_1^R(x_0)^2 \tag{13a}$$

$$v^L(x_0) = m_2^L(x_0) - m_1^L(x_0)^2 . \tag{13b}$$

Next, the process of synchronization can be characterized in terms of Markov model on S^1 – circle manifold.
The density function of transition from $\tilde{x} \in S^1$ to $\tilde{z} \in S^1$ is given by

$$\tilde{q}(\tilde{x}_0, \tilde{z}) = \sum_{l=-\infty}^{\infty} q(\tilde{x}_0, \tilde{z} + \pi l). \tag{14a}$$

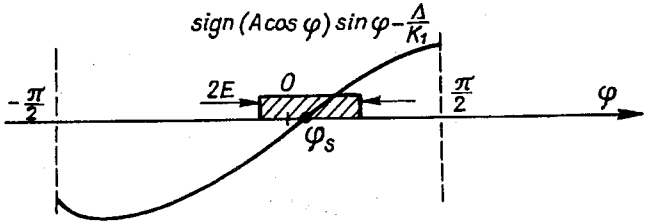

Fig. 5. The ilustration of synchronization on S^1 – circle manifold

The absorbing set A_s around the state of phase entrainment in noiseless case is

$$A_s = <\varphi_s - \epsilon, \varphi_s + \epsilon> \tag{14b}$$

That is why the mean number of steps m_1^s and mean square number m_2^s of steps to acquire from the initial state $\tilde{x}_0$ satisfy

$$m_1^s(\tilde{x}_0) - \int_{X \setminus A_s} \tilde{q}(\tilde{x}_0, \tilde{z}) m_1^s(\tilde{z}) \, d\tilde{z} = 1 \tag{15a}$$

$$m_2^s(\tilde{x}_0) - \int_{X \setminus A_s} \tilde{q}(\tilde{x}_0, \tilde{z}) m_2^s(\tilde{z}) \, d\tilde{z} = 2m_1(\tilde{x}_0) - 1. \tag{15b}$$

Moreover the variance of the number of steps to synchronization is

$$v_2^s(\tilde{x}_0) = m_2^s(\tilde{x}_0) - m_1^s(\tilde{x}_0)^2 . \tag{15c}$$

3. THE RESULTS OF COMPUTATIONS

The numerical results based on the theory of part I and part II are presented in this chapter. They are given in form of figures mainly. S_0 stands for the input signal power to noise power ratio. The cycle slipping phenomenon is described for the modified loop of first-order in terms of fig. 6 to fig. 11.

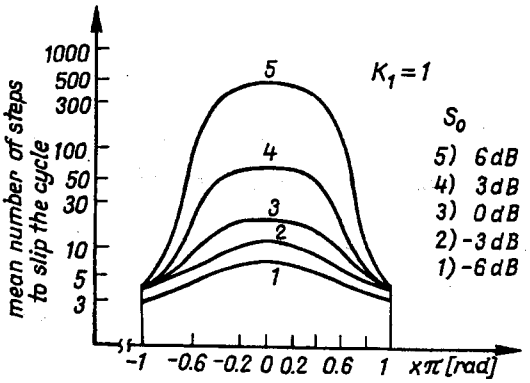

Fig. 6. The mean number of steps to slip the cycle. Modified first-order digital phase-locked loop. S_0 – input signal power to noise power ratio. Negligible quantization effects

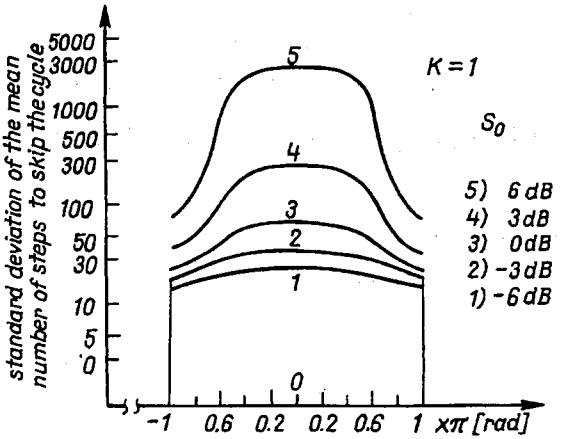

Fig. 7. The standard deviation of the number of steps to slip the cycle. Modified first-order digital phase-locked loop. Negligible quantization effects

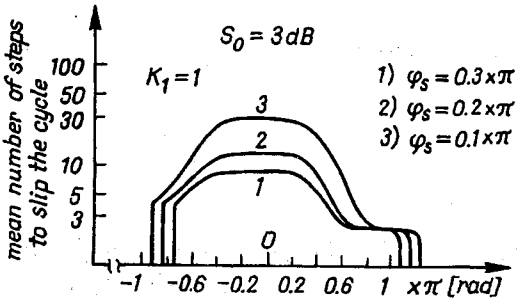

Fig. 8. The mean number of steps to slip the cycle Modified first-order DPLL with nonzero frequency offset. Negligible quantization effects

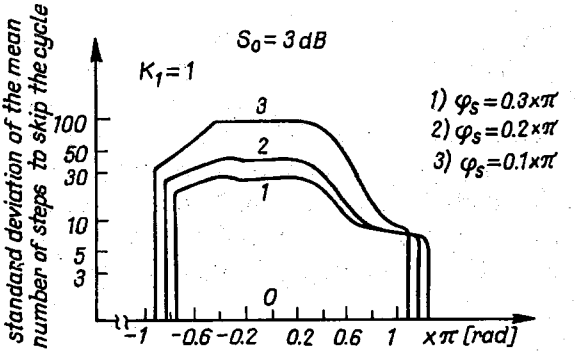

Fig. 9. The standard deviation of the mean number of steps to slip the cycle. Modified first-order DPLL with nonzero frequency offset. Negligible quantization effects

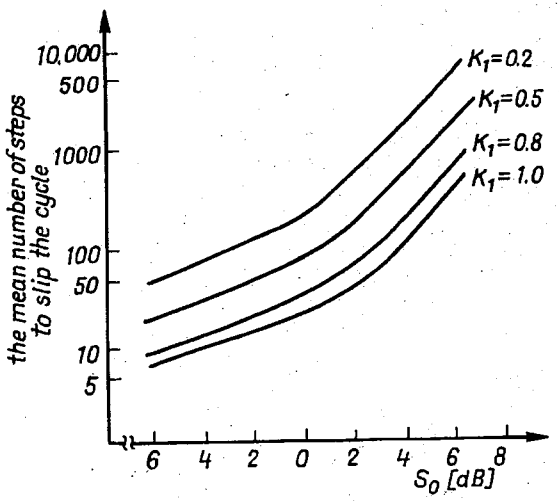

Fig. 10. The mean number of steps to splip the cycle from the state of 0 radians. First-order modified phase-locked loop. Treshold exhibited. Negligible quantization effects

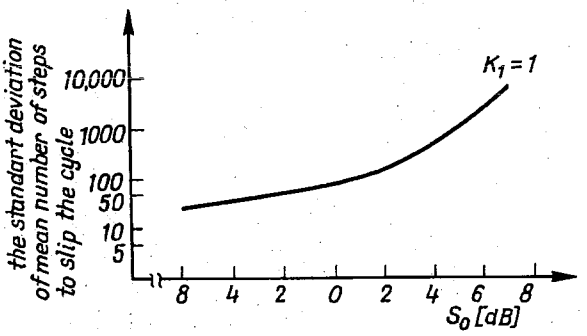

Fig. 11. The standard deviation of the mean number of steps to slip the cycle from the state of 0 — radians. First-order modified digital phase-locked loop. Treshold exhibited

The degradation which is due to the frequency offset resulting in nonzero steady phase error φ_s is shown in fig. 8 and fig. 9.
The existence of treshold phenomenon is shown in fig. 10 and fig. 11 in terms of parameters characterizing the cycle slipping.
The steady state distribution of the probabilistic measure is shown in fig. 12 to fig. 16 in the modified DPLL of first-order case. Moreover the steady state standard deviation of phase error process based on the steady state distribution of the probabilistic measure is shown in fig. 17 to fig. 19. The rest of the results of this chapter is computer modeling based.

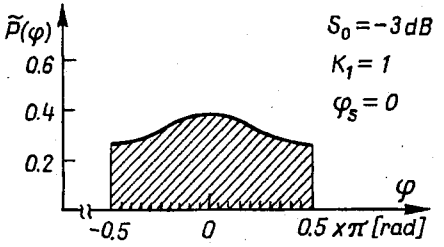

Fig. 12. The steady state distribution of probabilistic measure. First order modified DPLL. Negligible quantization effects

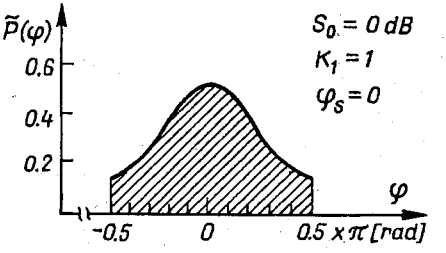

Fig. 13. The steady state distribution of probabilistic measure. First-order modified DPLL. Negligible quantization effects

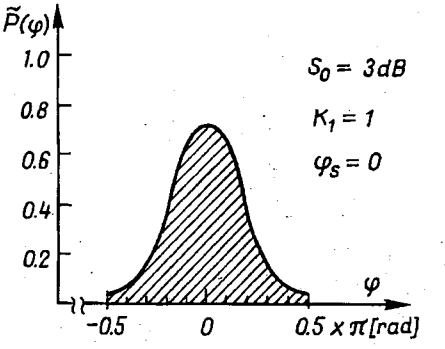

Fig. 14. The steady state distribution of probabilistic measure. First-order modified DPLL. Negligible quantization effects

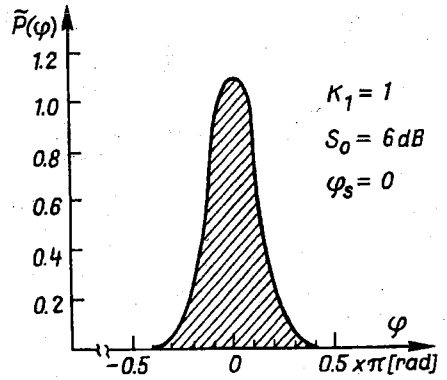

Fig. 15. The steady state distribution of probabilistic measure. First-order modified DPLL. Negligible quantization effects

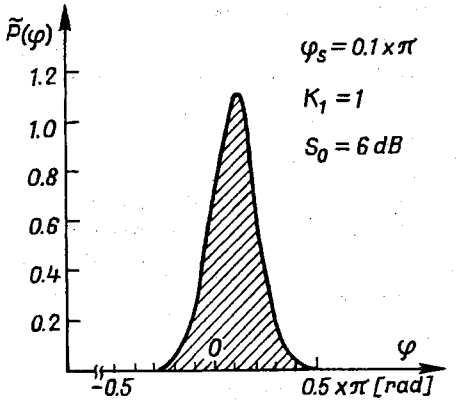

Fig. 16. The steady state distribution of probabilistic measure shifted due to frequency offset. First-order modified DPLL. Negligible quantization effects

The acquisition behaviour of first-order DPLL in modified and unmodified case is described in term of fig. 20 to fig. 25. The performance of the loop of second order is presented in next figures.

This case was of interest because of hang up phenomenon discovered in the loop of second order [2,3]. The modification of this loop is in order to avoid it. The prolonged acquisition due to chaotic transient hang up phenomenon is shown in fig. 26 and fig. 27 in the presence of noise. Whereas the experimental distribution of points showing the existence of stable trajectory of period 4 is shown in fig. 28. The evolution of probabilistic measure under the increasing impact of noise results in uniquely ergodic case. Thus the performance of modified DPLL overcomes the one of unmodified DPLL until the impact of noise is strong enough (fig. 26, fig. 27).

The steady state behaviour of both loops is quite similar to shown in fig. 29 and fig. 30. In addition the sensitivity due to initial conditions of the trajectories starting

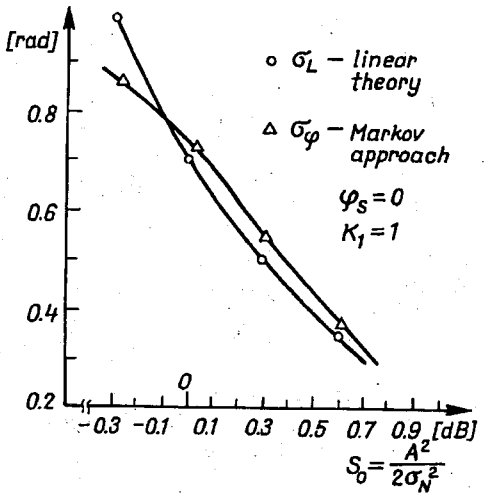

Fig. 17. The steady state standard deviation of phase-error process, $K_1 = 1$. First-order modified DPLL. Negligible quantization effects

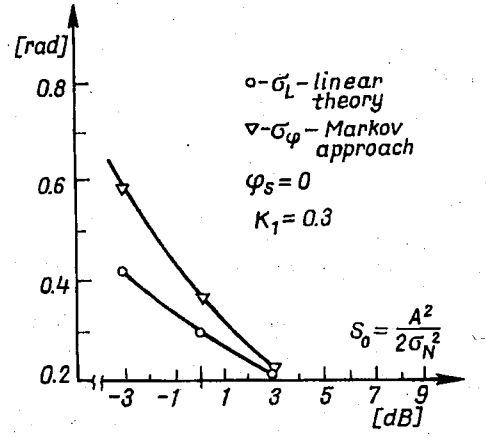

Fig. 18. The steady state standard deviation of phase error process, $K_1 = 3$. First-order modified DPLL. Negligible quantizaiotin effects

from the hiperbolic region in the unmodified DPLL case [2,3] results in the sensitivity of the standard deviation of the number of steps to acquisition as shown in table 1.

The last figures show the performance of the first-order DPLL with quantizer (see fig. 31) in modified and unmodified case.

It is noticeable that the increasing impact of noise makes no difference between the number of levels of quantizer. That is why the approach within continous state space is reasonable if either the number of steps of quantizer is high enough or the impact of noise is strong enough.

The performance depends also on the frequency offset resulting in nonzero φ_s.

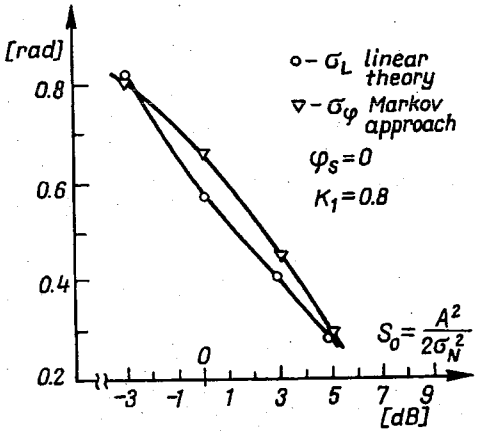

Fig. 19. The steady state standard deviation of phase error process, $K_1=0.8$. First-order modified DPLL. Negligible quantization effects

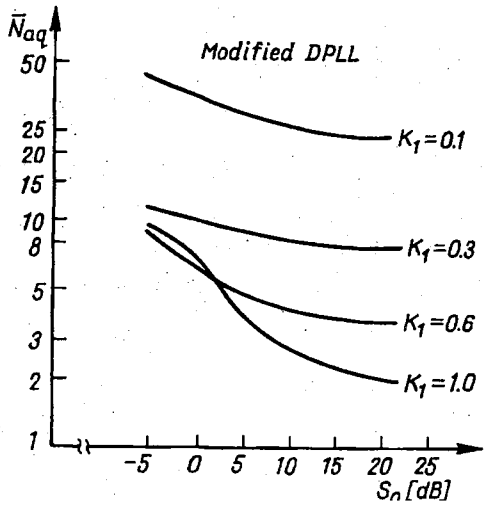

Fig. 20. The estimate $\bar{N}_{aq}$ of the mean number of steps to acquisition. First-order modified DPLL, $\epsilon=.05\times\pi$ [rad], $S_0=A^2/2\sigma_N^2$ [dB], $\Lambda=0$. Negligible quantization effects, $\varphi_0=0.95\,x\pi/2$ [rad]. Few thousand trajectories considered

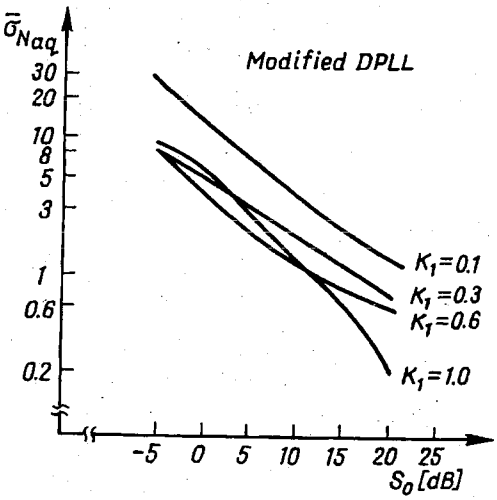

Fig. 21. The estimate $\sigma_{N_{aq}}$ of standard deviation of the distribution of the number of steps to acquisition. First-order modified DPLL, $\epsilon=0.05\,x\pi$ [rad], $S_0=A^2/2\delta_N^2$ [dB], $\Lambda=0$. Negligible quantization effects, $\varphi_0=0.95\,x\pi/2$ [rad]. Few thousand trajectories considered

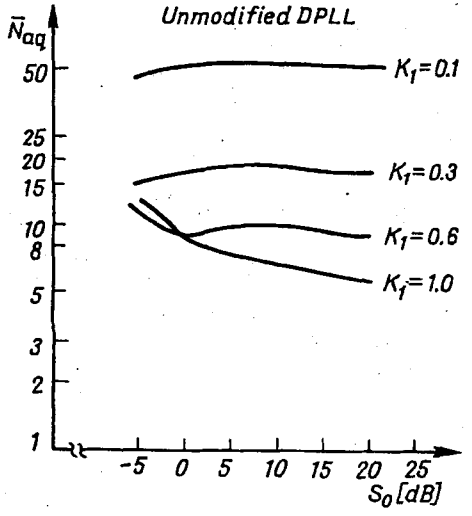

Fig. 22. The estimate $\bar{N}_{aq}$ of the mean number of steps to acquisition. First-order unmodified DPLL, $\epsilon=0.05\,x\pi$ [rad], $S_0=A^2/2\sigma_N^2$ [dB], $\Delta=0$. Negligible quantization effects, $\varphi_0=0.95\,x\pi/2$ [rad]. Few thousand trajectories considered

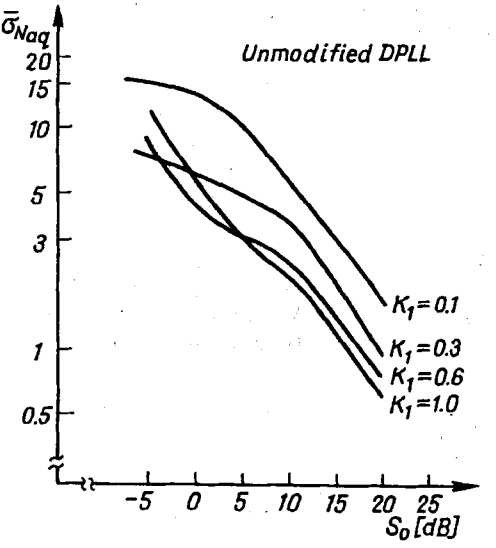

Fig. 23. The estimate $\sigma_{N_{aq}}$ of standard deviation of the distribution of the number of steps to acquisition. First-order unmodified DPLL, $\epsilon=0.05\,x\pi$ [rad], $\Delta=0$, $S_0=A^2/2\sigma_N^2$ [dB], $\Delta=0$. Negligible quantization effects, $\varphi_0=0.95\,x\pi/2$ [rad]. Few thousand trajectories considered

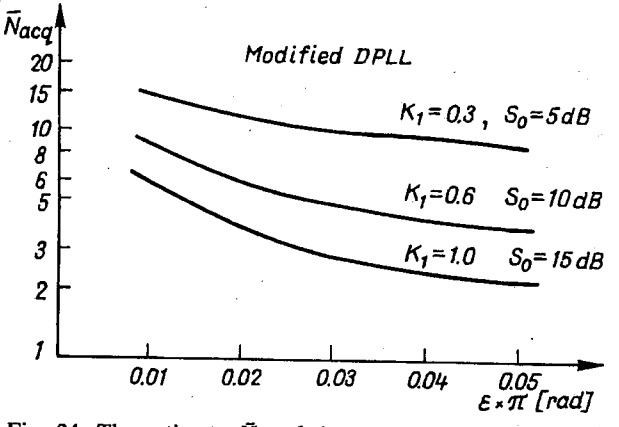

Fig. 24. The estimate $\bar{N}_{aq}$ of the mean number of steps to acquisition versus the radius of absorbing interval, $\Delta=0$. Modified first-order DPLL. Negligible quantization effects, $\varphi_0=0.95\,x\pi/2$ [rad]. Few thousand trajectories considered

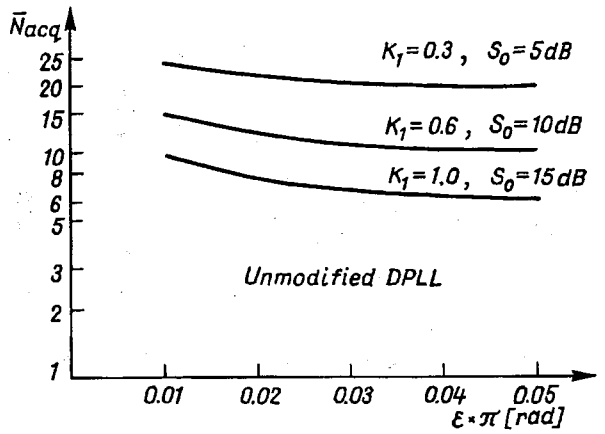

Fig. 25. The estimate $\bar{N}_{aq}$ of the mean number of steps to acquisition versus the radius of absorbing interval ϵ, $\Lambda=0$. Unmodified first-order DPLL. Negligible quantization effects, $\varphi_0=0.95\,x\pi/2$ [rad]. Few thousand trajectories considered

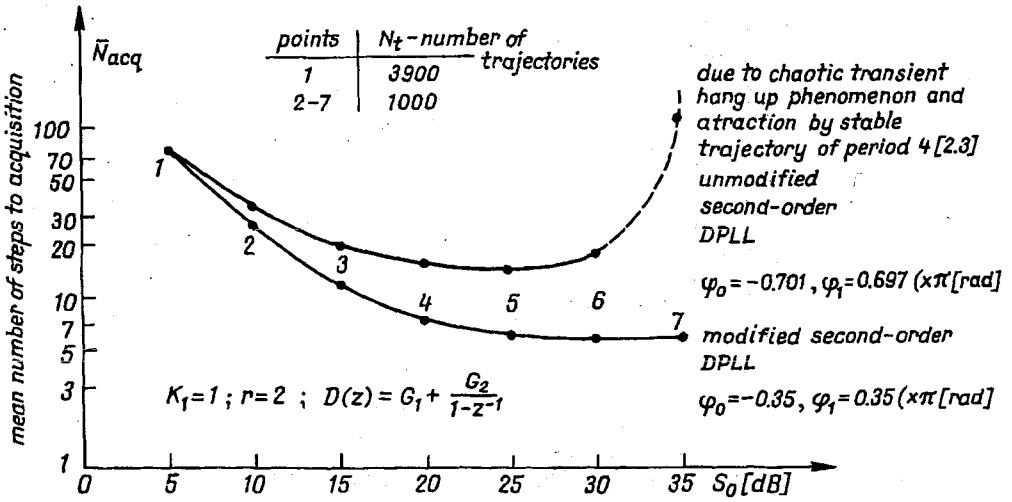

Fig. 26. The mean number of steps to acquisition. Second-order DPLL in modified and unmodified case. The acquisition occurs if the distance from the state of phase entrainment is less then 0.05 $x\pi$ [rad]. Negligible quantization effects

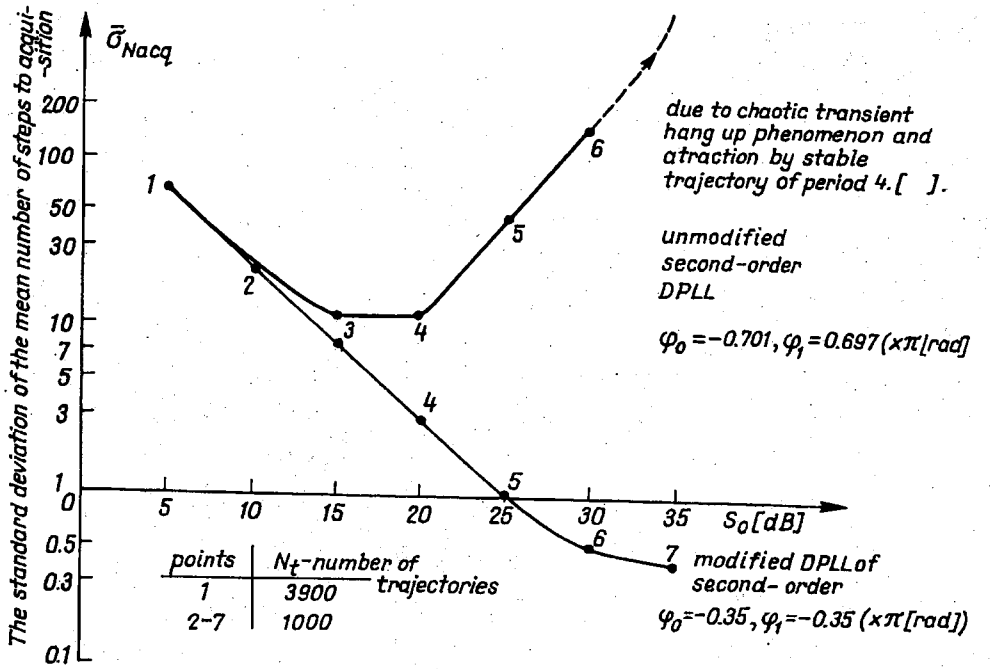

Fig. 27. The standard deviation of the number of steps to acquisition. Second-order DPLL. Acquisition region of 0.05 xπ [rad], radius. Negligible quantization effects

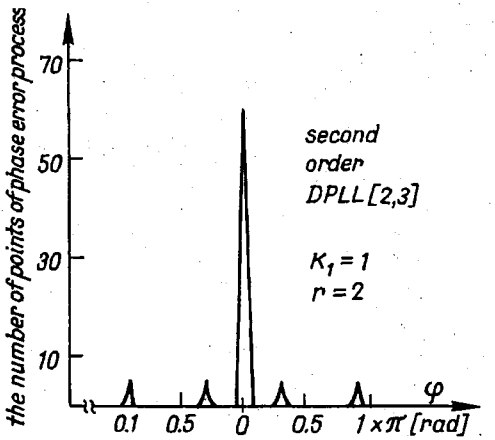

Fig. 28. The experimental distribution of trajectories. 1000 trajectories starting from hiperbolic region [2,3]. 30 initial points taken into account as transient while last 10 as distribution. Negligible noise. This distribution is due to the trajectory of period 4 and fixed point of N:1 phase entrainment

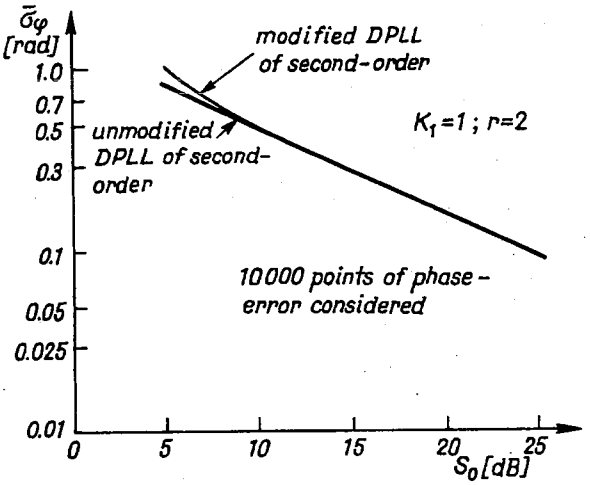

Fig. 29. The steady state standard deviation of the phase error process around the state of phase entrainment. Second-order DPLL in modified and unmodified case. Negligible quantization effects

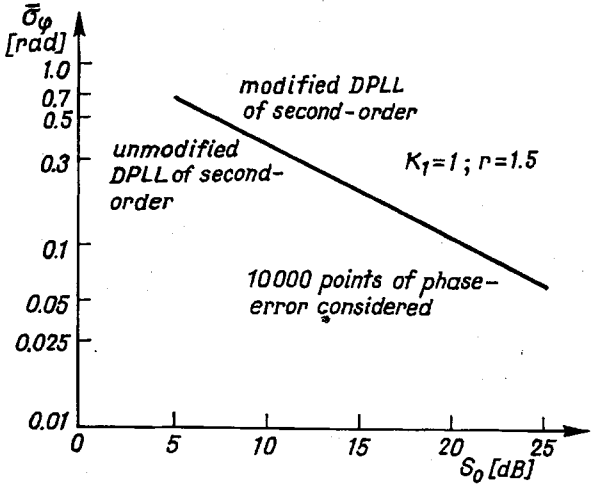

Fig. 30. The steady state standard deviation of the phase error process around the state of phase entrainment. Second-order DPLL in modified and unmodified case. Negligible quantization effects

Tablica 1

Loop's parameters $K_1=1$; $r=2$; $S_0=20$ dB (signal to noise ratio)

unmodified DPLL of second-order				modified DPLL of second-order			
φ_0 (x πrad)	φ_1 (x πrad)	$\bar{N}_{acq}$	$\bar{\sigma}_{\bar{N}}$	φ_0 (x πrad)	φ_1 (x πrad)	$\bar{N}_{acq}$	$\bar{\sigma}_{\bar{N}}$
−.705	.7	14.3	7.3	−.351	.35	7.3	2.8
−.703	.7	14.4	6.3	−.35	.35	7.3	2.7
−.701	.7	14.8	11.3	−.353	.35	7.2	2.5
−.7	.695	14.5	9.3	−.351	.346	7.4	2.9
−.701	.697	15.0	10.6	−.351	.348	7.3	2.8
sensitivity of $\sigma_{\bar{N}}$ due to chaotic transient hang up phenomenon							

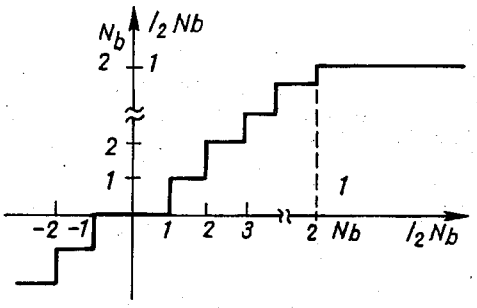

Fig. 31. The characteristics of quantizer with dead zone, symetric for positive and negative values, 2^{N_b} levels of quantization

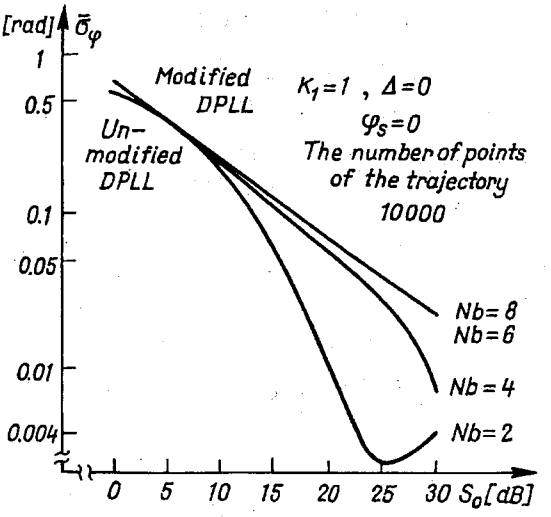

Fig. 32. The mean squared value $\bar{\sigma}_\varphi$ of steady state oscillations in the case of modified and unmodified DPLL of first-order: $K_1=1, \Delta=0$. The difference between unmodified and modified DPLL is slightly noticeable for signal power to noise power ratio less then 3 db. $S_0=A^2/2\sigma_N^2$, b_N – mean squared value of noise sequence

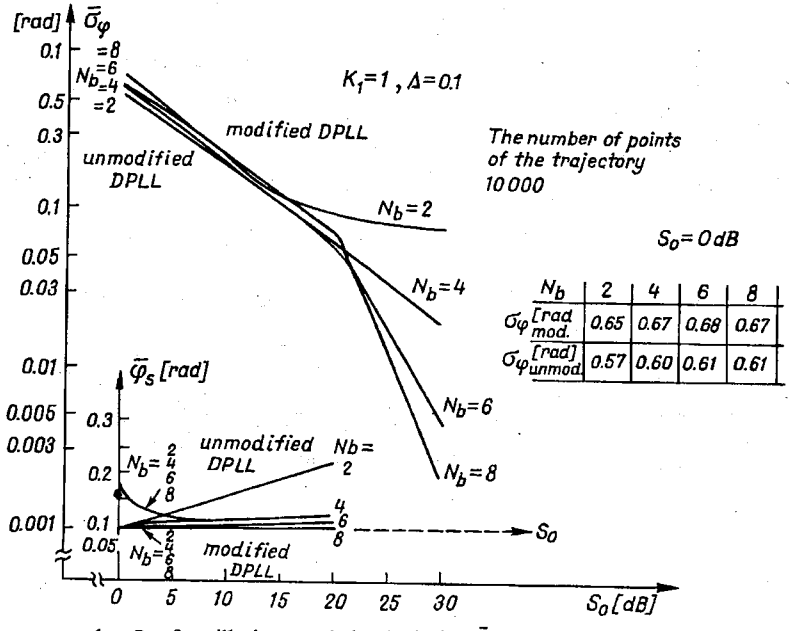

N_b	2	4	6	8
$\sigma_{\varphi\,\text{mod.}}$ [rad]	0.65	0.67	0.68	0.67
$\sigma_{\varphi\,\text{unmod.}}$ [rad]	0.57	0.60	0.61	0.61

Fig. 33. The mean value $\bar{\varphi}_s$ of oscillations and the deviation $\bar{\delta}_\varphi$ of the steady state oscillations in the case modified and unmodified DPLL of first-order, $K_1=1$, $\Delta=0{,}1$. The difference between unmodified and modified case is slightly noticeable for small signal power to noise power ratio

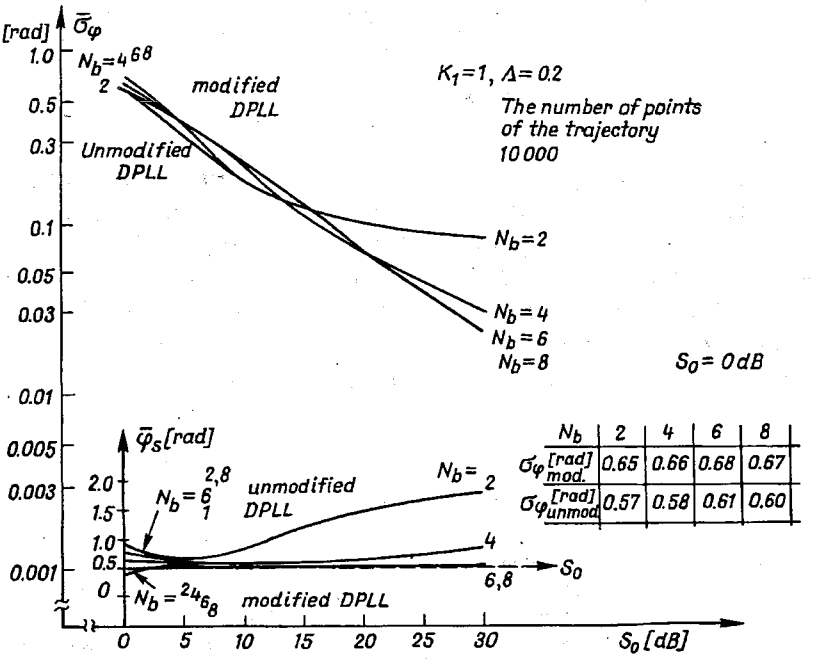

Fig. 34. The mean value $\bar{\varphi}_s$ of oscillations and the standard deviation $\bar{\sigma}_\varphi$ of the steady state oscillations in the case of modified and unmodified DPLL of first-order, $K_1 = 1$, $\Delta = 0{,}05$

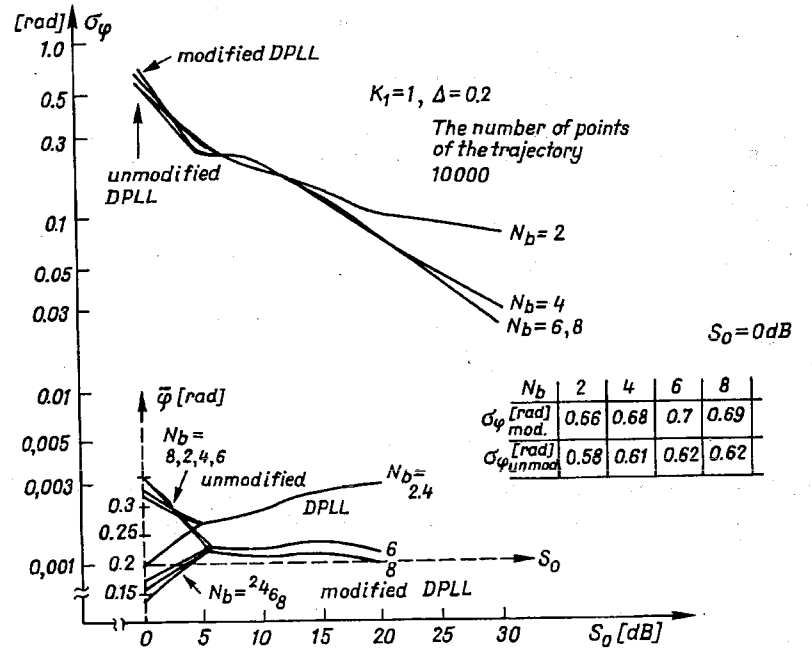

Fig. 35. The mean value $\bar{\varphi}_s$ of oscillations and the standard deviation of the steady state oscillations in the case of modified and unmodified DPLL of first-order, $K_1 = 1$, $\Delta = 0{,}2$

CONCLUSIONS

The nonuniform sampling digital phase-locked loop DPLL was modified in aim to get improved acquisition [2,3]. Its performance was verified in the presence of noise within Markov theory and computer modelling based approache. The results have been provided in chapter III and discussed. It results that the modified phase-locked loop overcomes the performance of unmodified one in the considered case. The hang up phenomenon does not occur in the modified loop case. The results of this part illustrate the general approach to the dynamics of part I.

REFERENCES

1. M. Żółtowski: *On the digital nonuniform sampling phase-locked loops in the presence of noise.* Part I
2. M. Żółtowski: *O globalnej stabilności synchronizmu pętli fazowej drugiego rzędu z niejednostajnym próbkowaniem.* Rozprawy Elektrotechniczne, 1988, 34, z. 4, pp. 37–58
3. M. Żółtowski: *Chaotic transient hang up phenomenon and N:1 phase entrainment in discrete time phase-locked loop of second order.* ECCTD, Paris 1987
4. D. E. Knuth: *The art of computer programming,* vol. 2, Addison-Wesley Series and Computer and Information Processing, 1969
5. D'Andrea, F. Russo: *Multilevel Quantized DPLL Behaviour with Phase — and Frequency — Step Plus noise Input.* IEEE Transactions on Communications, vol. COM–28, no 8, August 1980

APPENDIX 1

THE MATHEMATICAL MODEL OF THE MODIFIED NONUNIFORM SAMPLING PHASE-LOCKED LOOP OF FIRST-ORDER WITH NEGLIGIBLE QUANTIZATION EFFECTS

The waveform to the loop's input is

$$X(t) = A\sin(\omega_0 t + \theta(t)) + N(t) \qquad \text{(A1–1)}$$

A — amplitude ($A=\sqrt{2P}$, P — power of not disturbed $X(t)$), ω_0 — radian frequency, $\theta(t)$ modulation of phase, $N(t)$ — noise disturbance. Special simpler case is considered next;

$$\theta(t) = \Omega t + \theta_0 \qquad \text{(A1–2)}$$

i. e the input waveform is detuned in phase θ_0 and frequency Ω from the local reference and these detunations can appear as steps. The sampling instants are according to the algorithm of DCO

$$t_{k+1} = t_k + T - Y_k, \qquad k = 0, 1, \ldots \qquad \text{(A1–3)}$$

$T = \dfrac{2\pi}{\omega_0}\mathcal{N}$ is the nominal period of DCO waveform in the case of N:1 phase entrainment, while Y_k is the output of the loop's filter at t_k instant (see fig. 1). From (A1–3)

$$t_k \underset{t_0=0}{=} kT - \sum_{l=0}^{k-1} Y_l \qquad k = 0, 1, \ldots \tag{A1-4}$$

To avoid proliferation

$$X(t_k) = X_k;\ N(t_k) = N_k;\ \theta(t_k) = \theta_k. \tag{A1-5}$$

Next

$$\begin{aligned} X_k &= A \sin(\omega_0 t_k + \theta_k) + N_k = \\ &= A \sin\left(\omega_0 \left(kT - \sum_{l=0}^{k-1} Y_l\right) + \theta_k\right) + N_k = \\ &= A \sin\left(\theta_k - \omega_0 \sum_{l=0}^{k-1} Y_l\right) + N_k \\ & k = 0, 1, \ldots \end{aligned} \tag{A1-6}$$

The instantenous phase error, phase error shortly can be defined as

$$\varphi_k \overset{\text{df}}{=} \theta_k - \omega_0 \sum_{l=0}^{k-1} Y_l. \tag{A1-7}$$

The phase error describes the deviation from the state of phase entrainment. The equation of loop in terms of phase error is

$$\begin{aligned} \varphi_{k+1} &= \varphi_k - \theta_{k+1} - \theta_k - \omega_0 Y_k \\ & k = 0, 1, \ldots \end{aligned} \tag{A1-8}$$

Moreover

$$Y_k = G_1 \operatorname{sign} X_k^{\varepsilon} \cdot X_k, \qquad k = 0, 1, \ldots \tag{A1-9}$$

in the first-order loop case; $G_1 = D(z)$, while X_k^{ε} is $\pi/2$ radian shifted sample of input waveform $X(t)$.
Thus

$$\begin{aligned} \varphi_{k+1} &= \varphi_k + \Omega(T - Y_k) - \omega_0 Y_k = \varphi_k - (\Omega + \omega_0) Y_k + \Lambda = \\ &= \varphi_k - K_1 \operatorname{sign} X_k^{\varepsilon} \sin \varphi_k + \Lambda - \frac{K_1}{A} \operatorname{sign} X_k^{\varepsilon} \cdot N_k \\ K_1 &= (\omega_0 + \Omega) A \\ \Lambda &= \Omega T. \end{aligned} \tag{A1-10}$$

Finally, the equation of the loop of first-order is;

$$\begin{aligned} \varphi_{k+1} = \varphi_k &- K_1 \operatorname{sign}(A \cos \varphi_k + N_k^{\varepsilon}) \sin \varphi_k + \Lambda + \\ &- \frac{K_1}{A} \operatorname{sign}(A \cos \varphi_k + N_k^{\varepsilon}) N_k \\ & k = 0, 1, \ldots \end{aligned} \tag{A1-11}$$

N_k^c stands for the $\pi/2$ radian shifted sample of N_k. Both samples are assumed statistically independent.

APPENDIX 2

THE DISTRIBUTION OF DENSITY OF PROBABILITY ON S^1 CIRCLE MANIFOLD

Suppose the density of transition $q(x,y)$ from x to y in one step is given. Then the density $q^{(k+1)}(x_0, y)$ of transition from the initial state x_0 to state y in $k+1$ steps satisfies

$$q^{(k+1)}(x_0, y) = \int_{-\infty}^{\infty} q^{(k)}(x_0, x)\, q(x, y)\, \mathrm{d}x \qquad (A2-1)$$

$$k = 0, 1, \ldots$$

Now, the density of probability on S^1 circle manifold is of interest. Let $\tilde{x} \in S^1$. If $x \in R$ then
$\tilde{x} = \operatorname{Arg} e^{jx} \in <-\pi, \pi>$ closed interval with equivalent end points. That is why the density of transition from $\tilde{x}$ to $\tilde{y}$ on S^1 is

$$\tilde{q}^{(k)}(\tilde{x}_0, \tilde{y}) = \sum_{n=-\infty}^{\infty} q^{(k)}(\tilde{x}_0, \tilde{y} + 2\pi n). \qquad (A2-2)$$

Next from (A2−1)

$$\tilde{q}^{(k+1)}(\tilde{x}_0, \tilde{y}) = \sum_{n=-\infty}^{\infty} \int_{-\infty}^{\infty} q^{(k)}(\tilde{x}_0, x)\, q(x, \tilde{y} + 2\pi n)\, \mathrm{d}x =$$

$$= \sum_{n=-\infty}^{\infty} \sum_{m=-\infty}^{\infty} \int_{2\pi(m-1/2)}^{2\pi(m+1/2)} q^{(k)}(\tilde{x}_0, x)\, q(x, \tilde{y} + 2\pi n) \underset{x = \tilde{z} + 2\pi m}{\mathrm{d}x} =$$

$$= \sum_{n=-\infty}^{\infty} \sum_{m=-\infty}^{\infty} \int_{-\pi}^{\pi} q^{(k)}(\tilde{x}_0, \tilde{z} + 2\pi m)\, q(\tilde{z} + 2\pi m, \tilde{y} + 2\pi n)\, \mathrm{d}\tilde{z} =$$

$$= \int_{-\pi}^{\pi} \sum_{m=-\infty}^{\infty} q^{(k)}(\tilde{x}_0, \tilde{z} + 2\pi m) \sum_{n=-\infty}^{\infty} q(\tilde{z} + 2\pi m, y + 2\pi n)\, \mathrm{d}\tilde{z}. \qquad (A2-3)$$

But

$$\sum_{m=-\infty}^{\infty} q^{(k)}(\tilde{x}_0, \tilde{z} + 2\pi m) = \tilde{q}^{(k)}(\tilde{x}_0, \tilde{z}) \qquad (A2-4)$$

Also

$$q(\tilde{z} + 2\pi m, \tilde{y} + 2\pi n) = q(\tilde{z}, \tilde{y} + 2\pi(n-m)) \tag{A2-5}$$

Thus

$$\tilde{q}^{(k+1)}(x_0, y) = \int_{-\pi}^{\pi} \tilde{q}^{(k)}(\tilde{x}_0, \tilde{z}) \sum_{n=-\infty}^{\infty} q(\tilde{z}, \tilde{y} + 2\pi(n - m))\,d\tilde{z} =$$

$$= \int_{-\pi}^{\pi} \tilde{q}^{(k)}(\tilde{x}_0, \tilde{z}) \sum_{l=-\infty}^{\infty} q(\tilde{z}, \tilde{y} + 2\pi l)\,d\tilde{z}. \tag{A2-6}$$

From (A2-6)

$$\tilde{q}^{(k+1)}(x_0, y) = \int_{-\pi}^{\pi} \tilde{q}^{(k)}(\tilde{x}_0, \tilde{z})\,\tilde{q}(\tilde{z}, \tilde{y})\,d\tilde{z} \tag{A2-7a}$$

and

$$\tilde{q}(\tilde{z}, \tilde{y}) = \sum_{l=-\infty}^{\infty} q(\tilde{z}, \tilde{y} + 2\pi l) \tag{A2-7b}$$

APPENDIX 3

THE NUMERICAL SOLUTION OF THE EQUATION

$$q(y) = \int_{-\pi}^{\pi} q(z)\,q(z, y)\,dz \tag{A3-1}$$

Let the solution $q(y)$ of (A3-1) satisfy

$$q(y) \simeq q_n(y) = \sum_{k=1}^{n} c_k u_k(y) \tag{A3-2}$$

$\{u_k\}$ is the system of ortogonal functions and q_n converge to q uniformly while $n \nearrow \infty$.

Let also

$$< a(x) \mid b(x) > \stackrel{\text{df}}{=} \frac{1}{2\pi} \int_{-\pi}^{\pi} a(x)\,b(x)\,dx \tag{A3-3}$$

stands for the scalar product of mappings a and b from $<-\pi, \pi>$ interval onto R (the set of reals).

Then

$$<q_n(y) \mid u_k(y)> = \int_{-\pi}^{\pi} q(z, y) < q_n(y) \mid u_k(y) > \mathrm{d}z =$$

$$= \frac{1}{2\pi} \int_{-\pi}^{\pi} q(z, y) \int_{-\pi}^{\pi} \sum_{i=1}^{n} c_i u_i(z) u_k(y) \mathrm{d}y\mathrm{d}z =$$

$$= \frac{1}{\pi} \sum_{i=1}^{n} c_i \int_{-\pi}^{\pi} \int_{-\pi}^{\pi} q(z, y) u_i(z) u_k(y) \mathrm{d}y\mathrm{d}z = \sum_{i=1}^{n} c_i K_{ik} \qquad \text{(A3–4)}$$

and

$$q_{ik} = \frac{1}{2\pi} \int_{-\pi}^{\pi} \int_{-\pi}^{\pi} q(z, y) \mathrm{u}_i(z) u_k(y) \mathrm{d}y\mathrm{d}z . \qquad \text{(A3–5)}$$

Thus the system of equations is obtained

$$c_k = \sum_{i=1}^{n} c_i q_{ik} \qquad i, k = 1, \ldots, n \qquad \text{(A3–6)}$$

Moreover $u_i(y)$ used in the computation of this paper is shown in fig. A3–1. From the condition of normality

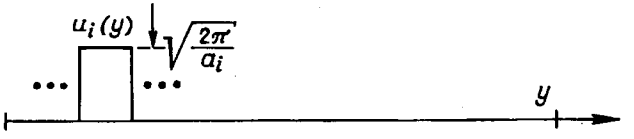

Fig. A3–1. The $u_i(y)$ of the ortonormal system of functions, $i=1,\ldots,n$

$$\frac{1}{2\pi} \int_{-\pi}^{\pi} u_i^2(y) \mathrm{d}y = 1 \qquad \max_{y \in <-\pi, \pi>} u_i(y) = \sqrt{\frac{2\pi}{a_i}} \qquad \text{(A3–7)}$$

The length a_i, $i=1,\ldots,n$ is chosen according to the expected density of

$$q_n(y) \approx \sum_{i=1}^{n} c_u u_i(y) . \qquad \text{(A3–8)}$$

Also

$$\int_{-\pi}^{\pi} \sum_{i=1}^{n} c_i u_i(y) \mathrm{d}y = \sum_{i=1}^{n} c_i \int_{-\pi}^{\pi} u_i(y) \mathrm{d}y =$$

$$= \sum_{i=1}^{n} c_i \sqrt{\frac{2\pi}{a_i}} a_i = \sum_{i=1}^{n} c_i \sqrt{2\pi a_i} = 1 \qquad \text{(A3-9)}$$

due to normalization.
Next

$$\sum_{k=1}^{n} c_k \sqrt{2\pi a_k} = \sum_{k=1}^{n} \sqrt{2\pi a_k} \sum_{i=1}^{n} c_i q_{ik} =$$
$$= \sum_{k=1}^{n} \sqrt{2\pi a_k} \sum_{i=1}^{n} c_i \sqrt{2\pi a_i} \frac{q_{ik}}{\sqrt{2\pi a_i}} =$$
$$= \sum_{i=1}^{n} c_i \sqrt{2\pi a_i} \sum_{k=1}^{n} \sqrt{\frac{2\pi a_k}{2\pi a_i}} q_{ik}. \qquad \text{(A3-10)}$$

Thus

$$\sum_{k=1}^{n} \sqrt{\frac{a_k}{a_i}} q_{ik} = 1. \qquad \text{(A3-11)}$$

Eventually by setting

$$c'_k = \sqrt{2\pi a_k}\, c_k, \qquad k = 1, \ldots, n \qquad \text{(A3-12a)}$$

$$q'_{ik} = q_{ik} \sqrt{\frac{a_k}{a_i}} \qquad \text{(A3-12b)}$$

the following equations are valid

$$c'_k = \sum_{i=1}^{n} c'_i q'_{i,k} \qquad k = 1, \ldots, n \qquad \text{(A3-13a)}$$

$$\sum_{k=1}^{n} c'_k = 1 \qquad \text{(A3-13b)}$$

$$\sum_{k=1}^{n} q'_{ik} = 1 \qquad i = 1, \ldots, n. \qquad \text{(A3-13c)}$$

The real height of rectangle $u_i(y)$, $i=1,\ldots,n$ is c'_i/a_i.
The set of equations (A3 – 13) has well established physical meaning. The coefficients c'_k, $k=1,\ldots,n$ form the distribution of Markov chain with transition probabilities q'_{ik}, $i,k=1,\ldots,n$.

APPENDIX 4

THE NUMERICAL SOLUTION OF THE EQUATION

$$m(x) - \int_a^b q(x, z)\, m(z)\, \mathrm{d}z = g(x) \qquad \text{(A4-1)}$$

Like in previous case

$$m(x) \simeq m_n(x) = \sum_{i=1}^{n} \alpha_i u_i(x) \qquad \text{(A4-2)}$$

and $\{u_i(x)\}$, $i=1,\ldots,n$ form the set ortogonal functions.
Also

$m_n(x)$ tends to $m(x)$ uniformly while $n \nearrow \infty$, $x \in <a, b>$.

Next

$$<m_n(x)\,|\,u_k(x)> = \int_a^b q(x, z) <m_n(z)\,|\,u_k(x)> \mathrm{d}z + <g(x)\,|\,u_k(x)> . \qquad \text{(A4-3)}$$

Or

$$<m_n(x)\,|\,u_k(x)> = \sum_{i=1}^{n} \alpha_i \int_a^b q(x, z) <u_i(z)\,|\,u_k(x)> \mathrm{d}z + <q(x)\,|\,u_k(x)> . \qquad \text{(A4-4)}$$

Finally

$$1)\ \alpha_k = \sum_{i=1}^{n} \alpha_i q_{ki} + b_k , \qquad k = 1, \ldots, \mathrm{n} \qquad \text{(A4-5a)}$$

$$2)\ \underset{a_i}{\rightarrow\square\leftarrow}\ u_i(x) \downarrow \sqrt{2\pi / a_i}$$

and a_i is adjusted according to the expected shape of $m(x)$, $x \in <a, b>$.

$$3)\ q_{ki} = \frac{1}{2\pi} \int_a^b \int_a^b q(x, z)\, u_i(z)\, u_k(x)\, \mathrm{d}x\, \mathrm{d}z \qquad \text{(A4-5b)}$$

$$k, i = 1, \ldots, \mathrm{n}$$

$$b_k = \frac{1}{2\pi} \int_a^b g(x)\, u_k(x)\, \mathrm{d}x, \qquad k = 1, \ldots, n . \qquad \text{(A4-5c)}$$

The original problem has been changed for the solution of the system of equations (A4-5).

APPENDIX 5

THE MODEL OF MARKOV FOR THE MODIFIED DPLL WITH THE EQUANTIZATION EFFECTS TAKEN INTO ACCOUNT

1) The levels of quantizer can be chosen to get linear depedence on the phase error in the case of sinusoid to the loop's filter. See fig. A5-1.

If the number of quantization levels is equal $2M+1$ then the steps of quantization in amplitude are (see fig. A5 – 1)

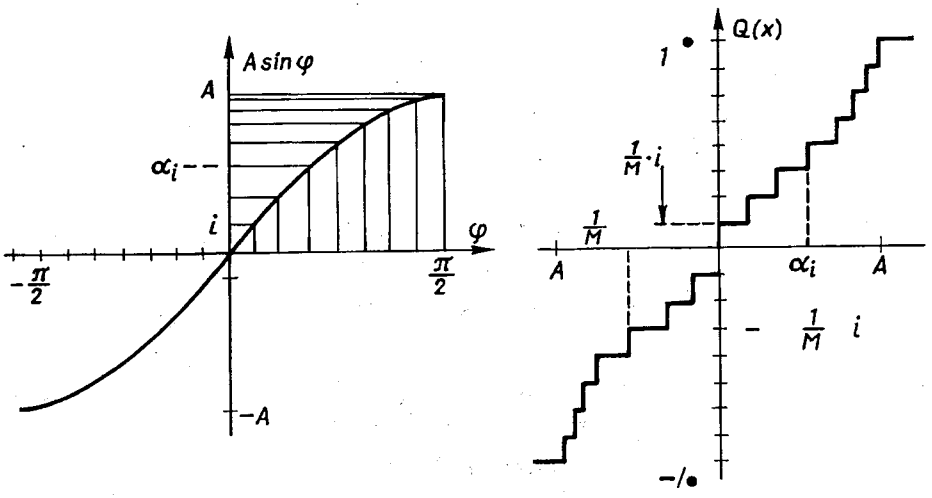

Fig. A5 – 1. Characteristics of quantizer in the case of sinusoid input

$$\alpha_i = A \sin \frac{\pi}{2} \frac{i}{M} \tag{A5-1}$$

$$\alpha_i = -\alpha_{-i}, \quad i = 1, \ldots, M-1$$

2) The equation of not modified DPLL of the first – order is

$$\varphi_{k+1} = \varphi_k - K_1 \left\{ Q(A \sin \varphi_k + N_k) - \frac{A}{K_1} \right\} \tag{A5-2}$$

$$k = 0, 1, \ldots$$

Now

$$Q(A \sin \varphi_k + N_k) \tag{A5-3a}$$

can take only the values

$$\frac{1}{M} i, \quad i = \pm 1, \ldots, M \tag{A5-3b}$$

at view of the characteristic of quantizer assumed.

Let

$$K_1 = \frac{2\pi}{L} \quad \text{and} \quad \frac{A}{K_1} = \frac{l_0}{M} < 1, \quad L, l_0 \text{ are integers.}$$

Thus the equation of the loop is

$$\varphi_{k+1} = \varphi_k - \frac{2\pi}{LM}\left(i - l_0\right) \tag{A5-4a}$$

if

$$Q(A \sin \varphi_k + N_k) = \frac{1}{M} i \tag{A5-4b}$$

i. e if

$$\alpha_{i-1} \leqslant A \sin \varphi_k + N_k < \alpha_i \tag{A5-4c}$$
$$i = 1, \ldots, M - 1$$

$$\alpha_i < A \sin \varphi_k + N_k \tag{A5-4d}$$
$$i = M - 1$$

$$\alpha_i \leqslant A \sin \varphi_k + N_k < \alpha_{i+1} \tag{A5-4e}$$
$$i = -1, \ldots, -(M - 1)$$

$$A \sin \varphi_k + N_k < \alpha_i$$
$$i = -(M - 1).$$

3) Thus if the attention is restricted to the $<-\pi, \pi>$ closed interval the distribution of adminissible states is shown in fig. A5–2 because the smallest step of the phase adjustment is $\pm 2\pi/LM$. The set of states is

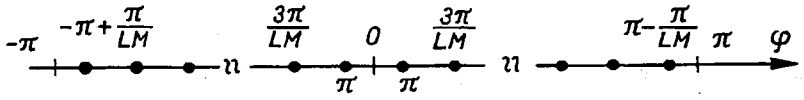

Fig. A5–2. The set of adminissible states in the case of Markov model (Markov chain)

$$X = \left\{\pm \frac{\pi}{LM}, \ldots, \pm \frac{\pi}{\mathrm{LM}}(2_i + 1), \ldots, \pm \frac{\pi}{LM}(LM - 1)\right\} \tag{A5-5}$$

Let $x \in X$ and

$$u(x) = K_1 (Q(A \sin x + N_k) - A/K_1) = \frac{2\pi}{LM}(i - l_0) = z. \tag{A5-6}$$

Thus according to (A5–4a)

$$y = x - z, \quad x \in X, \quad y \in X. \tag{A5-7}$$

Now the required probabilities can be determined

$$P_{xy} = \text{Probability that } z = x - y, P(z = x - y) \tag{A5-8}$$

Moreover

$$P(z) = P(u(x) = z) \tag{A5-9}$$

Let

$$\frac{2\pi}{LM} l_0 = z_0 \text{ and } \frac{2\pi}{LM} i = z'.$$

Then

$$z = z' - z_0 \tag{A5–10}$$

That is why

$$P(z) = P(z' = z + z_0). \tag{A5–11}$$

Finally

$$P(z') = \mathrm{P}\left(K_1(Q(A\sin x + N_k))) = z' = \frac{2\pi}{LM} j\right) =$$

$$= P\left(Q(A\sin x + N_k) = \frac{1}{M} j\right) \tag{A5–12}$$

(A5–3b)

The last probabilities can be readily obtained from (A5–4) while N_k is gaussian $k=0,1,\ldots$

4) The number of states on the circle S^1 is twice smaller in the case of modified loop. Also

$$P_m(z) = P(z' = z + z_0) P_+ + P(z' = -z + z_0) P_- \tag{A5–13}$$

P_m stands for the respective probability in modified case whereas

$$P_+ = P(A\cos x + N_k \geqslant 0) \tag{A5–14a}$$
$$P_- = P(A\cos x + N_k < 0) \tag{A5–14b}$$

5) The results of part I of this paper can be used to compute required parameters.

APPENDIX 6

COMPUTER BASED MODELLING OF DPLL

The idea of computer based modeling of DPLL is to implement its operation in software. The algorithm which generates random gaussian numbers is important for this reason. The disturbing noise can be formed by this numbers in sequence. The following algorithm which is due to Box, Mahler and Marsaglia can be used as noise generator. Though being rather slow it is perspicous and accurate. See the book of Knuth [4] for further assistance.

1. The method of polar coordinates

Step 1. Generate two independent random numbers U_1, U_2 of uniform distribution on (0, 1) interval.

Step 2. Transform these numbers into $(-1, 1)$ interval according to $V_1 = 2U_1 - 1$; $V_2 = 2U_2 - 1$

Step 3. Calculate

$$R^2 = V_1^2 + V_2^2$$

Step 4. If $R^2 \geqslant 1$ then go to step 1 else go to next step.

(The mean value of the sequence of steps from 1 to 3 is 1.27 while its deviation is 0.587).

Step 5. Generate two indepedent random numbers X_1, X_2 of normal distribution N(0,1) (of 0 mean value and standard deviation equal 1) according to

$$X_1 = V_1 \sqrt{-\frac{2\ln R^2}{R^2}}; \quad X_2 = V_2 \sqrt{-\frac{2\ln R^2}{R^2}}.$$

2. The justification of the method of polar coordinates

First of all if $R^2 < 1$ then the point (V_1, V_2) is from uniform distribution of the inside points of the circle of R radius. Secondly let $V_1 = R\cos\theta$ and $V_2 = R\sin\theta$. Then

$$X_1 = R'\cos\theta \quad \text{and} \quad X_2 = R'\sin\theta \tag{A6-1}$$

while

$$R' = \sqrt{-2\ln R^2} \tag{A6-2}$$

Also R^2 and θ are indepedent and from uniform distribution on (0,1) and $<-\pi,\pi>$ interval respectively. Thus

$$P(R' \leqslant r) = P(-2\ln R^2 \leqslant r^2) = P\left(R^2 \geqslant e^{\frac{-r^2}{2}}\right) = 1 - e - \frac{-r^2}{2} \tag{A6-3}$$

$P(A \ldots)$ stands for the probability of event that A ...

Now

$$P(r \leqslant R' \leqslant r + dr) = p(r)\,dr = re^{-r^2/2}\,dr \tag{A6-4a}$$

and

$$P(v \leqslant \theta \leqslant v + dv) = p(v)\,dv = \frac{1}{2\pi}dv \tag{A6-4b}$$

Thus the joint distribution function is

$$P(X_1 \leqslant x_1, X_2 \leqslant x_2) = P(r\cos v \leqslant x_1 r \sin v \leqslant x_2) = \int\limits_{\{(r,v:\ r\cos v \leqslant x_1,\ r\sin v \leqslant x_2\}} \frac{1}{2}\pi\, re^{-r^2/2}\,dr\,dv =$$

$$= \frac{1}{2}\pi \int\limits_{\{(x,y):x \leqslant x_1, y \leqslant x_2\}} e^{-(x^2+y^2)/2}\,dx\,dy = \frac{1}{\sqrt{2\pi}} \int\limits_{-\infty}^{x_1} e^{-x^2/2}\,dx \frac{1}{\sqrt{2\pi}} \int\limits_{-\infty}^{x_2} e^{-y^2/2}\,dy. \tag{A6-5}$$

Eventually X_1 and X_2 are gaussian and independent.

3) The estimate of mean value based on N_1 observations x_i of random variable X is

$$S_{N_1} = \frac{1}{N_1} \sum_{i=1}^{N_1} x_i$$

4) The estimate of variance based on N_1 observations x_1 of random variable X is

$$V_{N_1} = \frac{1}{N_1 - 1} \sum_{i=1}^{N_1} (x_i - S_N)^2 = \frac{1}{N_1 - 1} \sum_{i=1}^{N_1} x_i^2 - \frac{N_1}{N_1 - 1} S_{N_1}^2$$

5) The equation of I-order modyfied DPLL is

$$\varphi_{k+1} = \varphi_k - K_1 \operatorname{sign}(A \cos \varphi_k + N_k^c) \sin \varphi_k + \Lambda +$$

$$- \frac{K_1}{A} \operatorname{sign}(A \cos \varphi_k + N_k^c) N_k^s$$

$$k = 0, 1, \ldots$$

N_k^c, N_k^s, $k=0,1,\ldots$ are the sequences of indepedent gaussian variables of 0 mean value and σ_N standard deviation.

6. The equation of I – order unmodified DPLL is

$$\varphi_{k+1} = \varphi_k - K_1 \sin \varphi_k + \Lambda - \frac{K_1}{A} N_k$$

$$k = 0, 1, \ldots$$

N_k, $k=0,1,\ldots$ is white stationary gaussian sequence of θ mean value and δ_N standard deviation.

7. The equation of II – order DPLL is

$$\varphi_{k+2} - 2\varphi_{k+1} + \varphi_k = -K_1 r X_{k+1}/A + K_1 X_k/A$$

$$k = 0, 1, \ldots$$

$X_k/A = \sin\varphi_k + \frac{N_k}{A}$, $k = 0, 1, \ldots$ in the case of unmodified DPLL.

$$X_k/A = (\sin\varphi_k + N_k/A) \operatorname{sign}(A \cos\varphi_k + N_k^c), \quad k = 0, 1, \ldots$$

in the case of modified DPLL.

8. The characteristics of quantizer is shown in fig. 31.

9. The standard deviation is set equal σ according to transformation

$$N_s = \sigma X_i, \quad i = 1, 2,$$

while X_i is of standard deviation equal 1.

10. N_k/A k=0,1,...
is of standard deviation equal

$$\sigma = \sqrt{\frac{1}{2S_0}}, \quad S_0 = 10^{S_{0_{db}}/10}$$

while $S_{0_{db}}$ is the input signal power to noise power ratio (SNR, dB scale used).

11. The results of computer based modelling are shown in fig. 20÷35.

M. ŻÓŁTOWSKI

O CYFROWYCH PĘTLACH FAZOWYCH Z NIEJEDNOSTAJNYM PRÓBKOWANIEM W OBECNOŚCI ZAKŁÓCEŃ LOSOWYCH. CZĘŚĆ II

Streszczenie

Pętla cyfrowa z niejednostajnym próbkowaniem została zmodyfikowana w celu uzyskania korzystniejszych własności dotyczących osiągania stanu synchronizmu [2,3].
Jej parametry w obecności zakłóceń losowych zostały zbadane w ramach teorii przedstawionej w części I. Szczególnie istotny był wpływ modyfikacji na zjawisko poślizgu błędu fazy. Przeprowadzone obliczenia nie pokazują istotnej degradacji. Niezmodyfikowana pętla drugiego rzędu objawia zjawisko chaosu przejściowego [2,3]. Zjawisko to jest badane w obecności zakłócenia losowego.
Natomiast zjawisko zawieszenia stanu synchronizmu w pętli zmodyfikowanej nie występuje.

KWARTALNIK ELEKTRONIKI I TELEKOMUNIKACJI, 1991, 37, Z. 3–4, ss. 533–572

621.317.08

New stability criteria for the nonuniform sampling zero-crossing digital phase-locked loops of any order*

MARIUSZ ŻÓŁTOWSKI

Instytut Telekomunikacji, Politechnika Gdańska

Otrzymano 1990.04.25

Autoryzowano do druku 1990.11.27

Part I

New stability criteria for the digital nonuniform sampling zero-crossing phase-locked loops are derived. The functional nonlinear discrete-time equation on the S^1 – circle manifold is used to describe the phase error process in the loop of any order. Disturbed N:1 phase entrainment is studied while the perturbation is either the frequency offset or additional random noise and effects due to quantization. The class of loops with discontinous characteristics of phase-detector is recommended while fast acquisition regardless of the initial phase error conditions is required in the case of loop of any order. The notion of the covering space of the theory of dynamical systems is used to consider the dynamics of the loop on the S^1 – circle manifold. The presented approach is extendible to include the fading of the input waveform, AM and PM modulation or variable coefficient filter of the loop. This extension shall be presented in Part II and Part III.

1. INTRODUCTION

Digital phase-locked loops (DPLL – s) may be considered as heart parts of digital synchronization systems. Generally they can be referred to nonuniform sampling and uniform sampling schemes [1]. Just the class of nonuniform sampling loops shall be of interest in this paper. Namely, the sampling device acts as a phase detector in these loops while providing information about the deviation of the incoming signal versus the local reference generated in the digitally controlled oscillator (DCO) of the loop. Usually the nonuniform sampling DPLL takes the advantage of the N:1 phase entrainment only. It occurs while the loop is tracking the positive zerocrossings of the incoming signal. Then there are exactly N periods of the input waveform during 1 nominal period of the sampler. Nevertheless the $P:Q$ phase entrainment while P and

* Accepted for presentation at 1990 IEEE International Symposium on Circuits and Systems as regular (lecture) paper [11]

Q are integers may occur in the nonuniform sampling phase-locked loop also. However such a loop is not zero-crossing DPLL(ZC−DPLL) any more. The N:1 phase entrainment in the nonuniform sampling DPLL−s has been studied by Gill, Gupta, Reddy, Weinberg, Liu, Chie, Lindsey, Osborne, Andrea, Russo, Rudel and others [1]. Quantization, frequency offset and noise disturbance result in the perturbation of the state of phase entrainment in the loop. However in all cases the fast acquisition behaviour while not dependent on the initial phase error is of great importance from the practical point of view. On the other hand the possibility of existence of chaotic transient hang up phenomenon has been revealed in the DPLL of second order with sinusoidal-type nonlinearity [4,12,13,14]. This loop can achieve phase-lock even different from the N:1 phase entrainment for some region of the initial conditions of the phase error process (see also the discussion at the end of this part). As a matter of fact the exact conditions under which the N:1 phase entrainment is acquired are of interest. That is why they are considered in the this paper. Among the derivation of new stability criteria according to which the class of loops with discontinous nonlinearity may not exhibit chaotic behaviour a simple controlling algorithm is considered also. The aim of it is to improve the acquisition of the phase-lock in the case of nonuniform sampling DPLL with sinusoidal nonlinearity. Additionally it is pointed out that the approximations to hold in range and pull in range can be obtained within presented approach either. Pull in range is determined by the frequency interval while the phase-lock is acquired regardless of the initial conditions of the phase error. Whereas the hold in range by the one while phase-lock is maintained. The known estimates of this parameters have been provided in [2,5]. However less is known about the pull in range of the DPLL−s of higher order. In addition the constant component of the phase error process is known as static error while the variable one as dynamic one.

2. THE NOTION OF THE COVERING SPACE AND THE MATHEMATICAL MODEL OF THE NONUNIFORM SAMPLING DIGITAL PHASE-LOCKED LOOP IN THE CASE OF N:1 PHASE ENTRAINMENT

The notion of the covering space will be explained before begining with the model of the loop [10]. This notion is helpful while dealing with the dynamics on the S^1 − circle manifold instead of the straight line R.

DEFINITION 1

The continous mapping π: $Y \to X$ (Y, X topological spaces) is a covering if for every $x_0 \in X$ there exist its neighbourhood U, $x_0 \in U$ such that $\pi^{-1}(U)$ is a disjoint union of open subsets of Y. Each set of this union is mapped into U by homeomorphism i. e. Π is a local homeomorphism. The space Y is called a covering space of the base space X.

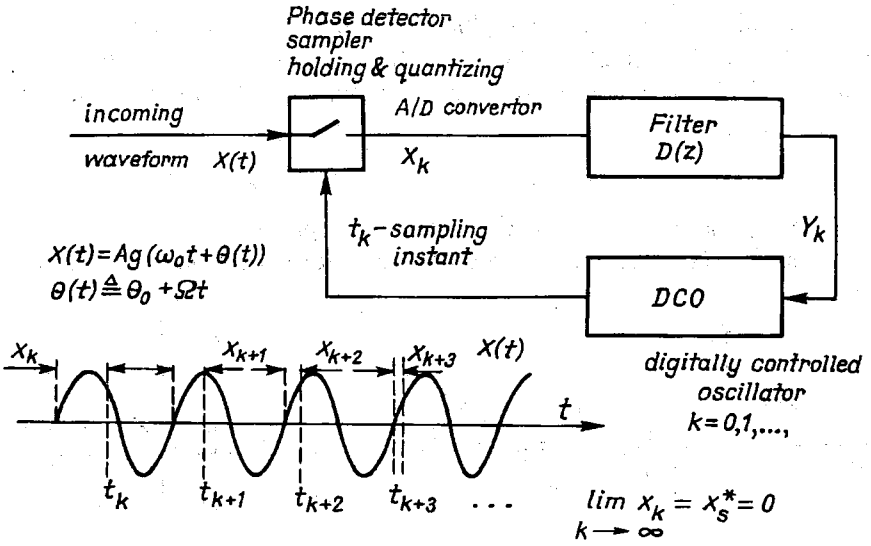

Fig. 1. The scheme of the digital nonuniform sampling ZC (zero crossing) phase-locked loops and the principle of synchronization ($N=1$, $g(\varphi)=\sin\varphi$, $\{x_k\}$ converges to the fixed point x_s^* of stable equilibrium)

Moreover the principle of synchronization by the loop is explained in fig. 1 and scheme of the loop's model is provided. The details concerning the derivation of this model are given in appendix 1 (A1). However, the incoming waveform being tracked by the loop is

$$X(t) = Ag(\omega_0 t + \theta(t)) + N(t). \qquad \text{(A1-1)}$$

The function g of (A1 – 1) describes the shape of the signal component of $X(t)$ and the following conditions are met:

1) $g : R \to <-1, 1>$ is periodic with period 2π

2) there is only one zero crossing in $(-\pi, \pi)$ open interval. A stands for the amplitude, ω_0 for the radian frequency whereas $\theta(t)$ for the phase of signal part of $X(t)$, θ_0 is an offset in phase while Ω_0 one in frequency. The linear discrete-time filter of the loop is described in terms of the transfer function $D(z)$. The effects of quantization are taken into account by nonlinear function Q. Moreover $N(t)$ of (A1 – 1) stands for the noise component disturbing loop's input signal. The digitally controlled oscillator (DCO) of the loop performs the calculations of the subsequent sampling instants according to the algorithm

$$t_{k+1} = T - Y_k + t_k, \qquad k = 0, 1, \ldots \qquad \text{(A1-2a)}$$

T of (A1 – 2a) is the period of sampling while Y_k is the output from the digital filter of the loop at instant k. The perturbed N:1 phase entrainment is of interest. This is consistent with

$$T = \frac{2\pi}{\omega_0} N \qquad \text{(A1-2b)}$$

and zero initial conditions of the loop's filter.

Let the disturbing noise be negligible. The extension to include the effects of noise on loop's dynamics will be presented further. In this case the dynamics of the loop of n^{th} order in respect to N:1 phase entrainmen can be shortly given by [1,2,5,13]

$$x_{k+1} = F(x_k, x_{k-1}, \ldots, x_{k-n+1}), \tag{1}$$

while $\{x_k\} \stackrel{\text{df}}{=} \{x_k : k = 0, 1, \ldots\}$ is the phase error process.
The mapping F of (1) is almost everywhere continous. The points of discontinuity

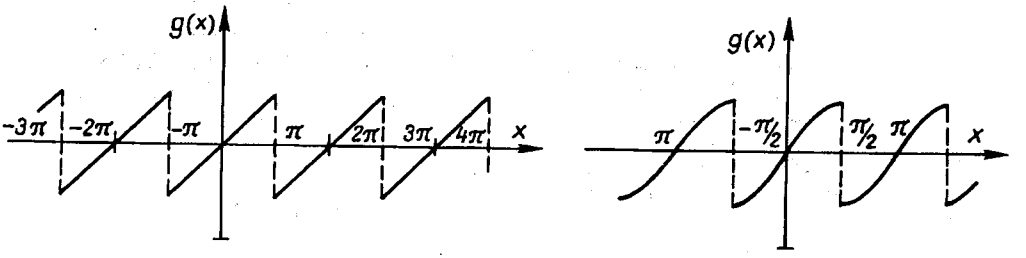

Fig. 2. The other shapes of the nonlinearity of the digital nonuniform sampling phase-locked loop

of F depend on the discontinuity of the nonlinearity g of the loop (see fig. 1) which contributes to the characteristics of the phase detector of the loop. Among the DPLL−s with sinusoidal nonlinearity there are also ones with g of fig. 2. Let the coefficients of the loop's filter be positive. Then the fixed points of (1)[1)]

$x_s^* = 2k\pi \subset \mathrm{R}$, k = ..., −1, 0, 1, ... are the points of stable equilibrium while

$x_u^* = (2k + 1)\pi \subset R$, $k = \ldots, -1, 0, 1, \ldots$ are the points of unstable equilibrium

provided, that the characteristic roots of the linearized equation (1) are all inside the unit circle of complex plane.
Let also

$$\hat{x}_k \stackrel{\text{df}}{=} \{x_k, x_{k-1}, \ldots, x_{k-n+1}\}, \; k = n - 1, n, n + 1, \ldots$$

and all x_k of the subsequent $\hat{x}_k$ appear according to (1).
That is why $\hat{x}_{n-1}$ represents the set of initial conditions of (1);

$$\hat{x}_{n-1} = \{x_{n-1}, x_{n-2}, \ldots, \mathrm{x}_0\}.$$

Suppose there is family of sets V_m such that for each m

$$\hat{x}_m \subset V_m \subset B(x_s^{*2k}, r_m) \quad m = n - 1, n, n + 1, \ldots$$

and there is no other set V_m of smaller diameter than r_m while showing this property. $B(x_s^{*2k}\, r_m)$ stands for the ball which is centered in x_s^{*2k} and has diameter r_m.
Now, if $x_s^{*2k} = 2k\pi \in R$ for certain $k \in Z$ (Z stands for the set of integers) then the following lemma 1 holds true.

[1)] The point x^* is a fixed point of (1) if $x^* = F(x^*,\ldots,x^*)$

Lemma 1

If $x^{*2k}_s \in U$ is the point of stable equilibrium of (1) and $U \subset R$ is sufficiently small then there exist: $\epsilon > 0$, integer k_0 and the family o sets $V_m \subset U \subset R$ such that

$$\text{diam } V_{k_0} = r_{k_0},\ V_{m+1},\ V_m \subset U,\ \bigcap_{m = k_0} V_m = x^{*2k}_s$$

and

$$\hat{x}_m \subset V_m \qquad m = k_0, k_0 + 1, \ldots$$

In other way lemma 1 states that every trajectory $\gamma(x)$ while the initial point is $x = \hat{x}$

$$\gamma(x) \stackrel{\text{df}}{=} \{y \in R: \exists_{k \in Z}\ y = x_k\}$$

of (1) converges locally to the point of stable equilibrium x^{*2k}_s. Now, the next lemma can be considered.

Lemma 2

Let $\gamma_s(x) = \pi(\gamma(x))$ be the trajectory of (1) projected on the circle $S^1 = <-\pi, \pi>$ closed interval with equivalent end points while the all characteristic roots of linearized counterpart of (1) are inside the unit circle of complex plane. Then the trajectory $\pi(\gamma(x))$ converges to the only fixed point of stable equilibrium $x^*_s = 0 \in S^1$ if and only if $\gamma(x)$ converges locally to certain point $x^{*2k}_s = 2k\pi \in R$ $(k \in Z)$, (Z is the set integers) of stable equilibrium. Space $R = R^1$ (R is the set of reals) is the covering space of S^1.

Proof

Suppose $\gamma_s(x)$ converges to the point $x^*_s = 0 \in S^1$ and the characteric roots of linearized counterpart of (1) are all inside the unit circle. Then there exist neighbourhood $U \subset S^1$ of $0 \in S^1$ such a that $\pi^{-1}(\gamma_s(x))$ converges in $\pi^{-1}(U)$ to $x^{*2k}_s = 2k\pi \in R$ for certain $k \in Z$ and vice versa [10]. Note that it may happen that $V_{m+1} \not\subset V_m$.
In other way Lemma 2 asserts the following:

1) Suppose the parameters of the loop are fixed and the equation (1) is valid in respect to the N:1 phase entrainment (see appendix 1 for the details).

2) All the characteristic roots of (1) are inside the unit circle while the phase entrainment with $x^*_s = 0 \in S^1$ occurs.

Then there is exactly only N:1 phase entrainment with the state $x^{*2k}_s \in R$ for certain k (the fixed point of stable equilibrium) and $\pi(x^{*2k}_s) = x^*_s \in S^1$ considered as phase-loock (see also fig. 3)
The projection of lemma 2 is:

$$\pi : R \to S^1$$

$$[x] \to [\mathrm{x}] = \arg(e^{jx}) \text{ and } [x] \in <-\pi, \pi>. \tag{2}$$

Equivalently $[x] = x(\mathrm{mod}\, 2\pi)$.

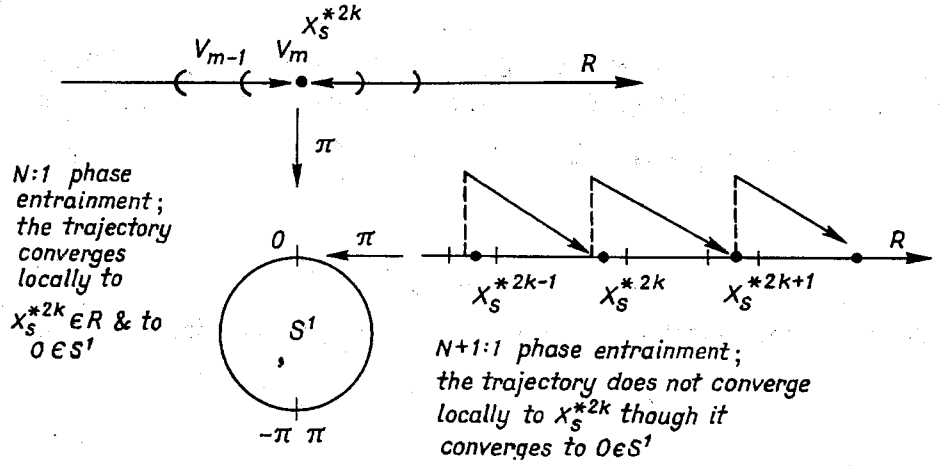

Fig. 3. The ilustration of lemma 2

Secondly, the following functional equation is proposed instead of (1) to describe the dynamics of the phase-locked loop

$$x(k+1) = \sum_{l=0}^{k} k_{\lambda,1}(k-l)\{g(x(l)) - \lambda x(l)\} + x_\lambda(k+1) + \sum_{l=0}^{k} k_{\lambda,2}(k-l)z(l) \tag{3}$$

$$k = 0, 1, \ldots$$

The interpretation of the new model of the loop is given in fig. 4. The equation (3) is equivalent to the equation (1) in the sense that the trajectories generated by (1) and (3)

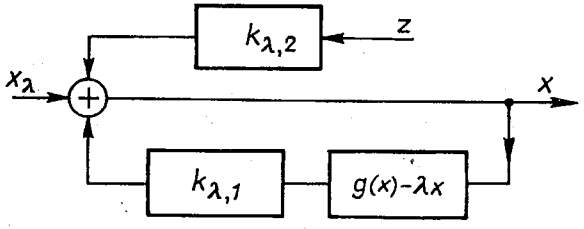

Fig. 4. The interpretation of the new model of the digital phase-locked loop given in terms of the equation (5)

are the same (the discrete time case is considered). Thus the initial points of every trajectory of (3) are $x(0), x(1), \ldots, x(n-1)$ for the loop of order n (generally the symbol $a(k)$ is equivalent to the symbol a_k). These initial conditions are included in the discrete time waveform $x_\lambda(k+1)$ of (3). The real parameter λ is positive. The derivation of the equation (3) which is based on $\mathcal{Z}$-transformation technique is presented in the appendices (A2–A4) of this paper. The $x(k)$ of (3) is the phase error process in the loop. It is defined to measure the deviation from the state of phase entrainment (see fig. 1 and the appendices for the details). The waveform $z(l)$ of (3) $l=0,1,\ldots$ stands for the disturbing noise sequence. As previously the nonlinearity of the loop is given in terms of periodic function g with 2π being the period in this case. It results either directly

from the shape of the waveform being tracked by the loop or from the image of the nonlinear processing algorithm while acting on this waveform. The functions $k_{\lambda,1}$, $k_{\lambda,2}$ of discrete time argument are the unit pulse responses of the new model of the loop. Whereas x_λ which depends on the n initial points in the order loop case n^{th} is the discrete time response of the linear part of the loop's model, being known (see fig. 4). Note that the nonlinear functional equation (3) is of 1 dimension whatever the order of the loop is. This stands in favour of it most of all. Now, the idea of this paper can be easily explained. The new model of the nonuniform sampling digital phase-locked loop while in terms of equation (3) is used to derive new stability criteria. The problem of this paper is similar to that considered by Tsypkin [9] while concering the nonlinear discrete-time control systems. However the S^1 – circle manifold is the state space of this approach instead of the euclidean one as usually is of concern. Just in view of lemma 2 one can consider the dynamics on the S^1 – circle manifold instead of the R^1 – euclidean space of 1 dimension.

3. THE DYNAMICS OF THE DIGITAL PHASE-LOCKED LOOP ON THE S^1 – CIRCLE MANIFOLD

One can begin with the argument that the phase error of the equation (3) is the cyclic variable at any discrete-time instant k, $k=0,1,\ldots$. This idea can be formulated in terms of the following Lemma 3.

Lemma 3

Let the phase error process $\{x(k)\}$, $k=0,1,\ldots$ satisfy the equation (3). Then the following diagram is commutative

$$\begin{array}{ccc} \{R\} & \overset{\mathscr{F}}{\to} & \{R\} \\ \downarrow & & \downarrow \\ \{S^1\} & \overset{\mathscr{F}}{\to} & \{S^1\}. \end{array} \tag{4}$$

The $\mathscr{F}$ of diagram (4) stands for the functional operator of the right hand side of the equation (3). This operator acts either on the space of sequences of elements from R denoted as $\{R\}$ or on the space of sequences of elements from S^1 denoted as $\{S^1\}$.

Remark

One can think that the proposition of Lemma 3 is obvious because the phase error process can be given the explicit definition as the sequence of variables which take their values from S^1. However a formal proof can be derived while being based on the recursive equivalent of (3). Namely, the right hand side of (1) is partly additive in subsequent phase errors and partly not sensitive to the shift by 2π radians due to the nonlinearity of the loop's model while being periodic. That is why the operations of (4) are really interchangeable.

Now, in view of lemmas 1 – 3 the examination of the equation (3) on the S^1 – circle manifold is well established.

4. THE N:1 PHASE ENTRAINMENT ONE THE S^1 – CIRCLE MANIFOLD. INTRODUCTION

The equation (5) will be considered:

$$x(k+1) = \sum_{l=0}^{k} k_{\lambda,1}(k-l)\left\{g(x(l)) - \lambda x(l)\right\} + x_\lambda(k+1) + \sum_{l=0}^{k} k_{\lambda,2}(k-l)\, z(l) (\mathrm{mod}\, 2\pi). \tag{5}$$

It results from the equation (3) by the projection on the S^1 – circle manifold. The first n points of (5) are specified as $x(0)(\mathrm{mod}\, 2\pi)$, $x(1)(\mathrm{mod}\, 2\pi)$, ..., $x(n-1)(\mathrm{mod}\, 2\pi)$. The order of the loop is equal n while $(\mathrm{mod}\, 2\pi)$ stands for the operation of projection which has been explained in the previous chapters.
Suppose first that

$u(l) \stackrel{\mathrm{df}}{=} g(x(l)) - \lambda x(l)$, $l = 0, 1, \ldots$ and $z(l) = 0$ (the noise is negligible).

Then the following observations are valid.

Observation 1

Let g be the linear function from S^1 to R such a that $u(l) = 0$ for all l, $l = 0,1,\ldots$. Then the trajectory of the phase error process is given by

$$x(k+1) = x_\lambda(k+1)(\mathrm{mod}\, 2\pi) \tag{6}$$

The n initial points are $x(0)(\mathrm{mod}\, 2\pi)$, $x(1)(\mathrm{mod}\, 2\pi)$, ..., $x(n-1)(\mathrm{mod}\, 2\pi)$.

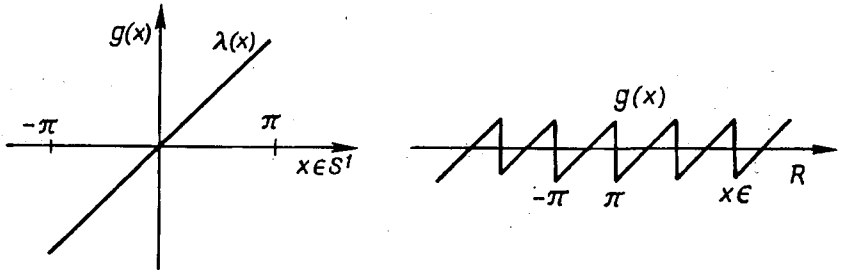

Fig. 5. The loop's phase detector nonlinearity: linear on S^1 – circle manifold and periodic on R straight line

Observation 2

Let the following approximation which is known as linearization be valid

$$g(x) = g'(0)x = \lambda x \tag{7}$$

for all x from the neighbourhood U of $0 \in S^1$. If the set U contains the whole trajectory of the phase error process then the equation (6) is also valid. Secondly, the following conclusions can be derived from the observations 1 and 2.

Conclusion 1

Let $u(l) = 0$ for all $x \in S^1$ $(g(x) = \lambda x)$ and

a) $r_x = \limsup_{m \to \infty} \sqrt[m]{|x_\lambda(m)|} < 1$, or equivalently

b) the function $X_\lambda(z) = \sum_{m=0}^{\infty} x_\lambda(m) z^{-m}$, $z \in C$ (C is the set of complex numbers) has the poles inside the unit circle of the complex plane. Then

$$\lim_{k \to \infty} x(k) \pmod{2\pi} = 0$$

for every initial points of the phase error process. The absolute value $|x(k)|$ diminishes not slower than $c r_x^k$ when k tends to infinity, $c > 0$, $c \in R$.

Conclusion 2

Let $\forall_{x \in U \subset S^1} g(x) = \lambda x$ and the trajectory of the phase error process is entirely in U. Then the proposition of conlusion 1 is also locally valid while the set U is of concern. The point $0 \in S^1$ is the point of stable equilibrium in this case.

Conclusion 3

Let $\lambda = g'(0)$, g is at least C^1. Then by localizing the poles of $X_\lambda(z)$ of the conclusion 1 one can determine the region of the parameters which assure the existence of the stable equilibrium $0 \in S^1$ and N:1 phase entrainment locally. The aim of further considerations is to extend the results given by conclusions 1 – 3 to more general case of the nonlinearity of the loop. Especially the conclusion 1 which asserts the global stability of loop's dynamics on S^1 – circle manifold is of interest in more general circumstances. The proposition of lemma 2 assets the correctness of such a approach in respect to N:1 phase entrainment.

5. THE N:1 PHASE ENTRAINMENT ON THE S^1 – CIRCLE MANIFOLD. GENERAL CASE

First one can easily check that the following properties hold true for any $x, y, \alpha \in R$ while $[x] = x \pmod{2\pi}$ stands for the projection on S^1 circle manifold

$$|[|x|]| = |[x]| \tag{8a}$$
$$[\alpha[x]] | \leqslant |\alpha| \quad |[x]| \tag{8b}$$
$$|[[x] + [y]]| \leqslant |[x]| \tag{8c}$$

$|x|$ stands for the absolute value of x.

Secondly, let $\{X\}$ stand for the space of the sequences $\{x\}$ which elements $x(n)$, $n \in Z_+$ (Z_+ is the set of nonnegative integers) are from the space X i. e.

$$\{X\} = \left\{\{x\} : Z_+ \to X, \quad n \to x(n) \in X\right\}. \tag{9}$$

The space $\{X\}$ is the vector space while

$$\begin{aligned} \{x\} &= \{x(0), x(1), \dots\} \\ \{x \pm y\} &= \{x(0) \pm y(0), x(1) \pm y(1), \dots\} \\ \{\alpha x\} &= \{\alpha x(0), \alpha x(1), \dots\} \end{aligned} \tag{10}$$

Also let $\{[X]\}$ stand for the space of the sequences $\{[x]\}$ which elements are from $[X]$ space

$$\begin{aligned} \{[X]\} &\stackrel{\text{df}}{=} \left\{\{[x]\} : Z_+ \to [X], n \to x(n) \in [X]\right\} \\ [X] &\stackrel{\text{df}}{=} \{[x] : x \in X\} \\ \{[x]\} &= \{[x(0)], [x(1)], \dots\} \end{aligned} \tag{11}$$

The operations of the $\{[X]\}$ space are induced by those of $\{X\}$. However $\{[X]\}$ is not a vector space any more (see (8b)) but is still similar to vector one. Now, let the function ρ from $\{X\}$ to R_+ (R_+ is the set of nonnegative reals) be given:

$$\begin{aligned} \rho &: \{X\} \to R_+ \\ &\{x\} \to \rho(\{x\}) < \infty \end{aligned} \tag{12}$$

The following properties of the function ρ which concern the space $\{[X]\}$ will be of importance:

$$\rho(\{[x]\}) = 0 \rightleftharpoons \{[x]\} = 0 \text{ while last 0 stands for zero of } \{[X]\} \tag{13a}$$

$$\rho(\{[\{[x]\}]\} + \{[y]\}]\} \leqslant \rho(\{[y]\}) + \rho(\{[y]\}) \tag{13b}$$

$$\rho(\{[\alpha\{[x]\}]\}) \leqslant |\alpha| \rho(\{[x]\}) \tag{13c}$$

The operations of addition, multiplication and projection of (13) are performed the point by point (see (10) and (11)). This concept of ρ function is quite similar to the notion of norm. However it should be identity in (13c) in the normed space case. The space $\{[X]\}$ with ρ function well defined for every element $\{[x]\} \in \{[X]\}$ is denoted by $(\{[X]\}, \rho)$. Next, let the following notation be introduced before the dynamics of the loop in respect to S^1 — circle manifold is considered:

$$A_{\lambda,1}\{u, k\} \stackrel{\text{df}}{=} \sum_{l=0}^{k} k_{\lambda,1}(k - 1)u(l) \tag{14a}$$

$$z_\lambda(k) \stackrel{\text{df}}{=} \sum_{l=0}^{k} k_{\lambda,2}(k - 1)z(l) = A_{\lambda,2}\{z, k\} \tag{14b}$$

$$u(k) \stackrel{\text{df}}{=} g(x(k)) - \lambda x(k), \quad k \in Z_+. \tag{14c}$$

Let also the sequence $\{A_{\lambda,1}\{u\}\}$ be introduced

$$\{A_{\lambda,1}\{u\}\} : Z_+ \times \{R\} \to \{R\}$$
$$(\{u\}, k) \to A_{\lambda,1}(\{u\}, k) \tag{14d}$$

$k \in Z_+$ and $\{u\} \in \{R\}$.
Now, if

$$\forall_{\{u\} \in \{R\}} \rho(\{[A_{\lambda,1}\{u\}]\}) \leqslant \alpha_1 \rho(\{u\}) \tag{15}$$
$$0 \leqslant \alpha_1 < \infty$$

then there exists the operator $A_{\lambda,1}$:

$$A_{\lambda,1} : (\{R\}, \rho) \to (\{S^1\}, \rho) : S^1 = [\mathrm{R}]$$
$$\{u\} \to \{[A_{\lambda,1}\{u\}]\}$$

and

$$\rho([A_{\lambda,1}u]) \stackrel{\mathrm{df}}{=} \rho(\{[A_{\lambda,1}\{u\}]\}) \leqslant \alpha_1 \rho(\{u\}). \tag{16}$$

Moreover suppose that the following constraint concerning the $\{u\}$ sequence is valid also

$$\forall_{\{u\} \in \{R\}} \rho(\{u\}) \leqslant \alpha_2 \rho(\{[x]\}) + a, \quad 0 < a \in R. \tag{17}$$

Now, in view of this chapter the equation (5) can be given the short form:

$$x = A_{\lambda,1}u + x_\lambda + z_\lambda (\mathrm{mod}\, 2\pi) \tag{18}$$

with $A_{\lambda,1}$ of (16), u of (14c) and z_λ of (14b).
Finally, the main result of this paper can be given in terms of the theorem 1.

Theorem 1

Let x_λ and z_λ belong to $(\{R\}, \rho) \cap (\{S^1\}, \rho)$ space. If

$$\alpha_1 \cdot \alpha_2 < 1 \ (\alpha_1 \text{ of (15) and } \alpha_2 \text{ of (17)})$$

then there is extractly one solution of (5) which belongs to $(\{S^1\}, \rho) \cap (\{R\}, \rho)$ space. Also, the following estimation holds true

$$\rho(\{[x]\}) \leqslant \frac{\rho(\{[x_\lambda]\}) + \rho(\{[z_\lambda]\}) + \alpha_1 a}{1 - \alpha_1 \alpha_2}. \tag{19}$$

The proof of theorem 1

While the equation (18) is equivalent to recurrent one there is always the unique solution of it for any initial points specified. Moreover from the functional form of (18) and the relations (13), (16) and (17) it follows that:

$$\rho(\{[x]\}) = \rho(\{[A_{\lambda,1}u + x_\lambda + z_\lambda]\}) = \rho(\{[[A_{\lambda,1}u] + [x_\lambda + z_\lambda]]\}) \leqslant$$
$$\leqslant \alpha_1 \rho(\{u\}) + \rho(\{[x_\lambda]\}) + \rho(\{[z_\lambda]\}) \leqslant \alpha_1 (\alpha_2 \rho(\{[x]\}) + a) +$$

$$+ \rho(\{[x_1]\}) + \rho(\{[z_1]\}).$$

Just the belongness of the solution $\{[x]\}$ to $(\{S^1\}, \rho)$ space follows from this inequality while its belongness to $(\{R\}, \rho)$ space is assured by lemma 2.

Now, the strategy of further approach can be clarified. The N:1 phase entrainment will be studied by theorem 1 while different functions ρ are used. These functions are to measure the process of acquisition of phase-lock by the loop while different constraints are posed on loop's nonlinearity. The various aspects of the process of acquisition can be studied this way.

6. THE EXAMPLES OF DIFFERENT $(\{[X]\}, \rho)$ SPACES

a) The space $(\{[X]\}, \rho_1)$ of the sequences of finite pseudoenergy

$$\rho_1 : \{[X]\} \to R_+$$

$$\{[x]\} \to \rho_1(\{[x]\}) = \sqrt{\sum_{m=0}^{k} |[x(m)]|^2 r_0^{-2m}} \tag{20}$$

$r_0 \in (0,1> \subset R$.

The sequence of null pseudoenergy is zero of this space.

b) The $(\{[X]\}, \rho_2)$ space.

$$\rho_2 : \{[X]\} \to R_+$$

$$\{[x]\} \to \rho_2([x]) = \lim_{N\to\infty} \sup_{n>N} |[x(m)]|. \tag{21}$$

Every sequence which converges to zero is zero of this space.

c) The space $(\{[X]\}, \rho_3)$ of the sequence of finite pseudopower.

$$\rho_3 : \{[X]\} \to R_+$$

$$\{[x]\} \to \rho_3(\{[x]\}) = \overline{\lim_{N\to\infty}} \sqrt{\frac{1}{N} \sum_{m=0}^{N} |[x(m)]|^2} \tag{22}$$

d) The space $(\{[X]\}, \rho_4)$ of the sequences of finite peak value.

$$\rho_4 : \{[X]\} \to R_+$$

$$\{[x]\} \to \rho_4(\{[x]\}) = \sup_{m\geqslant 0} |[x(m)]|. \tag{23}$$

It is not difficult to prove with aid of (8) that the properties (13) are met while the functions ρ_i $(i=1,2,3,4)$ of this chapter are of concern. The triangle inequality (13b) follows from the known triangle inequality

$$\sqrt{\sum (a_m + b_m)^2} \leqslant \sqrt{\sum (a_m)^2} + \sqrt{\sum |b_m|^2}$$

in the a) and c) cases.

7. THE CONSTRAINTS ON THE LOOP'S NONLINEARITY

The two kinds of constraints concerning the nonlinearity of the loop are considered first (see fig. 6 and fig. 7).

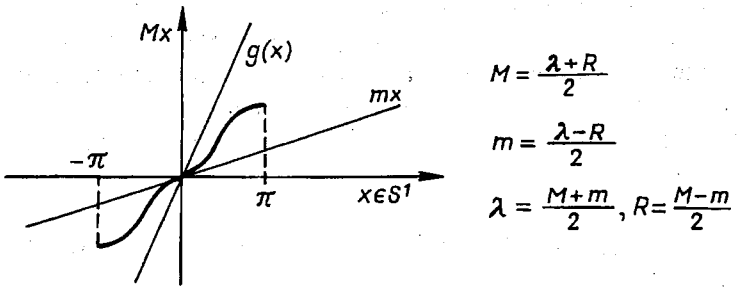

Fig. 6. The ilustration of the constraints (25) on loop's nonlinearity

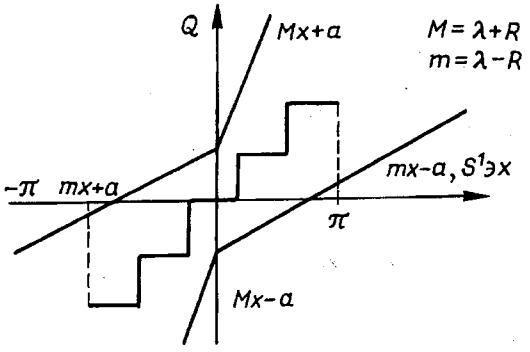

Fig. 7. The constraints on loop' nonlinearity while quantization effects are taken into account. The characteristic of quantizer

Constraint 1

$$|g(x) - \lambda x| \leqslant R\,|x|,\ x \in S^1,\ R \geqslant 0,\ \lambda > 0. \tag{24}$$

The geometrical meaning of constraint 1 is that $g(x)$ is contained among the straight lines of slopes determined by M and m while

$$M = \lambda + R \quad \text{and} \quad m = \lambda - R, \text{ (see fig. 6).} \tag{25}$$

Constraint 2

$$|g(x) - \lambda x| \leqslant R|x| + a, \quad a > 0. \tag{26}$$

This constraint is ilustrated in fig. 7. One can easily notice that these constraints are general in the sense that the wide class of nonlinear function is allowed while describing the nonlinearity of the phase-locked loop. Moreover if $u(l) = g(x(l)) - \lambda x(l)$, $l \in Z_+$ and the constraint 1 is considered then the inequality (17) holds for any $\{u\} \in \{R\}$, $i = 1,2,3,4$ with $\alpha_2 = R$ and $a = 0$.

$$\rho_i(\{u\}) \leqslant R\rho_i(\{[x]\}). \tag{17a}$$

On the other hand while the constraint 2 is considered then

$$\rho_i(\{u\}) \leqslant R\rho_i(\{[x]\}) + a, \quad i = 2, 4 \tag{17b}$$

and the inequality (17) holds with $\alpha_2 = R$ and $a > 0$. This constraint will be used for the spaces b) and d) only. Next the inequality (16) of the theorem 1 will be considered for the spaces of chapter 6 case in details. The specific counterparts of theorem 1 will be obtained for the subsequent spaces this way. These theorems will be of direct use while touching the different aspects of the phase entrainment in the loop.

8. THE SPACE $(\{[R]\}, \rho_1)$ OF THE SEQUENCES OF FINITE PSEUDOENERGY

Let begin with the following lemma;

Lemma 4

Suppose $\{y\} \in \{R\}$, $\{u\} \in \{R\}$ and

$$y(k) = \sum_{l=0}^{k} k_{\lambda,1}(k-l)u(l), \; k \in Z_+, \; (Z_+ \text{ is the set of nonnegative integers}). \tag{27}$$

Then

$$\rho_1(\{[y]\}) \leqslant \alpha_1 \rho_1(\{u\}) \tag{28}$$

and

$$\alpha_1 = \alpha_1(r_0) = \sup_{\omega} |K_{\lambda,1}(r_0, e^{j\omega})|, \; r_0 \in (0, 1>,$$

$$K_{\lambda,1}(r_0 e^{j\omega}) = \mathcal{Z}\{k_{\lambda,1}\}|z = r_0 e^{j\omega} = K_{\lambda,1}(z)|_{z=r_0 e^{j\omega}}$$

Proof

$$\sum_{m=0}^{\infty} |[y(m)]|^2 r_0^{-2m} \leqslant \sum_{m=0}^{\infty} |y(m)|^2 r_0^{-2m} = \frac{1}{2\pi} \int_{-\pi}^{\pi} |Y(r_0 e^{j\omega})|^2 \, d\omega \tag{29}$$

$r_0 \in (0,1>$, for any $\{[y]\} \in (\{[R]\}, \rho_1)$.

$$Y(r_0 e^{j\omega}) = \sum_{m=0}^{\infty} y(m) z^{-m}\Big|_{z=r_0 e^{j\omega}} = \mathcal{Z}\{y\} = Y(z)\Big|_{z=r_0 e^{j\omega}}$$

On the other hand if (27) holds true then [7]

$$Y(z) = K_{\lambda,1}(z)\, U(z); \quad U(z) = \mathcal{Z}\{u\}; \quad K_{\lambda,1}(z) = \mathcal{Z}\{k_{\lambda,1}\} \tag{30}$$

whereas $\mathcal{Z}$ stands for Laurent's series of the respective time sequence ($\mathcal{Z}$ transformation).

Now, from (29) and (30)

$$\rho_1(\{[y]\}) \leqslant \sqrt{\frac{1}{2\pi}\int_{\pi}^{\pi} |Y(r_0 e^{j\omega})|^2 \,d\omega} = \sqrt{\frac{1}{2\pi}\int_{-\pi}^{\pi} |K_{\lambda,1}(r_0 e^{j\omega})|^2 |U(r_0 e^{j\omega})|2 \,d\omega} \leqslant$$

$$\leqslant \operatorname{sun}|K_{\lambda,1}(r_0 e^{j\omega})|\rho_1(\{u\}) = \alpha_1 \rho_1(\{u\}) = \alpha_1(r_0)\rho_1(\{u\}); r_0 \in (0, 1>. \quad (31)$$

That is why (28) holds true in this case.

Note that

$$1 \geqslant r_0 = |r_0 e^{j\omega}| > \lim_{m\to\infty} \sup \sqrt[m]{|x_\lambda(m)|} \quad (32)$$

is sufficient for the belongness of $\{[x_\lambda]\}$ to $(\{[R]\}, \rho_1)$ space.
On the other hand

$$1 \geqslant r_0 = |r_0 e^{j\omega}| > \lim_{m\to\infty} \sup \sqrt[m]{k_{\lambda,1}(m)} \quad (33)$$

is sufficient for the existence of $K_{\lambda,1}(r_0 e^{j\omega})$. Note that the belongness of $\{x_\lambda\}$ to $(\{R\}, \rho_1)$ space is necessary for the existence of N:1 phase entrainment in the phase-locked loop. Moreover the lemma 4 asserts that the inequality (15) of theorem 1 is valid with α_1 specified in (28). That is why the theorem 2 can be stated as a consequence of the theorem 1 while $(\{[R]\}, \rho_1)$ space is of concern.

Theorem 2

Suppose

A1. The noise $z(l)$ is negligible, $l \in Z_+$

A2. There exists the closed interval $<r, 1>$, $r > 0$ such a that (34)

1) $\overset{\forall}{r_0} \in <r, 1>$ (32) and (33) hold

$$2)\ \alpha_1(r_0)\alpha_2 = \alpha_1 R < 1 \quad (35)$$

$$3)\ |\lambda[x] - g([x])| \leqslant R|[x]|.$$

Then the point of stable equilibrium $x = 0 \in S^1$ which represents the state of N:1 phase entrainment is the global attractor in the sense that every trajectory converges to it. Moreover every transient response i. e. the acquistition of the loop is not slower than

$$C r_0^m m^{-(1+\beta)/2} \quad (36)$$

while the discrete time m tends to the infinity, $R \in C > 0$. Moreover the constant $\beta > 0$ may be of any order of littleness, $r_0 \leqslant 1$.

Proof

The solution of (18) exists and is unique in view of theorem 1. It belongs to $(\{[R]\}, \varrho_1)$ space while $r_0 > r$. If the sequence $\{[x(m)]\}$ converges to zero slower than specified in (36) then it can be bounded the point by point from below by the sequence $\{C r_0^m m^{-1/2}\} = \{x_0\}$ for almost all m. But $\rho_1(\{x_0\}) = \infty$ and $\{[x]\} \notin (\{[R]\}, \rho_1)$ in this case. This contradicts the previous statements obviously. That is why the theorem 2 which specifies the N:1 phase entrainment in terms of pseudoenergy holds true.

9. THE SPACE $(\{[R]\}, \rho_3)$ OF THE SEQUENCES OF FINITE PSEUDOPOWER

It is not difficult to extend the results of previous chapter to prove that

$$\overline{\lim_{M\to\infty}} \sqrt{\frac{1}{M} \sum_{m=0}^{M} \left| \left[y(m) \right] \right|^2} = \rho_3(\{[y]\}) \leqslant \sup_{\omega} |K_{\lambda,2}(e^{j\omega})| \, \rho_3(\{u\}) \tag{37}$$

That is why (15) holds;

$$\rho_3(\{[y]\}) \leqslant \alpha_1 \rho_3(\{u\}) \tag{38}$$

and

$$\alpha_1 = \sup_{\omega} |K_{\lambda,1}(e^{j\omega})| \tag{39}$$

like in the case of finite pseudoenergy. The scope of this chapter is to take the random disturbing noise into account also. According to the model assumed the disturbing noise $z(l)$, $l \in Z_+$ affects the digital phase-locked loops as

$$z_\lambda(k) = \sum_{l=0}^{k} k_{\lambda,2}(k - l) z(l), \quad k \in Z_+ \tag{40}$$

The noise $z(l)$ is of finite power i. e. $\rho_3(\{z\}) < \infty$
Also the poles of $K_{\lambda,2}(z)$ which is $\mathscr{Z}$ transform of the unit pulse response $k_{\lambda,2}$ are all inside the unit circle:

$$\lim_{m\to\infty} \sup \sqrt[m]{k_{\lambda,2}(m)} < 1. \tag{41}$$

Let

$$z_\lambda(k)_M \stackrel{\text{df}}{=} \sum_{l=0}^{k} k_{\lambda,2}(k - l) z_M(l), \quad k \in Z_+ \tag{42}$$

and

$$z_M(l) = \begin{cases} z(l) & l \leqslant M \\ 0 & l > M \end{cases} \tag{43}$$

while the M of (42–43) is an positive integer.

Now

$$\frac{1}{M}\sum_{n=0}^{\infty}|z_\lambda(n)_M|^2 = \frac{1}{2\pi}\int_{-\pi}^{\pi}|K_{\lambda,2}(e^{j\omega})|^2\frac{|Z_M(e^{j\omega})|^2}{M}\,d\omega \tag{44}$$

and

$$Z_M(e^{j\omega}) \stackrel{\text{df}}{=} \mathscr{Z}\{z_M\}\Big|_{z=e^{j\omega}}.$$

Suppose that

$$\bar{P}_z(e^{j\omega}) \stackrel{\text{df}}{=} \overline{\lim_{M\to\infty}}\frac{|Z_M(e^{j\omega})|^2}{M}. \tag{45}$$

Then the following estimate holds true in this case

$$\rho_3(\{[z_\lambda]\}) \underset{(44)}{=} \sqrt{\frac{1}{2\pi}\int_{-\pi}^{\pi}|K_{\lambda,2}(e^{j\omega})^2\ \bar{P}_z(e^{j\omega})\,d\omega}. \tag{46}$$

Moreover suppose

$$\int_{-\pi}^{\pi}|K_{\lambda,2}(e^{j\omega})|^2\ \bar{P}_z(e^{j\omega})\,d\omega = \sigma_z^2\int_{-\pi}^{\pi}|K_{\lambda,2}(e^{j\omega})|^2\,d\omega. \tag{47}$$

This happens for instance while

$$\bar{P}_z(e^{j\omega}) = \sigma_z^2 = \text{const}. \tag{48}$$

Then

$$\rho_3(\{[z_\lambda]\}) = \sigma_z^2\int_{-\pi}^{\pi}\frac{1}{2\pi}|K_{\lambda,2}(e^{j\omega})|^2\,d\omega. \tag{49}$$

The (48) is valid while $z(l)$ is the stochastic process called the white noise. One can also notice that $x_\lambda(m)\to 0$ while the discrete time m tends to the infinity if the state of N:1 phase entrainment is locally stable. That is why $\rho_3(\{[x_\lambda]\})=0$.
Finally the following theorem results from the consideration of this paper.

Theorem 3

Suppose

A1. There exists the density $\bar{P}_z(e^{j\omega})$ of (45) and (41) holds true

A2. $|\lambda[x] - g([x])| \leqslant R|[x]|$

$$\text{A3. } \alpha_1 \alpha_2 = \alpha_1 \cdot R < 1$$

Then the mean squared value of oscillations of the phase error process $\rho_3(\{[x]\})$ can be estimated in the following way

$$\rho_3(\{[x]\}) \leqslant \frac{\rho_3(\{[z_\lambda]\})}{1 - \alpha_1 R}, \tag{50}$$

while α_1 is given by (39) and $\rho_3(\{[x_\lambda]\})$ by (46). See also (47 – 49) for the possible estimates of $\rho_3(\{[z_\lambda]\})$. The proof of this theorem is almost the same as of the previous one. Notice that $\{k_{\lambda,2}\} = \{k_{\lambda,1}\}$ for the almost all cases considered in this paper. The influence of quantization noise can be accounted for also. The additional parameter is $\sigma_{zq}^2 = q^2/12$. In this case σ_{zq} is the mean squared value of quantization noise while the quantization is uniform and symetric [7]. However not constant quantization step q may be of interest while optimazing the quantizer. Fortunately the integral of (49) can be given closed form in terms of the coefficients of $K_{\lambda,2}(z)$ which is loop's transfer function. While

$$I = \frac{1}{2\pi} \int_{-\pi}^{\pi} |K_{\lambda,2}(e^{j\omega})|^2 \, d\omega \tag{51}$$

one gets in particular cases [8].

$$1)\ K_{\lambda,2}(z) = \frac{a_0}{z - b_0} \quad : \quad I = \frac{a_0^2}{1 - b_0^2}$$

$$2)\ K_{\lambda,2}(z) = \frac{a_0 - a_1 z}{z^2 - b_1 z + b_0} \quad : \quad I = \frac{(a_1^2 + a_0^2)(1 + b_0) - 2a_0 a_1 b_1}{(1 + b_0)(1 - b_0^2) + b_1(b_1 b_0 - b_1)}$$

$$3)\ K_{\lambda,2}(z) = \frac{-a_2 z^2 + a_1 z - a_0}{z^3 - b_2 z^2 + b_1 z + b_0} : \quad I = \frac{B_0 Q_0 - B_1 Q_1 + B_2 Q_2}{(1 - b_0^2) Q_0 + (b_2 + b_1 b_0) Q_1 + Q_3}$$

$$B_0 = a_0^2 + a_1^2 + a_2^2,\ B = -2a_1(a_0 + a_2),\ B_2 = 2a_2 a_0,\ Q_0 = 1 + b_1 - b_0(b_0 - b_2),$$
$$Q_1 = -b_2 - b_1 b_0,\ Q_2 = -b_2(b_0 - b_2) - b_1(1 + b_1);\ Q_3 = (b_1 + b_2 b_0) Q_2$$

10. THE SPACE $(\{S^1\}, \rho_2)$ OF THE SEQUENCES WITH ASYMPTOTIC METRIC

Now, the space $(\{[R]\}, \rho_2)$ with

$$\rho_2(\{[x]\}) \triangleq \lim_{M \to \infty} \sup_{m > M} |[x(m)]| \tag{52}$$

is of interest. This space is particularly well suited to describe the steady state properties of the phase error process while the discrete time m tends to infinity. While the effects due to the quantizer of the analog to digital convertor of the loop are to be accounted for this feasibility is of importance. With the consttraints of fig. 7 while given analitically

by (26) one can take into account any quantizer. It is enough when its characteristics is within the admissible region bounded by the straight lines of fig. 7. In view of (26)

$$\rho_2(\{u\}) \leqslant R\rho_2(\{[x]\}) + a. \tag{17}$$

Now, let the following lemma be proved to proceed.

Lemma 5

Suppose

$$\alpha_1 \stackrel{\text{df}}{=} \sum_{m=0}^{\infty} |k_{\lambda,1}(m)| < \infty \tag{53}$$

and

$y(k)$, $k \in Z_+$ is given by (27).

Then

$$\rho_2(\{[y]\}) \leqslant \alpha_1 \cdot \rho_2(\{u\}). \tag{54}$$

Proof

$$\rho_2(\{[y]\}) = \lim_{M\to\infty} \sup_{m>2M} |[y(m)]| = \lim_{M\to\infty} \sup_{m>2M} \left|\left[\sum_{l=0}^{m} k_{\lambda,1}(l)\, u(m-l)\right]\right| =$$

$$= \lim_{M\to\infty} \sup_{m>2M} |\sum_{l=0}^{M} k_{\lambda,1}(l)\, u(m-l) + \sum_{l=M+1}^{m} k_{\lambda,1}(l)\, u(m-l)| \leqslant$$

$$\leqslant \lim_{M\to\infty} \sup_{m>2M} \left\{\sum_{l=0}^{\infty} k_{\lambda,1}(l) | \sup_{m-M\leqslant k\leqslant m} |u(k)| + \sum_{l=M+1}^{\infty} |k_{\lambda,1}(l)| \sup_{k\geqslant 0} |u(k)|\right\} =$$

$$= \sum_{l=0}^{\infty} |k_{\lambda,1}(l)| \lim_{M\to\infty} \sup_{k>M} |u(k)| = \alpha_1 \rho_2(\{u\}). \tag{55}$$

Now the inequality (54) of lemma 5 can be recognized as a special case of (15) with α_1 defined in (53). That is why the next theorem can be stated

Theorem 4

Suppose

A1. The noise is negligible

A2. $|\lambda[x] - g([x])| \leqslant R|[x]| + a$

A3. $\alpha_1 \cdot \alpha_2 = \alpha_1 R < 1$ while α_1 is given in (53)

A4. $x_\lambda(m) \to 0$ when $\to m$.

Then the steady state amplitude of oscillations is bounded according to

$$\rho_2(\{[x]\}) \leqslant \frac{\alpha_1 a}{1 - \alpha_1 \cdot R}, \tag{56}$$

while m tends to infinity. By following the previous cases the proof of theorem 4 can be easily completed. That is why it is left.

11. THE SPACE $(\{S^1\}, \rho_4)$ OF THE SEQUENCES OF FINITE PEAK VALUE

The elements from the space of the sequences of finite peak value satisfy

$$\rho_4(\{[x]\}) = \sup_{m \geqslant 0} |[x(m)]|, \quad m \in Z_+ . \tag{57}$$

Suppose first that the n initial points of the phase error process $[x(0)]$, $[x(1)]$, ..., $[x(n-1)]$ are given in the case of the phase-locked loop of n-th order. While represented by the point $0 \in S^1$ the state of N:1 phase entrainment is consistent with the zero sequence. Secondly if the question is posed what the extreme limits of the phase error process are then the answer can be gained by considering the solution in $(\{S^1\}, \rho_4)$ space. First of all one can notice that the following inequalities hold true in this case:

$$\rho_4(\{[y]\}) \leqslant \sum_{l=0}^{\infty} |k_{\lambda,1}(l)| \rho_4(\{u\}) \tag{15}$$

and

$$\rho(\{u\}) \leqslant R\rho(\{[x]\}). \tag{17a}$$

That is why while (15) and (17a) are valid the next theorem follows from the theorem 1.

Theorem 5

Suppose

A1. The noise disturbance $z(l)$ is negligible, $l \in Z_+$
A2. $\alpha_1 = \sum_{l=0}^{\infty} \left| k_{\lambda,1}(l) \right| < \infty$
A3. $|\lambda[x] - g([x])| \leqslant R|[x]|$
A4. $\alpha_1 R < 1$.

Then the upper bound to the peak value of the phase error is

$$\rho_4(\{[x]\}) \leqslant \frac{\rho_4(\{[x_i]\})}{1 - \alpha_1 R}. \tag{58}$$

A kind of Lapunov stability is asserted by the theorem 5. This is of interest while the dynamics of the loop is considered locally i. e in the neighbourhood of the state of phase entrainment. When the initial phase error points are near enough the point of N:1 phase entrainment then the same applies to the whole trajectory. However the asymptotic stability occurs also in view of the previous theorem.

12. THE EXAMPLES

While the nonuniform sampling digital phase-locked loops are of concern the scope of this chapter is to apply the results of the previous ones to concrete cases. Namely the

following expamples are to show how the different aspects of the acquisition in these loops can be studied within the presented approach.

1°. The first-order DPLL

The equation of the first-order DPLL is given in appendix 2 (the equation A2–6). While applying the theorem 2 the following relations should hold true

$$|1 - K_1' \lambda| < 1 \tag{59}$$

$$\alpha_1(r_0) = \sup_{\omega} \left| K_{\lambda,1}(r_0 e^{j\omega}) \right| = \frac{|K_1'|}{|r_0 - (1 - K_1' \lambda)|} \tag{60}$$

$$\alpha_2 = R. \tag{61}$$

$$\text{If } r_0 = 1 \quad \text{then} \quad \alpha_1 \cdot \alpha_2 = \frac{1}{|\lambda|} R. \tag{62}$$

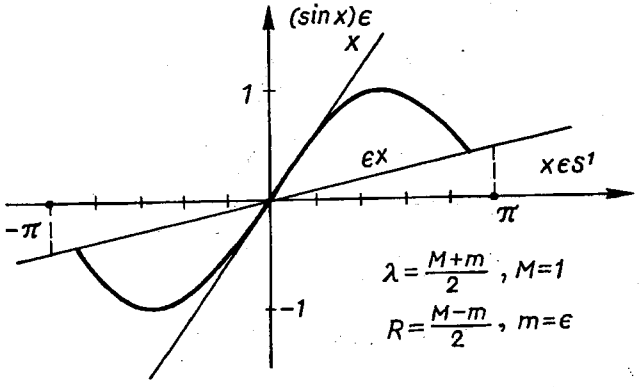

Fig. 8. The almost sinusoidal shape of loop's nonlinearity

Let $g_\epsilon(x) = (\sin x)_\epsilon$ of fig. 8 and $\Lambda = 0$. The parameter Λ describes the denuntion due to the frequency offset. Then (see fig. 8)

$$\lambda = \frac{1 + \epsilon}{2} \quad \text{and} \quad R = \frac{1 - \epsilon}{2}, \tag{63}$$

Also

$$\alpha_1 \alpha_2 = \frac{1 - \epsilon}{1 + \epsilon} \tag{64}$$

That is why the proposition of theorem 2 holds true for every $\epsilon > 0$ ($\alpha_1 \alpha_2 < 1$ in this case).

2°. The second-order DPLL

The equation of the loop of second order is given in appendix 3a

1) Let

$$K_1' = 1, \quad r_t = 2, \quad \lambda = \frac{1+\epsilon}{2}, \quad R = \frac{1-\epsilon}{2}, \tag{65}$$

$\epsilon > 0$ (see fig. 8).

If $r_0 = 1$ then

$$|K_{\lambda,1}(e^{j\omega})| = \frac{|1 - 2e^{j\omega}|}{|e^{2j\omega} - 2(1-\lambda)e^{j\omega} + 1 - \lambda|}. \tag{66}$$

The image of $|K_{\lambda,1}(e^{j\omega})|$ is shown in fig. 9. The proposition of theorem 2 holds true if

$$\alpha_1 \alpha_2 = \alpha_1(\epsilon) R = \alpha_1(\epsilon) \frac{1-\epsilon}{2} < 1. \tag{67}$$

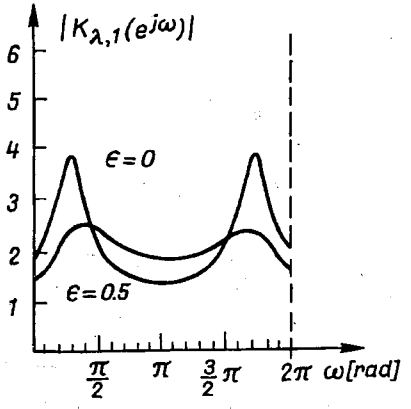

Fig. 9. The graph of $|K_{\lambda,1}(e^{j\omega})|$

The last inequality is met while $\epsilon > 0{,}35$ (the approximate result).

2) Let

$$K_1' = 0{,}5, \quad r_t = 2, \quad \lambda = (1+\epsilon)/2, \quad R = (1-\epsilon)/2,$$

$\epsilon > 0$ (see fig. 8).

If $r_0 = 1$ then

$$|K_{\lambda,1}(e^{j\omega})| = \frac{0{,}5|1 - 2e^{j\omega}|}{|e^{j2\omega} + (2-\lambda)e^{j\omega} + 1 - 0{,}5\lambda|}. \tag{68}$$

Now the image of $|K_{\lambda,1}(e^{j\omega})|$ is given in fig. 10. Approximately $\epsilon > 0{,}45$ while

$$\alpha_1(\epsilon) \frac{1-\epsilon}{2} < 1. \tag{69}$$

The proposition of theorem 2 holds true in this case.

3^0. The DPLL of the second-order with non perfect adder

The equation of this loop is given in appendix 3b. Let $K_1 = 1$, $r_t = 1+\beta$, $\lambda = (1+\epsilon)/2$, $R = (1-\epsilon)/2$, $\epsilon > 0$ (70)

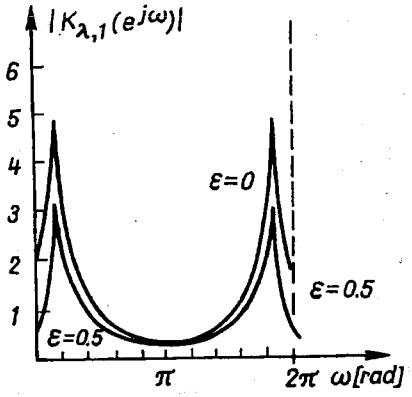

Fig. 10. The graph of $|K^{\lambda,1}(e^{j\omega})|$

If $r_0=1$ then

$$|K_{\lambda,1}(e^{j\omega})| = \left|\frac{\beta - e^{j\omega}(\beta + 1)}{e^{2j\omega} - (1 + \beta - \lambda(1 + \beta))e^{j\omega} + \beta(1 - \lambda)}\right| \tag{71}$$

$0 < \beta < 1$.

$|K_{\lambda,1}(e^{j\omega})|$ is ilustrated in fig. 11. In view of this graph the proposition of theorem 2 holds true if $\epsilon > 0{,}3$ (the approximate result).

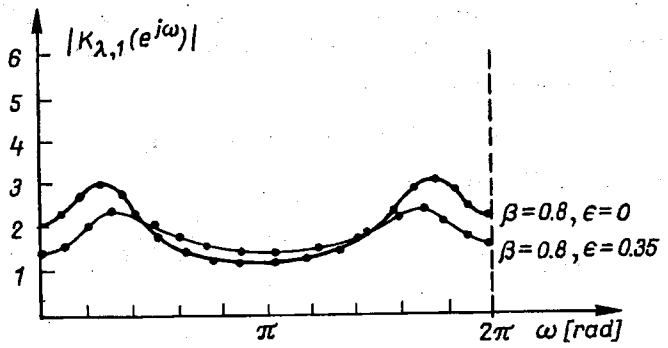

Fig. 11. The image of $|K_{\lambda,1}(e^{j\omega})|$. The loop of second order with nonperfect adder

4°. The DPLL of third-order

The equation of this loop is given in appendix 4. Let

$$K_1' = 1, \quad pK_1' = 3, \quad r_l = 2, \quad \lambda = (1 + \epsilon)/2, \quad R = (1 - \epsilon)/2, \quad \epsilon > 0 \tag{72}$$

If $r_0 = 1$, then

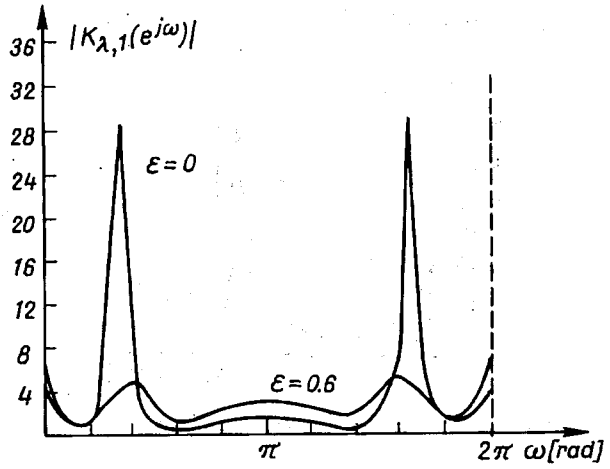

Fig. 12. The graph of $|K_{\lambda,1}(e^{j\omega})|$. The loop of third order

$$|K_{\lambda,1}(e^{j\omega})| = \frac{|-3e^{j2\omega} + 3e^{j\omega} - 1|}{|e^{3j\omega} - 3e^{2j\omega}(1-\lambda) + 3e^{j\omega}(1-\lambda) - (1-\lambda)|}. \tag{73}$$

The image of $|K_{\lambda,1}(e^{j\omega})|$ is given in fig. 12. It follows from this graph that the proposition of theorem 2 holds true if approximately $\epsilon > 0{,}6$. The parameters λ and R of the previous examples have been adjusted to the nonlinearity of the loop of fig. 8 while the sinusoidal waveform is being tracked. The additional graphs are provided regardless of the loop's nonlinearity next.

5°. The DPLL of second-oder

a) Let $K_1'\lambda = 1$, $r_l = 2$ $(\lambda > 0)$, then

$$|K_{\lambda,1}(r_0 e^{j\omega})| = \frac{\sqrt{1 - 4r_0\cos\omega + 4r_0^2}}{r_0^2}\frac{1}{|\lambda|} \leqslant$$

$$\leqslant \frac{1 + 2r_0}{r_0^2}\frac{1}{|\lambda|}, \quad r_0 > 0. \tag{74}$$

b) Let $K_1'\lambda = 1{,}2$, $r_l = 2$. Then $r_0 > 0{,}69$ and the graph of $K_{\lambda,1}(r_0 e^{j\omega})$ is shown in fig. 13 for the different values of r_0

c) Let $K_1' = 0{,}5$, $r_l = 2$. Then $r_0 > 0{,}29$ and the graph of $|K_{\lambda,1}(r_0 e^{j\omega})|$ is in fig. 14

d) Consider the loop of second-order with non perfect adder (see the appendix 3b) while $K_1'\lambda = 1$, $r_l = 1 + \beta$, $\lambda > 0$, $0 < \beta < 1$. Then for $r_0 > 0$

$$|K_{\lambda,1}(r_0 e^{j\omega})| = \frac{\sqrt{\beta^2 - 2\beta(1+\beta)r_0\cos\omega + (1+\beta)^2 r_0^2}}{r_0^2} \leqslant$$

$$\frac{\beta + (1+\beta)r_0}{r_0^2}\frac{1}{|\lambda|} \tag{75}$$

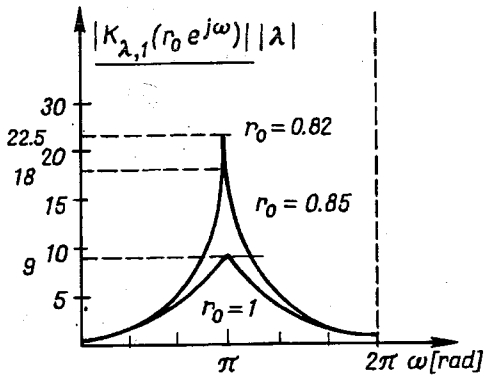

Fig. 13. The graph of $|K_{\lambda,1}(e^{j\omega})|$. The loop of second order, aperiodic case

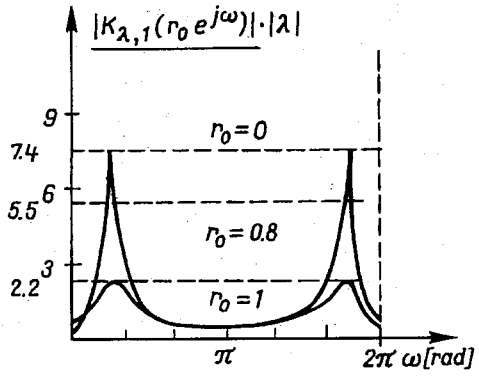

Fig. 14. The graph of $|K_{\lambda,1}(e^{j\omega})|$. The loop of second order, periodic case

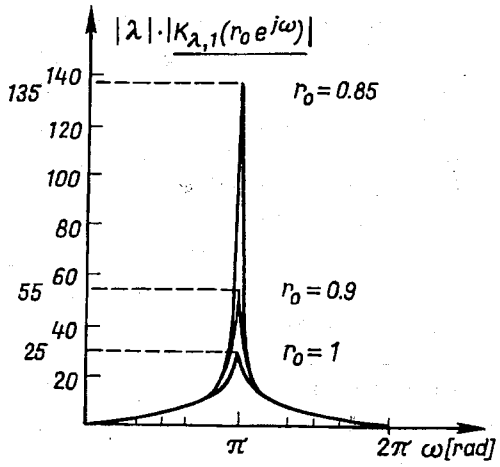

Fig. 15. The graph of $|K_{\lambda,1}(e^{j\omega})|$. The graph of $|K_{\lambda,1}(e^{j\omega})|$. The loop of third-order, aperiodic case

6°. The DPLL of third-order

Let $K_1'\lambda=1{,}1$, $r_l=2$, $p=3$, $\lambda>0$. Then $r_0>0{,}813$ and the image of $|K_{\lambda,1}(r_0 e^{j\omega})|$ is given in fig. 15.

13. THE CLASS OF THE NONUNIFORM SAMPLING PHASE-LOCKED LOOPS WHICH ACQUIRE THE PHASE-LOCK REGARDLESS OF THE INITIAL PHASE ERROR. THE N:1 PHASE ENTRAINMENT CONSIDERED

The class of the digital nonuniform sampling phase-locked loops which acquire the phase-lock regardless of the initial phase error can be specified in view of obtained results. This is referred to the N:1 phase entrainment admissibly perturbed. The mentioned classification can be accomplished in terms of the properties of the loop's nonlinearity. While it is of sinusoidal form the following conclusions can be derived from the examples of previous chapter. Namley, the examples 1–6 show that the proposition of theorem 2 holds true in the first-order loop case only. Moreover while the almost all trajectories are of concern. The trajectory $\gamma(x)=\{x: x=\pi\in S^1\}$ is the exeptional one in this case. However the point $x=\pi\in S^1$ is the point of unstable equilibrium. On the other hand the things are quite different in the case of the loops of higher order (the examples 2–3). It has been known since the paper of Osborne that the N:1 phase entrainment in the loop of higher order can occur for the initial phase error conditions from the region around the stable equilibrium only [2,4]. Unhesitatingly the whole S^1 x S^1 torus space is not this region while the DPLL of second order is considered [4]. Let in view of the theorems 2 and 5 the continuity of the phase error process in excitation x_λ in respect to pseudoenergy ρ_1 or the peak value ρ_4 metric be well established. Then the parameter ϵ of the previous chapter can be put into good account while discussing the size of the region of direct convergence around the stable equilibrium being responsible for the N:1 phase entrainment in the loop [1,2,4]. The smaller ϵ the greater this region is. The numerical calculations performed by Osborne are in good accord with this last statement. See the examples 2–6 while comparing with the results of Osborne. Nevertheless the propositions of all theorems under consideration can be met in the case of the DPLL of any order if the value of the parameter R is small enough. Just the schemes of the DPLL-s with the small value of this parameter are presented in the appendix 6. Whereas the effective nonlinearities of these loops are presented in fig. 16. They are the discontinous ones. The origin of the parameter φ_s – the steady phase error or static error is explained in the appendices 2 and 3. Presumably let the value of the parameter R which describes the loop's nonlinearity in general way be given. Then it may be compared with required one in view of the graph of $|K_{\lambda,1}(e^{j\omega})|$ in order to make the proposition of the theorem 2 hold true if of concern. Moreover the speed of convergence can be estimated. Namley consider the example 5a for instance. If $R=0(\lambda\neq 0)$ then r_0 can be small at will while the proposition of the theorem 2 is met. This is the case of the fastest acquisition of the

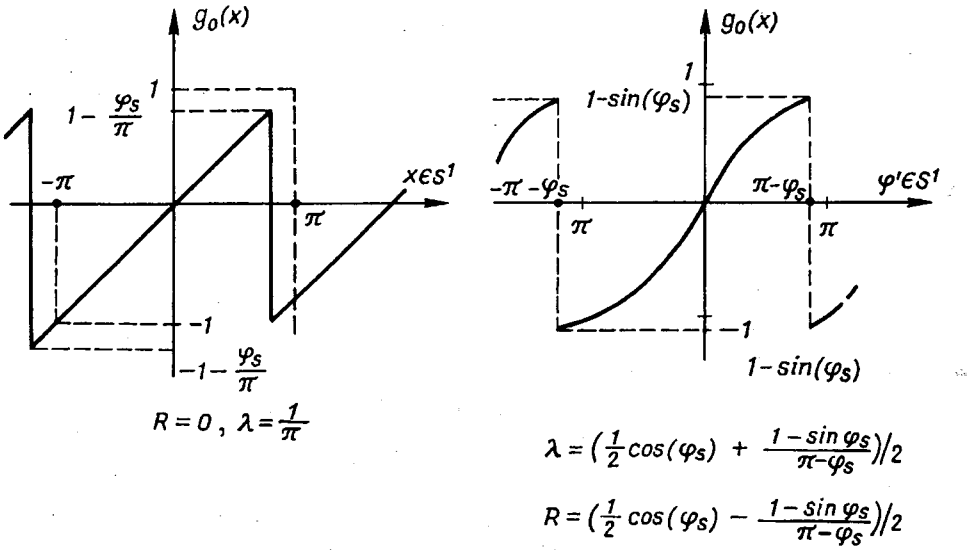

Fig. 16. The effective characteristics of the phase detector nonlinearity of the modified digital phase-locked loop from the appendix 6

phase-lock. In other cases the smallest value of r_0 can be found from the graphs like those of the last examples. The effect of noise disturbances can be accounted for by the theorem 3 while the quantization effects by the theorem 4. The mentioned class of loops which acquire the phase-lock regardless of the initial phase error conditions and fast can be easily identified now. Just the loops with the discontinous nonlinearity belong to it.

14. ON THE CONTROL OF THE ACQUISITION WHILE THE SINUSOIDAL WAVEFORM IS BEING TRACKED BY THE DPLL

The digital circuitry of the phase-locked loop is especially suitable for controlling the acquisition of the phase-lock. Just while putting into good account this fact a very simple algorithm for controlling the acquisition of the loop of any order with sinusoidal loop's nonlinearity will be presented. However a slight different constraint on nonlinearity will be used. If the nonlinearity of the loop is in the region bounded by the curves of fig. 17 then the following estimation holds true

$$|g([x]) - \lambda[x]| \leqslant R|[x]| + (a - M|[x]|)\, r_d(a/M) \tag{76}$$

while

$$r_d(u) \stackrel{\text{df}}{=} \begin{cases} 1 & \text{if } |[x]| \leqslant u \\ 0 & \text{if } |[x]| > u,\ u > 0. \end{cases}$$

If $|[x]| \leqslant a/M$ then

$$|g([x]) - \lambda[x]| \leqslant (R - M)|[x]| + a = a - \lambda|[x]| < a \qquad (77)$$

$a > 0$.

In view of the new constraints (77) the following new theorem can be proved.

Theorem 6

Suppose

A1. $\alpha_1 R < 1$, $\alpha_1 = \sum_{m=0}^{\infty} |k_{\lambda,1}(m)|$

A2. $x_\lambda(m) \to 0$ while $m \to \infty$

$$\text{A3. } |g([x]) - \lambda[x] \leqslant \begin{matrix} R|[x]| \text{ while } |[x]| > a/M \\ a \text{ while } |[x]| < a/M \end{matrix}$$

and $a/M < a$.

Then the steady state amplitude of oscillations $\rho_2(\{[x]\})$ is bounded according to

$$\rho_2(\{[x]\}) \leqslant \alpha_1 \cdot a. \qquad (78)$$

The proof of the theorem 6 while being very similar to that of theorem 4 is left. If a is small then small amplitude of oscillations can be established due to the value of parameter $\alpha_1 = \alpha_1(\lambda)$ small enough (sufficiently large $\lambda = (M+m)/2$). Just the proposition of the last theorem is met in this case. Now the declared algorithm can be explained while the sinusoidal waveform is being tracked by the loop of any order. Let the two

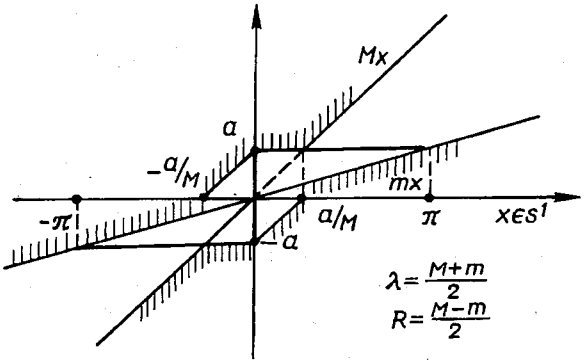

Fig. 17. The new constraints on loop's nonlinearity in the case of controlled digital phase-locked loop

level quantization of fig. 17 be performed until the phase error is in small enough neighbourhood of N:1 phase entrainment state. Then the multilevel quantization performed next reduces the amplitude of the phase error process to the required final value in view of the results of chapter 11.

15. CONCLUSIONS

The new stability criteria for the digital nonuniform sampling zero crossing phase-locked loops of any order have been provided. While stated in terms of theorems a kind of unified approach to the problem of N:1 phase entrainment in these loops has been framed. That is why the *„norm"* oriented approach has been released in some sense from the inconvinience pointed out by Linsdey and Chie in [1], pp. 426–427. The model of the loop in terms of the functional nonlinear discrete-time equation on the S^1 – circle manifold has been used. It has been proved that loop with discontinous characteristics of the phase detector (the loop's nonlinearity) can be designed to meet the requirement of fast convergence of all trajectories to the state of N:1 phase entrainment. This means fast acquisition behaviour. Moreover while extending the qualitative results of this paper the theorems in hand can be of assistance on designing stage. The effect of disturbing noise and the quantization in amplitude of the waveform being tracked have been taken into account either. The estimate of the seize of the region of direct convergence around the state of N:1 phase entrainment can be given in terms of ϵ parameter. It is wortwhile to remind that the lack of the continuity of the loop's nonlinearity is even necessary to avoid the spurious behaviour of loop's dynamics [4,12,13,14]. While sinusoidal nonlinearity is under consideration the chaotic transient hang up phenomenon has been discovered in the loop of second order and reported in [4,12,13]. Occasionally it has been confirmed by Bernstein, Liberman and Lichtenberg in [14] within an interesting phenomena oriented approach including the estimation of convergence rates. However the causal approach of Żółtowski [4,12,13] revealed great sensitivity to initial conditions from the hiperbolic region while the time to reach the phase-lock is of interest and numerical results concerining this time have been provided. That is why to get further information a measure oriented approach within Markov theory while taking the disturbing noise into account has been explored by the author. When the impact of noise is megligible (the quantization due to computer based experiment can be accounted for as quantization noise) the computer oriented approach is preferable in view of ergodic theorem and of practical loss of analytical properties in this case. While the noise grows stronger the different methods can be used and are considered in forthcoming paper by Żółtowski. Also the simple algorithm for controlling the acquisition while the harmonic waveform is being tracked by the loop of any order has been presented. The effect of quantization of incoming waveform results in additional oscillations of the phase error around the stable equilibrium in not perturbed case when steady state considered. The theorems of this paper can be given a very local interpretation also. Namely a certain subregion $U \subset S^1$ containing the state of phase entrainment may be of concern if every trajectory of the phase error process remains in U. Suppose the disturbing noise z(l) is taken into account in this case. Then $z_M(l)$ of chapter 9 with M equal up to the order of value to the mean time to leave the set U have to be considered. Also $\bar{P}_z(e^{j\omega})$ of (45) have to be replaced by the expression with the finite value of M. However the approximation with infinite value of M is reasonable if the signal to noise ratio is high enough.

Further information concerning the process o synchronization can be gained in the low signal to noise power ratio case within the theory of Markov processes [1]. However the theorems of this paper give the theoretical tools to establish

1) the local stability of the perturbed N:1 phase entrainment

2) the global stability of the perturbed N:1 phase entrainment on S^1 circle manifold. Clearly if 2) occurs then also but not vice versa. The hold in range parameter of the loop is determined by the conditions under which 1) occurs. On the other hand the pull in range parameter of the loop is determined by the ones under which 2) occurs. These parameters can be approximated in terms of the frequency intervals by using the approach of this paper. Suppose not perturbed by noise and quantization N:1 phase entrainment is studied by the theorems of this paper. Then the results of practical importance gained this way and by topological methods [1,2,5] are similar. Eventually this approach is extendible to consider the fading of input waveform, AM and PM modulation or variable coefficients filter of the loop. This is aimed to be presented in Part II and Part III.

REFERENCES

1. W. C. Lindsey, C. M. Chie: *A survey of digital phase-locked loops*, Proceedings of the IEEE, vol. 69, no. 4, April 1981, pp. 410–431
2. H. C. Osborne: *Stability analysis of N^{th} Power Digital Phase-Locked Loop – Part I: First Order DPLL and – Part II: Second and Third – Order DPLLs.* IEEE Transactions on Communication, vol. COM–28, no. 8, August 1980, pp. 1342–1346
3. J. C. Lee, C. K. Un: *Performance analysis of digital Tanlock loop.* IEEE Transaction on Communication, vol. COM–30, no. 10, October 1982, pp. 2398–2411
4. M. Żółtowski: *Chaotic transient hang up phenomenon and N:1 phase entrainment in the discrete-time phase-locked loop of second order.* ECCTD, Paris 1987
5. M. Żółtowski: *On the acquisition behaviour of a First-Order Digital phase-locked loop with negligible and Binary Quantization Effects.* Rozprawy Elektrotechniczne, 1984, 30, z. 2. ss. 401–412
6. F. Leja: *Funkcje zespolone.* W–wa: PWN, 1971, second edition.
7. A. V. Oppenheim, R. W. Schafer: *Cyfrowe przetwarzanie sygnałów,* W–wa, WKŁ 1979
8. E. I. Jury: *Przekształcenie Z i jego zastosowania.* W–wa. WNT, 1970
9. J. Z. Cypkin: *Teoria układów impulsowych.* W–wa; PWN, 1965
10. W. Szlenk: *Wstęp do teorii gładkich układów dynamicznych.* W–wa: PWN, 1982
11. M. Żółtowski: *New stability criteria for the Nonuniform Sampling Digital Phase-Locked Loops.* 1990, ISCAS, New Orlean, May 1–3, 1990
12. M. Żółtowski: *On the Global Stability of the Second Order Discrete Time Phase-Locked Loop.* IX National Conference on Circuit Theory and Electronic Networks, Wrocław–Szklarska Poręba, 22–24 Października 1986 (in polish)
13. M. Żółtowski: *On Global Stability of Phase Entrainment in Nonuniform sampling Discrete Time Phase-Locked Loop of Second Order.* Rozprawy Elektroniczne, 1988, 34, z. 4, ss. 37–58 (in polish)
14. G. M. Bernstein, M. A. Lieberman, A. J. Lichtenberg: *Nonlinear Dynamics of a Digital Phase-Locked Loop.* IEEE Transactions on Commun., vol. 17, no. 10, October 1989, pp. 1062–1070

APPENDIX 1

THE MODEL OF THE NONUNIFORM SAMPLING DIGITAL PHASE-LOCKED LOOP

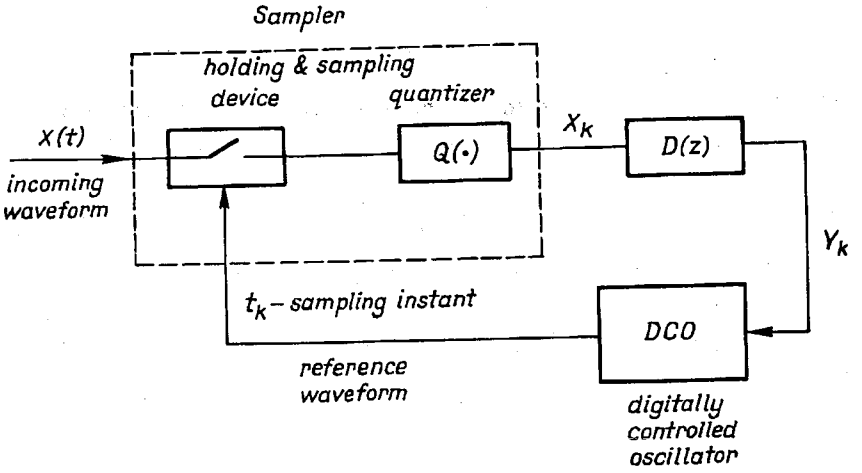

Fig. A1 – 1. The scheme of the nonuniform sampling digital phase-locked loop

From (A1 – 2) (see the begining of chapter 2)

$$t_{k+1} = t_0 + (k+1)T - \sum_{i=0}^{k} Y_i \underset{t_0=0}{=} (k+1)T - \sum_{i=0}^{k} Y_i \qquad \text{(A1-3)}$$

$t_0 = 0$ has been assumed without the loss of generality.
Shortly

$$X(t_k) = X_k,\ N(t_k) = N_k,\ \Theta(t_k) = \Theta_k,\ S_k = S(t_k) = \\ = A\,g(\omega_0 t_k + \Theta_k). \qquad \text{(A1-4)}$$

Next, in view of (A1 – 1) – (A1 – 4)

$$S_{k+1} = A\,g(\omega_0 t_{k+1} + \Theta_{k+1}) = A\,g(\omega_0 (k+1)T + \\ - \omega_0 \sum_{i=0}^{k} Y_i + \Theta_{k+1}) = A\,g(\Theta_{k+1} - \omega_0 \sum_{i=0}^{k} Y_i) \qquad \text{(A1-5a)}$$

and

$$X_k = S_k + N_k. \qquad \text{(A1-5b)}$$

Let the instantaneous phase error, phase error shortly be defined as

$$\varphi_k = \begin{cases} \Theta_0 & k = 0 \\ \Theta_k - \omega_0 \sum_{i=0}^{k-1} Y_i & k \neq 0. \end{cases} \qquad \text{(A1-6a)}$$

The phase error process is defined to measure the deviation from the state of N:1 phase entrainment admissibly perturbed. It follows from (A1 – 6a) that

$$S_k = A\,g(\varphi_k) \tag{A1-6b}$$

and

$$\varphi_{k+1} = \varphi_k + \Theta_{k+1} - \Theta_k - \omega_0 Y_k, \quad k = 0, 1, \ldots \tag{A1-6c}$$

That is why $S_k = 0$ if the N:1 phase entrainment occurs while the noise is negligible. On the other hand the output waveform Y_k and the input waveform X'_k of the loop's filter are related according to

$$\mathcal{Z}\{Y_k\} = \mathcal{Z}\{X'_k\}\,D(z) + Y_0(z). \tag{A1-7a}$$

$\mathcal{Z}\{\cdot\}$ stands for $\mathcal{Z}$ – Laurent transformation of the adequate time series. The sequence $\{Y_k^0\} = \mathcal{Z}^{-1}\{Y_0(z)\}$ of (A1 – 7) is the response of the loop's filter due to nonzero initial conduitions. $\mathcal{Z}^{-1}$ stands for the inverse Laurent transformation of the function of complex variable z. Also

$$X'_k = Q(x_k). \tag{A1-7b}$$

Next, in view of (A1 – 4), (A1 – 6), (A1 – 7) one gets

$$\Phi(z) = \Theta(z) - \frac{\omega_0}{z-1}\,\mathcal{Z}\{Q(A\,g(\varphi_k) + N_k)\}\,D(z) + \\ - \frac{\omega_0\,Y^0(z)}{z-1} \tag{A1-8}$$

and

$$\Phi(z) = \mathcal{Z}\{\varphi_k\}; \quad \Theta(z) = \mathcal{Z}\{\Theta_k\}.$$

Now, from (A1 – 6c), (A1 – 2a) and (A1 – 7a) while $\{d_k\} = \mathcal{Z}^{-1}\{D(z)\}$ is the unit pulse response of the loop's filter, the following equations are obtained

$$\varphi_{k+1} = \varphi_k + \Theta_{k+1} - \Theta_k - \omega_0 \sum_{i=0}^{k} Q(A\,g(\varphi_k) + N_i)\,d_{k-1} + \\ - \omega_0 Y_k^0 \tag{A1-9}$$

and

$$t_{k+1} = t_k + T - \sum_{i=0}^{k} Q(A\,g(\varphi_i) + N_i)\,d_{k-1} - Y_k^0 \\ t_0 = 0 \tag{A1-10}$$

This couple of equations describe the dynamics of the nonuniform sampling digital phase-locked loop in terms of the phase error process. The baseband model of the digital phase-locked loop which results from the equation just derived is shown in fig. A1 – 2. Now let simpler case of perturbed N:1 phase entrainment be considered (zero initial conditions of the loop's filter) while

$$\Theta_k = \Theta_0 + \Omega_0 t_k \tag{A1-11a}$$

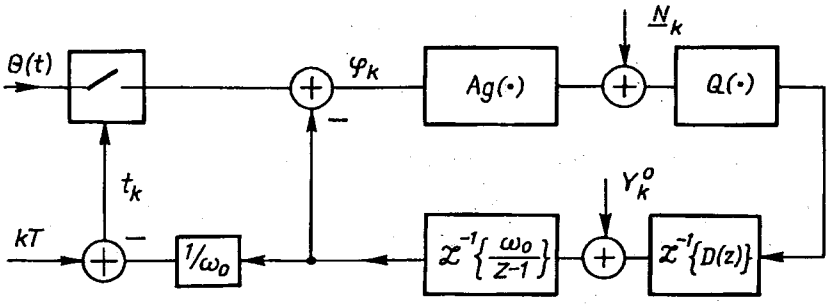

Fig. A1 – 2. The model of the noniniform sampling phase-locked loop

The initial conditions of the filter can be easily controlled within the digital circuitry of the loop whereas in view of (A1 – 11a) the input waveforms while detuned in phase Θ_0 and radian frequency Ω_0 are of concern. Now

$$\Theta_{k+1} - \Theta_k = \Omega_0 T - \Omega_0 \sum_{i=0}^{k} Q(Ag(\varphi_i) + N_i) d_{k-i} \qquad \text{(A1 – 11b)}$$

and

$$\varphi_{k+1} = \varphi_k - (\omega_0 + \Omega_0) \sum_{i=0}^{k} Q(Ag(\varphi_i) + N_i) d_{k-i} + \Omega_0 T. \qquad \text{(A1 – 11c)}$$

The equation (A1 – 11c) after $\mathscr{Z}$ transformation is

$$z(\Phi(z) - \varphi_0) = \Phi(z) - (\omega_0 + \Omega_0) \mathscr{Z}\{Q(Ag(\varphi_i) + N_i)\} D(z) + \Omega_0 T/(1 - z^{-1}) \qquad \text{(A1 – 12)}$$

Next the special cases of the equations (A1 – 11) are of interest.

1) The loop of first order: $D(z) = G_1$. From (A1 – 12)

$$\varphi_{k+1} = \varphi_k - (\omega_0 + \Omega_0) G_1 Q(Ag(\varphi_k) + N_k) + \Omega_0 T \qquad \text{(A1 – 13)}$$

or

$$\varphi_{k+1} = \varphi_k - K_1 Q(Ag(\varphi_k) + N_k) + \Lambda, \quad k = 0, 1, \ldots \qquad \text{(A1 – 14)}$$

with φ_0 as initial condition, $K_1 = (\omega_0 + \Omega_0) G_1$, $\Omega_0 T = \Lambda$.

2) The loop of second order: $D(z) = G_1 + G_2/(1 - z^{-1})$

From (A1 – 12) the equation of the loop of the second order is

$$\varphi_{k+2} - 2\varphi_{k+1} + \varphi_k = K_1 Q(Ag(\varphi_k) + N_k) - K_1 r_l Q(Ag(\varphi_{k+1}) + N_{k+1}) \qquad \text{(A1 – 15)}$$

with φ_0, φ_1 as initial conditions,

$$K_2 = (\omega_0 + \Omega_0) G_2, \quad r_l = 1 + K_2/K_1.$$

3) The loop of the second order with non-perfect adder:

$$D(z) = G_1 + \frac{G_2}{1 - \beta z^{-1}}, \quad 0 < \beta < 1.$$

From (A1−12) the equation of the loop of second order is

$$\varphi_{k+2} + (1 + \beta)\varphi_{k+1} + \beta\varphi_k = -K_1 r_l Q(Ag(\varphi_{k+1}) + N_{k+1}) + \\ + \beta K_1 Q(Ag(\varphi_k) + N_k) + \beta K_1 Q(Ag(\varphi_k) + N_k) + \Delta(1 - \beta) \quad \text{(A1−16)}$$

with φ_0, φ_1 as initial conditions.

4) The loop of third-order:

$$D(z) = G_1 + G_2/(1 - z^{-1}) + G_3/(1 - z^{-1})^2.$$

From (A1−12) the equation of the loop of third-order is

$$\varphi_{k+3} - 3\varphi_{k+2} + 3\varphi_{k+1} - \varphi_k = -pK_1 Q(Ag(\varphi_{k+2}) + N_{k+2}) + \\ + K_1(1 + r_l) Q(Ag(\varphi_{k+1}) + N_{k+1}) - K_1 Q(Ag(\varphi_k) + N_k) \quad \text{(A1-17)}$$

with φ_0, φ_1, φ_2 as initial conditions,

$$r_l = 1 + K_2/K_1, \quad p = 1 + K_2/K_1 + K_3/K_1, \quad K_3 = (\omega_0 + \Omega_0)G_3.$$

In the following appendices 2−4 the model of the nonuniform sampling digital phase-locked loop in terms of the discrete-time functional equation of convolutional form is derived in patricular cases.

APPENDIX 2

THE FIRST-ORDER DIGITAL PHASE-LOCKED LOOP WITH NEGLIGIBLE NOISE AND QUANTIZATION EFFECTS

While $Q(x)=x$, $N_k=0$ the equation of the loop is (see appendix A1)

$$\varphi_{k+1} = \varphi_k - K_1' g(\varphi_k) + \Delta, \quad k = 0, 1, \ldots \quad \text{(A2−1)}$$

$K_1'=K_1/A$. If $|\Delta/K_1'|<1$ then there exists the fixed point φ_s of (A2−1) while $g(\varphi_s)=\Delta/K_1'$.

However, the transformation

$$\tilde{\varphi}_k = \varphi_k - \varphi_s \qquad k = 0, 1, \ldots$$

maps the phase error process into the neighbourhood of 0 instead of φ_s. That is why one gets instead of (A2−1)

$$\tilde{\varphi}_{k+1} = \tilde{\varphi}_k - K_1' g_0(\tilde{\varphi}_k) \quad \text{(A2−2)}$$

while

$$g_0(x) \stackrel{\text{df}}{=} g(x + \varphi_s) - g(\varphi_s). \quad \text{(A2−3)}$$

Moreover one can consider

$$x_{k+1} = x_k - K_1' \lambda x_k - K_1'(g_0(x_k) - \lambda x_k) \tag{A2-4}$$

instead of (A2–2) with $x_k = \tilde{\varphi}_k$, $k \in Z_+$, Z_+ is the set of nonnegative integers. With help of $\mathscr{Z}$ – Laurent transformation (direct and reverse) one gets from (A2–2) subsequently

$$X(z) = \frac{z x_0}{z - (1 - K_1' \lambda)} - \frac{\mathscr{Z}\{K_1'(g_0(x_k) - \lambda x_k)\}}{z - (1 - K_1' \lambda)} \tag{A2-5}$$

$X(z) = \mathscr{Z}\{x_k\}$

and

$$x(k) = \sum_{l=0}^{k-1} k_{\lambda,1}(k - l)\{g_0(x(l)) - \lambda x(l)\} + x_\lambda(k), \quad k = 1, 2, \ldots \tag{A2-6}$$

while $x(k) = x_k$, $k = 0,1,\ldots$
Also

$$k_{\lambda,1}(k) = -K_1'(1 - K_1' \lambda)_{k-1} 1|(k - 1) \tag{A2-7}$$

$$K_{\lambda,1}(z) = \mathscr{Z}\{k_{\lambda,1}(k)\} = \frac{-K_1'}{z - (1 - K_1' \lambda)} \tag{A2-8}$$

$$x_\lambda(k) = x_0(1 - K_1' \lambda)^k 1|(k) \tag{A2-9}$$

$$X(z) = \frac{z x_0}{z - (1 - K_1' \lambda)} = \mathscr{Z}\{x_\lambda(k)\} \tag{A2-10}$$

$$r_x = \lim_{m \to \infty} \sup \sqrt[m]{|x_\lambda(m)|} = |1 - K_1' \lambda| \tag{A2-11}$$

$$r_{\lambda,1} = \lim_{m \to \infty} \sup \sqrt[m]{|k_{\lambda,1}(m)|} = |1 - K_1' \lambda| \tag{A2-12}$$

$$K_{\lambda,1}(r_0 e^{j\omega}) = \frac{K_1'}{e^{j\omega} r_0 - (1 - K_1' \lambda)} \tag{A2-13}$$

$$\sup_\omega |K_{\lambda,1}(r_0 e^{j\omega})| = \frac{|K_1'|}{|r_0 - (1 - K_1' \lambda)|} \tag{A2-14}$$

$$1|(k) = \begin{cases} 1 & k \geqslant 0 \\ 0 & k < 0. \end{cases}$$

The equation (A2–6) is the required one of the convolutional form.

APPENDIX 3

1. THE SECOND ORDER DIGITAL PHASE-LOCKED LOOP WITH PERFECT ADDER

Negligible noise and quantization effects: $Q(x) = x$, $N_k = 0$, $k = 0,1,\ldots$. The equation of this loop while $K_1' = K_1 A$ and $x_k = \varphi_k$ is (see appendix 1)

$$x_{k+2} - 2x_{k+1} + x_k = K_1' \lambda x_k - K_1' r_l \lambda x_{k+1} + \\ + K_1'(g(x_k) - \lambda x_k) - K_1' r_l (g(x_{k+1}) - \lambda x_{k+1}) \tag{A3-1}$$

Next while performing direct and reverse $\mathscr{Z}$ – Laurent transformations one gets $(x(k)=x_k)$

$$X(z) = \frac{z^2 x_0 + z(x_1 - 2x_0 - K_1' r_l g(x_0))}{z^2 - (2 - K_1' r_l \lambda) z + 1 - K_1' \lambda} + \\ + \frac{(K_1' - K_1' r_l z)\, \mathscr{Z}\{g(x_k) - \lambda x_k\}}{z^2 - (2 - K_1' r_l \lambda) z + 1 - K_1' \lambda} \tag{A3-2}$$

and

$$x(k) = \sum_{l=0}^{k-1} k_{\lambda,1}(k - l)\{g(x(l)) - \lambda x(l)\} + x_\lambda(k) \tag{A3-3}$$

$k = 1, 2, 3, \ldots$

Also

$$k_{\lambda,1}(\mathrm{k}) = \mathscr{Z}^{-1}\{K_{\lambda,1}(z)\} = \mathscr{Z}^{-1}\left\{\frac{K_1' - K_1' r_l z}{z^2 - (2 - K_1' r_l \lambda) z + 1 - K_1' \lambda}\right\} \tag{A3-4}$$

and

$$x_\lambda(k) = \mathscr{Z}^{-1}\{X_\lambda(z)\} = \mathscr{Z}^{-1}\left\{\frac{z^2 x_0 + z(x_1 - 2x_0 + K_1' r_l g(x_0))}{z^2 - (2 - K_1' r_l \lambda) z + 1 - K_1' \lambda}\right\} \tag{A3-5}$$

The equation (A3–3) is the functional one of convolutional form.

2. THE SECOND-ORDER DIGITAL PHASE LOCKED WITH NONPERFECT ADDER

The equation of the loop while the disturbing noise and quantization effects are negligible i. e.: $Q(x)=x$ and $N_k=0$, $k=0,1,\ldots$ is (appendix 1)

$$\varphi_{k+2} - (1 + \beta)\varphi_{k+1} + \beta\varphi_k = K_{1g}'(\varphi_k) - K_1' r_l g(\varphi_{k+1}) + \Lambda(1 - \beta) \tag{A3-6}$$

and $K_1' = K_1 \mathrm{A}$, $\mathrm{k} \in Z_+$.

If $\left|\frac{(1 - \beta)\Lambda}{(\beta - r_l) K_1'}\right| < 1$ then there exists the fixed point φ_s of (A3–6) and

$$g(\varphi_s) = -\frac{(1 - \beta)\Lambda}{(\beta - r_l) K_1'} \tag{A3-7}$$

By

$$\tilde{\varphi}_k = \varphi_k - \varphi_s$$

the equation (A3–6) is transformed into

$$\tilde{\varphi}_{k+2} - (1 + \beta)\tilde{\varphi}_{k+1} + \beta\tilde{\varphi}_k = K_1' g_0(\varphi_k) - K_1' r_l g_0(\tilde{\varphi}_{k+1}) \tag{A3-8}$$

while

$$g_0(x) \stackrel{\text{df}}{=} g(x + \varphi_s) - g(\varphi_s), \quad 0 < \beta < 1.$$

Next while using the direct and reverse $\mathscr{Z}$ transformations (A3 – 8) can be changed ($x_k = \tilde{\varphi}_k$) into

$$x_{k+2} - (1 + \beta)x_{k+1} + \beta x_k = \beta K_1' \lambda x_k - K_1' r_l \lambda x_{k+1} + \\ + \beta K_1'(g_0(x_k) - \lambda x_k) - K_1' r_l (g_0(x_{k+1}) - \lambda x_{k+1}) \tag{A3-9}$$

$$X(z) = \frac{z^2 x_0 + (x_1 - (1 + \beta)x_0 - K_1' r_l g_0(x_0))}{z^2 - (1 + \beta - K_1' r_l \lambda)z + \beta(1 - K_1' \lambda)} + \\ + \frac{(\beta K_1' - z K_1' r_l)\, \mathscr{Z}\{g_0(x_k) - \lambda x_k\}}{z^2 - (1 + \beta - K_1' r_l \lambda)z + \beta(1 - K_1' \lambda)}. \tag{A3-10}$$

While $x(k) = x_k$ it follows from (A3 – 10)

$$x(k) = \sum_{l=0}^{k-1} k_{\lambda,1}(k - l)\{g(l) - \lambda x(l)\} + x_\lambda(k), \tag{A3-11}$$

$k = 1, 2, 3, \ldots$.

Moreover

$$\mathrm{k}_{\lambda,1}(\mathrm{k}) = \mathscr{Z}^{-1}\{K_{\lambda,1}(\mathrm{z})\} = \mathscr{Z}^{-1}\left\{\frac{\mathrm{K}_1' - \mathrm{z}\mathrm{K}_1' \mathrm{r}_l}{z^2 - (1 + \beta - \mathrm{K}_1' \mathrm{r}_l \lambda)\mathrm{z} + \beta(1 - \mathrm{K}_1' \lambda)}\right\} \tag{A3-12}$$

and

$$x_\lambda(k) = \mathscr{Z}^{-1}\left\{\frac{z^2 x_0 + (x_1 - (1+\beta)x_0 + K_1' r_l g_0(x_0))}{z^2 - (1 + \beta - K_1' r_l \lambda)z + \beta(1 - K_1' \lambda)}\right\}. \tag{A3-13}$$

The equation (A3 – 13) is the required one of the convolutional form.

APPENDIX 4

DIGITAL PHASE LOCKED LOOP OF THIRD-ORDER WITH NEGLIGIBLE QUANTIZATION EFFECTS

$Q(x) = x$ and $N_k = 0$, $k = 0, 1, \ldots$

The equation of the loop of third-order while $x_k = \varphi_k$ is (see appendix 1):

$$x_{k+3} - 3x_{k+2} + 3x_{k+1} - x_k = -pK_1' \lambda x_{k+2} - pK_1'(g(x_{k+2}) - \lambda x_{k+2}) + \\ + K_1'(1 + r_l)(g(x_{k+1}) - \lambda x_{k+1}) - K_1'(g(x_k) - \lambda x_k) + \\ + K_1'(1 + r_l)\lambda x_{k+1} - K_1' \lambda x_k \tag{A4-1}$$

$k = 0, 1, \ldots$

Next with aid of direct and inverse Laurent transformations one gets

$$X(z)=\frac{\mathscr{Z}\{g(x_k)-\lambda x_k\}(-pK_1'z^2+K_1'(1+r_l)z-K_1')}{z^3-z^2(3-pK_1'\lambda)+z(3-K_1'(1+r_l)\lambda)+K_1'\lambda-1}+$$
$$+\frac{z^3x_0+z^2(x_1-3x_0+pK_1'g(x_0)+z(x_2-3x_1+3x_0+pK_1'g(x_1)-K_1'(1+r_l)g(x_0))}{z^3-z^2(3-pK_1'\lambda)+z(3-K_1'(1+r_l)\lambda)+K_1'\lambda-1} \quad \text{(A4-2)}$$

and

$$x(k)=\sum_{l=0}^{k-1}k_{\lambda,1}(k-l)\{g(x(l))-\lambda x(l)\}+x_\lambda(k) \quad \text{(A4-3)}$$

$k = 1, 2, \ldots$

Also

$$k_{\lambda,1}(k)=\mathscr{Z}^{-1}\left\{\frac{-pK_1'z^2+K_1'(1+r_l)z-K_1'}{z^3-z^2(3-pK_1'\lambda)+z(3-K_1'(1+r_l)\lambda)+K_1'\lambda-1}\right\} \quad \text{(A4-4)}$$

$$x_\lambda(k)=\mathscr{Z}^{-1}\left\{\frac{z^3x_0+z^2(x_1-3x_0+pK_1'g(x_0))+z(x_2-3x_1+3x_0+pK_1'g(x_1))-K_1'(1+r_l)g(x_0)}{z^3-z^2(3-pK_1'\lambda)+z(3-K_1'(1+r_l)\lambda)+K_1'\lambda-1}\right\} \quad \text{(A4-5)}$$

The equation (A4−3) of convolutional form is the required one.

APPENDIX 5

THE FUNCTIONAL EQUATION OF THE DIGITAL PHASE-LOCKED LOOP OF THE CONVOLUTIONAL FORM WITH DISTURBING NOISE AND NEGLIGIBLE QUANTIZATION EFFECTS: $Q(x) = x$

It follows from appendix 1 that the disturbing noise can be taken into account by substitution $g_0(x)+N/A$ in place of $g_0(x)$ ($g_0x=g(x)$ if $\varphi_s=0$) in the case of DPLL of any order. That is why the equation of the loop with disturbing noise is

$$x(k)=\sum_{l=0}^{k-1}k_{\lambda,1}(k-l)(g_0(x(l))-\lambda x(l))+x_\lambda(k)+\sum_{l=0}^{k-1}k_{\lambda,2}(k-l)z(l) \quad \text{(A5-1)}$$

$z(k) = N_k/A$, $k_{\lambda,1}(k) = k_{\lambda,2}(k)$, $k = 0, 1, \ldots$

The equation (A5−1) is the required one.

APPENDIX 6

THE MODEL OF MODIFIED NONUNIFORM DIGITAL PHASE-LOCKED LOOPS

According to fig. A6−1, fig. A6−2 and the appendix 1 the following relations are valid while $\pi/2$ radian shift is taken into account

$$s_k = A\sin\varphi_k + N_k \quad \text{(A6-1)}$$

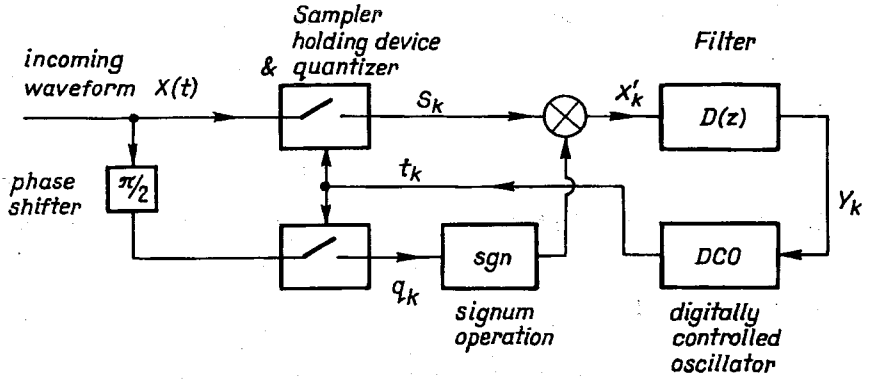

Fig. A6–1. The scheme of the modified nonuniform sampling digital phase-locked loop by the author of this paper

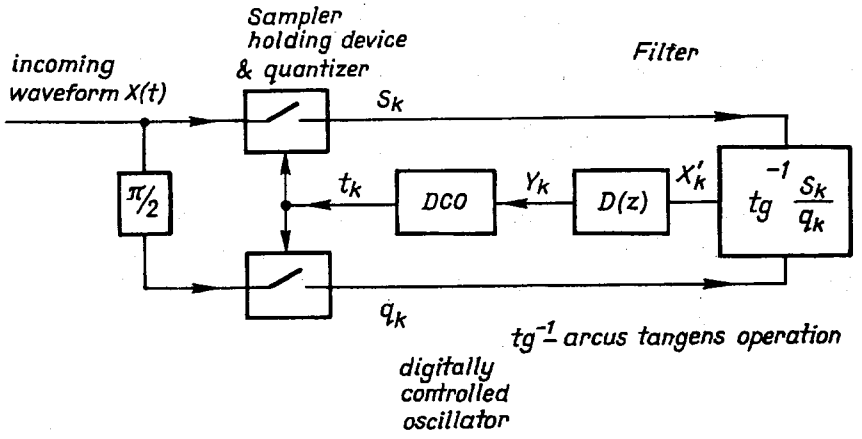

Fig. A6–2. The scheme of the nonuniform sampling DTPLL [3]

$$q_k = A\cos\varphi_k + N'_k. \tag{A6–2}$$

1. The modified loop of fig. A6–1.

In this case

$$X'_k = (A\sin\varphi_k + N_k)\operatorname{sgn}(A\cos\varphi_k + N'_k) = s_k \operatorname{sgn} q_k = \\ = A g^*(\varphi_k) + N^*_k \tag{A6–3}$$

and

$$g^*(\varphi) = \sin\varphi \operatorname{sgn}(A\cos\varphi) \tag{A6–4}$$

sign stands for signum. On the other hand

$$N^*_k = N_k \operatorname{sgn}(A\cos\varphi_k + N'_k) + A\sin\varphi_k(\operatorname{sgn}(A\cos\varphi_k + N'_k) + \\ - \operatorname{sgn}(A\cos\varphi_k)). \tag{A6–5}$$

By substitution

$$\varphi = \varphi'/2, \quad \Theta' = 2\Theta, \quad Y' = 2Y \tag{A6–6}$$

the equation (A1 – 6c) of appendix 1 is changed into

$$\varphi'_{k+1} = \varphi'_k + \Theta'_{k+1} - \Theta'_k - \omega_0 Y'_k. \qquad \text{(A6–7)}$$

The effective nonlinearity of the loop is

$$g^*(\varphi') = \sin(\varphi'/2)\ \operatorname{sgn}(A\cos(\varphi'/2)) \qquad \text{(A6–8)}$$

However while estimating the parameters of noise (A6–5) should be taken into account.

2. The loop of fig. A6–2

$$X'_k = \operatorname{tg}^{-1} s_k/q_k = \operatorname{tg}^{-1}\left(\frac{A\sin\varphi_k + N_k}{A\cos\varphi_k + N'_k}\right) = g^*(\varphi) + N_k. \qquad \text{(A6–9)}$$

The effective nonlinearity of the loop is

$$g^*(\varphi) = \operatorname{tg}^{-1}(\operatorname{tg}\varphi). \qquad \text{(A6–10)}$$

Whereas the effective noise in the loop is

$$N_k = \operatorname{tg}^{-1}\left(\frac{A\sin\varphi_k + N_k}{A\cos\varphi_k + N'_k}\right) - \operatorname{tg}^{-1}(\operatorname{tg}\varphi) \qquad \text{(A6–11)}$$

The g^* of (A6–10) is a sawtooth function. The estimates of the required parameters of the effective noise should take (A6–11) into account [3]. Moreover tg^{-1} of (A6–9) and (A6–11) is understood as the operation of argument [3,6]. The operation of argument can be used in case 1 also.

M. ŻÓŁTOWSKI

NOWE KRYTERIA STABILNOŚCI DLA CYFROWYCH PĘTLI FAZOWYCH Z NIEJEDNOSTAJNYM PRÓBKOWANIEM DOWOLNEGO RZĘDU ŚLEDZĄCYCH PRZEJŚCIA PRZEZ POZIOM ZEROWY. CZĘŚĆ I

Streszczenie

Odkryto nowe kryteria stabilności dla cyfrowych pętli fazowych z niejednostajnym próbkowaniem śledzących przejścia przez poziom zerowy. Do opisu przebiegu błędu fazy w pętli dowolnego rzędu użyto nieliniowe funkcjonalne równanie dotyczące rozmaitości S^1 – okręgu. Zbadano zaburzony synchronizm N:1, gdy zaburzeniem jest albo odstrojenie w częstotliwości lub dodatkowy szum losowy i efekt kwantowania. Klasa pętli z nieciągłą charakterystyką detektora fazy jest godna polecenia, gdy wymagany jest szybki proces synchronizacji w pętli dowolnego rzędu niezależnie od początkowych warunków błędu fazy. Przedstawioną analizę można rozszerzyć w celu uwzględnienia zaników przebiegu wejściowego, modulacji AM i PM lub filtru o zmiennych współczynnikach. Rozszerzenie takie zostanie przedstawione w części II i części III.

KWARTALNIK ELEKTRONIKI I TELEKOMUNIKACJI, 1991, 37, Z. 3–4, ss. 573–592

621.317.08

New stability criteria for the nonuniform sampling zero-crossing digital phase-locked loops of any order

MARIUSZ ŻÓŁTOWSKI

Instytut Telekomunikacji, Politechnika Gdańska

Recived 1990.04.25

Authorized 1990.11.27

Part II

New stability criteria for the digital nonuniform sampling zero-crossing phase-locked loops are derived in the case of perturbed N:1 phase entrainment. The approach of Part I is extended to include the fading of the input waveform, AM and PM modulation. The functional nonlinear discrete-time equation on the S^1 circle manifold is used to describe the phase error in the loop of any order.

I. INTRODUCTION

Digital zero-crossing phase-locked loops (DPLL-s) are the phase locked loops (PLL-s) while implemented within digital circuitry. The resulting reliability, immunity to drifts and flexibility are of interest in communication, communication by satellite, space communication, the communication of deep space, telemetry, measuring, control and guidance. The DPLL is a nonlinear feedback device which tracs the phase of incoming waveform while the error of keeping up is called the instantenous phase error or phase error process shortly. The phase error is obtained from the phase detector of the loop. Just the sampling device acts as a phase detector in the nonuniform sampling DPLL-s. That is why the acquisition of phase-lock (the state of phase entrainment) relies on the changeable time interval between the subsequent samples of the waveform being tracked by the loop. The purpose of presented extension of Part I is to consider the fading of input waveform, amplitude AM and phase PM modulations. So far, the phase modulation in the loop of first-order only has been considered by Gill and Gupta [3]. The presented approach is of the worst case type while assuring the existence of the required phenomena if the parameters are kept within prescribed limits. The different aspects of the acquisition of the phase-lock can be discussed while various estimates can be obtained. This approach can be helpful to

plan the very detailed computer studies of the loop of special interest in the case of N:1 phase entrainment.

2. THE MODE OF THE DIGITAL NONUNIFORM SAMPLING PHASE-LOCKED LOOP

The principle of synchronization is shown in fig. 1 while the model of the digital phase-locked loop of fig. 1 is derived in appendices 2–4 in this case. See also the second

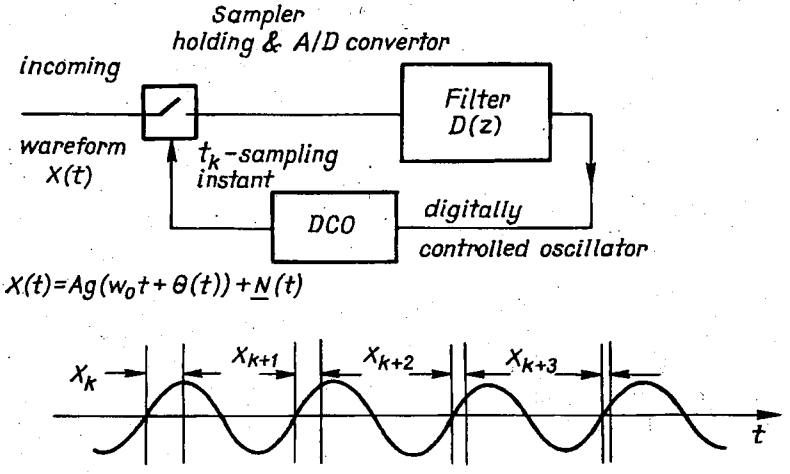

Fig. 1. The model of the nonuniform sampling DPLL and the principle of N:1 phase entrainment

chapter of Part I for introductory explanation of loop's model. It has been shown (see the appendices for the details) that the new model of the loop can be given in terms of functional equation on S^1 circle manifold of the form

$$x(k) = \sum_{l=0}^{k-1} k_{\lambda,1}(k-l)\big(Q(g_0(l, x(l))) - \lambda x(l)\big) + \sum_{l=0}^{k} k_{m,\lambda}(k-l)\theta_0(l) + \sum_{l=0}^{k-1} k_{\lambda,1}(k-l)z(l, x(l)) + x_\lambda(k) \pmod{2\pi}. \quad (1)$$

The discrete time waveform x of (1) is the phase error process. The discrete time functions $k_{\lambda,1}$, $k_{m,\lambda}$ are the unit pulse responses [4] of the model of the loop. The θ_0 of (1) stands for the discrete time waveform describing the phase of the incoming waveform. Whereas $x_\lambda(\lambda>0)$ while depedent on n initial conditions in the loop of n^{th}-order case is the known waveform standing for the linear part of the model of the loop. The nonlinear function g_0 of (1) represents the effective nonlinearity of the loop (the characteristic of the phase detector). The main features of the new model are: the phase error x is the sum of the known waveform x affected by the modulation θ_0, the noise z and the nonlinear term from the feedback loop (see fig. 2). The modulation in

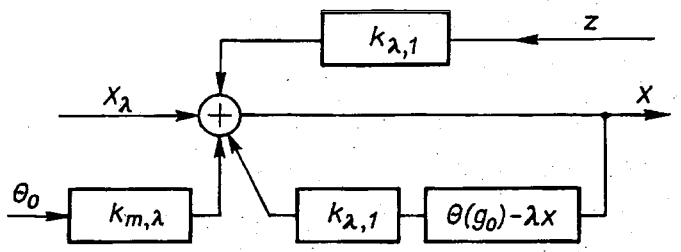

Fig. 2. The model of the DPLL in respect to N:1 phase-entrainment in terms of convolutional functional equation

amplitude is taken into account throughout g_0 function while parameter λ is carefully chosen. Finaly Q of (1) represents the quantization effects. In view of the cyclic nature of phase error (see part I for the details) the dynamics of the DPLL is considered on S^1 – circle manifold. The operation of projection is given by

$$\pi : R \to S^1$$
$$x \to \pi(x) = \arg e^{jx} \in <-\pi, \pi> \text{ closed interval with equivalent ends}$$
$$R - \text{straight line of reals.}$$

The equivalent notations for $\pi(x)$ are: $[x]$ and $x \pmod{2\pi}$. The all subsequent points of the phase error trajectory of (1) are projected on S^1.

3. THE PERTURBED N:1 PHASE ENTRAINMENT ON S^1 – CIRCLE MANIFOLD

The purpose of perturbed N:1 phase entrainment considerations is to obtained the different kinds of estimates which are to show that the phase error trajectory in the perturbed case does not essentially differ from one in the unperturbed one. The perturbation of N:1 phase entrainment occurs while the frequency offset, disturbing noise, phase modulation or quantization of the incoming waveform being tracked by the loop are present.

This approach is quite similar to that of Part I. Let $\{X\}$ stands for the space of the sequences $\{x\}$ which elements are from X space. Whereas $\{[X]\}$ for the space of the sequences $\{[x]\}$ which elements are from $[X]$ space. In the considered case $X=R^1=R$ and $[X]=[R]=S^1=<-\pi, \pi>$. The operation of projection onto S^1 circle manifold is denoted by $[\ ]$ of (mod 2π). Moreover the following statements hold true for all x,y,α from $R,\alpha>0$, while $|\ |$ stands for absolute value

$$|[|x|]| = |[x]| \tag{2a}$$
$$|[\alpha[x]]| \leqslant |\alpha||[x]| \tag{2b}$$
$$|[[x] + [y]]| \leqslant |[y]| \tag{2c}$$

Now, let the function ρ with properties concerning the space $\{[X]\}$ be defined:

$$\rho : \{X\} \to R_+ \text{ (the set of nonnegative reals)}$$

$$\{x\} \to \rho(\{x\}) < \infty$$

Further properties of ρ are:

$$\rho(\{[x]\}) = 0 \rightleftharpoons \{[x]\} = 0 \tag{3a}$$

Last 0 stands for zero element of $(\{[X]\}, \rho)$ space.

$$\rho(\{[\lambda\{[x]\}]\}) \leqslant |\lambda|\,\rho(\{[x]\}) \tag{3b}$$

$$\rho(\{[\{[x]\} + \{[y]\}]\}) \leqslant \rho(\{[x]\}) + \rho(\{[y]\}) \tag{3c}$$

$(\{[X]\}, \rho)$ stands for the space $\{[X]\}$ with ρ well defined for every $\{[x]\} \in \{[X]\}$. The addition, multiplication and projection of (3) are the operations being performed coordinate point by coordinate point on vectors. Let the following notation be introduced first

$$A_{\lambda,l}\{k, u\} \stackrel{\text{df}}{=} \sum_{l=0}^{k-1} k_{\lambda,l}(k - l)\,u(l), \tag{4a}$$

$$z_\lambda(k) = A_{\lambda,l}\{k, z\} = \sum_{l=0}^{k-1} k_{\lambda,l}(k - l)\,z(l, x(l)), \tag{4b}$$

$$\theta_\lambda(k) = \sum_{l=0}^{k} k_{m,\lambda}(k - l)\,\theta_0(l) = A_{\lambda,m}\{k, \theta\} \tag{4c}$$

$$u(l) = Q(g_0(l, x(l))) - \lambda x, \quad l = 0, 1, \ldots \tag{4d}$$

The depedence on $x(l)$ in (4b) is not present if quantization effects are either negligible or modelled by additional quantization noise. The parameters of quantization noise (the mean squared value) depend on quantizer [4]. Now if

$$\underset{\{u\}}{\forall} \in \{R\} \quad \rho(\{[A_{\lambda,l}\{u\}]\}) \leqslant \alpha_1\,\rho(\{u\}) \tag{5}$$

and $0 \leqslant \alpha_1 < \infty$ then there exists operator

$$A_{\lambda,l} : \{R\} \to (\{S^1\}, \rho),\ S^1 = [R]$$

$$\underset{\{u\}\in\{R\}}{\forall} \to \{[\mathrm{A}_{\lambda,l}\{u\}]\} \in (\{S^1\}, \rho)$$

and

$$\underset{\{u\}}{\forall} \in \{R\}\ \rho(\{[\mathrm{A}_{\lambda,l}\{u\}]\}) \leqslant \alpha_1\,\rho(\{u\}). \tag{6}$$

Secondly, let the following constraint on the loop's nonlinearity be valid

$$\underset{\{u\}\in\{R\}}{\forall} \rho(\{u\}) \leqslant \alpha_2\,\rho(\{[x]\}) + a \tag{7}$$

$$\alpha_2 \geqslant 0, \quad a > 0.$$

Then the theorem 1 can be stated. While being basic for all considerations of this paper it is the counterpart of the similar one of Part I.

Theorem 1

Suppose $\{x_\lambda\}$, $\{z_\lambda\}$, $\{\theta_\lambda\}$ are from $(\{R\}, \rho) \cap (\{S^1\}, \rho)$ space.
Let also

$$\alpha_1 \alpha_2 < 1, \quad \alpha_1 \text{ of (6) and } \alpha_2 \text{ of (7)}.$$

Then the solution $\{x\}$ of the equation (1) is unique and belong to $(\{S^1\}, \rho) \cap (\{R\}, \rho)$ space if $\rho(\{[x]\})$ is sufficiently small. Moreover the following estimate holds true

$$\rho(\{[x]\}) \leqslant \frac{\rho(\{[x_\lambda]\}) + \rho(\{[z_\lambda]\}) + \rho(\{[\theta_\lambda]\}) + \alpha_1 a}{1 - \alpha_1 \cdot \alpha_2} \tag{8}$$

The proof of theorem 1

The solution of (1) exists and is unique because the reccurent equation is under consideration. Moreover the equation (1) in simplified notation is (see (4))

$$x = A_{\lambda,1} u + x_\lambda + \theta_\lambda + z_\lambda.$$

Next, in view of (3), (6), (7)

$$\begin{aligned} \rho(\{[x]\}) &= \rho(\{[A_{\lambda,1} u + x_\lambda + \theta_\lambda + z_\lambda]\}) = \\ = \rho(\{[[A_{\lambda,1} u] + [[x_\lambda + \theta_\lambda] + z_\lambda]]\}) &\leqslant \rho(\{[A_{\lambda,1} u]\}) + \rho(\{[[x_\lambda + \theta_\lambda] + z_\lambda]\}) \leqslant \\ &\leqslant \alpha_1 \rho(\{u\}) + \rho(\{[x_\lambda + \theta_\lambda]\}) + \rho(\{[z_\lambda]\}) \leqslant \\ \leqslant \alpha_1 \cdot \alpha_2 \rho(\{[x]\}) + \alpha_1 \cdot a + (\rho(\{[x_\lambda]\}) + \rho(\{[\theta_\lambda]\})) + \rho(\{[z_\lambda]\}) &= \\ = \alpha_1 \cdot \alpha_2 \rho(\{[x]\}) + \alpha_1 \cdot a + \rho(\{[x_\lambda]\}) + \rho(\{[\theta_\lambda]\}) + \rho(\{[z_\lambda]\}) & \end{aligned} \tag{9}$$

The proposition of last theorem follows from this inequality directly. The belongness to $(\{R\}, \rho)$ space can be established in view of the local stability of the loop within the covering space concept of Part I. While the perturbed N:1 phase entrainment is considered the continuity of the phase error x considering the excitation occurs and the phase error should change slightly arround the state of N:1 phase entrainment. This is assured if $\rho(\{[x]\})$ is sufficiently small. The small oscillations occur in the covering space in this case.
Now the different aspects of perturbed N:1 phase entrainment can be studied by the theorem 1 in the case of various constraints on loop's nonlinearity. However the calculations of $\rho(\{[\theta_\lambda]\})$ and $\rho(\{[z_\lambda]\})$ require additional estimates especially in the modified DPLL-s case. Just the exact estimates of $\rho(\{[\theta_\lambda]\})$ are impossible because of nonlinear depedence on x. This depedence is present because the equations according to which the phase error and the sampling instants change in the loop are coupled (see appendix 1). The are decoupled in simpler case of Part I. However, since the phase modulation $\theta(t)$ is known up to required parameters it is still possible to find the estimates of $\rho(\{[\theta_\lambda]\})$ which do not depend on $x(l)$ for all $l \in Z_+$.

4. THE EXAMPLES OF $(\{[X]\}, \rho)$ SPACES

a) The $(\{[X]\}, \rho_1)$ space of the sequences of finite pseudoenergy:

$$\rho_1 : \{[X]\} \to R_+$$

$$\{[x]\} \to \rho_1(\{[x]\}) = \sqrt{\sum_{m=0}^{\infty} [x(m)]^2 r_0^{-2m}} \tag{10a}$$

$r_0 \in (0,1> \subset R$.

b) The $(\{[X]\}, \rho_2)$ space of the sequences with asymptotic metric

$$\rho_2 : \{[X]\} \to R_+$$

$$\{[x]\} \to \rho_2(\{[x]\}) = \lim_{M\to\infty} \sup_{m>M} |[x(m)]| \tag{10b}$$

c) The space $(\{[X]\}, \rho_3)$ of the sequences of finite pseudopower

$$\rho_3 : \{[X]\} \to R_+$$

$$\{[x]\} \to \rho_3(\{[x]\}) = \overline{\lim_{M\to\infty}} \sqrt{\frac{1}{M} \sum_{m=0}^{M} |[x(m)]|^2} \tag{10c}$$

d) The space $(\{[X]\}, \rho_4)$ of the sequences with finite peak value

$$\rho_4 : \{[X]\} \to R_+$$

$$\{[x]\} \to \rho_4(\{[x]\}) = \sup_{m\geqslant 0} |[x(m)]| \tag{10d}$$

Moreover $X=R$ and $[R]=S^1$ in the all cases.

5. THE NONLINEARITY CONSTRAINTS

Three different constraints on loop's nonlinearity are used:
a) The case when the effects of quantization of the incoming waveform are negligible; $Q(x)=x$

$$|Q(g_0(l, x)) - \lambda x| \leqslant R|x| \tag{11a}$$
$$x \in S^1, \quad R > 0, \quad \lambda > 0.$$

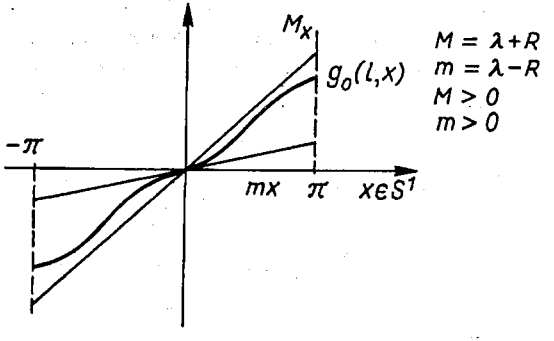

Fig. 3. The first exapmle of constraints on loop's nonlinearity

According to geometrical meaning of (11a) the loop's nonlinearity is within the region bounded by the straight lines of M and m slopes respectively (see fig. 3).

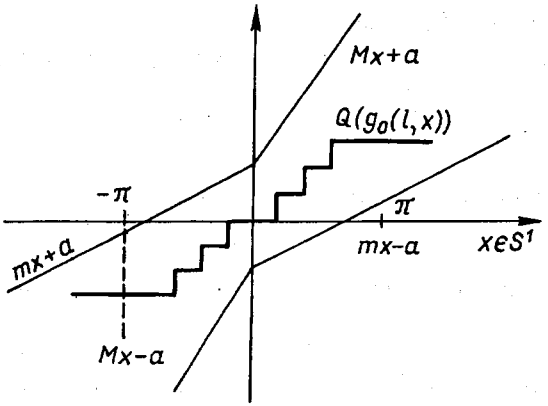

Fig. 4. The second example of constraints on loop's nonlinearity

b) The case when the equantization effects are taken into account

$$|Q(g_0(l, x)) - \lambda x| \leqslant R|x| + a, \quad R > 0, \quad a > 0. \tag{11b}$$

c) Another case of constraints while the quantization effects are accounted for by the model

$$|Q(g_0(l, x)) - \lambda x| \leqslant R|x| + (a - M|x|) r_d(a/M) \tag{11c}$$

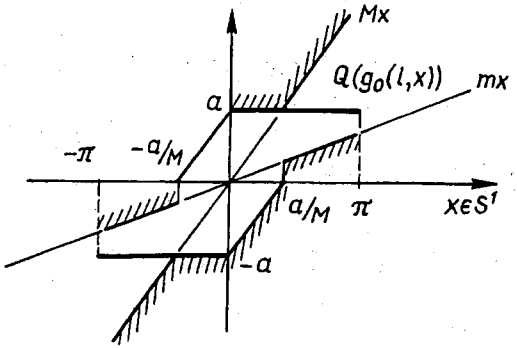

Fig. 5. The third example of constraints on loop's nonlinearity

while

$$r_d(u_1) \stackrel{\text{df}}{=} \begin{cases} 1 & \text{when } |x| \leqslant u_1 \\ 0 & \text{when } |x| > u_1, \ u_1 > 0 \end{cases}$$

$$x \in S^1, \quad R > 0, \quad a > 0, \quad M > 0, \quad m \geqslant 0.$$

If $x \in S^1$, $\in |x| \leqslant a/M$ then

$$|Q(g_0(l, x)) - \lambda x| \leqslant a - \lambda|x| \leqslant a. \tag{11d}$$

See the Part I for the use of this constraint.
Now while the constraints on loop's nonlinearity are valid it is easy to estimate the parameters α_2 and a of theorem 1.

6. THE ESTIMATES CONCERNING THE OPERATOR OF CONVOLUTION

Let the discrete-time sequences $\{y\}$ and $\{u\}$ are related each to other by the operation of convolution i.e

$$y(l) = \sum_{m=0}^{l} k(l - m)\, u(m) \quad \text{for all } l \in Z_+, \ (Z_+ \text{ is the set of nonnegative integers}) \tag{12}$$

The discrete-time sequence $\{k\}$ of (12) is the unit pulse response of the linear discrete time system while described in terms of (12). That is why the equation (12) after $\mathscr{Z}$ – Laurent transformation takes form

$$Y(z) = K(z)\, U(z) \tag{13a}$$

$$Y(z) = \sum_{m=0}^{\infty} y(m) z^{-m} = \mathscr{Z}(\{y\}) \tag{13b}$$

$U(z) = \mathscr{Z}(\{u\}), K(z) = \mathscr{Z}(\{k\}), z \in C$ (C is the set of complex numbers).

Just the relations while concerning the convolutions operator of (12) will be considered next for the subsequent spaces of chapter 4.
a) The space $(\{S^1\}, \rho_1)$ of the sequences of finite pseudoenergy. The following estimate holds true for any element $\{[y]\}$ of this space:

$$\rho_1^2(\{[y]\}) = \sum_{m=0}^{\infty} |[y(m)]|^2 r_0^{-2m} \leqslant \sum_{m=0}^{\infty} |y(m)|^2 r_0^{-2m} = \frac{1}{2\pi} \int_{-\pi}^{\pi} |Y(r_0 e^{j\omega})|^2 \, d\omega \tag{14}$$

$$r_0 \in (0,1>, \ Y(r_0 e^{j\omega}) = \mathscr{Z}(\{y\})\Big|_{z = r_0 e^{j\omega}}$$

Also

$$\rho_1(\{[y]\}) \leqslant \sqrt{\frac{1}{2\pi} \int_{-\pi}^{\pi} |Y(r_0 e^{j\omega})|^2 \, d\omega} = \sqrt{\frac{1}{2\pi} \int_{-\pi}^{\pi} |K(r_0 e^{j\omega})|^2 |U(r_0 e^{j\omega})|^2 \, d\omega} =$$

$$\leqslant \sup_{\omega} |K(r_0 e^{j\omega})| \, \rho_1(\{u\}). \tag{15}$$

The last expression can be given a short form also

$$\rho_1(\{[x]\}) \leqslant \alpha_1 \cdot \rho_1(\{u\}) \tag{16a}$$

while

$$\alpha_1 = \alpha_1(r_0) = \sup_{\omega} |K(r_0 e^{j\omega})|. \tag{16b}$$

Suppose there exists r_0 satisfying

$$1 \geqslant r_0 = |r_0 e^{j\omega}| > \lim_{m\to\infty} \sup \sqrt[m]{|k(m)|}. \tag{17}$$

Then the function $K(r_0 e^{j\omega})$ exists.

b) The space $(\{S^1\}, \rho_3)$ of the sequence of finite pseudopower.

$$\rho_3(\{[y]\}) = \overline{\lim_{M\to\infty}} \sqrt{\frac{1}{M} \sum_{m=0}^{M} |[y(m)]|^2} \leqslant \alpha_1 \rho_3(\{u\}) \tag{18}$$

with α_1 defined in (16b), $r_0 = 1$ in this case while $\overline{\lim}$ stands for limes superior. Also, the following estimate is valid in view of (15)

$$\rho_3(\{[y]\}) \leqslant \sqrt{\frac{1}{2\pi} \int_{-\pi}^{\pi} |K(e^{j\omega})|^2 \; \bar{P}_u(e^{j\omega}) \, d\omega} \tag{19a}$$

$$\bar{P}_u(e^{j\omega}) \stackrel{\text{df}}{=} \overline{\lim_{M\to\infty}} \frac{|U_M(e^{j\omega})|^2}{M} \tag{19b}$$

$$U_M(e^{j\omega}) = \mathscr{Z}(\{u_M\})\Big|_{z=e^{j\omega}} \tag{19c}$$

$$u_M(l) \stackrel{\text{df}}{=} \begin{cases} u(l) & l \leqslant M \\ 0 & l > M. \end{cases} \tag{19d}$$

c) The space $(\{S^1\}, \rho_2)$ of the sequences with asymptotic metric. In this case (see Part I)

$$\rho_2(\{[y]\}) = \lim_{M\to\infty} \sup_{m>M} |[y(m)]| \leqslant \alpha_1 \cdot \rho_2\{u\} \tag{20a}$$

while

$$\alpha_1 \stackrel{\text{df}}{=} \sum_{m=0}^{\infty} |k(m)| \tag{20b}$$

d) The $(\{S^1\}, \rho_4)$ space of the sequences with finite peak value metric.
This case is quite similar to the previous one

$$\rho_4(\{[y]\}) = \sup_{m>0} |[y(m)]| \leqslant \alpha_1 \rho_4(\{u\}) \tag{21}$$

while α_1 is defined in (20b).

7. EXAMPLES

In this chapter the examples of using theorem 1 in respect to the nonuniform sampling DPLL-s are presented. In different situations the existence of perturbed N:1 phase entrainment is shown this way and upper bounds concerning the phase error process are given.

a) The case of negligible noise disturbances.

Let the nonlinearity of the loop of any order satisfy (11b).

Suppose

$$\rho = \rho_2 \text{ and the assumptions of theorem 1 are valid :}$$

$$\alpha_1 = \sum_{m=0}^{\infty} |k_{\lambda,1}(m)| \tag{22a}$$

$$\alpha_2 = R \tag{22b}$$

$$\alpha_1 \cdot \alpha_2 < 1. \tag{22c}$$

Then

$$\rho_2(\{[x]\}) \leqslant \frac{\alpha_1 a + \rho_2(\{[\theta_\lambda]\})}{1 - \alpha_1 \alpha_2}. \tag{22d}$$

Moreover

$$\rho_2(\{[\theta_\lambda]\}) \leqslant \sum_{l=0}^{\infty} |k_{m,\lambda}(l)| \, \rho_2(\{\theta_0\})$$

$$\leqslant \sum_{l=0}^{\infty} |k_{m,\lambda}(l)| \lim_{t_M \to \infty} \sup_{t > t_M} |\theta_0(t)|. \tag{22e}$$

Whereas $\theta_0(t)$ of (22e) is the known phase modulation of zero mean value. However the estimation of (22c) is a pessimistic one. Much more realistic one can be obtained by considering (4c) directly. Namely $\rho_2(\{[\theta_\lambda]\})$ can be approximated according to

$$\rho_2(\{[\theta_\lambda]\}) = \sup_{n>0} \left[\left| \sum_{l=0}^{\infty} k_{m,\lambda}(l) \, \theta_0(n - l) \right| \right]. \tag{22f}$$

The approximation of (22f) results from the assumption that the samples $\theta_0(l)$ of (22f), $l \in Z_+$ are uniformly spaced in time. On the other hand if the nonlinearity of the loop is constrained according to (11d) then

$$\rho_2(\{[x]\}) \leqslant \max\left\{ \alpha_1 a + \rho_2(\{[\theta_\lambda]\}), \frac{\rho_2(\{[\theta_\lambda]\})}{1 - \alpha_1 \cdot \alpha_2} \right\}. \tag{22g}$$

The α_1 of (22g) is given in (22a) and $\rho_2(\{[\theta_\lambda]\})$ can be estimated like in the previous case.

b) The negligible effects of quantization case

Let the nonlinearity of the loop of any order be constrained according to (11a). Suppose $\rho = \rho_3$ and the assumptions of theorem 1 are valid, i.e.

$$\alpha_1 = \sup_{\omega} |K_{\lambda,1}(e^{j\omega})| \tag{23a}$$

$$\lim_{m\to\infty} \sup \sqrt[m]{k_{\lambda,1}(m)} < 1 \tag{23b}$$

$$\alpha_2 = R \tag{23c}$$

$$\alpha_1 \cdot \alpha_2 < 1. \tag{23d}$$

Then

$$\rho_3(\{[x]\}) \leqslant \frac{\rho_3(\{[z_\lambda]\}) + \rho_3(\{[\theta_\lambda]\})}{1 - \alpha_1 \cdot \alpha_2}. \tag{23e}$$

Now, while (19) in hand

$$\rho_3(\{[z_\lambda]\}) \leqslant \frac{1}{2\pi} \int_{-\pi}^{\pi} |K_{\lambda,1}(e^{j\omega})|^2 \bar{P}_z(e^{j\omega})\, d\omega \tag{24a}$$

$$\bar{P}_z(e^{j\omega}) \stackrel{df}{=} \overline{\lim_{M\to\infty}} \frac{|Z_M(e^{j\omega})|^2}{M} \tag{24b}$$

$$\rho_3(\{[\theta_\lambda]\}) \leqslant \sqrt{\frac{1}{2\pi} \int_{-\pi}^{\pi} |K_{m,\lambda}(e^{j\omega})|^2 \bar{P}_\theta(e^{j\omega})\, d\omega} \tag{25a}$$

$$\bar{P}_\theta(e^{j\omega}) \stackrel{df}{=} \overline{\lim_{M\to\infty}} \frac{|\theta_M(e^{j\omega})|^2}{M}. \tag{25b}$$

$Z_M(e^{j\omega})$ and $\theta_M(e^{j\omega})$ are defined exactly as $U_M(e^{j\omega})$ of (19) is. The estimates of $\rho_3(\{[z_\lambda]\})$ and $\rho_3(\{[\theta_\lambda]\})$ can be obtained while the expressions (24) and (25) and information about $\{[z_\lambda]\}$ and $\{[\theta]\}$ in hand.

c) Let the peak value metric ρ_4 is considered and the nonlinearity of the loop is constrained according to (11b). Suppose the assumptions of the theorem 1 are valid i.e.

$$\alpha_1 = \sum_{m=0}^{\infty} |k_{\lambda,1}(m)| \tag{26a}$$

$$\alpha_2 = R \tag{26b}$$

$$\alpha_1 \cdot \alpha_2 < 1. \tag{26c}$$

Then

$$\rho_4(\{[x]\}) \leqslant \frac{\alpha_1 a + \rho_4(\{[\theta_\lambda]\}) + \rho_4(\{[z_\lambda]\}) + \rho_4(\{[x_\lambda]\})}{1 - \alpha_1 \cdot \alpha_2} \tag{26d}$$

Moreover suppose that $a \simeq 0$, $\rho_4(\{[z_\lambda]\}) \simeq 0$ and $\rho_4(\{[x_\lambda]\}) \simeq 0$ $\rho_4(\{[x_y]\}) \simeq 0$. The last is true while the initial phase error conditions are not far from the state of N:1 phase entrainment. Then $\rho_4(\{[x]\})$ is also small according to (26d). It means that the perturbation of N:1 phase entrainment is small. That is why one can consider local

constraints on loop's nonlinearity which are valid for sufficiently small neighbourhood of the point $0 \in S^1$ in this case. This point is the state of unperturbed N:1 phase entrainment.

d) Taking AM amplitude modulation into account

Note that the amplitude modulation is taken into account by the extended nonlinearity of the loop. This nonlinearity enters the loop's equation as

$$\underset{A_M}{Q}\,(A_M(\tilde{A}_i g(x_i) + \tilde{N}_i)).$$

The maximal amplitude due to modulation is A_M whereas

$$\tilde{A}_i = A_i / A_M, \quad i \in Z_+$$

stands for the instantenous amplitude of the incoming waveform. That is why the constraints on loop's nonlinearity are additionally affected by variable $\tilde{A}_i$, especially by minimal value of it. Maximal $\tilde{A}_i$ is equal 1. See fig. 6 for illustration and the appendices for the details.

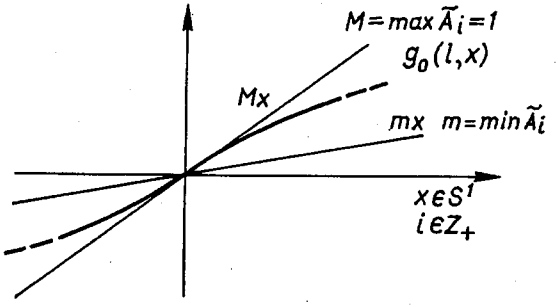

Fig. 6. The modulation AM effect on the nonlinearity constraints — the modulation index less than 1

FINAL REMARKS

The extension of approach of Part I while the stability of the nonuniform sampling DPLL-s is of concern has been presented. The existence of perturbed N:1 phase entrainment in the case of AM amplitude modulation and PM phase modulation has been well established. The estimates concerning the phenomenon of phase entrainment have been provided. The results obtained may be of assistance on designing stage. The exact study of the considered problem forces one to deal with coupled nonlinear discrete-time equation of high enought degree of complexity. That is why the use of computer while looking for very detailed results is advised. The Markov theory based approach can be used in particular cases to obtain analitical results of practical value. The functional nonlinear discrete-time equation on the S^1 circle manifold has been used to describe the phase error process in the loop of any order.

REFERENCES

1. W. C. Lindsey, C. M. Chie: *A survey of digital phase-locked loops.* Proc. IEEE vol. 69, no 4, April 1981, pp. 410–431
2. M. Żółtowski: *New stability criteria for the digital nonuniform sampling zero-crossing phase-locked loops of any order. Part I, this issue*
3. G. S. Gill, S. C. Gupta: *First-Order Discrete Phase-locked Loop with applications to demodulation of angle modulated carrier,* IEEE Ttans. Commun. vol. COM–70, June 1972, pp. 454–462
4. A. V. Oppenheim, R. W. Schafer: *Cyfrowe przetwarzanie sygnałów,* Warszawa, WKŁ: 1979, (polish translation from english)

APPENDIX 1

THE MODEL OF DIGITAL ZERO-CROSSING NONUNIFORM SAMPLING PHASE-LOCKED LOOP (DPLL)

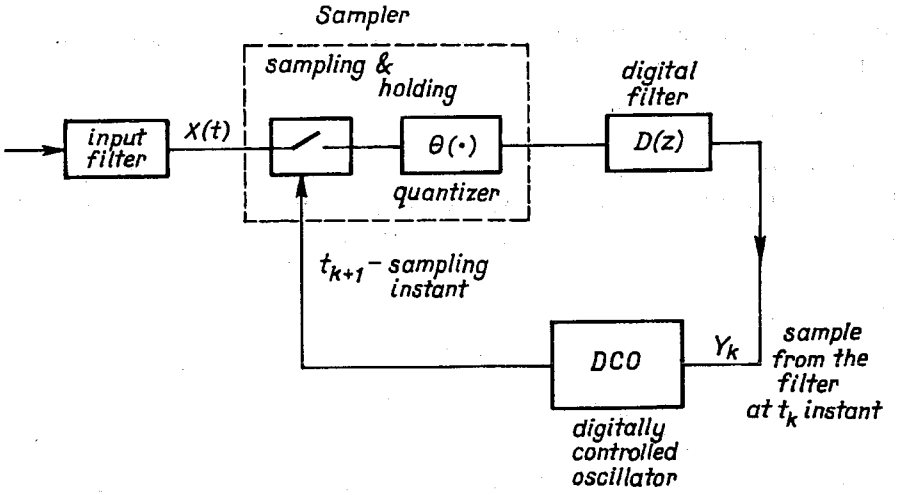

Fig. A1–1. The model of the nonuniform sampling digital phase-locked loop (DPLL)

While following the derivation of Part I one arrives at couple of equations

$$\varphi_{k+1} = \varphi_k + \theta_{ok+1} - \theta_{ok} - (\omega_0 + \Omega_0) \sum_{i=0}^{k} d_{k-1} Q(A_i g(\varphi_i) + N_i) + \Omega_0 T \tag{A1–1a}$$

$$t_{k+1} = t_k + T - \sum_{i=0}^{k} d_{k-1} Q(A_i g(\varphi_i) + N_i). \tag{A1–1b}$$

The notation introduced is the same as one of Part I.
Let

$$\omega \triangleq \omega_0 + \Omega_0 \quad \text{and} \quad \tilde{A}_i \triangleq A_i / A_M, \quad i \in Z_+$$

whereas $A_M > 0$ is the maximal value of variable amplitude A(t) in this case. Then (A1 – 1a) is now

$$\varphi_{k+1} = \varphi_k + \theta_{ok+1} - \theta_{ok} - \omega A_M \sum_{i=0}^{k} d_{k-1} \underline{Q}\,(A_M(\tilde{A}_i g(\varphi_i) + N_i)) + \Omega_0 T \tag{A1–2}$$

and

$$\tilde{N}_i = N_i / A_M, \quad i \in Z_+ .$$

Last equation after $\mathscr{Z}$ – Laurent transformation is

$$z\Phi(z) - z\varphi_0 = \Phi(z) + z\theta_0(z) - z\theta_0 - \theta_0(z) + \Omega_0 T/(1 - z^{-1}) + - A_M D(z)\mathscr{Z}\left\{\underline{Q}\left(A_M(\tilde{A}_i g(\varphi_i) + N_i)\right)\right\}. \tag{A1–3}$$

This equation is the basic one for further considerations. The particular cases are derived from it. Moreover

$$\Phi(z) = \mathscr{Z}\{\varphi_i\}; \quad \theta_0(z) = \mathscr{Z}\{\theta_{0i}\}; \quad D(z) = \mathscr{Z}\{d_i\}, \quad i \in Z_+ .$$

The initial conditions of the loop's filter are all assumed zero. Non-zero initial conditions are due to certain modulation and this way can be additionally introduced if necessary.

APPENDIX 2

THE EQUATION OF THE FIRST-ORDER DPLL

From (A1 – 3) (appendix 1) while $D(z) = G_1$; $\omega A_M G_1 = K_1$; $\Omega_0 T = \Lambda$ (A2–1) one obtains

$$\varphi_{k+1} = \varphi_k + \theta_{ok+1} - \theta_{ok} - K_1 \underline{Q}\left(A_M(\tilde{A}_k g(\varphi_k) + N_k)\right) + \Lambda =$$

$$= \varphi_k - K_1 g(\varphi_s) + \Lambda + \theta_{ok+1} - \theta_{ok} +$$

$$- K_1\left(\frac{Q}{A_M}(A_M(\tilde{A}_k g(\varphi_k) + \tilde{N}_k)) - g(\varphi_s)\right). \tag{A2–2}$$

Let $\varphi_s \overset{\text{df}}{=} g^{-1}(\Lambda/K_1)$ is well established. The change of variables introduced next is in order to consider the phase error process around 0 phase point. It is accomplished by

$$\varphi_k = \tilde{\varphi}_k + \varphi_s, \quad k \in Z_+ . \tag{A2–3}$$

The change of variables results in

$$\tilde{\varphi}_{k+1} = \tilde{\varphi}_k - K_1\left(\frac{Q}{A_M}(A_M(\tilde{A}_k \cdot g(\varphi_k + \varphi_s) + \tilde{N}_k)) - g(\varphi_s)\right) + \\ + \theta_{ok+1} - \theta_{ok} \tag{A2–4}$$

Now let $x_k = \varphi_k$, $k \in Z_+$

$$Q(g_0(k, \tilde{\varphi}_k)) \stackrel{\text{df}}{=} \frac{Q}{A_M}\left(A_M \tilde{A}_k g(\tilde{\varphi}_k + \varphi_s)\right) - g(\varphi_s) \tag{A2–5a}$$

and

$$\tilde{N}_0(k, \tilde{\varphi}_k) = \frac{Q}{A_M}\left((A_k g(\tilde{\varphi}_k + \varphi_s) + \tilde{N}_k)\right) - \frac{Q}{A_M}\left(A_M \tilde{A}_k g(\tilde{\varphi}_k + \varphi_s)\right). \tag{A2–5b}$$

Last substitutions results in new form of the equation (A2–4):

$$x_{k+1} = x_k - K_1 Q(g_0(k, x_k)) + \theta_{ok+1} - \theta_{ok} - K_1 \tilde{N}_0(k, x_k). \tag{A2–6}$$

The next transformations are in order to derive the equivalent form of (A2–6) in terms of functional equation. First, $\mathscr{Z}$ – Laurent transform of (A2–6) is

$$zX(z) - zx_0 = X(z) - K_1 \mathscr{Z}\{Q(g_0(k, x_k) - \lambda x_k\} - K_1 \lambda X(z) + \\ - \theta(z) + z\theta_0(z) - \theta_0 z - K_1 \mathscr{Z}\{\tilde{N}_0(k, x_k)\} \tag{A2–7}$$
$$\lambda \in R_+ \quad (R_+ \text{ is the set of nonnegative reals}).$$

Secondly let

$$K_{\lambda,1}(z) = -\frac{K_1}{z - (1 - K_1\lambda)} = \mathscr{Z}\{k_{\lambda,1}(l)\} \tag{A2–8a}$$

$$X_\lambda(z) = \frac{z(x_0 - \theta_0)}{z - (1 - K_1\lambda)} = \mathscr{Z}\{x_\lambda(l)\} \tag{A2–8b}$$

$$K_{m,\lambda}(z) = \frac{z - 1}{z - (1 - K_1\lambda)} = \mathscr{Z}\{k_{m,\lambda}(l)\}. \tag{A2–8c}$$

Then (A2–7) is equivalent to

$$X(z) = K_{\lambda,1}(z)\mathscr{Z}\{Q(g_0(k, x_k)) - \lambda x_k\} + K_{m,\lambda}(z)\theta_0(z) + \\ + K_{\lambda,1}(z)\mathscr{Z}\{\tilde{N}_0(k, x_k)\} + X_\lambda(z), \quad k \in Z_+. \tag{A2–9}$$

On the other hand the last equation after inverse $\mathscr{Z}$ – transformation is

$$x(k) = \sum_{l=0}^{k-1} k_{\lambda,1}(k - l)(Q(g_0(l, x_l)) - \lambda x(l)) + \sum_{l=0}^{k} k_{m,\lambda}(k - l)\theta_0(l) + \\ + \sum_{l=0}^{k-1} k_{\lambda,1}(k - l)z(l, x(l)) + x_\lambda(k), \quad k \in Z_+. \tag{A2–10}$$

Last equation is the required one of convolutional form. Moreover

$$x_l = x(l), \quad \theta_0(1) = \theta_{ol}(l), \quad \tilde{N}_0(l, x_l) = z(l, x(l)). \tag{A2–11}$$

APPENDIX 3

THE EQUATION OF SECOND-ORDER DPLL

1) $D(z) = G_1 + \dfrac{G_2}{1 - z^{-1}}$ while adding and proportional filter is of concern

(A3–1)

From (A1–3) one obtains

$$z\Phi(z) - z\varphi_0 = \Phi(z) + z\theta_0(z) - Q_0(z) + \theta_0(z) + \frac{\Omega_0 T}{1 - z^{-1}} + \\ - A_M\left(G_1 + \frac{z G_2}{z - 1}\right)\mathscr{Z}\left\{\frac{Q}{A_M}(A_M(\tilde{A}_i g(\varphi_i) + \tilde{N}_i))\right\}. \quad \text{(A3–2)}$$

First, let

$$Q(g_0(i, \varphi_i)) \stackrel{\text{df}}{=} \frac{Q}{A_M}(A_M \tilde{A}_i(\varphi_i)) \quad \text{(A3–3a)}$$

and

$$\tilde{N}_0(i, \varphi_i) = \frac{Q}{A_M}\left(A_M(\tilde{A}_i g(\varphi_i) + \tilde{N}_i)\right) - \frac{Q}{A_M}\left(A_M \tilde{A}_i g(\varphi_i)\right), \quad \text{(A3–3b)}$$

while

$$\Omega_0 T = \Lambda \quad \text{(A3–3c)}$$
$$K_1 = \omega A_M G_1 \quad \text{(A3–3d)}$$
$$K_2 = \omega A_M G_2 \quad \text{(A3–3e)}$$
$$r_l = 1 + K_2/K_1. \quad \text{(A3–3f)}$$

Secondly, let also

$$X_\lambda(z) = \frac{(z - 1)z(\varphi_0 - \theta_0) + z\Lambda}{z^2 - (2 - K_1 r_l \lambda)z + 1 - K_1 \lambda} = \mathscr{Z}\{x_\lambda(k)\}, \quad \text{(A3–4a)}$$

$$K_{\lambda,l}(z) = \frac{K_1 - z K_1 r_l}{z^2 - (2 - K_1 r_l \lambda)z + 1 - K_1 \lambda} = \mathscr{Z}\{k_{\lambda,l}(k)\}, \quad \text{(A3–4b)}$$

$$K_{m,\lambda}(z) = \frac{z^2 - 2z + 1}{z^2 - (2 - K_1 r_l \lambda)z + 1 - K_1 \lambda} = \mathscr{Z}\{k_{m,\lambda}(k)\} \quad \text{(A3–4c)}$$

and

$$\varphi_i = x_i = x(i), \quad i \in Z_+. \quad \text{(A3–4d)}$$

While using the notation just introduced the equation (A3–2) is equivalent to

$$X(z) = K_{\lambda,l}(z)\mathscr{Z}\{Q(g_0(l, x(l))) - \lambda x(l)\} + K_{m,\lambda}(z)\theta_0(z) + \\ + K_{\lambda,l}(z))\mathscr{Z}\{\tilde{N}_0(l, x(l))\} + X_\lambda(z). \quad \text{(A3–5)}$$

By inverse $\mathscr{Z}$ transformation (A3 – 5) can be transformed to

$$x(k) = \sum_{l=0}^{k-1} k_{\lambda,1}(k-l)\,Q(g_0(l, x(l)) - \lambda x(l)) + \sum_{l=0}^{k} k_{m,\lambda}(k-l)\,\theta(l) + \\ + \sum_{l=0}^{k-1} k_{\lambda,1}(k-l)\,z(l, x(l)) + x_\lambda(k), \quad k \in Z_+ \tag{A3-6}$$

while

$$z(l, x(l)) = \tilde{N}_0(l, x(l)). \tag{A3-7}$$

The last equation is the required one of convolutional form.

$$2)\ D(z) = G_1 + \frac{G_2 z}{z - \beta}, \quad 0 < \beta < 1.$$

The filter of the second-order DPLL with nonperfect adder.
From (A1 – 2) one gets

$$z\Phi(z) - z\varphi_0 = \Phi(z) + z\theta_0(z) - z\theta_0 - \theta_0(z) + \\ - \omega A_M\left(G_1 + \frac{G_2 z}{z-\beta}\right)\mathscr{Z}\left\{\frac{Q}{A_M}(A_M(\tilde{A}_i g(\varphi_i) + \tilde{N}_i))\right\} + \\ + \Omega_0 T/(1 - z^{-1}). \tag{A3-8}$$

Now let

$$\varphi_s = g^{-1}\left(\frac{\Delta(\beta - 1)}{(\beta - r_l)K_1}\right) \tag{A3-9}$$

be well established while

$$\Delta = \Omega_0 T \tag{A3-10a}$$
$$\omega A_M \cdot G_1 = K_1 \tag{A3-10b}$$
$$\omega A_M \cdot G_2 = K_2 \tag{A3-10c}$$
$$r_l = 1 + K_2/K_1. \tag{A3-10d}$$

Then like in the first-order DPLL case the phase error process can be transformed according to

$$\varphi_k = \tilde{\varphi}_k + \varphi_s \tag{A3-11a}$$

or

$$\Phi(z) = \tilde{\Phi}(z) + \varphi_s z/(z-1) \tag{A3-11b}$$
$$k \in Z_+, \quad \Phi(z) = \mathscr{Z}\{\varphi_i\}, \quad \tilde{\Phi}(z) = \mathscr{Z}\{\tilde{\varphi}_i\}.$$

This transformation while applied to (A3 – 8) results in

$$(z-1)(z-\beta)\tilde{\Phi}(z) = z(z-\beta)(\tilde{\varphi}_0 - \theta_{00}) + (z-1)(z-\beta)\theta_0(z) + (K_1\beta - K_1 r_l z).$$

$$\mathscr{Z}\{Q(g_0(i, \tilde{\varphi}_i))\} + (K_1\beta - K_1 r_l z)\mathscr{Z}\{N_0(i, \tilde{\varphi}_i)\} + \frac{\Delta z\beta(1 - r_l)}{\beta - r_l}. \tag{A3-12}$$

Whereas

$$Q(g_0(i, \tilde{\varphi}_i)) = \frac{Q}{A_M}\left(A_M \tilde{A}_i g(\tilde{\varphi}_i + \varphi_s)\right) - g(\varphi_s) \tag{A3-13a}$$

and

$$\tilde{N}_0(i, \tilde{\varphi}_i) = \frac{Q}{A_M}\left(A_M(\tilde{A}_i g(\varphi_i + \varphi_s) + \tilde{N}_i)\right) - \frac{Q}{A_M}\left(A_M \tilde{A}_i g(\tilde{\varphi}_i + \varphi_s)\right). \tag{A3-13b}$$

Let next

$$\tilde{\Phi}(z) = X(z), \tilde{\varphi}_k = x(k), X(z) = \mathscr{Z}\{x_k\}, \tilde{\Phi}(z) = \mathscr{Z}\{\tilde{\varphi}_k\}, \tilde{N}_0(k, \tilde{\varphi}_k) = z(k, x(k)). \tag{A3-14a}$$

$k \in Z_+$.

In view of (A3-14a) the equation (A3-12) is equivalent to

$$X(z) = K_{\lambda,1}(z)\mathscr{Z}\{Q(g_0(l, x(l)) - \lambda x(l)\} + X_\lambda(z) + K_{m,\lambda}(z)\theta_0(z) + \\ + K_{\lambda,1}(z)\mathscr{Z}\{z(l, x(l))\}, \quad \lambda \in R_+ \tag{A3-14b}$$

while

$$X_\lambda(z) = \mathscr{Z}\{x_\lambda(k)\} = \frac{z(z - \beta)(\tilde{\varphi}_0 - \theta_{00}) + z\tilde{\Delta}}{z^2 - z(\beta + 1 - \lambda K_1 r_l) + \beta(1 - K_1\lambda)} \tag{A3-15a}$$

$$\tilde{\Delta} \underline{\text{df}} \frac{\Delta\beta(1 - r_l)}{\beta - r_l}$$

$$K_{m,\lambda}(z) = \mathscr{Z}\{k_{m,\lambda}(k)\} = \frac{z^2 - z(\beta + 1) + \beta}{z^2 - z(\beta + 1 - \lambda K_1 r_l) + \beta(1 - \lambda K_1)} \tag{A3-15b}$$

$$K_{\lambda,1}(z) = \mathscr{Z}\{k_{\lambda,1}(k)\} = \frac{K_1(\beta - r_l z)}{z^2 - z(\beta + 1 - \lambda K_1 r_l) + \beta(1 - K_1\lambda)}. \tag{A3-15c}$$

The equation (A3-14b) after the inverse $\mathscr{Z}$ transformation is

$$x(k) = \sum_{l=0}^{k-1} k_{\lambda,1}(k - l)(Q(g_0(l, x(l)) - \lambda x(l)) + x_\lambda(k) + \\ + \sum_{l=0}^{k} k_{m,\lambda}(k - l)\theta_0(l) + \sum_{l=0}^{k-1} k_{\lambda,1}(k - l)z(l, x(l)). \tag{A3-16}$$

This equation is the required one of convolutional form.

APPENDIX 4

THE EQUATION OF THIRD-ORDER DPLL

In this case

$$D(z) = G_1 + \frac{G_2}{1 - z^{-1}} + \frac{G_3}{(1 - z^{-1})^2}. \tag{A4-1}$$

Moreover in view of (A1–3) the equation of the loop is

$$z\Phi(z) - z\varphi_0 = \Phi(z) + z\theta_0(z) - z\theta_0 - \theta_0(z) + \\ - \left(K_1 + \frac{zK_2}{z-1} + \frac{z^2 K_3}{(z-1)^2}\right) \mathscr{Z}\left\{\frac{Q}{A_M}(A_M(\tilde{A}_i g(\varphi_i) + \tilde{N}_i))\right\} + \\ + \frac{\Lambda}{1 - z^{-1}}. \tag{A4-2}$$

Let as before

$$N_0(i, \varphi_i) \overset{\text{df}}{=} \frac{Q}{A_M}\left(A_M(\tilde{A}_i g(\varphi_i) + \tilde{N}_i)\right) - \frac{Q}{A_M}\left(A_M A_i g(\varphi_i)\right) \tag{A4-3a}$$

and

$$Q(g_0(i, \varphi_i)) \overset{\text{df}}{=} \frac{Q}{A_M}\left(A_M \tilde{A}_i g(\varphi_i)\right), \quad i \in Z_+. \tag{A4-3b}$$

Also

$$K_1 = \omega A_M G_1 : K_2 = \omega A_M G_2 : K_3 = \omega A_M G_3 : \Lambda = \Omega_0 T : \\ r_l = 1 + K_2/K_1 : p = 1 + K_2/K_1 + K_3/K_1 \tag{A4-3c}$$

Then (A4–2) is equivalent to

$$(z^3 + z^2(3 - pK_1\lambda) + z(3 - K_1(1 + r_l)\lambda) + K_1\lambda - 1)\Phi(z) = \\ = z(\varphi_0 - \theta_0)(z-1)^2 + \Lambda z(z-1) + (z-1)^3\theta_0(z) + \\ + (K_1(1 + r_l)z - K_1 p z^2 - K_1)\mathscr{Z}\{Q(g_0(i, \varphi_i) - \lambda\varphi_i\} + \\ + (K_1(1 + r_l)z - K_1 p z^2 - K_1)\mathscr{Z}\{N_0(i, \varphi_i)\}. \tag{A4-4}$$

Let the following notation be introduced

$$x(i) = \varphi_i : X(z) = \Phi(z) \tag{A4-5a}$$

$$N_0(i, \varphi_i) = z(i, x(i)), \quad i \in Z_+ \tag{A4-5b}$$

$$X_\lambda(z) = \mathscr{Z}\{x_\lambda(k)\} = \frac{z(\varphi_0 - \theta_0)(z-1)^2 + \Lambda z(z-1)}{z^3 - z^2(3 - pK_1\lambda) + z(3 - K_1(1 + r_l)\lambda) + K_1\lambda - 1} \tag{A4-6a}$$

$$K_{\lambda,1}(z) = \frac{K_1(1 + r_l)z - K_1 p z^2 - K_1}{z^3 - z^2(3 - pK_1\lambda) + z(3 - K_1(1 + r_l)\lambda) + K_1\lambda - 1} \tag{A4-6b}$$

$$K_{m,\lambda}(z) = \frac{(z-1)^3}{z^3 - z^2(3 - pK_1\lambda) + z(3 - K_1(1 + r_l)\lambda) + K_1\lambda - 1} \tag{A4-6c}$$

While using this notation the equation (A4—4) is equivalent to

$$X(z) = K_{\lambda,1}(z)\mathscr{Z}\{Q(g_0(i, x(i)) - \lambda x(i)\} + K_{m,\lambda}(z)\theta_0(z) + K_{\lambda,1}(z)\mathscr{Z}\{z(i, x(i)\} \tag{A4-7}$$

The required equation of convolutional form can be obtained from last one by inverse $\mathscr{Z}$ — Laurent transformation

$$x(k) = x_\lambda(k) + \sum_{l=0}^{k-1} k_{\lambda,1}(k-l)(Q(g_0(l, x(l))) - \lambda x(l)) + \sum_{l=0}^{k-1} k_{\lambda,1}(k-l)z(l, x(l)) + , k \in Z_+ + \sum_{l=0}^{k} k_{m,\lambda}(k-l)\theta(l). \tag{A4-8}$$

M. ŻÓŁTOWSKI

NOWE KRYTERIA STABILNOŚCI DLA CYFROWYCH PĘTLI Z NIEJEDNOSTAJNYM PRÓBKOWANIEM DOWOLNEGO RZĘDU ŚLEDZĄCYCH PRZEJŚCIA PRZEZ POZIOM ZEROWY. CZĘŚĆ II

Streszczenie

Odkryto nowe kryteria stabilności dla cyfrowych pętli fazowych z niejednostajnym próbkowaniem śledzących przejścia przez poziom zerowy w przypadku zaburzonego synchronizmu N:1. Rozważania z części I rozszerzono by uwzględnić zaniki przebiegu wejściowego i modulacje AM i PM. Do opisu przebiegu błędu fazy w pętli dowolnego rzędu użyto nieliniowe funkcjonalne równanie na rozmaitości S^1 — okręgu.

KWARTALNIK ELEKTRONIKI I TELEKOMUNIKACJI, 1991, 37, Z. 3–4, ss. 593–632

621.317.08

New stability criteria for the nonuniform sampling zero-crossing digital phase-locked loops of any order

MARIUSZ ŻÓŁTOWSKI

Instytut Telekomunikacji, Politechnika Gdańska

Recived 1990.04.25

Authorized 1990.11.27

Part III

This paper is the third part of the approach in which new stability criteria for the nonuniform sampling digital phase-locked loops (DPLL-s) are of concern. The dynamics of the loop is modelled by the discrete-time functional equation on S^1 – circle manifold. It is shown how the unified approach of the previous parts can be extended to consider the case of DPLL-s with variable parameters in different situations of practical interest. Namely, the DPLL for Doppler rate tracking and DPLL with variable filter for improved acquisition in noise presence are considered.

1. INTRODUCTION

While the flexibility of the digital circuitry is put into good account the different controlling algorithms including adaptive ones can be introduced also in the digital phase-locked loop case. This is in order to assure the acquisition of phase-lock more reliable, more accurate and fast. The approach of parts I and II is extended in this paper to consider two cases of variable parameter DPLL-s which are interesting from the practical point of view. First one is the case considered previously by Chie [8]. It occurs while the frequency ramp signal is introduced to the loop's input. The second one is the case of speeding up the acquisition while the presence of noise is important and can not be neglected. This last case while considered by Rocha [9] first was studied in [4] in more details. These both cases can be considered within the model in terms of discrete-time functional equation on S^1 – circle manifold. The philosophy is to give the theoretical insight into different effects in DPLL-s first. Then the detailed analysis and anticipations can be accomplished by computer based modelling. As mentioned before it is intended to consider the special cases of adaptation in the digital phase-locked loop only. Further research concerning this area is in progress. Digital phase-locked loop is a nonlinear device. Its dynamics can be complicated even while

simplified models are used. That is why the dynamics of the loop of first-order with constant parameters is considered first. This is to give the answer to what can happen in this simplest nevertheless important case. This knowledge may be useful to recognize the different forms of dynamics in order to control the acquisition of phase-lock.

2. THE MODEL OF THE DIGITAL PHASE-LOCKED LOOP (DPLL)

The model of the loop is derived in appendix 1. $X(t)$ stands for the incoming waveform being tracked while Q represents quantization effects due to analog to digital conversion. A stands for amplitude, g describes the shape of the waveform to the loop's input, ω_0 stands for radian frequency and $N(t)$ for disturbing noise. The discrete time waveform Y_k $k = 0,1,..$ from the filter output controls the local oscillator of the

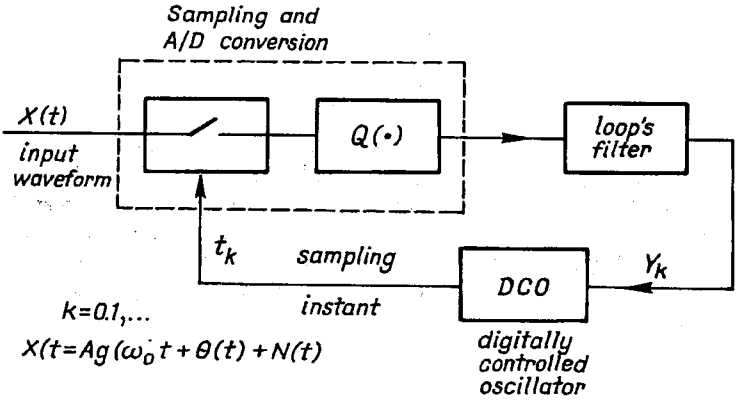

Fig. 1. The model of the nonuniform sampling DPLL

loop in order to gain phase entrainment with the incoming waveform. Information about deviation from the state of phase entrainment is provided by the phase detector of the loop which is the sampling device in this case. The model of the nonuniform sampling DPLL of any order is given in respect to $\mathcal{N}:\mathcal{M}$ phase entrainment in Appendix 1, while the baseband model of the loop is shown in fig. 2. See appendix 1 for the required details. However $\theta(t)$ is the phase modulation of the signal component of $X(t)$, t_k stands for sampling instant at k discrete moment, $k = 0,1,\ldots$, $\theta_k = \theta(t_k)$, $N_k = N(t_k)$, φ_k is the phase error process, $D(z)$ is z – domain transfer function of the loop's filter while the parameters of the filter are constant, $\mathcal{Z}$ and $\mathcal{Z}^{-1}$ stand for the direct and inverse $\mathcal{Z}$ – Laurent transformations. The time domain equations of the loop of fig. 2 are (see Appendix 1)

$$\varphi_{k+1} = \varphi_k + \theta_{k+1} - \theta_k - \omega_0 \sum_{i=0}^{k} Q(A\,g(\varphi_i) + N_i)\, d_{k-i} + \\ + \left(2\pi \frac{\mathcal{N}}{\mathcal{M}}\right) \bmod 2\pi, \tag{1a}$$

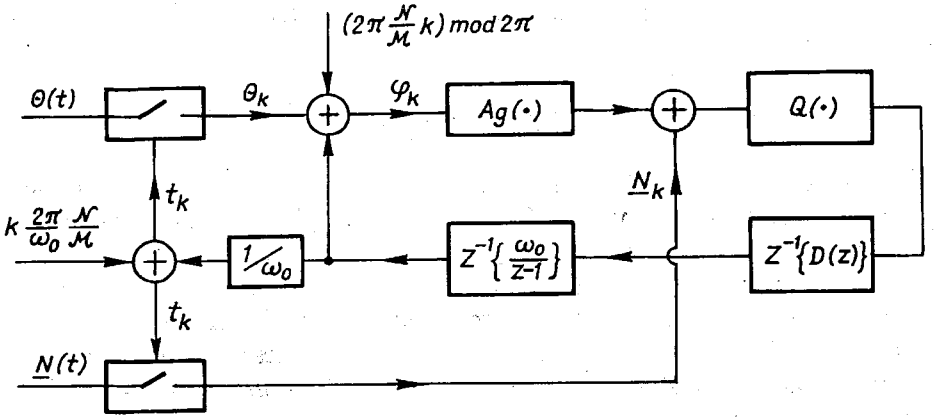

Fig. 2. The baseband model of the nonuniform sampling DPLL with respect to $\mathcal{N}:\mathcal{M}$ phase entrainment

$$t_{k+1} = t_k + \frac{2\pi\mathcal{N}}{\omega_0\mathcal{M}} - \sum_{i=0}^{k} Q(Ag(\varphi_i) + N_i)\, d_{k-i}. \tag{1b}$$

$\{d_k\} = \mathcal{Z}^{-1}\{D(z)\}$ is the discrete time pulse response of the loop's filter, $k=0,1,\ldots$. The $\mathcal{N}:\mathcal{M}$ phase entrainment in the loop depends on the properties of the phase error process which changes according to (1a). The phase error describes the deviation from zero-crossing of the incoming waveform. On the other hand the sequence of sampling instants is given by (1b). These equations are both coupled. However they can be decoupled in some cases. Just such a case will be considered next.

3. THE DYNAMICS OF THE LOOP OF FIRST-ORDER

The simplified model of the DPLL of first-order is derived in Appendix 2 in details and is given in terms of the following equation

$$\varphi_{k+1} = \varphi_k - K_1 g(\varphi_k) + \Lambda + \left(2\pi\frac{\mathcal{N}}{\mathcal{M}}\right) \bmod 2\pi. \tag{2}$$

Moreover

$$K_1 = \omega GA > 0,\ \Lambda = 2\pi\frac{\Omega_0\mathcal{N}}{\omega_0\mathcal{M}},\ \omega = \omega_0 + \Omega_0,\ {}^{a}\bmod 2 = \arg e^{ja} \in <-\pi, \pi>$$

The equation (2) is valid while the quantization effects are negligible, no disturbing noise is present, the incoming waveform is detuned in frequency Ω_0 and phase θ_0 from the reference: $\theta(t) = \Omega_0 t + \theta_0$, and $D(z)$ of the loop's filter is $D(z) = G$. This model while referred to $\mathcal{N}:\mathcal{M}$ phase entrainment disturbed in frequency only posesses all properties concerning the homeomorphism of the circle (being stated in Appendix 3 and

Appendix 4). The problem of $\mathcal{N}$:1 phase entrainment was in [4,6,7] of concern in details Suppose the mapping

$$h(\varphi) \stackrel{\text{df}}{=} \varphi - K_1 g(\varphi) + \Delta + \left(2\pi \frac{\mathcal{N}}{\mathcal{M}}\right) \bmod 2\pi \tag{3}$$

has a stable periodic point of period $\mathcal{M}$ in S^1 circle space. Then there is stable time aligment between the incoming waveform and the sampling one (see appendix 2). If $\Delta \neq 0$ then the perturbed in frequency $\mathcal{N}$:$\mathcal{M}$ phase entrainment may occur while Δ equals zero in unperturbed case. The regions on the (K_1, Δ) plane of perturbed in frequency $\mathcal{N}$:$\mathcal{M}$ phase entrainment existence are called the frequency acquisition regions of the DPLL. These regions are the subsets of the ones associated with periodic points either stable or unstable (fixed point is a periodic point of period 1). Some of these latter regions are plotted in fig. 3–8 for different $\mathcal{N}$,$\mathcal{M}$, K_1, Δ [rad] while $g(\varphi) = \sin\varphi$. The shaded regions being the subsets of the frequency acquisition regions

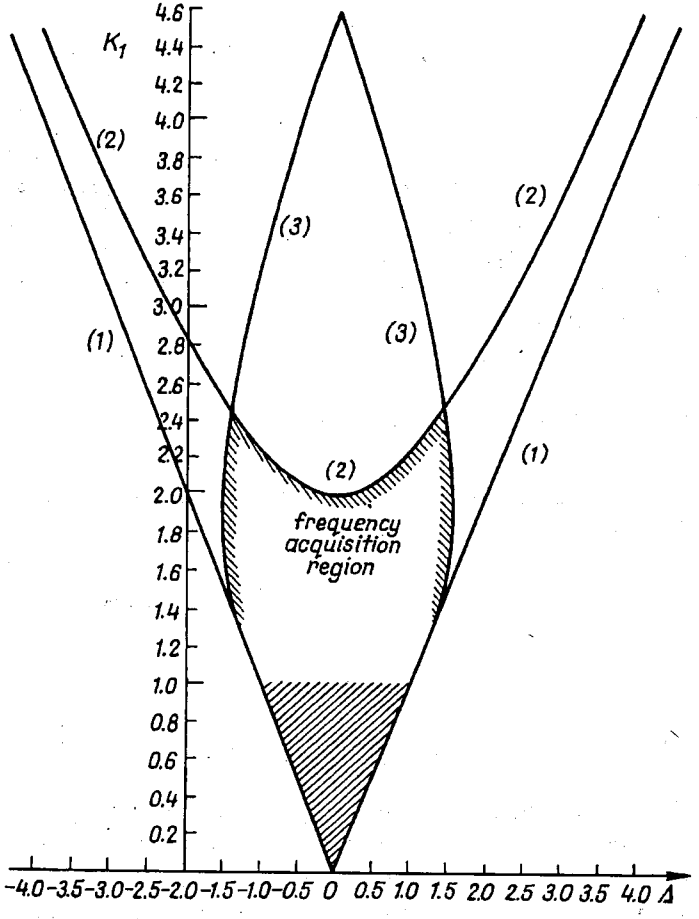

Fig. 3. The frequency acquisition region of the DPLL of first-order, $g(\varphi) = \sin\varphi$, $(\mathcal{N}/\mathcal{M}) \bmod 2\pi = 0$

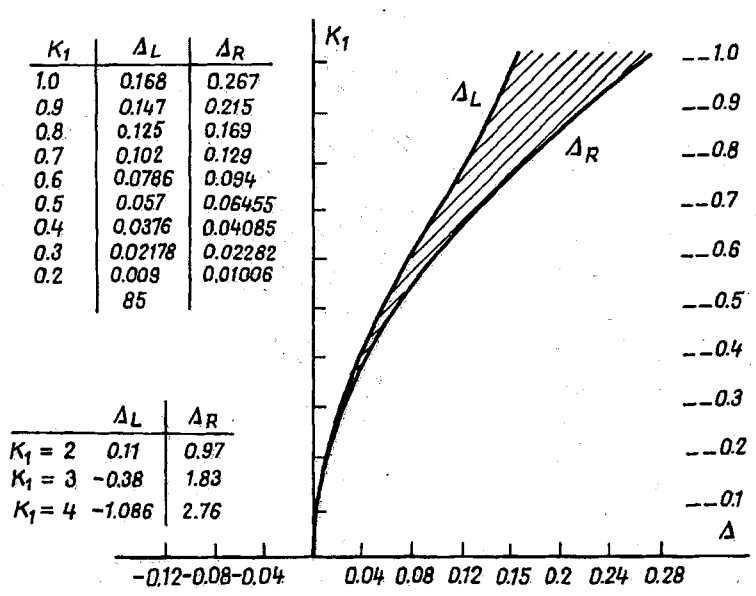

Fig. 4. The frequency region of periodic point $(\mathcal{N}|\mathcal{M})$ mod $2\pi = 1/4$ of first-order DPLL, $g(\varphi)=\sin\varphi$

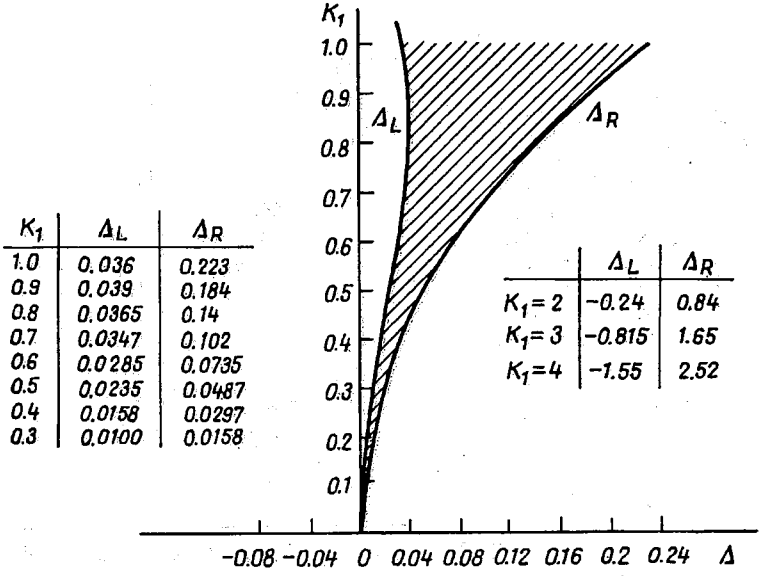

Fig. 5. The frequency region of periodic point $(\mathcal{N}|\mathcal{M})$ mod $2\pi = 1/3$ of first-order DPLL, $g(\varphi)=\sin\varphi$

correspond to homeomorphic mapping of S^1 onto S^1. All particular figures are collected in fig. 9 and are universal in view of the observations of appendix 2. The bottom parts of the shaded regions corresponding to the small values of parameter K_1 have been known as Arnold tongues [10]. The perturbed $\mathcal{N}:\mathcal{M}$ phase entrainment surely occurs for the values of K_1 less than 1 while (K_1, Λ) belongs to the frequency

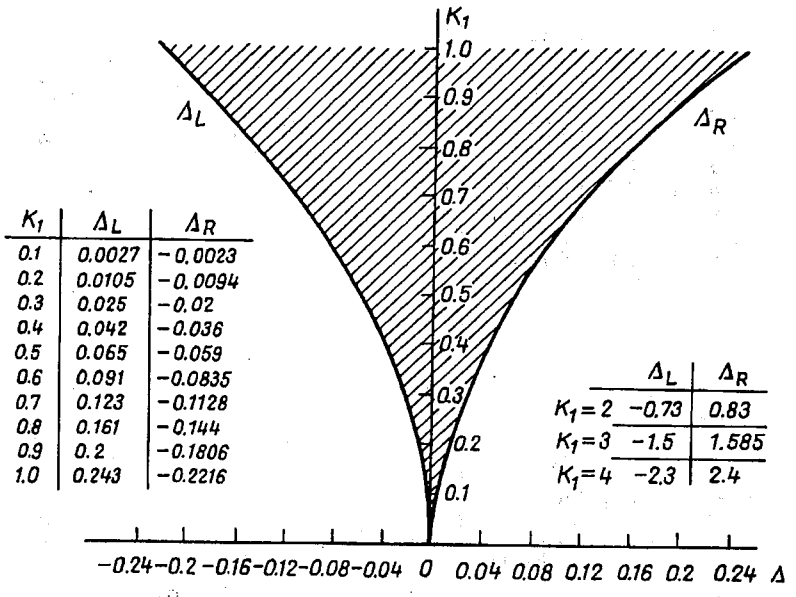

K_1	Δ_L	Δ_R
0.1	0.0027	−0.0023
0.2	0.0105	−0.0094
0.3	0.025	−0.02
0.4	0.042	−0.036
0.5	0.065	−0.059
0.6	0.091	−0.0835
0.7	0.123	−0.1128
0.8	0.161	−0.144
0.9	0.2	−0.1806
1.0	0.243	−0.2216

	Δ_L	Δ_R
$K_1=2$	−0.73	0.83
$K_1=3$	−1.5	1.585
$K_1=4$	−2.3	2.4

Fig. 6. The frequency region of periodic point $(\mathcal{N}/\mathcal{M})$ mod $2\pi = 1/2$ of first-order DPLL, $g(\varphi)=\sin\varphi$

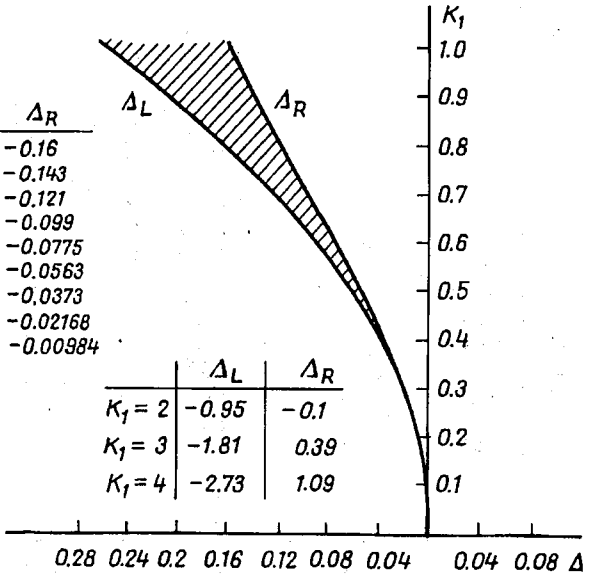

K_1	Δ_L	Δ_R
1.0	−0.26	−0.16
0.9	−0.21	−0.143
0.8	−0.165	−0.121
0.7	−0.126	−0.099
0.6	−0.08	−0.0775
0.5	−0.0639	−0.0563
0.4	−0.0405	−0.0373
0.3	−0.02263	−0.02168
0.2	−0.01003	−0.00984

	Δ_L	Δ_R
$K_1=2$	−0.95	−0.1
$K_1=3$	−1.81	0.39
$K_1=4$	−2.73	1.09

Fig. 7. The frequency region of periodic point $(\mathcal{N}/\mathcal{M})$ mod $2\pi = 3/4$ of first-order DPLL, $g(\varphi)=\sin\varphi$

region of periodic point of $\mathcal{M}$ period and $(\mathcal{N}/\mathcal{M})$ mod 2π type. Moreover, in view of homeomorphic properties of the mapping h of (2) being described in Appendix 3, the $\mathcal{N}$:$\mathcal{M}$ perturbed phase entrainment occurs regardless of the initial phase error condition. However the detailed frequency acquisition region while the perturbed in frequency phase entrainment (occurs regardless of the initial condition is given in fig. 3 in $\mathcal{N}$:1 phase entrainment case ($\mathcal{N}$:$\mathcal{M}$) strictly while ($\mathcal{N}$:$\mathcal{M}$) mod $2\pi=0$).

K_1	Δ_L	Δ_R
1.0	−0.205	−0.014
0.9	−0.165	−0.024
0.8	−0.128	−0.026
0.7	−0.097	−0.0271
0.6	−0.0678	−0.0245
0.5	−0.0468	−0.0203
0.4	−0.0288	−0.015
0.3	−0.0155	−0.0097
0.2	−0.0065	−0.00476

	Δ_L	Δ_R
$K_1 = 2$	−0.81	0.27
$K_1 = 3$	−1.61	0.85
$K_1 = 4$	−2.5	1.58

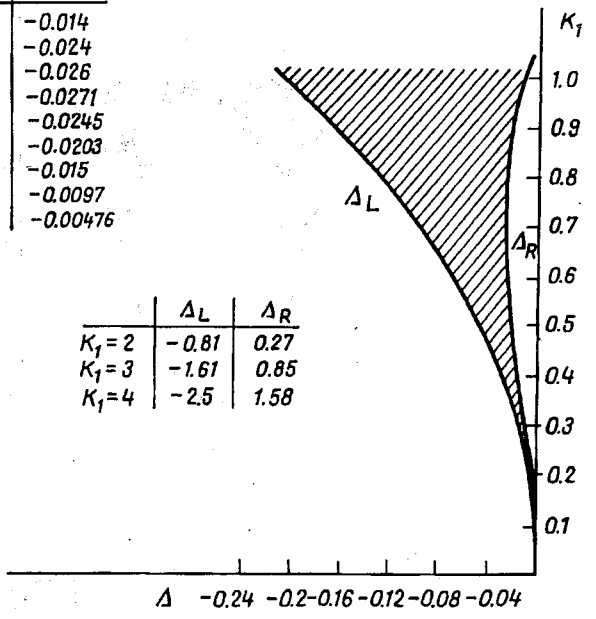

Fig. 8. The frequency region of periodic point ($\mathcal{N}/\mathcal{M}$) mod $2\pi = 2/3$ of first-order DPLL, $g(\varphi)=\sin\varphi$

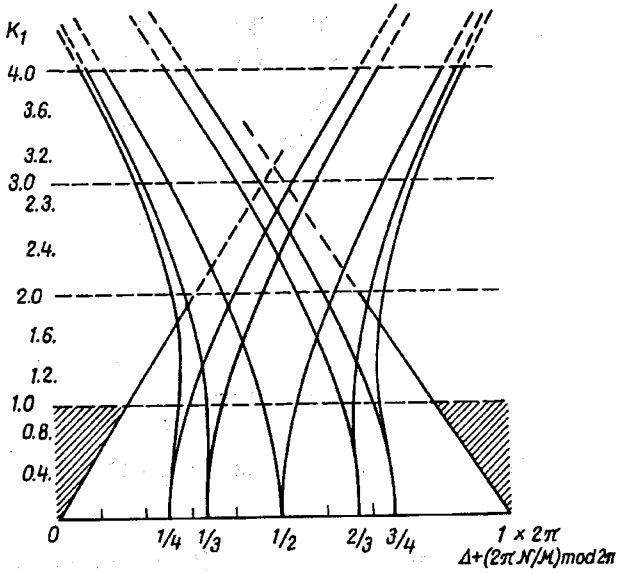

Fig. 9. The frequency regions of the periodic points of the first-order DPLL associated with $\mathcal{N}:\mathcal{M}$ phase entrainment, $g(\varphi)=\sin\varphi$

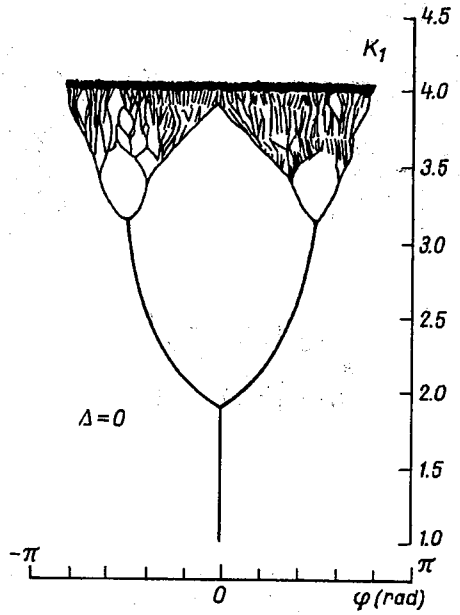

Fig. 10. Bifurcation diagram of I-order DPLL

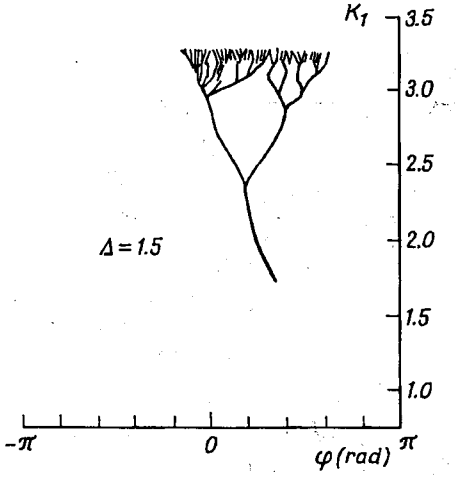

Fig. 11. Bifurcation diagram of I-order DPLL

The frequency acquisition region presented in [6,7] is different from that of fig. 3 because the dependence on ω was taken into account. The regions of fixed and periodic points of mapping h overlapp. When parameter K_1 is greater than 1 and is still increasing then the prior stability is being lost and the sequence of bifurcations occurs. The bifurcation diagrams are given in the next figures in the case of $\mathcal{N}$:1 phase entrainment. They show subsequent bifurcations from the single stable fixed point of